IDENTIFICATION OF AC ELECTRO-THERMAL AGEING MARKERS FROM ARTEMIS CABLE PEELINGS

Thesis submitted for the degree of

Doctor of Philosophy

at the University of Leicester

by

Antonios Tzimas, MSc, BEng (Hons)

Department of Engineering

University of Leicester

May 2008

Acknowledgements

To begin with I wish to thank my parents, Stelios and Pashalitsa, my grandmother, Anna, my sister, Vana and my aunt Elena for their support and encouragement throughout this study.

Then I thank Professor Len Dissado for his excellent guidance, support, understanding and expansion of my scientific as well as general knowledge, without him I would not be the same person I am now and this piece of work either.

I thank Professor John Fothergill for being present at the right time with the right piece of advice and support despite his busy schedule.

I thank Dr. Fu for his experimental guidance, supervision and moral support.

I would like to thank all the technical and clerical staff of the department of engineering for their help in one way or another that contributed to the completion of this work and making this department a friendly place to work at. Especially I would like to thank Jenny and Julie from the general office, the technicians; Tony, Dipak, Alan and Julian; Andy Willby and Paul Williams for the pleasant discussions about work and life in general.

I would also like to thank Borealis AB for the financial support during this study as well as my project co-ordinators Alfred Campus, Ulf Nilsson and Nigel Hampton for the fruitful discussions and support.

I also take this opportunity to thank my current boss Dr Simon Rowland for his understanding and tolerance near the submission of my thesis.

I also wish to thank my friends for being there for me when I needed them, Dr Gauthier Torricelli, Dr Gail Iles, Dr Nick Benzhavili, Dr Chen Zou, Dr Severine Leroy, Dr Kien Ling Khoo, Enid, Jo and Alan, Panos, Dionisis and Erriketi, Haider and Tanvir, Francesca and Ricky, Giorgo and Maria, Garber and others whose lack of acknowledgement may not be taken as lack of gratitude.

Last but not least I would like to thank my partner in life, Alexandra, for her patience understanding and support through the hardest pieces of this work. Not to forget to thank her mum for the enlightening holy pie that she made me.

I would like to dedicate this thesis to my grandfather, Antonios Tzimas, for the excellent moral foundation that he provided for me.

IDENTIFICATION OF AC ELECTRO-THERMAL AGEING MARKERS FROM ARTEMIS CABLE PEELINGS

Antonios Tzimas

ABSTRACT

XLPE cable peelings taken from underground High-Voltage cables that had previously been stressed under different ac electro-thermal conditions are investigated, with the aim of identifying properties indicative of the changes brought about by ageing. The inherent endurance ability of these peelings has been tested for three different endurance conditions of high ac electrical and thermal stresses. Space charge measurements via Pulse-Electro-Acoustic and Thermally-Stimulated-Currents are utilised to evaluate the state of the peelings before and after the endurance test in comparison with unstressed material.

It was found that the pre-stressing altered the inherent endurance capability of the peelings especially for materials that had experienced thermal and electro-thermal stressing as a cable. The space charge behaviour also showed changes due to the stressing, related to the accumulation and transport of charge, with ac-electrical stressing reducing the time for heterocharge accumulation at the anode and AC electro-thermal stressing facilitating positive charge injection and propagation to the cathode. A double positive peak near one electrode was identified as indicative of irreversible degradation.

CONTENTS

1 CHAPTER: INTRODUCTION AND PROJECT OVERVIEW

The possibility of identifying ac thermo-electric "ageing markers", i.e. measurable properties that altered irreversibly during ac electro-thermal stress with the reduction of the material life as a consequence, is investigated for cable insulation material. Cable peelings that were produced during a European funded programme called ARTEMIS were used as test objects. The insulation of these cables is cross-linked polyethylene (XLPE). In this chapter the material that was used as an insulator is introduced as well as the complications of its use in High Voltage (HV) power cables. The experimental techniques that have been used to search for ageing markers are also introduced here.

1.1 XLPE AND ITS APPLICATIONS

Dielectric systems are used extensively for many applications such as communication, electrical, and electronic systems. They range from simple capacitors to high voltage (HV) apparatus and power cables. Electrical insulation and conductor assemblies are manufactured with many configurations, but share the common feature of an insulator sandwiched between conducting electrodes. Because of its excellent electrical properties combined with good physical characteristics one of the most common insulation materials used for High Voltage (HV) cables, see Figure 1.1.1, is cross-linked polyethylene (XLPE) and over time it has replaced the traditional oil-filled paper cables (Hampton et al, 2007). XLPE insulated cables are preferred over the fluid filled ones as the hydraulic system is eliminated thus their installation and maintenance is less

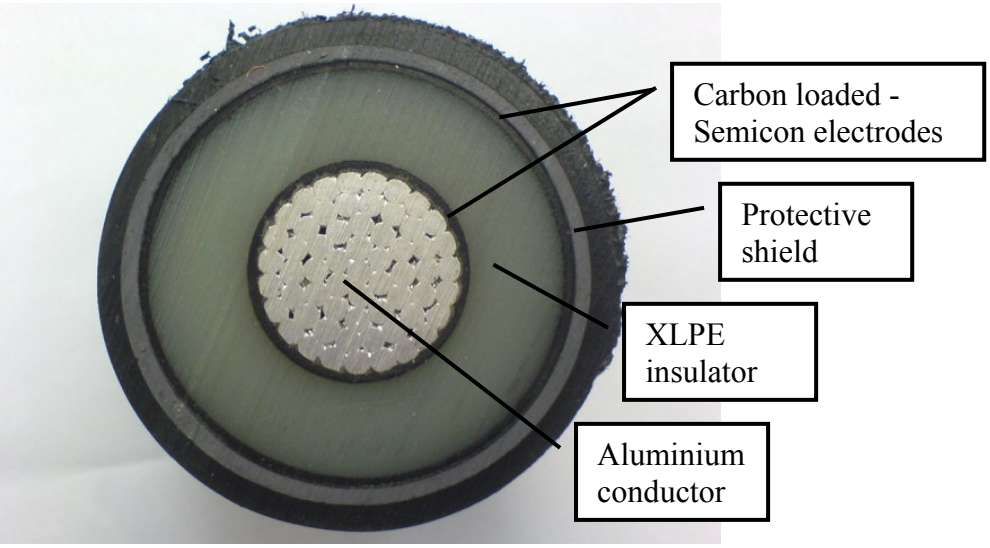

Figure 1.1.1: Photograph of a sectioned HV cable produced for the ARTEMIS programme.

troublesome. Oil-filled systems are also an environmental hazard when used as underground cables and for this reason they are being phased out.

1.1.1 XLPE and its limitations as an insulator in HV cables

Catastrophic failure of electrical cable insulation is still a major problem for the electricity generation and supply industries, and underwater telecommunication systems (Alison & Hill, 1994 and Brown et al, 2000). The technical limitations of extruded high and extra high voltage cables are related to lack of understanding of the degradation mechanisms. It is believed that the most harmful defects for the dielectric performance of HV cables are due to, protrusions from the semiconductive screens, contaminants and voids in the insulation, see Figure 1.1.2. However it has not been possible to quantify their effect on the degradation rate. This is one of the reasons why the design stress currently employed for XLPE is lower than for oil-filled cables (Dissado & Fothergill, 1992), resulting in larger cables and consequently higher installation cost.

Figure 1.1.2: Typical defects (contaminants – left & right, and semiconductor screen distortion – right) found in extruded cables. Taken from Hampton et al (2007).

Typical XLPE cables have a life expectancy of 30 years, and some of them have been operating for over 20 years. History has shown that the life time of some of these early cables was far shorter than expected as engineers and scientists at the time were not aware of the above complications. A common failure mechanism that extruded HV cables suffer from when located in a moist environment and placed under ac-electric stress is the generation of water trees from the inner and outer semiconductive (carbon-loaded polymer) screens, see Figure 1.1.3. The electric field at the branches of the water tree is enhanced and could lead to the formation of electrical trees and cable failure (Dissado & Fothergill, 1992). At the present time insulation materials and manufacturing process have been developed that prevent the growth of water trees

altogether and promise power cable longevity (Hampton et al, 2007). The present rate of unexplained failure is 0.8/100 km/yr and the industrial objective is to reach 0.2 (Borealis, 2003). This is only possible through the development of an effective Diagnosis System.

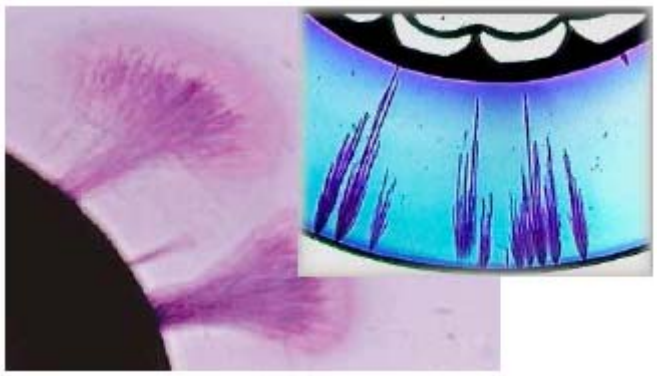

Figure 1.1.3: Water Trees growing from the Inner (bottom) and Outer (top) Semiconductive Screens. Taken from Hampton et al (2007).

Hence, there is still a need to monitor and diagnose the state of the earlier cables and monitor the ones that have just been installed. It has been suggested that the accumulation of charges in a dielectric, referred to as "space charge" in literature that modify the local electric field via Poisson's equation, are responsible for void expansion, partial discharges and consequently generation of electrical trees that lead to inevitable insulation breakdown (Dissado et al, 1997). Experiments have been carried out to study and measure the behaviour of space charge generated in dielectric insulating material (Dissado & Fothergill, 1998). Despite the achievement of the experiments, there is no established method to 'predict' the behaviour of the space charge in insulation dielectric materials under different operating conditions. Different operating parameters such as applied field and temperature alter the behaviour of the space charge in the material. At the moment accelerated ageing tests are conducted during the component design stage to allow engineers to gather statistical information on the HV performance, with the intention of extrapolating the data to service conditions and voltages, and ensuring low failure probability under service conditions. However, premature failures do occur under service conditions (Dissado & Fothergill, 1992). Developing an understanding of the mechanism causing the insulation to break down/degrade in order to determine a more accurate design life of the cables and develop a diagnostic tool to monitor their state is essential. The utilities would ideally like to be able to assess the remaining life for their cable systems and in order to do this

they need experimentally available indicators for the current state of their system vis-à-vis insulation that is in imminent risk of failure.

1.2 ARTEMIS PROGRAM

It has been reported that under high electric field stress, trapped or low mobility electrical charge within the bulk can increase the space charge accumulation, resulting in localized field enhancement and electromechanical force which may lead to premature failure of the cable well below its designed value. The increasing needs for energy quality and insulation system reliability are pushing strongly the research on new techniques for the diagnosis of insulation ageing. For that reason a European project, called "**ARTEMIS**" (**A**geing and **R**eliability **TE**sting and **M**onitoring of power cables; diagnosis for **I**nsulation **S**ystem) was carried out involving the collaboration of a great number of research and university institutes.

1.2.1 ARTEMIS overview

Two 90 kV cables were produced by two cable manufacturers, Pirelli Cavi (IT) and Nexans Benelux (BE), using a single batch of commercial XLPE supplied by another partner, Borealis A/S (DK). These cables were stressed in dry conditions for various times, voltage and temperature levels. The selected temperatures levels were 20 and 90°C, while three voltage levels were used: 145, 225 and 325 kV corresponding to fields of 14.1, 21.8 and 31.2 kV/mm at the inner semiconductive layer. The longest ageing time was 10 000 hours (417 days). The partners involved in the cable ageing were Pirelli Cavi, Nexans Benelux and EDF (FR).

Samples from both unstressed and electro-thermally stressed cables were distributed to the partners as both cable pieces shown in Figure 1.1.1 and 150 μm thick tape peeled from the insulation Figure 1.2.1. In addition, 150 μm tapes from unstressed cable were used for ageing tests at fields up to a value of 80 kV/mm that it was not possible to accomplish with full sized cables. A multitude of electrical, chemical and physical techniques were employed to characterise the status of the cable insulation (Fothergill et al, 2003). Although attention was focussed on a position located 2.0 mm from the inner semiconductive layer, some selected properties were determined throughout the whole insulation. The main part of this experimental work was performed by the universities of Bologna (IT), Leicester (UK), Montpellier (FR), Surrey (UK) and Toulouse (FR) and by the research organisations Alcatel CIT (FR) and Laborelec (BE).

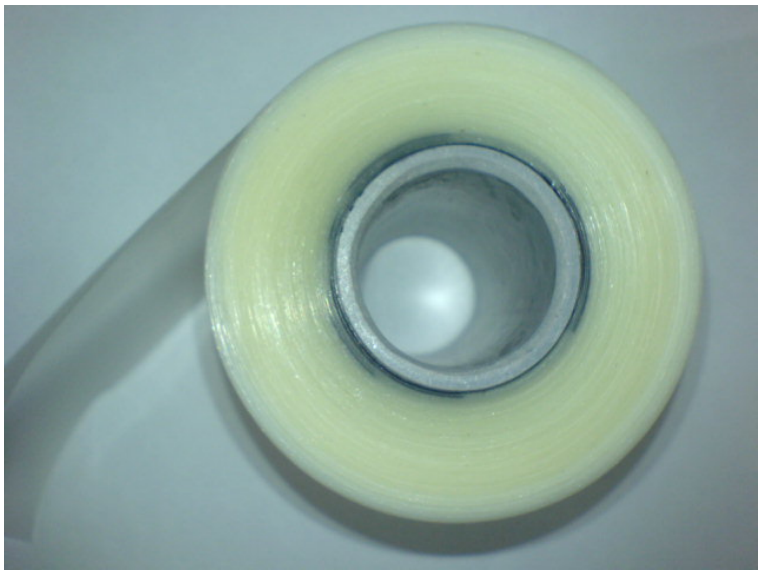

Figure 1.2.1: 150µm thick tapes peeled from XLPE cable insulation for Artemis programme.

1.2.2 ARTEMIS aims and objectives;

The main objectives of the ARTEMIS project were:

a) to assess the state of ageing of cable materials under combined stresses,

b) to develop a Diagnostic System to predict their remaining life time.

The Diagnostic System will provide:

- Definition of the range of critical values of relevant "markers". These "markers" (ageing observables) result from the identification of local material properties that change with ageing,
- Determination of electrical and thermal thresholds for ageing.
- Estimation of the time to breakdown.

The main tasks of ARTEMIS comprise: development of a model of ageing and remaining life time based on characterisation of AC power cables, development of the Diagnostic System using the model, advanced characterisation techniques and evaluation using operating cables removed from service.

1.2.3 ARTEMIS outcome

The project demonstrated that a very low rate of degradation of the cable materials with no significant degradation taking place during the cable stressing in spite of the use of very high electric stress levels at elevated temperatures. It is clear that the project did not provide a definitive indication of the techniques that should be used to evaluate life

expectancy, as the key degradation indicators were not identified. Nevertheless, the parameters that are likely to form such a set of indicators can be stated:

- the most promising are space charge measurements with PEA/TSM;
- analysis of the size and distribution of microvoids.

The stressed ARTEMIS cables have been compared to an 18 years old 150 kV cable removed from the Belgian network. This study reinforces the conclusion that space charge properties may be used as indicators of ageing.

A software tool to determine possible correlations between properties and ageing parameters (voltage, temperature and time) and determine the extent of degradation was developed at the end of the project. As ageing markers have not been identified, this diagnostic tool, called the Automated Diagnostic System, was designed as a general-purpose tool able to process any kind of data.

1.3 AIMS AND OBJECTIVES OF THE CURRENT WORK

The aim of the current work is to carry the "ARTEMIS" work forward through endurance testing towards a definite statement on ageing markers.

In order to achieve the aim of this work the following objectives were carried out:

- Characterisation of the peelings from the ARTEMIS project before endurance testing;
- Comparison of the inherent endurance capability of the peelings under high electro-thermal stressing;
- Relate the characterisations before and after the endurance tests to their prehistory and the endurance test survival time.

1.4 INTRODUCTION TO POLYMERS: FROM POLYETHYLENE TO XLPE

The purpose of this section is to introduce the chemical and morphological features of polyethylene (PE) and consequently cross-linked polyethylene (XLPE) as this is the material under study. Polyethylene has a wide range of applications in dielectrics because of its good electrical properties, i.e. large band gap insulator (~8.8eV), in combination with excellent mechanical properties. Hence, the study of the chemical and morphological properties of polymers and more specifically polyethylene has received a lot of interest (Dissado & Fothergill, 1992, Hoffmann et al, 1991, Stevens & Baird, 2005) as it is believed that they are responsible for the charge transport and conduction

mechanics of the material (Blaise, 2001), on which polymer charge transport (Teyssedre & Laurent, 2005) and life (Dissado, 2002) models are based.

1.4.1 Overview of polyethylene

Polymers are macromolecules made of long chains of with repeating monomers such as hydrocarbons. The chemical construction of polyethylene is shown in Figure 1.4.1. A more detailed description of its chemical and physical picture has been given by Hoffmann et al (1991) and Dissado & Fothergill (1992).

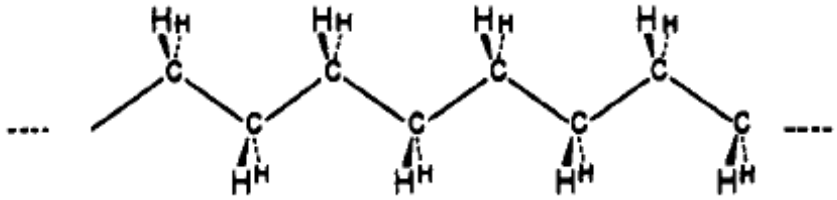

Figure 1.4.1: Polyethylene carbon hydrogen molecular chain. Taken from (Hoffmann et al, 1991).

The construction of the energy band structure of polyethylene from the orbital levels of a series of closely related olefins (C_nH_{2n+2}), such as methane, ethane, propane and butane is shown in Figure 1.4.2. From, this diagram it can be seen that the separation between the electron orbital energies gets smaller as the molecular size increases leading to overlapping orbitals where an idealized continuous band can be formed such as the valence and conduction ones in semiconductors. It can also be seen that polyethylene has a large band gap (~8.8eV), which means that there are no accessible energy levels for charges between the top of the valence band and the bottom of the conduction band. Theoretically this makes polyethylene a perfect insulator. However, the reality is a lot more complex as other sources, such as impurities and chemical

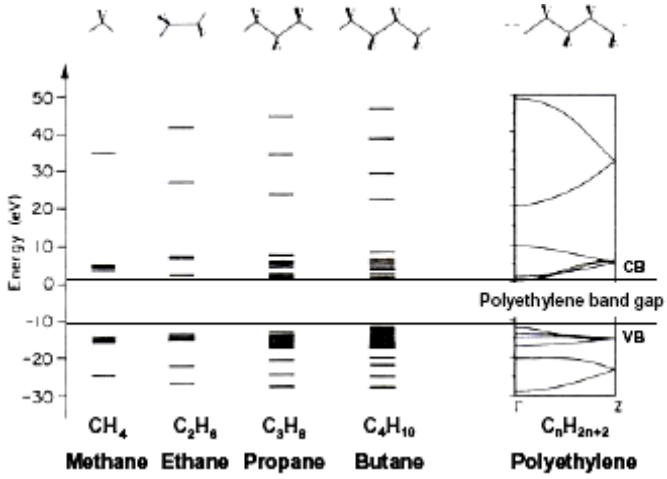

Figure 1.4.2: Distribution of orbital levels going from methane to polyethylene band structure diagram. CB and VB stands for conduction and valence band respectively. Taken from Hoffmann et al (1991).

conformational disorders (i.e. the amorphous nature of polyethylene), which according to Blaise (2001) arise from the metastability of the polymer structure, are able to supply/transport carriers by the introduction of localized energy states. In order to have a more realistic picture of the band diagram of polyethylene these physical, and chemical disorders, and their influence on the charge transport have been extensively discussed in literature by Dissado & Fothergill (1992) and Blaise (2001). The effect of these features is the introduction of localized states into the forbidden gap, see Figure 1.4.3, which have been included in recent charge transport models (Teyssedre and Laurent, 2005).

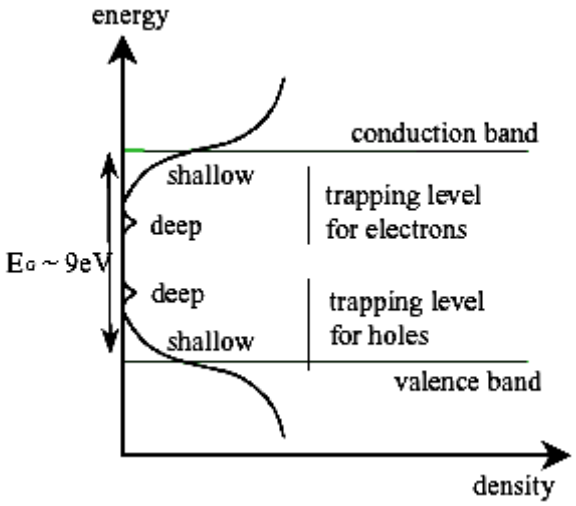

Figure 1.4.3: Schematic representation of the energy state density in a disordered dielectric material. Shallow and deep traps are related to physical and chemical disorder, respectively. Taken from (Teyssedre and Laurent, 2005).

The energies that these localized states correspond to are also referred to as traps in the literature, and are divided into shallow traps and deep traps, see Figure 1.4.3. Shallow traps lie close to the energy bands, and deep traps far from the band states. Electron-empty states may trap electrons, whereas electron-full states function as hole traps. These states therefore govern the ability of the charges to move through the insulator, i.e. they are responsible for the charge transport/accumulation in solid dielectrics. Because the shallow traps are localized energy states near to the edges of the forbidden gap charge transport, i.e. trapping and de-trapping mechanism, occurs a lot faster via them than via the deep traps. This leads to a fast charge transit of injected charges from one electrode to the other. Deep traps are located nearer to the centre of the forbidden gap, and it therefore takes more energy to release charges from them and hence a longer time for charges to transit the material via them. It may also take a longer time for charges to release sufficient energy for them to become localized in the deep traps than

in the shallow traps. It is believed that shallow and deep traps are related to the physical/morphological and chemical defects respectively.

(a) Physical defects

Polyethylene (PE) is a semi-crystalline material. It consist of crystalline regions, i.e. lamella (ribbon-like) sheets, surrounded by amorphous inter-lamella regions as shown very well schematically in Figure 1.4.4a by Jones et al (2005) and also captured with an Atomic Force Microscopy (AFM) in Figure 1.4.4b by Stevens & Baird (2005). The crystalline structure is achieved by the folding of long polymer chains into an alignment parallel to one another in the form of lamellar sheets, see Figure 1.4.4a. The crystallinity (volume percentage of polymer in the crystalline phase) of polyethylene depends on the manufacturing process and can vary from ~50% in low density PE (LDPE) to ~90% in high density PE (Phillips, 1983). The amorphous regions are almost liquid, even at room temperature and contain most of the chemical impurities that are rejected as the crystalline lamellar forms.

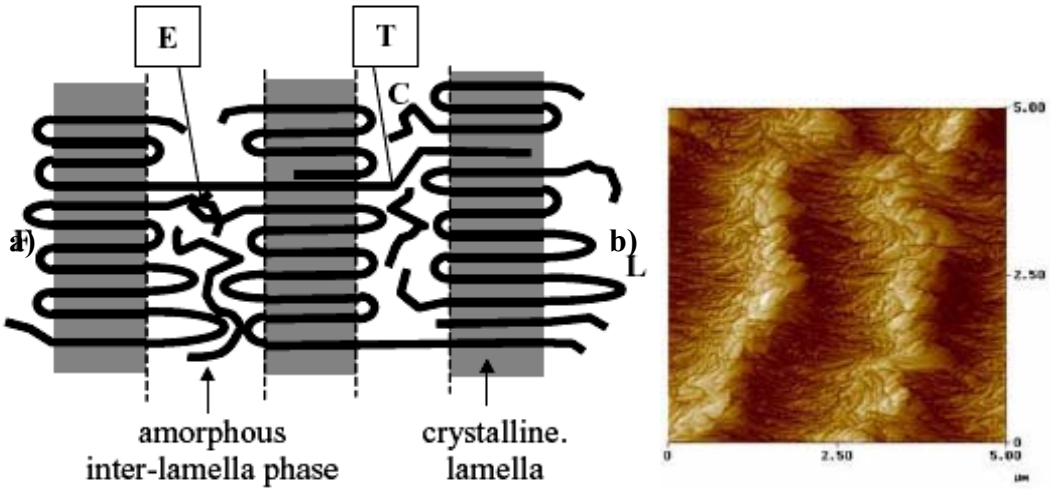

Figure 1.4.4: a) Idealized elements of PE morphology. F, lamellar chain folds. C, cilia. L, loops. T, ties. E, entanglements. Taken from Jones et al (2005). b) Atomic force microscopy photograph showing the crystalline (lamella) and amorphous region. Adapted from Stevens & Baird (2005).

Morphological defects in PE are associated with the lamellar structure and the way it is formed. For example, chain ends may be present within the lamellar or the amorphous phase and is also possible that there may be chain folds, loops and entanglements as is indicated in Figure 1.4.4a. It is also possible that a polyethylene chain is interrupted with an incorrect polymer unit such as polypropylene, with a consequence to alter the crystallinity. When PE is crystallised from a melt phase, lamellar may grow from a single nucleus to form spherulites that can have a diameter of more than 10 μm, as is shown in Figure 1.4.5. Lamellar sheets are typically 10-20nm thick, about 1 μm long

and about 0.1-1μm wide (Dissado and Fothergill, 1992). In XLPE it is unlikely for lamellar sheets to form spherulites when the cross-linking occurs at temperatures higher than the melting point of PE allowing macro-structural rearrangements to occur. Thus in XLPE the spherulites are normally replaced by lamellar stacks.

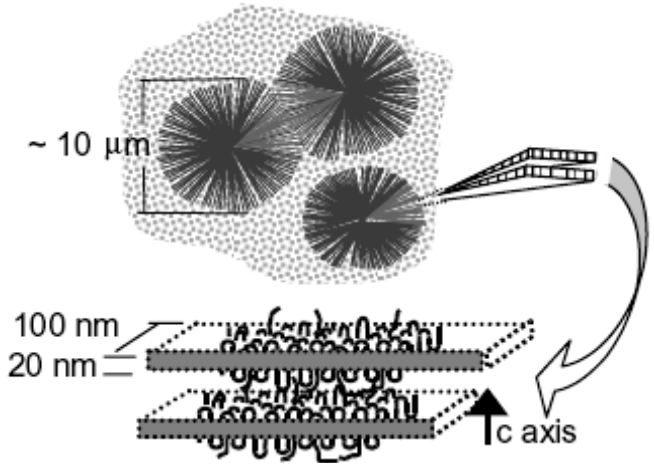

Figure 1.4.5: Morphology of semi-crystalline PE showing spherulites composed of crystalline-amorphous ribbons. Taken from Jones et al (2005).

Polyethylene is cross-linked in order to improve the mechanical properties by chemically attaching the chains together in a strong, cross-linked carbon bond creating a solid integrated mass. There are typically about one crosslink for every thousand monomer units. Cross-linking is achieved by heat, chemicals or radiation. The most common method to achieve cross-linking is by triggering a thermally-activated catalyst, such as peroxide, and raising the temperature above the melting temperature as cross-linking takes place when the polymer is in the amorphous melt phase (Dissado & Fothergill, 1992). The crystallinity of XLPE depends on the manufacturing process, i.e. the speed the temperature is increased and consequently decreased during the cross-linking. During manufacture microvoids can be formed by the evaporation of volatile decomposition products from various chemical reactions such as those used for cross-linking.

Markey & Stevens (2003) have investigated the void concentration and distribution in the XLPE material that is also used in this study for unaged and aged samples. Their investigation focussed on the extremely small so-called nano-voids, and showed that the size of these voids ranged between 30 and 50nm close to the inner semiconductive screen and between 50 and 80nm a radial distance of 4mm away. A higher concentration of voids less than 50nm was found near to the inner semiconductive

screen. The total number of voids and their internal surface area was also estimated and is presented in Table 1.4.1. It can be seen that the number of voids and their internal surface area is much higher close to the inner cable screen than away from it.

Distance from screen (mm)	Cable condition	Total number	Total void internal surface area (m^2 cm^{-3})
0	Unaged	107	5.39E−06
	Aged	49	6.70E−06
4	Unaged	35	3.85E−06
	Aged	50	3.99E−06

Table 1.4.1: Total void concentration and total void internal surface area calculated for unaged and aged samples at 0 and 4 mm away from the inner semicon. In all cases, the actual evaluated surface area was in the range 0.01–0.1mm^2 and this was taken from an inspection area that is typically 1–2mm in size. Adapted from Markey and Stevens (2003).

(a) Chemical defects

Chemical defects in polyethylene may consist of side chains, additives and crosslinking reaction products. In high voltage applications polyethylene very rarely is used in the pure state. Manufacturers tend to use additives to enhance their performance and improve the mechanical properties (Smedberg et al, 2004). Such additives are general features of polymeric insulation and can be divided into three main categories. The first one consists of the catalysts that are used for crosslinking, such as peroxide, and are meant to be used up during the manufacturing process and thereafter only their by-products remain. However, this is not normally the case as they are often not completely used up and remain in the insulation thereafter (Dissado & Fothergill, 1992). By-products of crosslinking reactions using dicumyl-peroxide, the most common catalyst, consist of α-methylstyrene, cumylalcohol, acetophenone and cumene. The proportion of by-products produced during peroxide initiated cross-linking depends on proportion of the route (a) or (b) shown in Figure 1.4.6, that the decomposition of the peroxide will follow during the reaction. The second category of additives are added in small concentrations (<10%) and do not alter the structure of the polymer. These could include stabilizers to protect the material from heat and ultra-violet radiation, antioxidants to prevent oxidation and others such as flexibilizers, antimicrobials, antistatic agents, and flame retardants. There are two common kinds of anti-oxidant a) a phenolic based one (methylenebis) that is classified into “primary antioxidants”, and b) a sulfur based one (dilauryl thiodipropinate) that is classified into secondary

antioxidants (Sekii Y. et al, 2001 and 2007). It should be noted that antioxidants could alter the crystallinity of the polyethylene (Boudou & Guastavino, 2002) and its space charge behaviour as they prevent the dissociation of hydro-peroxide (ROOH) into RO- and –OH which eventually interrupts oxidative degradation of polyethylene (Sekii Y. et al, 2003). The third category involves compounding ingredients such as fillers and plasticisers which are used in large concentrations (10-70%) to change the properties of the polymer during manufacture and use. These ingredients are used principally to improve the mechanical properties of the polymer, but there a special set of propriety ingredients that are aimed at inhibiting the inception and growth of the electrical pre-breakdown phenomena of water trees and electrical trees (Dissado & Fothergill, 1992). The exact nature of these ingredients is a matter of commercial confidentiality. All of these additives can increase the concentration and modify the energy of the localized states, and hence alter the energy distribution of the band diagram.

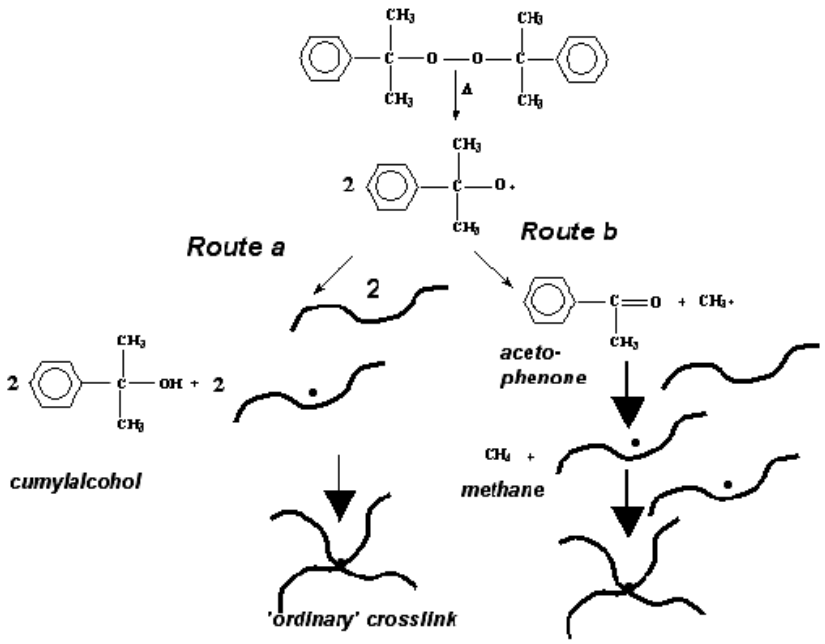

Figure 1.4.6: Peroxide initiated crosslinking of PE. Taken from Andrews et al (2006).

Modifications in the distribution of the localized states could also be introduced from side chains or in chain imperfections such as hydroxyl and ketone functions, and double or triple carbon-carbon bonds. The trap depths of chemical defects and by-products were estimated using ab-initio methods taking the n-$C_{13}H_{18}$ molecule as a reference for electron affinity. The values quoted in Table 1.4.2 for electrons and holes are from Menuier et al (2000) and Teyssedre et al (2001), and were used in the modelling of

charge transport (Teyssedre & Laurent, 2005). It is observed that the by-products, such as α-methylstyrene and acetophenone introduce the deepest trap depths for electrons. The deepest trap depths for holes could be provided by the tri-decene molecule and the α-methylstyrene by-product. Trap depths less than 0.79eV would be difficult to observe by experimental methods using the Pulse-Electro-Acoustic (see below section 1.7.1 for details) technique using the proposed model in (Dissado et al, 2007) to estimate trap depths because of the high mobility of charge and low rate of acquisition measurements.

Nature of chemical defect		Molecule with:	Depth of trap (eV)	
			For electrons	For holes (when available)
6-tridecene* ($C_{13}H_{26}$)		In-chain C=C	0.16	0.57
5,7 tri-decene* ($C_{13}H_{24}$)		In-chain conjugated C=C	0.51	1.35
6-tridecanone* ($C_{13}H_{26}O$)		Side chain C=O	0.49	0.43
5-decanone** ($C_{10}H_{20}O$)		Side chain C=O	0.453	
5-decene** ($C_{10}H_{20}$)		In-chain non conjugated C=C	0.122	
4, 6-decene** ($C_{10}H_{18}$)		In-chain conjugated C=C	0.443	
5-decyne** ($C_{10}H_{18}$)		In-chain non conjugated triple bond	0.041	
5-vinyl nonane** ($C_{10}H_{20}$)		Non conjugated C=C	0.157	
5-decanol** ($C_{10}H_{21}O$)		Hydroxyl	0.186	
5-decanal** ($C_{10}H_{20}O$)		Carbonyl group	0.445	
4-propyl heptane** ($C_{10}H_{22}$)		Saturated	0.121	
By-products of cross-linking reactions when using decumyl-peroxide as a cross-linking agent	Alpha-methylstyrene* (C_9H_{10})	Conjugated double bond	1.53	0.79
	Cumylalcohol* ($C_9H_{12}O$)	Hydroxyl	0.28	0.36
	Acetophenone* (C_8H_8O)	Carbonyl group	0.9	0.04
	Cumene** (C_9H_{12})		0.04	

Table 1.4.2: Summary of the trap depth values calculated using *ab-initio* methods for different chemical defects. Taken from Teyssedre & Laurent (2005).

1.5 SPACE CHARGE DYNAMICS

Space charge is the charge in a dielectric that modifies the local field via Poisson's equation:

$$\frac{dE(x)}{dx} = \frac{\rho(x)}{\varepsilon_o \varepsilon_r} \qquad \text{Equation (1)}$$

Where $E(x)$ is the electric field as a function of position in space (x);

$\rho(x)$ is the local space charge density;

$\varepsilon_o \varepsilon_r$ are the permittivity of free space and the relative permittivity respectively.

Space charge could consist of electronic charge carriers such as electrons and holes that are injected from the electrodes, and/or ionic charge carriers from molecular dissociation. Space charge can be characterized as homocharge or heterocharge depending on the polarity of the net charge that is accumulated adjacent to the electrodes. In the case where the charge accumulated has the same polarity as the adjacent electrode it is referred to as homocharge. In the other case where the charge accumulated has the opposite polarity to the adjacent electrode it is referred to as

heterocharge. Homocharge reduces the interfacial field at the electrode and the dielectric and increases the electric field in the bulk, while heterocharge enhances the interfacial field and reduces the electric field in the bulk, see Figure 1.5.1.

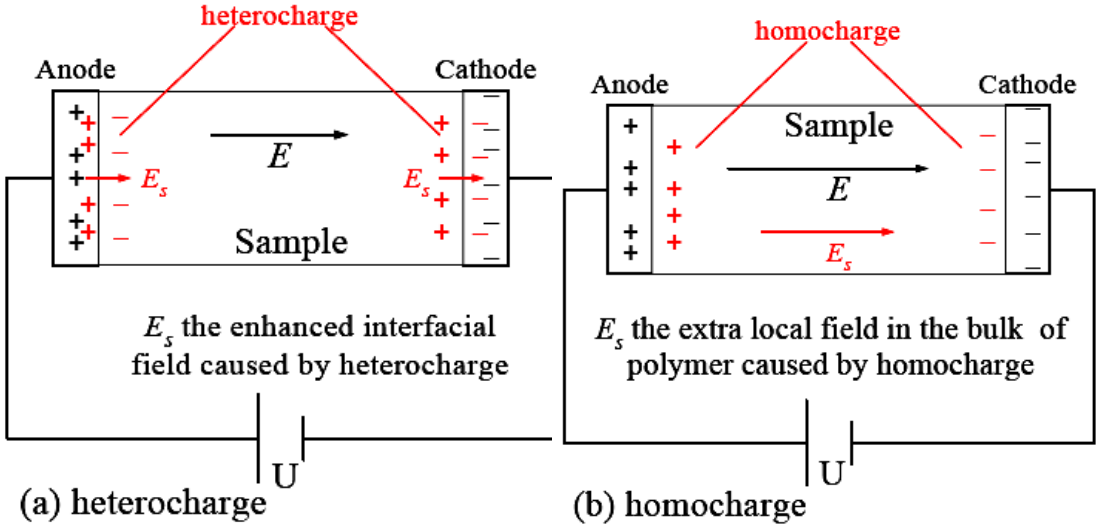

Figure 1.5.1: Influence of (a) heterocharge and (b) homocharge on the electric field distribution. Taken from C. Zou (2007).

1.5.1 Space charge and dielectrics

Space charge presence in dielectrics plays an important role in the state (health) and consequently longevity of an insulator, as:

- Space charge can change the electric field distribution by enhancing local electrical stress above the design value of the insulator, i.e. it is reported by Mazzanti et al (2005) that the Poissonian field inside the insulation can be greater than the Laplacian dc field by a factor of two;
- Space charge injection is responsible for electrical tree initiation and growth that leads to insulation failure (Dissado, 2002b);
- Space charge accumulation gives local energy concentrations that drive ageing mechanisms (Dissado et al, 2001) and place a system at risk;
- Space charge can be used as an indicator of charge traps formed during the ageing of dielectrics (Mazzanti et al, 2003a and 2003b).

Hence, space charge dynamics are discussed a lot in the literature. A great collection of papers can be found in Fothergill & Dissado (1998), which covers topics from measurement techniques to micro-physical descriptions.

1.5.2 Charge injection and transport mechanisms

The localized states in the energy-band diagram of polyethylene, which appear due to morphological disorder and chemical species, can trap injected charge carriers or themselves relate to ionic charge carriers. They therefore hold the charge for some time before de-trapping allows the charge to displace in the field, and hence they will control transport and allow charge to accumulate in the material. The injection of electronic charges as well as their transport depends upon the electric field, and a more detailed description can be found in Dissado & Fothergill (1992). Charge injection requires the transfer of an electron between the electrode and the polymer. This is opposed by a potential barrier. Two distinct processes are possible, electron tunnelling through the potential barrier and electron activation over the barrier (Dissado and Fothergill 1992). The Fowler-Nordheim theory describes the effect of electric field on tunnelling injection and will occur predominantly at very low ($T < 150$ K) temperatures, and very high fields ($E > 5x10^8$ V/m). At room temperature and moderate fields the Schottky process is presumed to dominate. In this mechanism the electric field reduces this potential barrier at the electrode/insulation interface making injection of electrons easier. Theoretical expressions for each process have been obtained under the assumption of a simple form of potential surface. In reality the electrode/insulation interface is very complex because of the presence of physical and chemical defects such as surface roughness, chemical impurities and dangling bonds (Jones et al, 2005), and hence the injection current is more complicated than the simple expressions derived.

Some basic mechanisms that describe charge transport in dielectrics are shown in Figure 1.5.2.

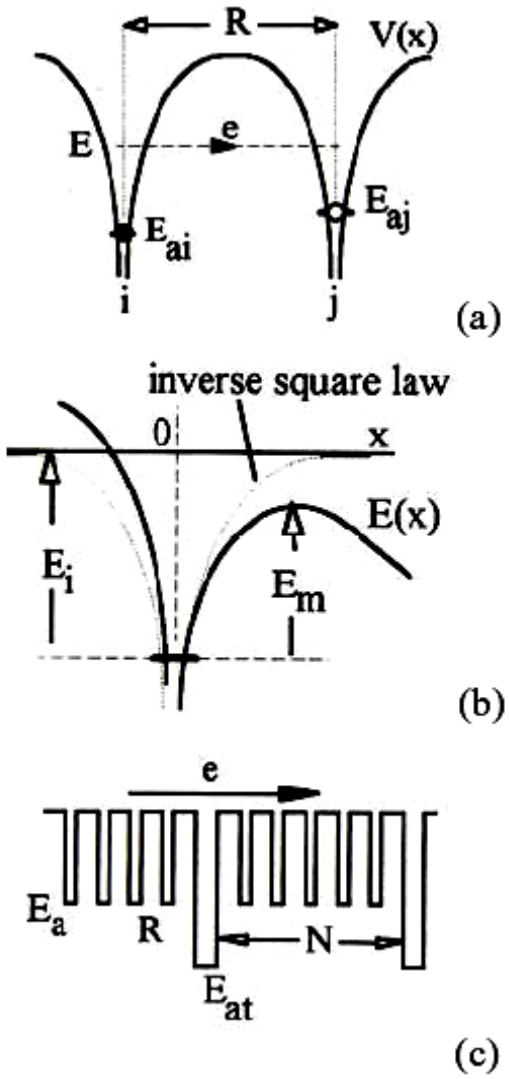

(a) Resonant tunnelling between two states. An electron in state *i* is thermally excited to an energy *E* at which it proceeds by resonance tunnelling through the intermolecular energy barrier *V(x)* to a state *j*. In this example *i* and *j* are acceptor states.

(b) Poole-Frenkel mechanism. The potential energy E_i of the site is assumed to be of Coulombic form. In the presence of a field, the energy of the site is modified (lowering the barrier in the drift direction).

(c) Trap controlled mobility. The migration of an electron occurs through trapping in successive states. Mobility is deduced from the average time that charges stay in traps.

Figure 1.5.2: Some basic principles for charge transport. Note the Coulombic shape of barriers in case (a) and (b) trap sites interactions by the influence of the electric field and the square shape in case (c). Note that the diagrams (a) and (c) are represented in zero field conditions. Taken from Teyssedre & Laurent (2005).

1.6 AGEING MECHANISMS AND MODELS

The understanding of ageing, degradation and breakdown mechanisms of dielectrics have occupied the interest of scientists for decades because of the wide range of application of dielectrics. The degradation and breakdown mechanisms are better understood than the ageing one whose existence is still a debatable topic (Fothergill, 2007 and Dissado, 2007), see Figure 1.6.1 and Table 1.6.1 where the characteristics of the mechanisms are summarized. Figure 1.6.1 shows that at different electric fields different mechanisms may lead the insulation to failure. Breakdown mechanisms occur at a field where a sample of insulation will fail in a short time, of the order of micro-seconds and are distinguished mainly as electrical, electromechanical or thermal in

origin. In these cases failure is caused by a mechanism that is unable to reach a stable state in the presence of a high electric field, and accelerates rapidly to breakdown when the field exceeds a mechanism-dependent critical value.

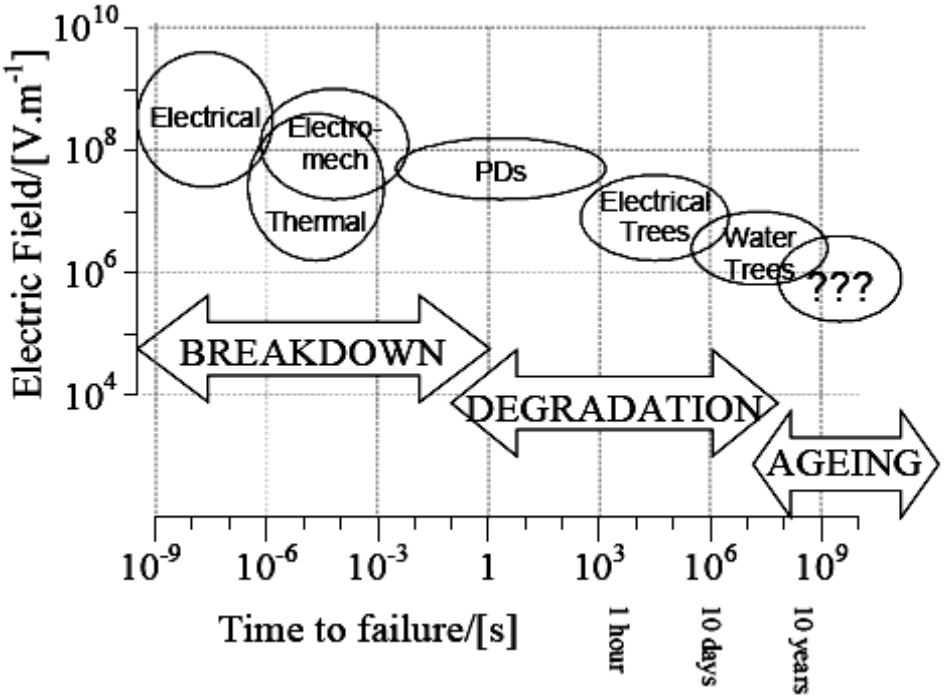

Figure 1.6.1: Indicative times and electric fields over which various electrical breakdown and degradation mechanisms are operative. Taken from Fothergill (2007).

At lower fields it is expected that these deterministic processes come into equilibrium, and hence failure should not occur. Nevertheless failure does occur but it requires a much longer time as other mechanisms are needed to bring the system to a point at which damage generation can accelerate to form a short-circuit. This is acceptable as long as the time required is long enough, for instance utilities expect that failure time should exceed 40 years at service stresses. This increase in time to failure may take place because the waiting time for the occurrence of an event that is severe enough to cause a rapid failure in an undamaged polymer becomes longer at lower fields (Dissado, 2007). This effect has been demonstrated in induced partial discharges by Temmen (2000), see Figure 1.6.2. Temmen argued that the surface conductivity of cavities could increase due to accumulated moisture, which in the presence of an electric field could generate local partial discharges that cause erosion of the surface and chemical degradation of the insulator. Thereafter, a pit may be formed by further increase of partial discharges that leads to electrical tree growth and consequent breakdown.

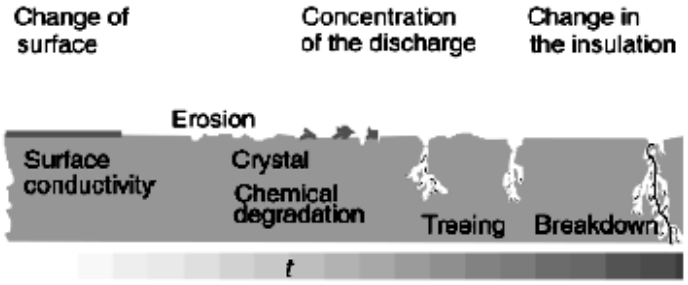

Figure 1.6.2: Stages of PD-induced damage at the insulator surface. Taken from Temmen (2000).

	Breakdown	***Degradation***	***Ageing***
Effect	Catastrophic: **insulation cannot be used afterwards**	Leads to breakdown: **reduces breakdown voltage**	May lead to degradation: **may not reduce breakdown voltage**
Speed	Fast: **occurs in <<1s**	Less than required service life**: ~hours-years**	Continuous process: **whole service life**
Evidenc	Direct observation: **normally by eye-hole through the insulation**	Observable directly: **may require microscopic or chemical techniques**	Difficult to observe: **may even be difficult to prove existence**
Place	Continuous filament: **bridges electrodes**	Occurs in weak parts: **may form fractal structures**	Assumed to occur throughout insulation
Size	>mm: **dependent on energy of event**	>μm: **may form larger structures**	>nm: **molecular scale**
Examples	**Thermal** **Electromechanical** **Mixed mode** **Avalanche** **Intrinsic**	**Electrical Trees** **Water Trees** **Partial Discharges**	**Bond scission** **Nano-voids** **Trap formation** **Non-electrical changes (oxidation etc)**

Table 1.6.1: Characteristics of Breakdown, Degradation and Ageing Processes. Taken from Fothergill (2007).

1.6.1 Deterministic breakdown

Theories of breakdown in which a process becomes unstable and unable to reach an equilibrium in the current or energy density above a critical field are denoted as

deterministic. In this category of model each step of the response to an applied field is determined by the previous conditions and the current step determines future events. A model-dependent breakdown field, E_b, can be determined for which the system response to the applied field just becomes unstable.

Deterministic models of breakdown are classified according to the process that leads to them. Four basic categories for polymeric insulating systems can be considered (see Figure 1.6.1 for ranges of the breakdown field, E_b, that can occur):

- **Thermal breakdown**, in which the applied power causes local heating and a self-reinforcing concurrent increase in conductivity;
- **Electro-mechanical**, in which the self-reinforcing electrostatic attraction of the electrodes due to local softening or cracking causes the dielectric to collapse;
- **Electronic**, in which breakdown is initiated by acceleration of charge carriers in (local) high electric fields;
- And **partial discharge breakdown**, in which gas in voids in the dielectric breakdown and deposit high-energy charges upon the void surface and thereby cause progressive deterioration.

1.6.2 Theoretical ageing models

Insulating polymers may alter both chemically and morphologically even in the absence of an electric field. It is usually assumed that during the period under service stress some mechanism causes small local modifications in the insulation, which either grow in number or extend until a point is reached at which a conducting path is rapidly formed between the electrodes resulting in a short circuit (Dissado, 2007). This process is given the name of electrical ageing.

In order to describe electrical ageing a number of models have been proposed by Jones et al (2005), Dissado et al (1997), Crine (2005) and Wu K. & Dissado (2004a). Dissado (2007) splits them into two categories: a) electrical field driven mechanical damage (Jones et al, 2005 and Dissado et al, 1997) and b) damage inducing energy transfer to the polymer from local electrical currents (Crine, 2005 and Wu K. & Dissado, 2004a). The physical features of these models are briefly described below.

(a) Electromechanical Ageing Models

The basis of these models is that mechanical stresses causes cracking and crazing in insulating polymers such as low density polyethylene (LDPE) and XLPE and that electrical fields produce a mechanical tension perpendicular to the field direction see Figure 1.6.3. Such electromechanical stresses depending on the local electric field strength can cause local extensions of the inter-lamella tie molecules and eventually when the stresses are high enough the breaking of tie molecules causing local cracks, see Figure 1.6.4. At some stage these will extend or join together to either produce a cavity where partial discharges could occur, leading to electrical tree failure or a runaway crack growth. In the model by Jones et al (2005) the electric field driving the process is essentially the applied field and morphological variations of the polymer structure are responsible for high electromechanical stresses. For this model a threshold field for crack generation can be defined, where the application of local fields below

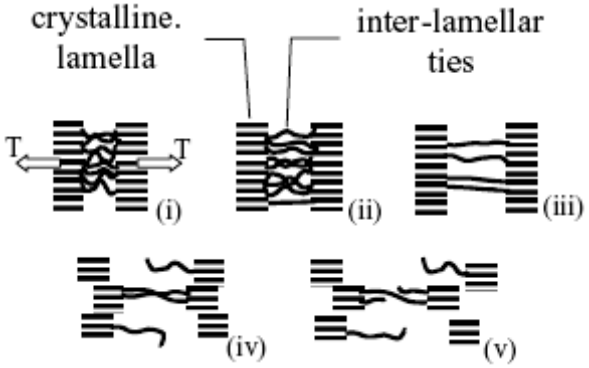

Figure 1.6.3: Response of tie molecules in an element of the amorphous phase to a tensile stress T; (i) at low stress, (ii) and (iii) progressive ductile extension of ties at higher stress,. (iv) and (v) break up of ties and ultimately of lamellae at highest stress. Taken from Jones et al (2005).

this value lead to local deformations that come into equilibrium. An expression for the ageing rate has been obtained using this model but even though it is intended to describe a progressive change over time, i.e. ageing, no expression for the lifetime has been derived. In contrast a lifetime expression is derived in the model by Dissado et al (1997). This model assumes that in the absence of an electric field the morphology changes slowly due to physical ageing of the polymer, but that the changes are insufficient to cause significant damage. The presence of space charge when an electrical field is applied leads to a local field enhancement and enhances the changes to the local morphology. The local deformation reaction is accelerated and the equilibrium deformation level is altered. In weak regions the equilibrium deformation will exceed

that required for bond breaking and cracks will be formed. Thereafter the process follows the same route as that described by Jones et al (2005).

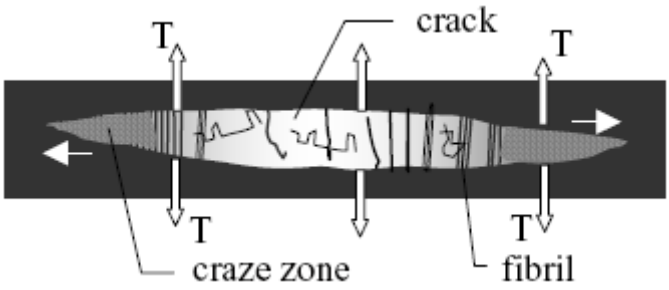

Figure 1.6.4: Craze and crack development in an inter-lamellar space under tension T. Fibrils develop and break to propagate crack. Taken from Jones et al (2005).

The lifetime expression for the model by Dissado et al (1997) is obtained by defining the deformation reaction in terms of an energy barrier between the un-deformed and deformed states that is lowered by the electromechanical stress. The system moves towards an equilibrium between the two states, and reaches an irreversible modification when a critical quantity of conversion has been achieved. The life expression has been fitted to the characteristic endurance life of a number of polymers (Mazzanti e al, 2005). Failure statistics can be deduced for the mechanism by assuming that the parameters have a spatial distribution of values and that rapid failure is initiated at the site whose parameter values (Dissado, 2002) give the shortest time for damage generation. The major achievement of this model was to fit the full endurance life data of a given polymer over a range of temperatures and fields with the same parameter set (Mazzanti et al, 2005).

(b) Ageing caused by Local Currents

In these models (Crine, 2005 and Wu K. & Dissado, 2004a) energy is transferred to the polymer from local currents causing damage that eventually leads to breakdown via a short-circuit. In the model developed by Crine (2005) electronic charges are accelerated in voids or free volume and transfer energy to the polymeric surfaces that provide an energy barrier for the electron to escape from the void. Continual transfer from either ac-currents or repetitive dc-currents builds up the energy retained locally and are said ‘to break Van der Waals bonds’. Van der Waals forces act attractively between neutral molecules and do not have a specific direction, but are the energies that hold molecules together in a solid. Therefore, the physical damage visualized here is a reduction of the energy that holds molecules together and is equivalent to local plastic deformation.

Thus, the mechanism described by this model is an alternative route to the first stages of damage described in the electromechanical models.

In the percolation ageing model developed by Wu K. & Dissado (2004a) electronic charges are located in traps that are neutral when occupied. In the presence of a field the energy barrier for the transfer of the charge carrier between traps is lowered and if the field is high enough the barrier can be removed altogether allowing groups of traps to be connected in the form of a field-dependent conducting path. These groups behave as percolation clusters and charges on the paths in the clusters can gain enough energy in the field to cause bond scission in the polymer both along the path and particularly on its boundaries. The broken bonds are taken to act as traps with low energy barriers and their generation extends the percolation cluster until it eventually bridges the insulating material under the applied field and causes a short circuit.

1.6.3 Space Charge and Ageing

All the theoretical models described above envisage ageing as mechanism that leads to local deformation by breaking up molecular ties, bond scission and inevitable crack formation. Hence, it is believed that ageing alters the polymer's conformational structure leading to creation of additional traps whose depth depends on the nature of the disorders caused by ageing. This has, as a consequence, to change the way charge accumulates and transports in the insulator suggesting that space charge measurements could be used as an indicator for ageing. Quantities that can be extracted from space charge measurements, such as mobility of charge packets (Lanca et al, 2007a and 2007b) as well as the mobility and trap depths of the charge carriers alone, are sensitive to ageing of polymers (Mazzanti et al, 2003a).

1.6.4 ARTEMIS Outcomes Related to Ageing

During the Artemis programme a great amount of data was produced from a wide range of techniques with the aim of characterising the material under study and identifying possible changes in the matrix. The outcome of the programme is summarized below.

1. The output from the experimental work was used as input to a theoretical ageing model that was developed during the project by the universities of Leicester and Bologna with contributions from EDF. This model related ageing to void aggregation by electro-mechanical stresses generated by localised space charge

regions, and is specific case of the model in (Dissado et al, 2001). The values of the parameters in the mathematical model were estimated on the basis of the experimental data.

2. The characterisation of chemical properties, using techniques such as infrared spectroscopy, differential scanning calorimetry (DSC) and chemiluminescence, indicate that they have not significantly changed during the cable ageing, not even under the most severe stress conditions. It is apparent that the stressing had not generated measurable oxidation of the XLPE insulation material.
3. The effects on the physical structure of the insulation have been investigated by small angle X-ray scattering (SAXS), transmission electron microscopy (TEM) and DSC giving information about the polyethylene crystals (lamellae) and microvoids less than 10 μm in size (Fothergill et al, 2003). The dimensions of the crystals are not significantly changed during the stressing, but the stressing might have had an influence on the microvoid distribution as indicated by extensive TEM and optical microscopy studies. Although no differences could be proved close to the inner semiconductive layer, there is evidence for an increased concentration 4 mm away from this layer (Markey & Stevens, 1999 and 2003).
4. AC breakdown strength tests of the 150μm tapes show only small (< 5%) differences between unstressed and stressed cable samples (Borealis, 2003). Such small differences support the conclusions from the chemical and physical investigations; that no significant degradation has taken place.
5. Space charge accumulation is the fundamental mechanism behind the proposed ageing model proposed in the Artemis programme. Thus, very extensive space charge measurements were performed using several different complementary techniques. The pulsed electro-acoustic measurements on the 150 μm tapes showed an increasing trend for the space charge amount with ageing time and electro-thermal stress (Borealis, 2003). In particular, the measured voltage threshold for space charge accumulation displayed a reduction with increased voltage stress (Mazzanti et al, 2003a and 2003b). Measurements on complete cable samples with the thermal step method (TSM) showed that the technique was able to detect a significant increase of space charge as a function of ageing voltage and, to a lesser degree, stressing time.

6. Electroluminescence (EL) tests, i.e. the measurements of photons emitted from a sample under voltage stress, could not identify any obvious relationship between ac or dc EL threshold and stressing factors although both can be related to chemical changes in the polymer (Borealis, 2003).

1.7 EXPERIMENTAL METHODS TO OBSERVE SPACE CHARGE

A great number of techniques have been developed in the last 30 years in order to observe space charge in solid dielectrics (Fleming, 2005). These can be divided into two main techniques; one where space charge is observed via external current measurements induced by a thermal excitation of trapped charges (Suh K. S. et al, 1992) and one where space charge is observed via pressure wave propagation that creates an acoustic signal directly related to the distribution of charges thereby making possible their spatial resolution (Lewiner et al, 2005). The former technique is known as thermally-stimulated currents (TSC) or thermally-stimulated-discharge-currents (TSDC). The latter technique is known as pressure-wave-propagation (PWP) from which alternative methods derive depending on how the pressure-wave is generated. Two well known ways to generate the pressure-wave are the laser-induced-pressure-pulse (LIPP) and the pulse-electro-acoustic (PEA). In order to observe space charge in this study the TSC and PEA techniques are employed and the basic principles of their implementation follow.

1.7.1 Pulse-Electro-Acoustic (PEA) technique

Measurements to observe space charge in solid dielectrics have been routinely made by researchers around the world since the development of the pulse-electro-acoustic technique (known as PEA these days) as it is a non-destructive method. The PEA method relies on the disturbance of the equilibrium between the electrostatic and elastic forces of the material under study. The disturbance of the equilibrium is achieved by the application of rapid high voltage pulses causing the elastic forces to react which in turn generate elastic waves, i.e. acoustic waves. By placing a piezoelectric transducer adjacent to the sample these acoustic waves can be converted into an electrical signal which can easily be observed with an oscilloscope. The time dependence of this signal is directly related to the distribution of space charge in the sample as is shown in Figure 1.7.1. This signal contains information on the position, and the net charge density as well as the polarity of the charges in the sample.

The protocols that were followed to conduct the space charge measurements via PEA as well as the information that can be extracted from such measurements are described in the following experimental chapters.

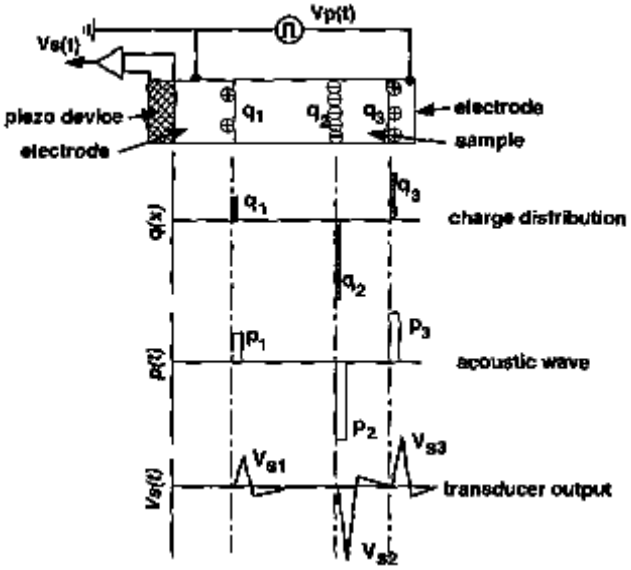

Figure 1.7.1: Schematic diagram of a PEA system. Taken from Fu M. & Chen G. (2003).

1.7.2 Thermally-Stimulated-Current (TSC) technique

The TSC technique relies on the thermal excitation of charges via temperature ramps to release charges from traps giving a current in the external circuit. The release of the charges is correlated with the de-trapping rate and hence with the trap depths of the material under study (Mizutani T. et al, 1977, 1980 and 1982). A general experimental procedure of TSC measurements involves the following steps (Suh K. S. et al, 1992):

1. Application of a dc voltage, V_p, at a poling temperature, T_p, during a poling time, t_p;
2. Cooling under this voltage to a lower temperature, T_{min};
3. Holding the sample at T_{min} for some time to eliminate current spikes from transients;
4. Changing the voltage at T_{min} to another voltage, V_d, such as zero;
5. Measurement of the current produced by relaxation of charges in the sample as a function of temperature which is programmed to rise linearly in time.

In the first step the dielectric is charged, then in the second the charges are frozen to prevent relaxation and in the last step, the charged dielectric relaxes as the temperature increases. The protocols that were followed to conduct such measurements as well as

the information that can be extracted are described in the following experimental chapters.

1.8 THESIS OVERVIEW

The chapters that follow include three experimental chapters, a discussion chapter and a chapter with conclusions and future work. The three experimental chapters carry forward the work that was undertaken during the Artemis programme. Thus in the first of the three the Artemis peelings are characterized via space charge measurements and the information that can be extracted from these measurements is reported. Therefore, the effect of electro-thermal stressing that the peelings experienced as a cable has on the space charge behaviour is investigated before any further stressing is applied. In the next chapter reports the results of electro-thermal endurance tests on ARTEMIS peelings at three different conditions; high temperature and high electric field, low temperature and high electric field and high temperature and a lower electric field. The aim of this investigation was to check whether the inherent electro-thermal pre-stressing of the peelings had an effect on the endurance capability of the material. In the last experimental chapter the peelings that participated in the endurance test reported in the previous chapter are characterized via space charge measurements and their space charge behaviour is compared with those obtained before any further electro-thermal endurance stressing. The discussion chapter brings the outcomes of the three experimental chapters together and highlights physical features in terms of possible ac-ageing mechanisms and the effect that different types of stressing have on the endurance capability and space charge behaviour of the material under study. The conclusions and future directions of this work follow after the discussion chapter.

2 CHAPTER: SPACE CHARGE CHARACTERISATION OF ARTEMIS XLPE PEELINGS

2.1 INTRODUCTION

The aim of this chapter is to characterise via space charge measurements the insulation peelings that were electrically, thermally, electro-thermally and serviced stressed as a cable during the Artemis programme. The investigation is carried out by two very well known techniques, the pulse-electro-acoustic (PEA) and the thermally-stimulated-current (TSC) (Y. Tanaka et al, 1998), for more information on the description of these techniques, see chapter 1. The results allow the behaviour of space charge in each material to be measured and compared.

2.1.1 The Artemis Programme

Cross- linked- polyethylene (XLPE) from a single supplier was used by two different companies to manufacture 90kV cables to the same Medium Voltage (MV)-design. The XLPE insulated cable was then stressed under various electro-thermal conditions during an EU-sponsored programme called ARTEMIS (Fothergill et al, 2003), see chapter 1. Sections from the cable were placed under electrical, thermal, and electro-thermal stress for varying lengths of time (up to about two years), after which their insulation was peeled and the peeling subjected to a number of diagnostic measurements designed to characterise the state of the insulating material in comparison to its state in an unstressed (i.e. unaged) cable. The peelings have a thickness of 150μm and they possess all the characteristics that the insulation of the MV-design cable does. This means that all the defects if any, that were introduced during the manufacturing process, i.e. the extrusion of the cables, are also present in the peelings. An analysis of the results did not show an unambiguous trend in the properties that were examined. The Artemis project demonstrated a very low rate of degradation of the cable materials in spite of the use of very high electric stress levels at elevated temperatures as demonstrated in the report by Borealis (2003) and Fothergill et al (2003). Nevertheless, it did provide a definite indication of the measurements that should be used to evaluate the state of the insulation, one of which is the space charge behaviour. In this chapter the results of PEA and TSC measurements are reported and assessed for a range of peelings with different pre-histories.

2.1.2 Space charge dynamics of polyethylene

This section will summarise the behaviour of space charge in XLPE with different electrode interfaces. The differences between space charge profiles from plaque, mini cables and MV-design cables such as the ones used in ARTEMIS will be discussed. These differences could be due to the cross-linking process, manufacturing process, by-products and concentration of volatiles, (Henryk et al, 2005). The Artemis peelings were conditioned at 50^{o}C for 48 hours so as to remove as much of the volatiles as possible.

In the past two decades, a great number of studies have been carried out on the space charge behaviour in polymeric insulation materials and more specifically XLPE in order to gain a better understanding of space charge dynamics and its effect on material selection and processing (see Dissado & Fothergill, 1992). These studies involved extensive investigations of space charge accumulation and transport mechanism in the dielectrics by Dissado et al, (1999a, 1999b and 2006), Mazzanti et al, (2003b), A. See et al, (2001) and also the influence that the electrode interfaces have on its dynamics in low density polyethylene, LDPE, by G. Chen et al (2001 and 2004) and XLPE by Bambery & Fleming (1998), Y.L. Chong et al (2007), Fleming (2000) and Y. F. F. Ho (2003). It is shown by G. Chen et al (2001) that the material of the electrodes plays a key role in charge injection and extraction processes and consequently amount of charge available for trapping in the bulk. The rate of injection/extraction as well as the type of the charge that is injected or extracted depends on the dielectric-electrode interfaces. For instance, carbon loaded electrodes (hereafter called semicon) injected more electrons and holes into LDPE than metal electrodes. Furthermore, there is a difference in charge injection/extraction rate between the different types of metal or semicons, e.g. aluminium electrodes have a higher injection rate of charges than gold ones (G. Chen et al, 2001). Thus, in a comparative study of space charge behaviour it is essential to ensure that the electrode/polymer interfaces remain the same throughout the experimental work.

The electrode/polymer interface is one factor that influences the space charge behaviour. Another one is the concentration of additives, cross-linking by-products and oxidation products in low density polyethylene and XLPE. It has been shown that the

introduction of cross-linking agents, such as the most commonly used dicumyl peroxide (DCP), enhances a number of mechanical properties such as the deformation resistance at higher temperatures, tensile strength and creep properties (Smedberg et al, 2004). On the other hand the effect of the additives and cross-linking agents on the electrical properties of the material is still under investigation. Nevertheless, it was found that in LDPE the addition of anti-oxidant agent induces deep trap sites in the system (Y. Tanaka et al, 2003) and the addition of cross-linking by-products can affect both the distribution and the density of deep and shallow traps (Montanari et al, 2004). Although it is not clear whether the above agents improve the electrical properties of polyethylene or not they definitely change its space charge dynamics. Further attention has also been given to how the by-products, such as acetophenone, α-methylstyrene and cumyl alcohol, influence the space charge distribution and trapping process in LDPE and XLPE by N. Hirai et al (2003) and Y. Maeno et al (2005) respectively. It was found that the by-products give rise to trapped charges, and that their polarity and the magnitude of the charge density depends on the type of the by-product. The space charge density can be reduced significantly if a treatment is applied to extract or at least reduce the concentration of by-products. A common treatment for XLPE is to remove volatile by-products by subjecting the material to an elevated temperature and under vacuum condition if necessary. It was found out that the space charge distribution is highly dependent on the degassing temperature duration that the insulation is subjected to (Y.L. Chong et al, 2005).

Most of these studies have been focused on plaque samples as it is easier to perform space charge measurements by PEA and TSC techniques, so cable geometries have received very little attention. The exact manufacturing process of High Voltage cables is also not always known, which means that the cross-linking agents are confidential.

2.1.3 Space Charge outcomes of the ARTEMIS programme

The pulse-electro-acoustic (**PEA**) apparatus for space charge measurements can perform space charge measurements on them with and without an electric field applied to the specimen, so that it is particularly appropriate for investigation of electrical properties such as charge injection and transport (Y. Tanaka et al, 1998). Space charge accumulation is the fundamental mechanism behind the ageing model proposed in the report by Borealis (2003) and Fothergill et al (2003) first described by Dissado et al

(2001). Thus, very extensive space charge measurements were performed using several different complementary techniques. The pulsed electro-acoustic measurements on the 150 μm tapes showed that the space charge amount accumulated at steady-state tended to increase with ageing time and electro-thermal stress as was found by Mazzanti & Montanari (2003a), Mazzanti et al (2003b) and Montanari (2000). In particular, the measured voltage threshold for space charge accumulation displayed a reduction with increased voltage stress during the cable pre-history. Measurements on complete cable samples with the thermal step method (TSM) detected a significant increase in space charge accumulation as a function of ageing voltage and, to a lesser degree, stressing time (Fothergill et al, 2003).

Artemis identified possible indicators that can be measured with the PEA and could be used as ageing markers. These are as described by Fothergill et al (2003):

- The mean stored charge density (preferably measured at a given polarization time) can be plotted as a function of poling fields and an estimate can be made of the dc charge threshold, i.e. the level of electrical field above which space charge begins to accumulate significantly. This threshold was suggested to be an ageing marker by Mazzanti and Montanari, (2003a), Montanari (2000) and Montanari et al (1999).
- The trap-controlled mobility can also be derived using the depolarisation characteristic and should decrease with time as the charges are emptied from even deeper trap sites Mazzanti et al (2003b) and Montanari et al (2001).
    - Hence, the rate of change of mobility with time at a specific depolarization could be used as an ageing marker.

Table 2.1.1 shows the ranking of a laboratory stressed peeling (that did not experience either thermal or electrical stress as a cable) according to the dc threshold estimation for a number of specimens (cable peelings) that experienced different electro-thermal stressing during the Artemis programme. The threshold value becomes lower and lower as the stressing time and field increases. However, stressing at a lower field for a long time may produce less modification than stressing at a higher field for a short time. Differences can also be observed between specimens stressed at the same field for almost the same duration, but at two different temperatures 20 and 90^{o}C. At the higher temperature of electro-thermal stress, the threshold level is lower than for just electrical

or thermal stress on their own. The dc threshold value seems sensitive to stressing, i.e. decreases as stressing increases.

Specimen rank	Field (kV/mm)	Temperature (^{o}C)	Stress time (hours)	DC Threshold (kV/mm)
0	0	20	0	20
1	0	130	300	9
2	50	20	65	8
3	45	20	3410	7
4	60	20	325	6
5	70	20	56.6	4
5	50	90	60	4
6	60	20	1935	3
7	70	90	34.8	2

Table 2.1.1: Data extracted from Artemis reports (Borealis, 2003) and publications (Mazzanti et al, 2003b) on dc threshold estimation.

The behaviour of charge packets in unstressed and stressed specimens under high fields was also investigated by Carmo Lança et al (2007). At high local fields (150kV/mm) charge packets cross the specimen thickness and the apparent speed of the packets seems to be sensitive to prior stressing, both duration and type of stress. Specimens weakly stressed or experiencing only thermal stressing have large charge packets which are slower than those detected in the unstressed specimen. Most of the specimens that were electro-thermally stressed showed faster and smaller charge packets than those found in the unstressed ones during the ARTEMIS programme by Montanari and his group as reported by Borealis (2003).

The depolarisation characteristic was also examined and showed a slower rate of charge depletion for specimens from stressed cables with respect to those from unstressed cables. The decline of the charge mobility during long times of depolarization was found to be greater in the electro-thermally or thermally stressed specimens in comparison with the electrically stressed and unstressed cables (Mazzanti et al, 2003a).

2.2 CHARACTERISATION MEASUREMENTS UTILISED

These measurements are the ones used here to identify quantities that have been altered during stressing. All samples were thermally treated to remove volatiles before measurement and ensure reproducible measurements appropriate to just the state of the polymer. Measurements of the concentration of cross-linking by-products that were made during the Artemis programme by FTIR and HPLC (High Precision Liquid Chromatography) revealed that after 24 hours of thermal treatment at 50^{o}C they were below the detection limit of these techniques as shown in Table 2.2.1. Hence, the materials used in this study were conditioned at this temperature and above for more than 24 hours to minimise the concentration of volatiles. Both the Pulsed-Electro-Acoustic (PEA) and Thermally-Stimulated-Current (TSC) techniques were used. This allowed us to obtain information both on the ability of the polymer to transport and accumulate charge, and the trap depth distribution and relaxation barriers in the various XLPE samples. The combination of both techniques gives a more detailed picture of the state of the XLPE specimens than each technique on its own.

Substance	0 hours	5 hours	24 hours
Cumyl alcohol	13350	2420	0
Acetophenone	3700	88	0
α-methylstyrene	116	0	0
Cumene	0	0	0

Table 2.2.1 (Taken form Fothergill et al, 2003): Concentration (in ppm) of cross-linking by-products as a function of treatment time (50^{o}C, ambient pressure) by HPLC and confirmed by FTIR.

The experiments reported relate to the trapping and release of space charge under a specified protocol, with measurements being made via the PEA (Y. Tanaka et al, 1998) and TSC (T. Mizutani et al, 1977) techniques. These two techniques are carried out at different DC applied voltage/field levels, and are used in a complementary way, with PEA measurements used to characterise the accumulated space charge distribution and its manner of decay upon removal of the voltage, and the TSC measurements being used to gain a clearer idea as to the energy distribution of the trapped charge (T. Mizutani et al, 1982).

2.2.1 Experimental set up and protocols

(a) PEA

In the PEA measurements, the HV electrode side consists of semicon material whereas the ground electrode is aluminium. A drop of silicone oil at the electrode/samples interfaces ensured good acoustic propagation. Four DC poling voltages of 5, 6, 7 and 7.5 kV were applied to the specimens for 120 min unless specified otherwise.

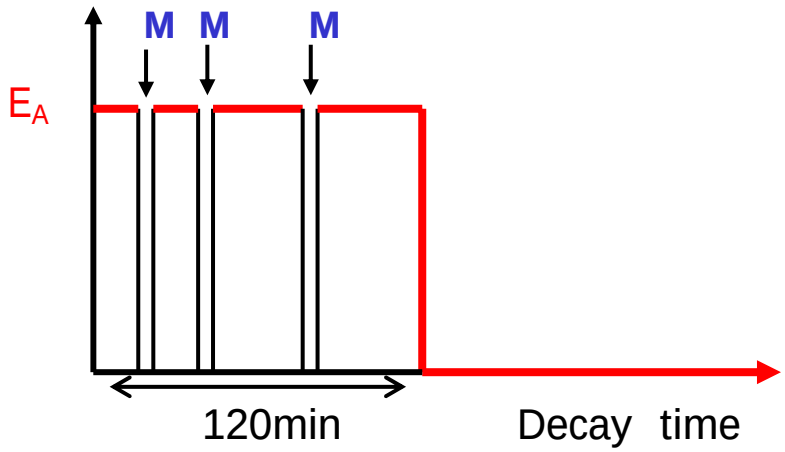

Figure 2.2.1: PEA protocol where E_A is the applied electric field and M the measurement intervals.

During the poling period the voltage was removed for a short time to enable a measurement to be made, and then the voltage was re-applied. The results therefore yield the space charge and corresponding image charges on the electrodes without an overlay of capacitive charge on the electrodes. The space charge decay was also measured at appropriate time intervals during 120 minutes or more of depolarization following removal of the applied voltage. The space charge profile was similar for all voltages, with only a small increase in the magnitude of the space charge density as the voltage increased. Therefore, the measurements taken under the higher voltages of 6, 7 and 7.5kV are presented in this study as changes due to ageing are more likely to be observable at higher fields.

(b) TSC protocol

The TSC measurements were taken by poling the samples at an electric field $\mathbf{E_p}$ and a poling temperature $\mathbf{T_p}$ which was kept constant at 90°C for a given duration $\mathbf{t_p}$. Once the poling duration is reached the sample is rapidly cooled down with liquid Nitrogen till the required minimum temperature $\mathbf{T_{min}}$ while the poling voltage is still applied. Then the poling field is removed and the only electric field remaining is due to space charge, $\mathbf{E_{SC}}$, which thereafter governs the movement of trapped charges and current magnitude.

The TSC currents are measured using a Keithley-167 pico-Ammeter while the temperature is increased at a constant rate β till $\mathbf{T_{max}}$ is reached using a Eurotherm temperature controller. A schematic diagram of the above procedure is shown in Figure 2.2.2. The poling electric-field and temperature were varied in order to investigate the effect that the charge that is injected has on the magnitude and temperature at which the current peaks occur. The rate β at which the temperature was increased was also varied in order to be able to estimate the activation energies or trap depths at a given temperature where a current peak occurs.

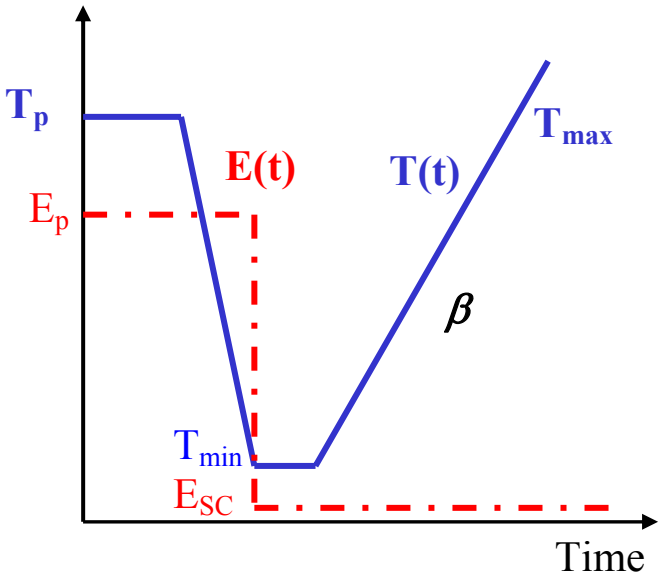

Figure 2.2.2: Thermally-Stimulated-Current protocol.

(c) Materials used

The material's stressing pre-histories as cables which are used to characterise their space charge behaviour, are presented in Table 2.2.2. It should be noted that two different conditioning processes were used to remove volatile cross-linking by-products after the cables were peeled and they are listed below:

- during the first type of conditioning, the specimens were thermally treated at 80^{o}C in vacuum for 48 hours: -**Type A**
- during the second type of conditioning, the specimens were thermally treated at 50^{o}C in ambient atmospheric pressure for 48 hours: -**Type B**

Thus, the space charge behaviour of the samples that experienced the same conditioning process will be compared together, in order to avoid changes in the space charge behaviour due to different by-product concentrations. In Table 2.2.2 the conditioning type of each material is specified. It should also be noted that in the case where both of

the types of conditioning are specified, it means that some specimens of this material conditioned at one type and some other specimens at the other type were used. The small case letter in the reference name indicates the manufacturer. It should not be forgotten that although the cables were made from exactly the same batch of XLPE, the cables were manufactured by two different companies, where different cross-linking methods were used and also different duration under thermal conditioning as a cable was used to remove methane gas from the peroxide decomposition. In one case the duration was 79 hours and the other case was 96 hours both at a temperature of 70^{o}C.

No	Ref. name	REF. CODE	Conditioning type	E. stress AC (kV/mm)	Temp. (^{o}C)	Time (h)
1.	US_p	P11	B	-	23	-
2.	US_a	E22	A, B	-	23	-
3.	E_S1p	P20U6	B	19.5	20	5000
4.	E_S2p	PTHT 6/2 No11	B	19.5	20	7747
5.	E_S1a	ATHT 4/2 No3	B	19.5	20	5581
6.	_TS1p	PVT11	B	0	90	5000
7.	_TS1a	AVT12	A	0	90	5000
8.	_TS2p	P90T3	B	0	90	10000
9.	ETS1p	P90TU11	A, B	19.5	90	5000
10.	ETS2p	PSM9	B	28	90	6000
11.	SA	ABBV1	A	SERVICE	SERVICE	>18 YEARS

Table 2.2.2: ARTEMIS pre-history of peelings used to measure the space charge. The indices 'a' and 'p' refer to the two different cable manufactures. The rest of the reference name of the materials under study is constructed according to acronyms of the stress that they experienced as a cable, i.e. US stands for Un-Stressed, ETS for Electro-Thermally-Stressed and so on.

2.3 RESULT OF PEA AND TSC MEASUREMENTS

Before describing the experimental results obtained by the two techniques, it should be noted that each of the PEA and TSC measurements were conducted on a different specimen in order to avoid introducing changes into the space charge profile of the material due to a former experimental procedure unless stated otherwise.

2.3.1 De-trapping Analysis of Depolarisation

Figure 2.3.1 shows how from the space charge versus log-time plot the minimum, Δ_{min}, and maximum, Δ_{max}, trap depths in a polymeric insulation could be estimated according to a model proposed by Dissado et al (1999 and 2006). This model proposes that

logarithm of the time at the start, $\mathbf{t_1}$, and end, $\mathbf{t_2}$, of a linear region of sigmoidal shape decay at a given temperature is proportional to the depth of the trap from which the charge is de-trapped, as is shown in Figure 2.3.1. Hence, at a given decay time, $t \geq t_1$, and temperature the depth of the trap from which the space charge escaped from can be determined.

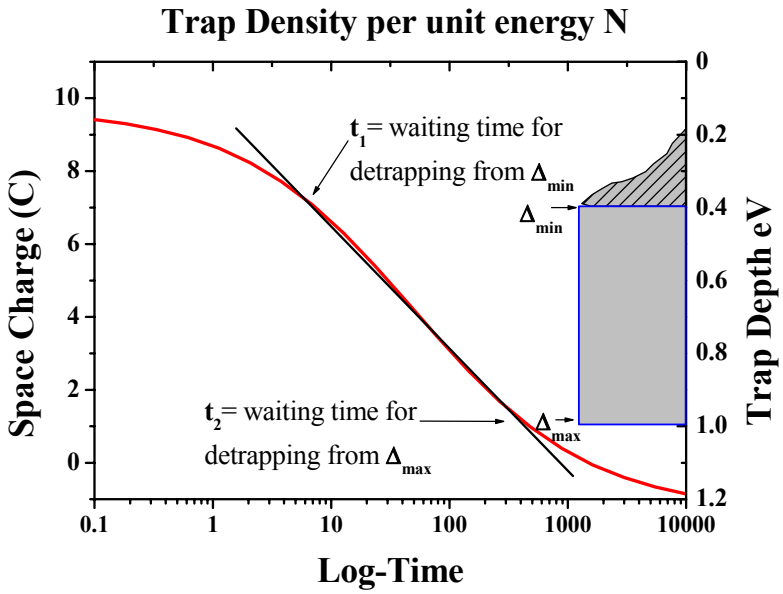

Figure 2.3.1: Theoretical model visualization proposed by Dissado et al (2006) to estimate trap depth range in insulators by the space charge decay plot.

Space charge decay during the depolarisation period has been analysed using the de-trapping model (Dissado et al, 2006) so as to deduce information on the trap depth distribution and rate of decay. The space charge at time **t** (either during voltage application or during subsequent depolarisation) is estimated via the absolute charge stored, **Q(t)**, in the sample calculated with Equation (1).

$$Q(t) = A\int_{x_1}^{x_o} |\rho(x,t)|dx \qquad \text{Equation (1)}$$

Here ***A*** is the surface area of the HV electrode, ***ρ(x,t)*** is the space charge density, and ***t*** is the time at which the measurement is carried out. The integral is taken between positions $\boldsymbol{x_0}$ and $\boldsymbol{x_1}$ and includes the image charges on the electrodes as it is difficult to estimate exactly where the electrode charge ends and the space charge begins. The actual space charge is taken to be half the amount deduced from Equation (1). The space charge decay behaviour, after voltage removal, is characterised by a plot of ***Q(t)*** vs ***log (t)*** (t = decay time). As long as the space charge profile retains its shape during

the decay, which is essentially the case here, the decay of the absolute charge ***Q(t)*** can be related to the charge de-trapping as shown by Mazzanti et al (2003b) and Dissado et al (1999). It was shown by Dissado et al (2006) that if it can be assumed that charges are trapped in states whose density has a top-hat energy distribution, the decay follows the form

$$Q(t) \approx eNkT(C - \ln(t)) \qquad \text{Equation (2)}$$

over the decay time range, t, defined by the equation below:

$$\exp\left(\frac{\Delta_{\min}}{kT}\right) < \nu t < \exp\left(\frac{\Delta_{\max}}{kT}\right) \qquad \text{Equation (3)}$$

Here ***N*** is the density of states per unit energy interval. Δ_{min} and Δ_{max} are the depths of the minimum-filled and maximum trap depths respectively. These can be obtained from the times at which the plot deviates from a straight line, as long as, **ν**, the de-trapping attempt frequency can be estimated. We have taken $\nu = kT/h$ for our estimation as this frequency relates to incoherent thermal vibrations of the trap site.

2.3.2 Estimation of activation energies using the TSC current peaks

The ramp rate of the TSC experiments was varied between 2-4^{o}C/min as the activation energies at the current peaks could be estimated according to a method proposed by Booth (cited in T. Mizutani et al, 1982), where the trapping level or activation energy *E* is defined as:

$$E_B = \frac{kT_1T_2}{T_1 - T_2} \ln\left\{\frac{\beta_1 T_2^2}{\beta_2 T_1^2}\right\} \qquad \text{Equation (4)}$$

where k is Boltzmann's constant in 8.617x10^{-5}eVK^{-1}, β_1 and β_2 are the two temperature ramp rates and T_1 and T_2 the corresponding temperatures at which current peaks occur.

The activation energy could also be estimated at a single ramp rate or even an unknown one from Grossweiner's equation (cited in Antonijevic, 2005), which is used to characterise first order kinetic processes and in theory could be applied to dipolar data. The activation energy in this case is defined as:

$$E_G = 1.51\frac{kT_1T_{\max}}{T_{\max} - T_1} \qquad \text{Equation (5)}$$

where T_{max} is the temperature the current peak occurs and T_1 is the temperature of the half-peak on the increasing part.

The above equations are used in the results section to estimate the activation energies and compare them with the ones obtained using the depolarisation characteristics.

2.3.3 Thermal conditioning type A

(a) Space Charge under Polarization

In the unstressed sample, **US_a**, Figure 2.3.2, a negative and positive space charge is near the electrodes. Over time the negative space charge region penetrates deeper into the insulation.

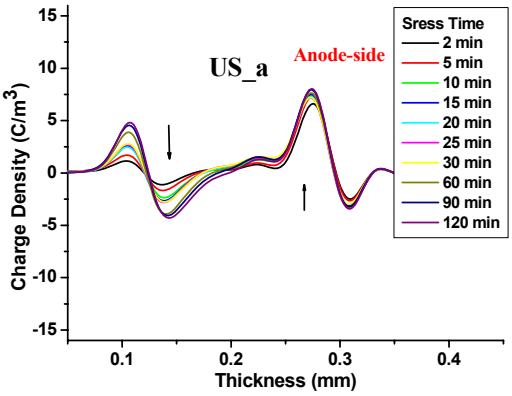

Figure 2.3.2: Space charge in the US_a sample during voltage stress at 6kV.

Figure 2.3.3 to Figure 2.3.7 show the space charge accumulation during 120mins of polarisation under two voltage stresses of 6 and 7 kV, for all three materials (i.e. with unstressed, thermally stressed and electro-thermally stressed pre-histories). The space charge behaviour of the thermally stressed sample, **_TS1a** shown in Figure 2.3.3, is almost identical to that of the unstressed sample, but here the transport of the negative carriers across the sample is even slower. The space charge behaviour at both voltages, 6 and 7 kV, is very similar with negative charge migrating closer to the anode when 7 kV was applied as shown in Figure 2.3.3b.

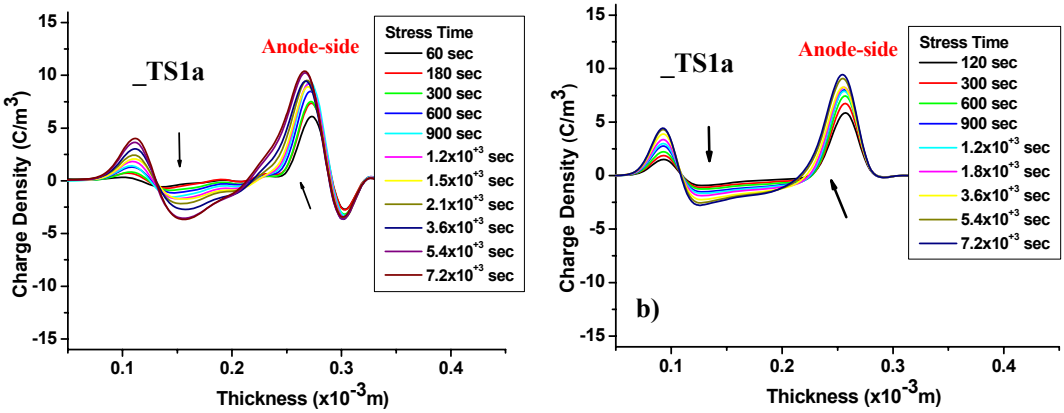

Figure 2.3.3: Space charge in the _TS1a samples during voltage stress at a) 6kV and b) 7kV.

Negative space charge dominates in the electro-thermally aged sample, **ETS1p**, but here the charge density under a voltage of 6kV reaches significantly higher values (6 Cm^{-3}), as shown in Figure 2.3.4a, than in the **US_a** (4 Cm^{-3}) and **_TS1a** (3 Cm^{-3}) samples. It should also be noted that after $3.6x10^3$ seconds of stressing, Figure 2.3.4b, the positive charge injected is greater than after the same period of stressing at 6kV, but the negative charge density is similar in both cases, Figure 2.3.4a.

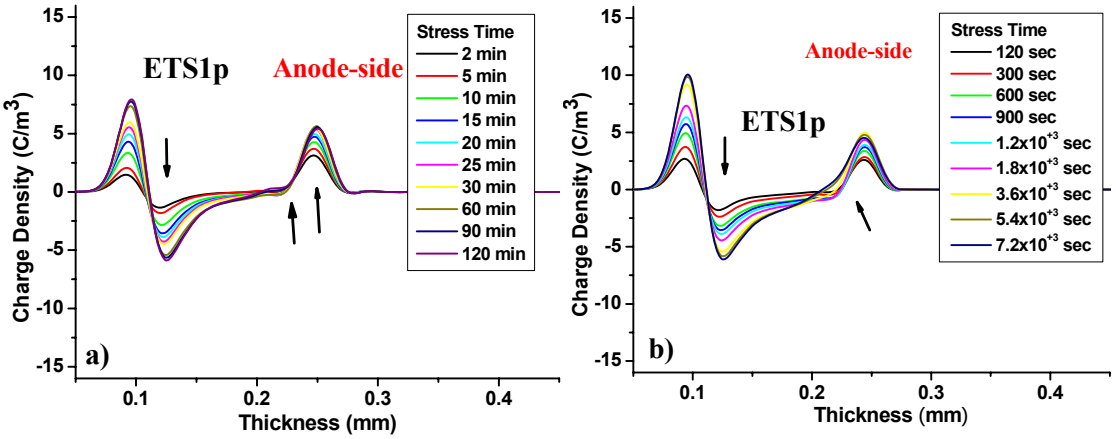

Figure 2.3.4: Space charge in the ETS1p samples during voltage stress a) 6kV and b) 7kV.

In the service-aged sample, **SA**, the space charge behaviour has significant differences to those of the other samples. Although negative space charge is still dominant, it has now accumulated next to the anode with a larger density, especially under 7kV (12 Cm^{-3}) as shown in Figure 2.3.5b.

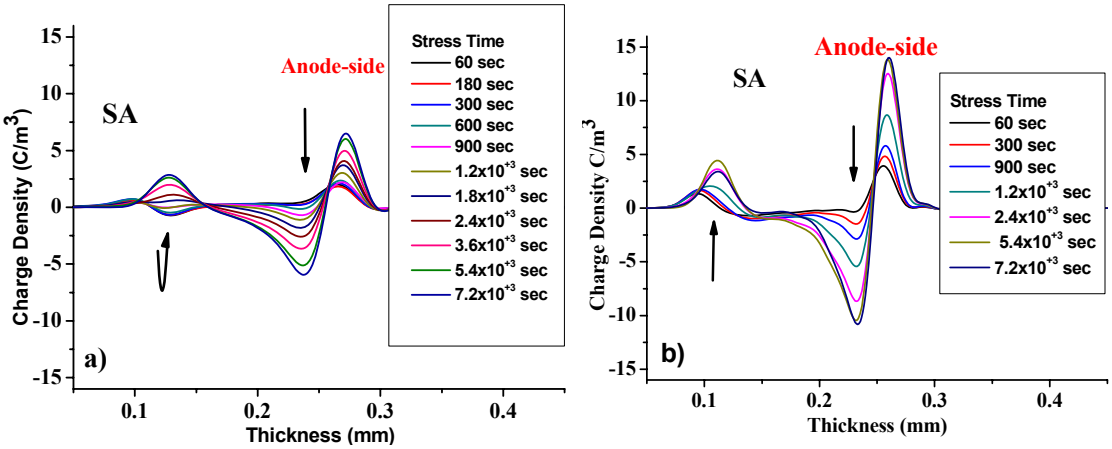

Figure 2.3.5: Space charge in the SA samples during voltage stress at a) 6kV and b) 7kV.

In Figure 2.3.5a, negative charge accumulates near the cathode within the first 60 secs of voltage application at 6kV and then decreases over the next 900secs. Over the same period the negative charge near the anode increases by a large amount. In order to find

out if the space charge profile is a characteristic of the material rather than the specific sample, replicate measurements were made. Figure 2.3.6 shows replicate measurements that were made during space charge accumulation under different voltages, and thus the change in charge density with applied field.

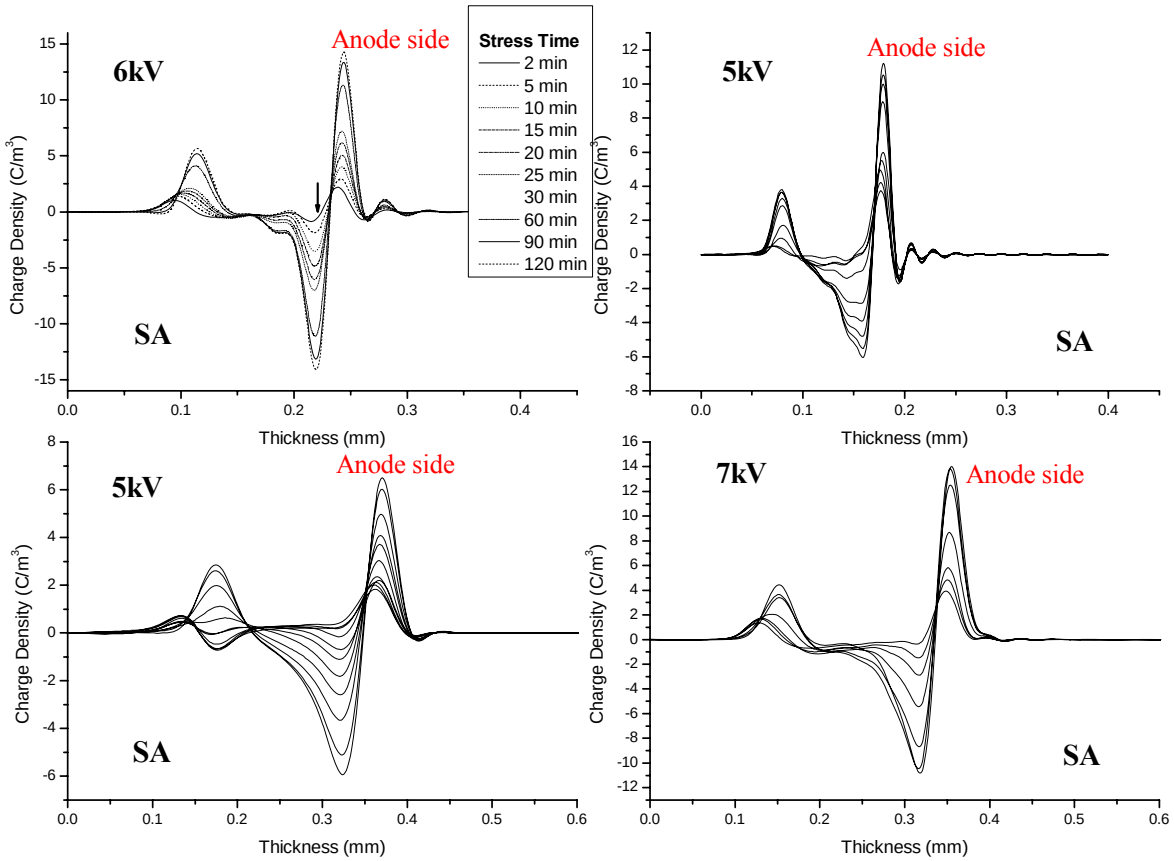

Figure 2.3.6: Replicate space charge profiles for the SA material under different applied voltage stresses, as stated on individual plots.

2.3.4 Thermal conditioning type B

(a) Unstressed materials

In the unstressed material **US_p**, Figure 2.3.7, homocharge accumulation is observed as in **US_a** and the magnitude of the space charge density as well as its behaviour is very similar, see Figure 2.3.2. The main difference that is observed is that the space charge density reaches its maximum value faster in the case of **US_p** than in the **US_a**. The decay of the space charge, Figure 2.3.7b, also occurs faster. Most of the charge has escaped within the first 10mins as is shown in Figure 2.3.7b.

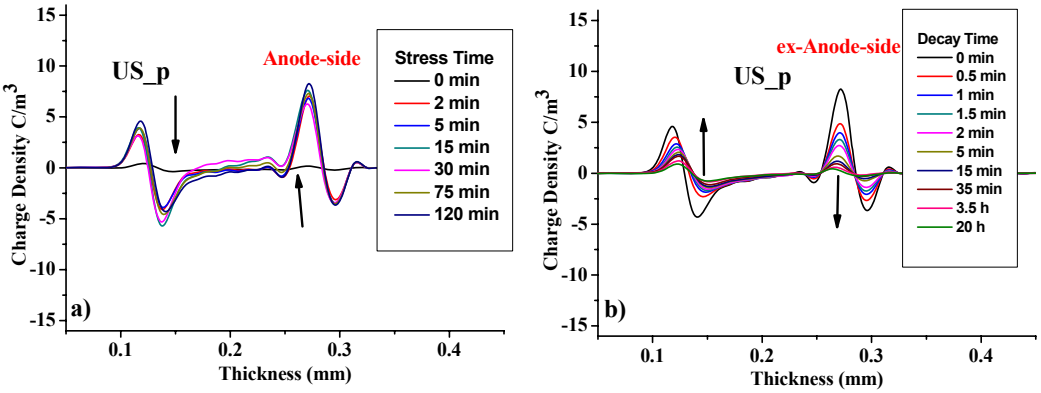

Figure 2.3.7: Space charge in the US_p sample during a) voltage stress at 7.5kV and b) decay.

The unstressed material **US_a** was also given type **B** conditioning. Its space charge behaviour at two different poling times, 120 minutes and 26 hours, is shown in Figure 2.3.8a and Figure 2.3.8b respectively. Again in both cases negative homocharge is observed that slowly penetrates into the material and eventually reaches the anode. The negative space charge increases in magnitude of charge density over time, Figure 2.3.9, and only saturates after 21 hours of poling when a great amount has already migrated, Figure 2.3.8. It should also be noted from Figure 2.3.8c that the negative charge

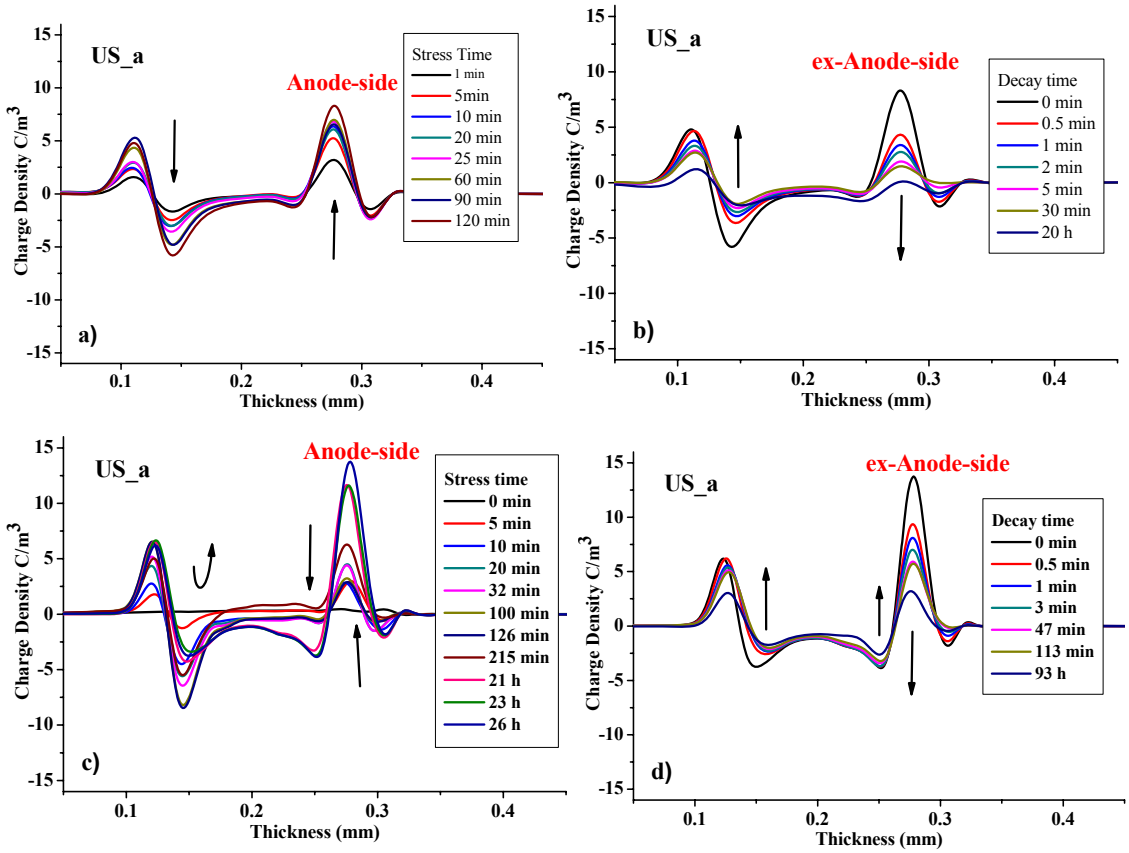

Figure 2.3.8: Space charge in US_a under voltage stress of 7.5kV: a) over 120min c) over 26h and b) and d) their consequent decays.

adjacent to the cathode decreases as it migrates to the anode where its magnitude increases. The build up of negative charge at the anode implies its extraction there is very slow, and thus that the extraction rate governs the establishment of a steady-state distribution after 21 hours. To summarise, Figure 2.3.9 shows that a steady-state amount of negative charge exists after 21 hours and Figure 2.3.8c shows that its distribution is unchanged-i.e. the system is in a steady-state.

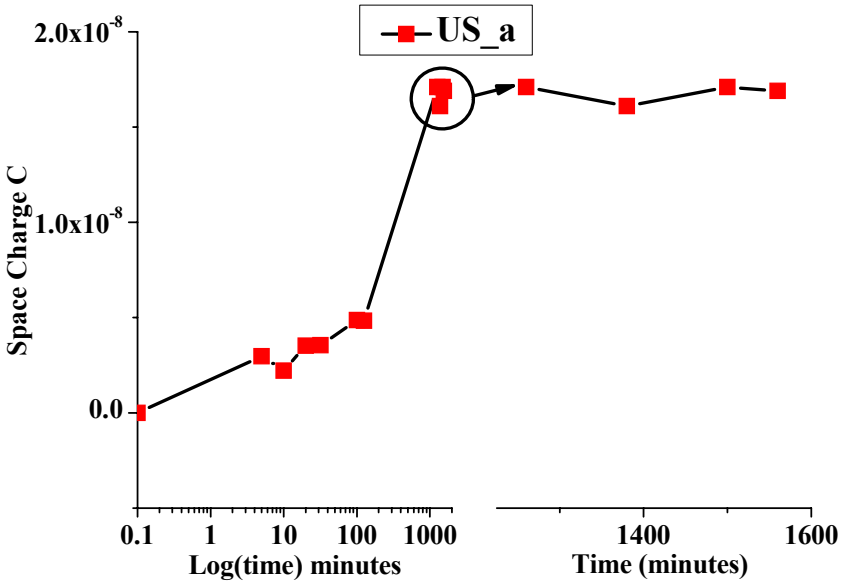

Figure 2.3.9: Total Space charge in US_a calculated using equation (1) over 26 hours of poling after the "zero minute". It should be noted that this figure shows the increase of the space charge only, as the influence of the capacitive charge on the electrodes is removed by subtracting the measurement at "zero minute" from every subsequent measurement.

(b) Electrically stressed materials

Figure 2.3.10 shows the space charge behaviour in a material, **E_S1p** that experienced a mean field of 19.5kV/mm for 5000 hours before it was peeled. During space charge accumulation, Figure 2.3.10a, negative charge which is most probably injected from the cathode reaches a negative peak value of 5 C/m^3 very quickly and then does not change in magnitude. However, negative charge slowly penetrates further into the material till it eventually reaches the anode. The space charge decay plot, Figure 2.3.10b, shows that the negative charge adjacent to the cathode escapes the sample as rapidly as it was formed during accumulation. The negative charge that builds up across the sample does not change significantly during 20 hours of depolarisation.

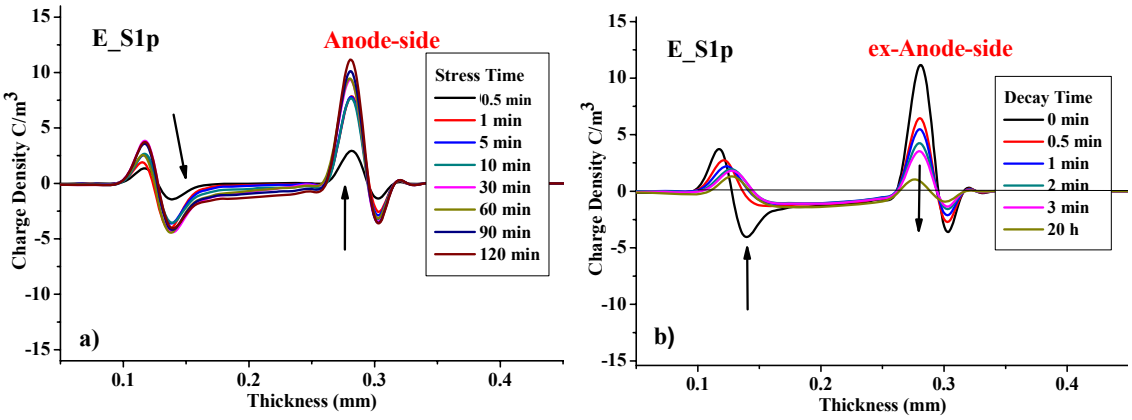

Figure 2.3.10: Space charge in the E_S1p sample during a) voltage stress at 7.5kV and b) decay.

E_S2p (pre-stressing history 19.5kV/mm for 7747h) shows a similar behaviour to that of **E_S1p** under a voltage stress of 6kV as is shown in Figure 2.3.11, but in this case positive charge seems to transport across the sample towards the cathode and decay slower than the anode and cathode peaks (this may also be due to measurement offset).

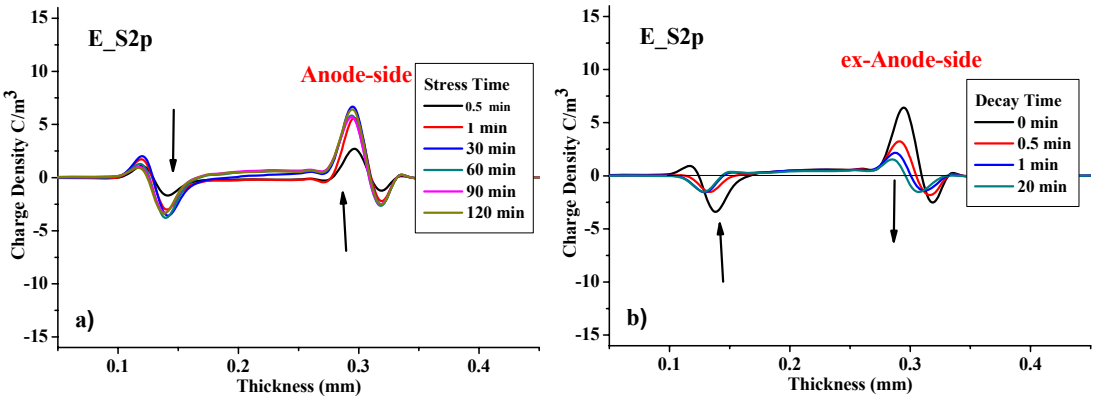

Figure 2.3.11: Space charge in the E_S2p sample during a) voltage stress at 6kV and b) decay.

Figure 2.3.12 shows the space charge dynamics of a material from a different manufacturer in the ARTEMIS programme, **E_S1a,** that experienced 19.5kV/mm for 5581 hours before it was peeled. During the space charge accumulation, negative charge carriers transit from the cathode to the anode where they start to accumulate, as is shown in Figure 2.3.12a. In this material the transit of the negative charge to the anode is noticeable after 30 minutes whereas Figure 2.3.8c shows that it only becomes noticeable in the corresponding unstressed material, **US_a**, at about 215 minutes. The negative charge density begins to decrease thereafter as is demonstrated in Figure 2.3.12 while the negative charge adjacent to the anode increases. Furthermore, during the space charge decay which is shown in Figure 2.3.12b the negative charge which accumulated near the anode decays very slowly in contrast to the negative charge adjacent to the cathode which escapes very fast leaving behind positive charge.

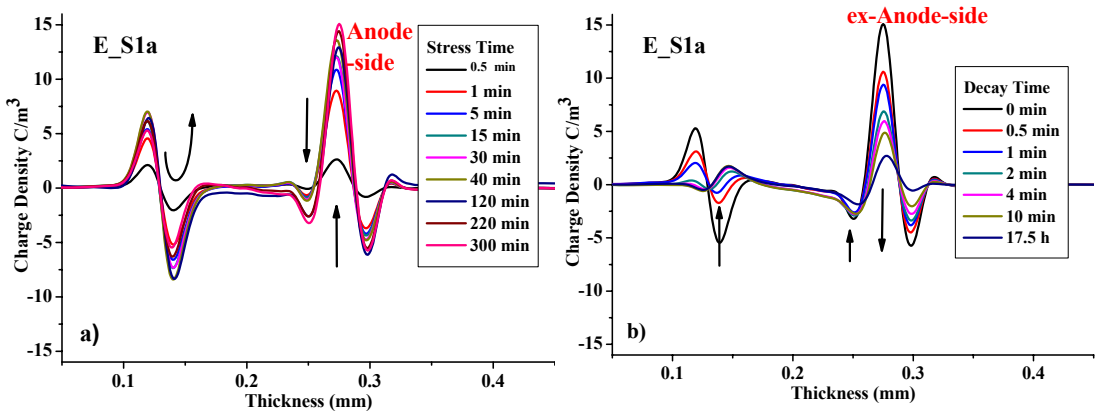

Figure 2.3.12: Space charge in the E_S1a sample during a) voltage stress at 7.5kV and b) decay.

(c) Thermally stressed

Figure 2.3.13a shows the space charge accumulation profile of the **_TS1p** (thermally pre-stressed at 90°C for 5000 hours) under a voltage stress of 6kV. There is a continuous accumulation of negative space charge, but during the first 20 minutes it is located near the cathode, and after that it starts to extend into the bulk of the sample and eventually reaches the anode. During decay, Figure 2.3.13b, the negative charge that has built up across the sample decays slowly as in the **E_S1p** material described above in Figure 2.3.10.

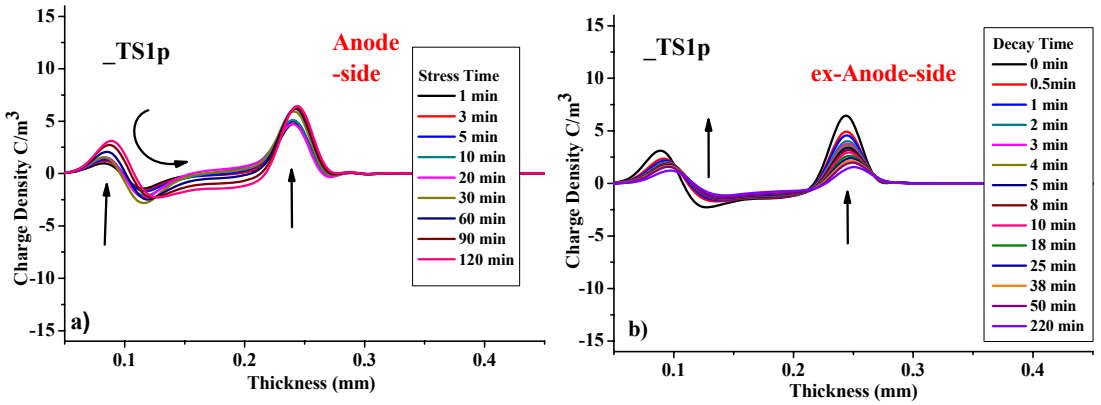

Figure 2.3.13: Space charge in _TS1p under voltage stress of 6kV a) accumulation and b) decay. Note that this measurement had experienced 90 minutes of voltage stress but the test was terminated as there was a voltage offset.

Figure 2.3.14 shows the space charge behaviour during accumulation at 7.5kV and the subsequent decay of a thermally pre-stressed material, **_TS2p**, that experienced 90°C for 10000 hours. The space charge in this material builds rapidly during the 120 minutes of poling and decays rapidly, too. This may suggest that the space charge is trapped in very shallow traps with high density.

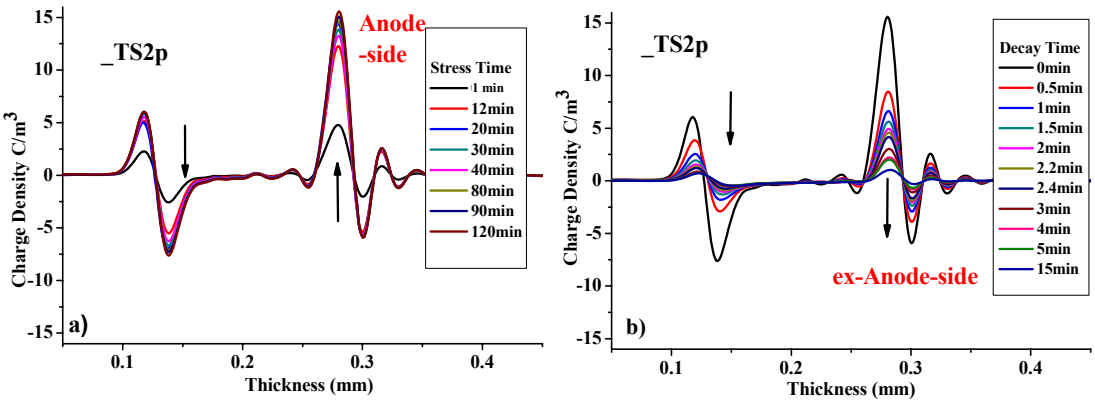

Figure 2.3.14: Space charge in the _TS2p sample during a) voltage stress at 7.5kV and b) decay.

(d) Electro-thermally stressed

The space charge behaviour of the electro-thermally pre-stressed material **ETS2p**, shown in Figure 2.3.15, shows almost no difference to that of the purely thermally stressed sample from the same manufacturer, **_TS2p**, see Figure 2.3.14.

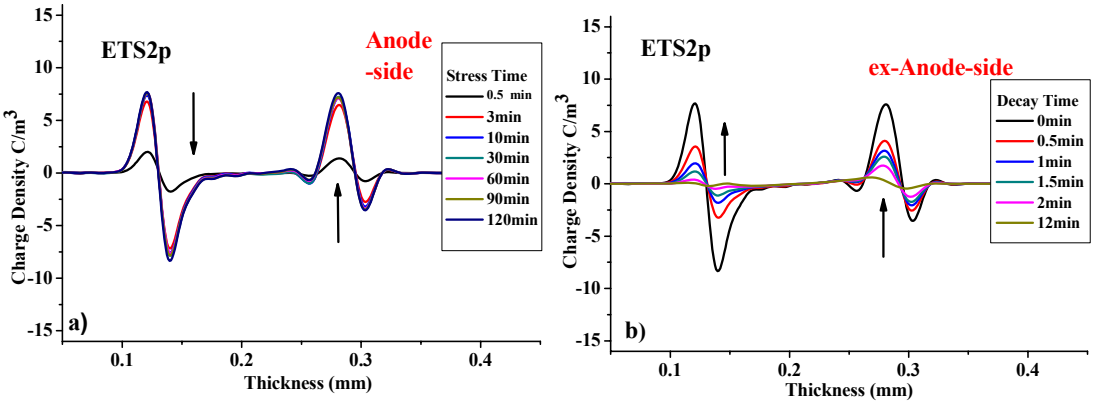

Figure 2.3.15: Space charge in the ETS2p sample during a) voltage stress at 7.5kV and b) decay.

2.3.5 Analysis of space charge measurements obtained by the PEA

(a) Time dependence of anode and cathode charge of type A thermally conditioned materials

Figure 2.3.16 and Figure 2.3.17 show how the charge density changes adjacent to the Anode and Cathode during 120min of dc poling for peelings with different electro-thermal histories. For the unstressed material, **US_a**, the charge density is increasing positively adjacent to the anode as is shown in Figure 2.3.16a. On the other hand the charge density of the service aged, **SA**, material increases negatively down to –15 C/m^3. The thermally and electro-thermally stressed (**ETS1p**) materials behave initially in a similar way to the **SA** material, but after a while the charge density magnitude starts to reduce till it eventually reverses polarity.

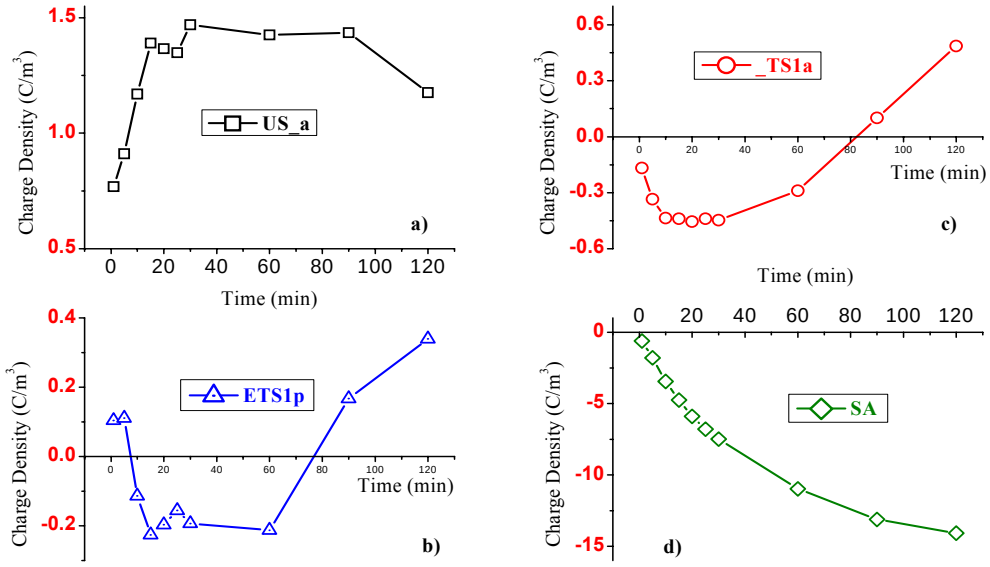

Figure 2.3.16: Change in charge density adjacent to the Anode (0.248mm from an arbitrary origin with respect to space charge diagrams) during space charge accumulation.

The change in charge density near to the cathode, Figure 2.3.17, is very similar in all materials from the ARTEMIS programme and shows a gradual increase in magnitude. In contrast the **SA** material has a very small negative homo-charge in this region that initially increases a little and then eventually decreases to a near constant value as is shown in Figure 2.3.17d.

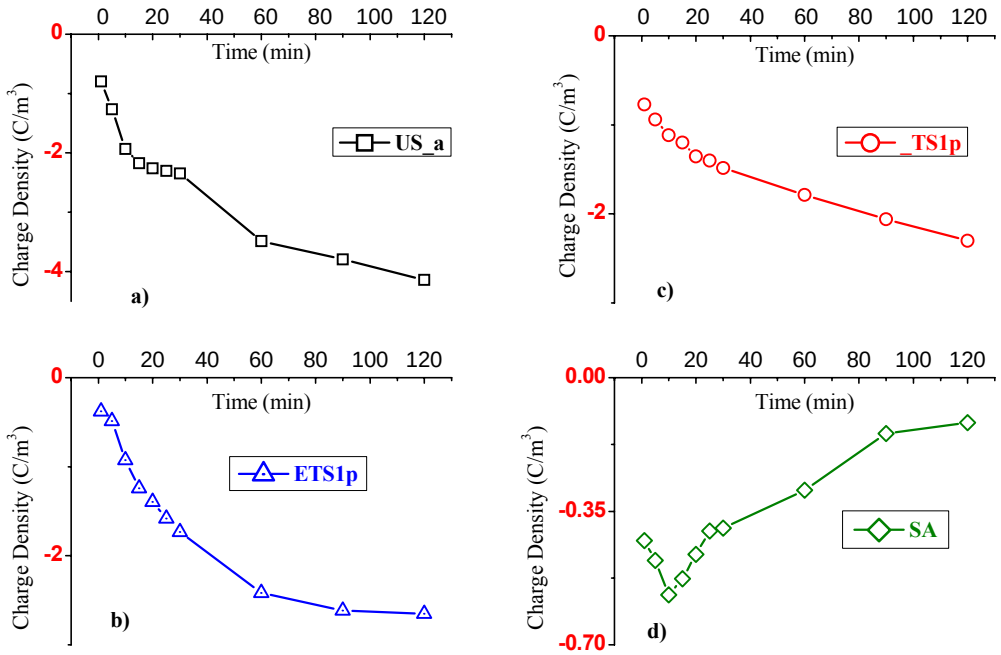

Figure 2.3.17: Change in negative peak charge density adjacent to the Cathode during space charge accumulation.

(b) Time dependence of anode and cathode charge of type B thermally conditioned materials

Unstressed materials

Figure 2.3.18 shows the change of space charge density of **US_p** over time at three points, two of the points are taken to be as near as possible to the peaks near the electrodes and the third one is taken in the middle of the other two, i.e. in the bulk of the material. The distance of these points is measured from an arbitrary origin which is related to the space charge diagrams presented previously. This is also the case for all the following figures. Figure 2.3.18a reveals that in polarisation, as the positive charge density near the anode peak increases the negative charge density near the cathode peak increases and vice versa during depolarisation, Figure 2.3.18b. It can also be observed that some positive charge is crossing the sample causing the positive peak at the anode to decrease, but at the same time the negative peak at the cathode increases. This is not possible unless the rate of negative charge injection from the cathode is greater than the rate of positive charge transport to the cathode region.

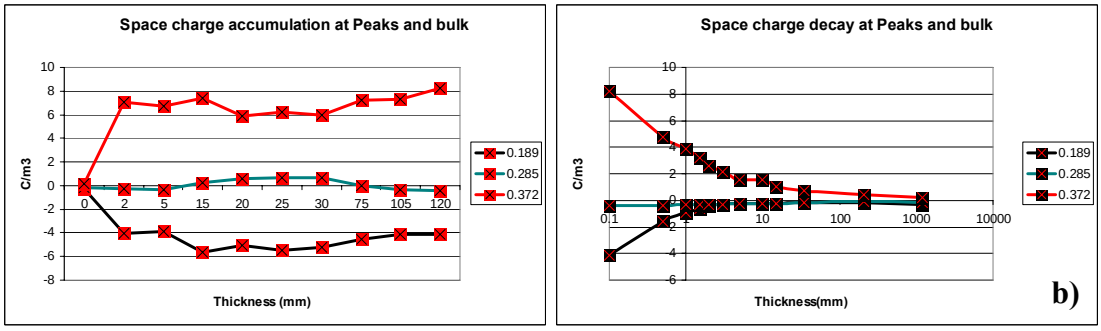

Figure 2.3.18: Change of space charge density at peaks 0.189mm (near cathode) and 0.372mm (near anode) from an arbitrary origin related to the space charge diagrams and bulk 0.285mm during a) accumulation and b) decay of the US_p space charge profile shown in Figure 2.3.7.

Electrically pre-stressed vs unstressed material

Figure 2.3.19 compares the change in charge density at positions adjacent to the electrodes of the electrically pre-stressed material, **E_S1a**, with the unstressed one, **US_a**. They were both poled at the same voltage but experienced different poling times. The **E_S1a** material was poled for 300 minutes and the **US_a** one for 26 hours. This figure shows that negative charge is injected from the cathode during accumulation and as the poling time increases the negative charge migrates adjacent to the anode where it builds up without getting extracted or recombined with possible positive charges that could be injected from the anode. From the decay plots of both materials it seems that

the negative charge adjacent to the anode is less mobile or more difficult to extract than the negative charge adjacent to the cathode, which in the case of the **E_S1a** escape very fast and eventually leaves behind positive charge. In the case of the **US_a** it just reduces very fast. It should be noted that the negative charge transit to the anode occurs a lot faster in the **E_S1a** than in the **US_a** which may indicate that the electrical stress that the **E_S1a** material experienced as a cable has altered its space charge behaviour.

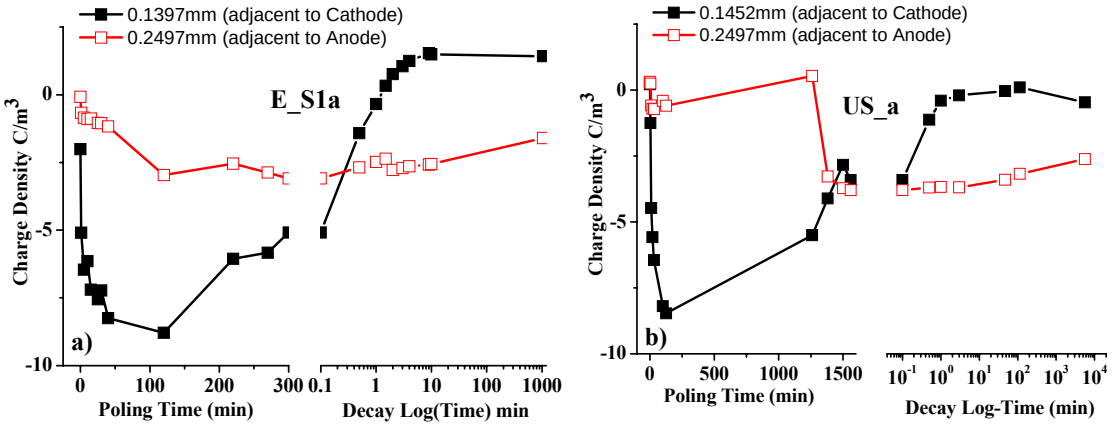

Figure 2.3.19: Change in magnitude of the charge density adjacent to the anode and cathode during accumulation and decay for a) the electrically pre-stressed material poled for 300 minutes, E_S1a, and b) the unstressed material US_a poled for 26 hours.

Comparison of different pre-stressing conditions

Figure 2.3.19 and Figure 2.3.20 show how the charge density changes adjacent to the anode and cathode for peelings with different electro-thermal histories and the type B conditioning. The materials that experienced this type of conditioning and mainly the unstressed and electrically stressed ones show no evidence of positive charge injection adjacent to the anode, Figure 2.3.19, unlike the ones with conditioning type A, Figure 2.3.16. The electrically pre-stressed material, **E_S1a**, in Figure 2.3.19 shows a constant increase of the negative charge density. In the thermally pre-stressed material, **_TS1p**, positive charge is injected within the first 20 minutes till the negative charge that is injected from the cathode transit adjacent to the anode. Thereafter, the charge density increases negatively. It can be observed that the space charge behaviour of **E_S1a** and **_TS1p** materials adjacent to the anode is similar to the serviced aged one, **SA**, shown in Figure 2.3.16, which under service has undergone some electrical and thermal stressing. The electro-thermally pre-stressed material, **ETS1p**, shows some evidence of positive charge injection after the 30th minute and its space charge behaviour is similar to the thermally and electro-thermally materials under conditioning type A in Figure 2.3.16.

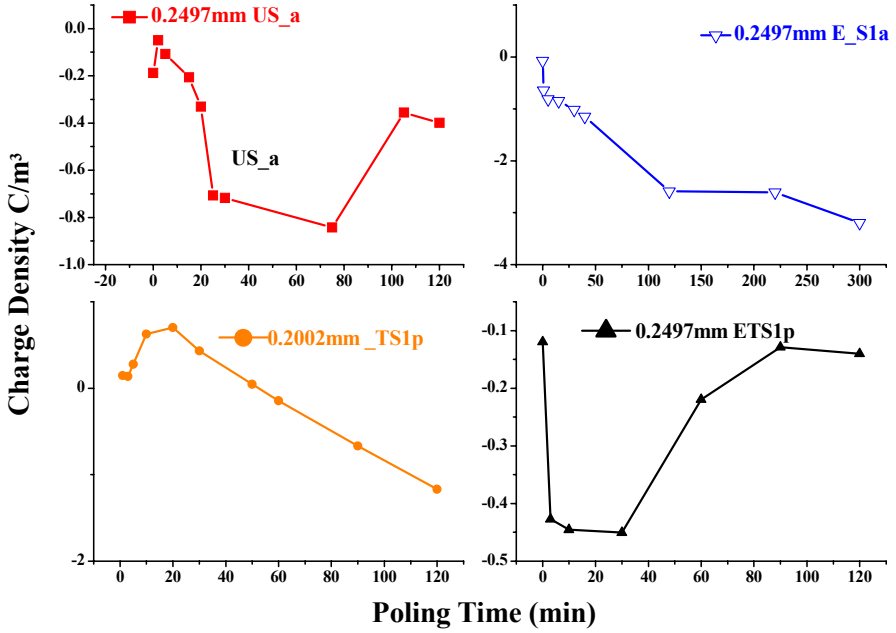

Figure 2.3.20: Change in charge density adjacent to the Anode during space charge accumulation.

Adjacent to the cathode, Figure 2.3.21, the space charge behaviour is dominated in all the materials by negative charge injection from the cathode. The negative charge is increasing the fastest in the electrically pre-stressed material, **E_S1a**, and electro-thermally one, **ETS1p**, reaching greater magnitudes than the other two materials.

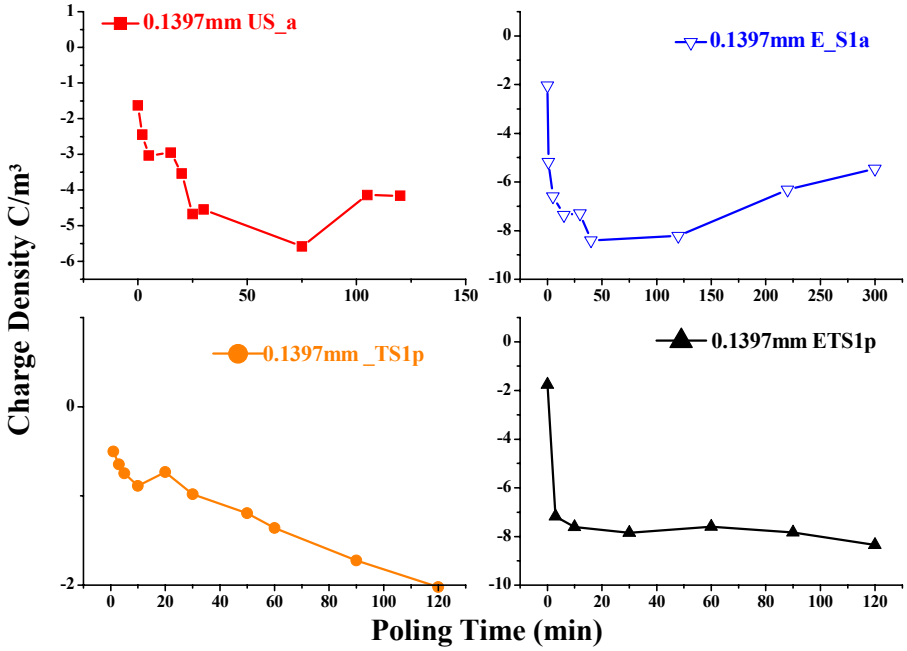

Figure 2.3.21: Change in charge density adjacent to the Cathode during space charge accumulation.

However, the negative charge density of the **E_S1a** material decreases after the 125th minute which also supports the idea of negative charge transit to the anode that is speculated by Tzimas et al (2005) for the service aged, **SA**, material. Hence, the space charge of the **E_S1a** material adjacent to the cathode again behaves similar to the **SA** one. In the **SA** material though, the negative charge density reduces a lot faster than the **E_S1a** suggesting that the negative charge is more mobile in the **SA**.

(c) Depolarization analysis of thermally conditioning type A materials

Figure 2.3.22 shows the decay of **Q(t)** with time once the voltage has been removed after 120 minutes of stressing. It is clear that the **SA** sample has the most space charge initially and that it decays fastest. For both the **US_a** and **_TS1a** samples the charge decay is very slow. In all cases the space charge decay obeys Equation (2) over a range of times. Using Equation (3), estimates of the minimum depth, Δ_{min}, of filled trap can be made. These lie around **0.93eV** for **SA** and **0.94** to **0.95eV** for the other samples. However it is noticeable that the two electro-thermally aged samples contain some charge that is removed quicker and hence that may lie in shallower traps (Dissado et al, 2006), or be quickly neutralized by Schottky charge injection (Mitsimoto et al, 2006).

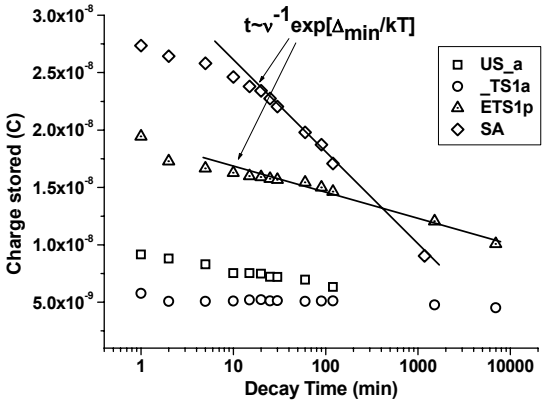

Figure 2.3.22: Decay of the stored space charge after voltage removal. The lines show the region of fit to equation (2) for SA and ETS1p.

No evidence for a cessation of the de-trapping process can be found and hence only a bound can be obtained for the deepest occupied traps using the longest time of the experiment (~ 7000 minutes). This gives $\Delta_{max} \geq$ **1.10eV.** The range of filled trap energies is therefore similar for all the materials, i.e. traps with depths between **~0.93eV** and **≥ 1.10eV**, but the service aged, **SA**, and electro-thermally aged samples, **ETS1**, contain more charge and have higher decay rates than others. Since the measuring

temperature is the same, Equation (2) implies that **N** is bigger in these two materials, than the others, with **N** being the largest in the service aged sample, as the trapped charge density is $\mathbf{eN(\Delta_{max}-\Delta_{min})}$ and the gradient of the **ln(t)** region of the plot is proportional to **–eNkT**.

(d) Depolarization analysis of thermally conditioning type B materials

Unstressed materials

Figure 2.3.23 shows the space charge decay after 26 and 2 hours of poling at 7.5kV. The linear region of the sigmoidal decay in Figure 2.3.23b gives the minimum filled trap depth $\mathbf{\Delta_{min}}$ and the deep trap limit $\mathbf{\Delta_{max}}$ according to Equation (3). After 26 hours of poling it was found that $\mathbf{\Delta_{min}}$ **~0.98eV** (when t_1=113 min) and $\mathbf{\Delta_{max}}$ is more than or equal to **1.08eV** (when t_2=5580 min) at T=298^{o}K. On the other hand after 2 hours of poling it is not possible to fit a sigmoidal function to the charge decay plot, but a linear region can be identified. Thus, if we assume that the linear region corresponds to a top-hat-trap (energy) distribution, $\mathbf{\Delta_{min}}$ and $\mathbf{\Delta_{max}}$ values correspond to **0.90eV** and **≥ 1.05eV** respectively. Although the trap depth range seems to be bigger in the case of 2h poling, it is possible that **N** for the accessible range of traps is smaller leading to a smaller amount of trapped space charge. This could mean that the poling time was not long enough to allow charges to access all the traps available at a given trap depth. There is also strong evidence that a large proportion of the charges reside in traps at depths less than **0.90eV**, and are extracted in less than ~1-2 minutes. Figure 2.3.23a shows how the charge density decays at the space charge peaks formed adjacent to both electrodes during 26 hours of poling and only near the cathode during 2 hours of poling. If we assume that the trap range at the position where the space charge peaks are formed have a top-hat energy distribution, then the trap depth at the beginning and end of the linear region can be estimated. Furthermore, the mirror image of the bottom end of the sigmoidal function described by Dissado et al (2006) is formed, as the space charge peaks that we are looking at, consist of negative charge. Hence, the maximum trap depth in this location can be estimated from Equation (3). It is found that the energy levels $\mathbf{\Delta_{min}}$ and $\mathbf{\Delta_{max}}$ adjacent to the cathode are the same during both poling times 2 and 26 hours, see Figure 2.3.23a. On the other hand the negative space charge that is trapped near the anode decreases very slowly indicating that these charges reside in very deep traps states, $\Delta_{max} \geq 1.08eV$, or that it is hard for them to escape/neutralise because of their nature.

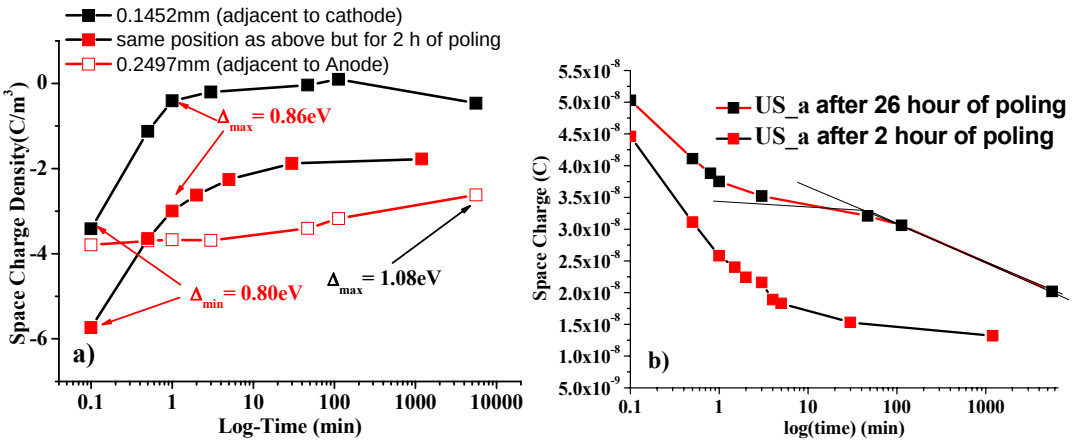

Figure 2.3.23: Space charge decay a) at peaks adjacent to electrodes after 26 hours of poling b) following Figure 2.3.9 of US_a after 2 and 26 hour of poling, calculated using Equation (1).

Electrically stressed materials

From Figure 2.3.24a, it can be deduced that the trap distribution lies between **0.87eV** to **1.05eV** as it does for the **US_a** material when poled for the same length of time. However, it should be noted that the charge in the **E_S1p** material which lies at trap depth of Δ_{max} has a greater charge density than in the **US_a** material, hence the electric field may have increased the trap density per eV, **N**. Figure 2.3.24b shows the space charge decay again but on a log-log plot in order to check if the decay mechanism follows a power law. Clearly from the shape of the plot this is not the case. Once again if we look at how the charge density changes at the peaks adjacent to the electrodes (Figure 2.3.25) we find out that the negative charge accumulated next to the cathode resides in very shallow energy states and the negative charge stored further away from that point is in trap states with a greater trap depth.

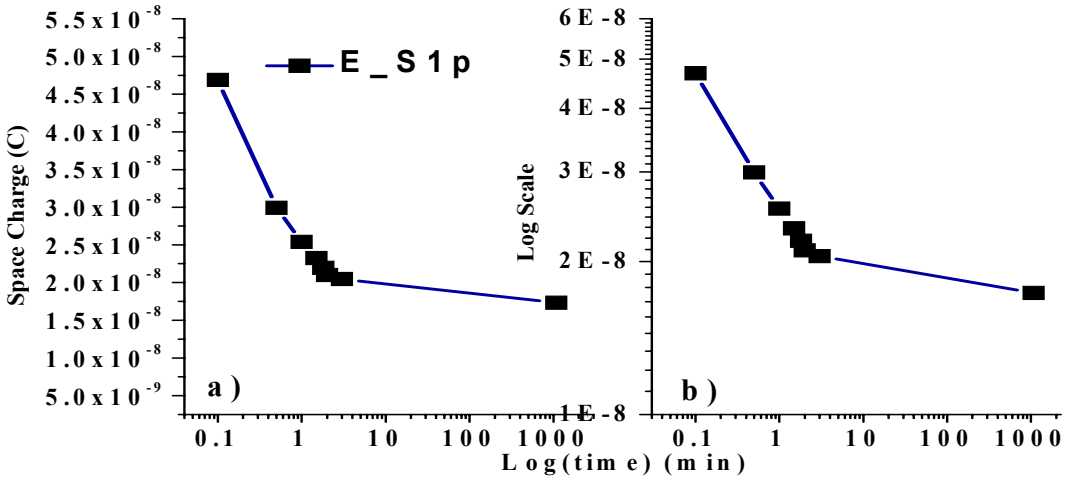

Figure 2.3.24: a) Space charge decay of Figure 2.3.10b of E_S1p after 2 hours of poling, calculated using equation (1) divided by a factor of 2 and b) plotted on a log-log scale.

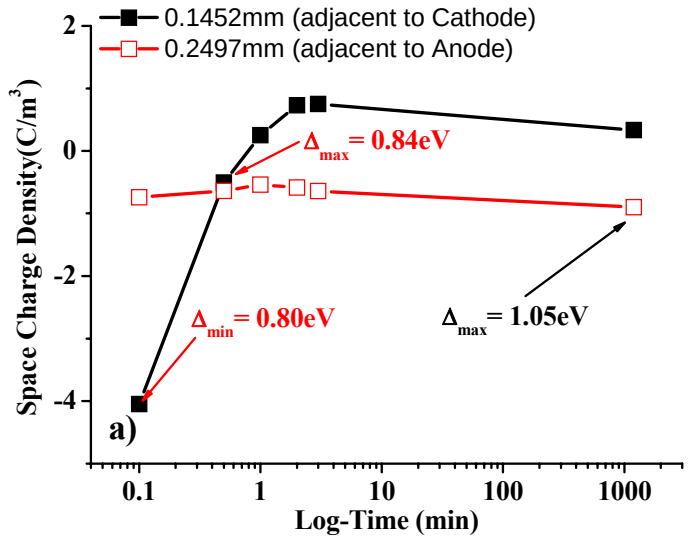

Figure 2.3.25: Space charge decay of E_S1p at peaks adjacent to electrodes after 2 hours of poling.

A similar behaviour is observed in the **E_S1a** material also where the trap depth distribution was found to lie between **0.88eV** and **1.04eV** as was deduced from Figure 2.3.26b. This suggests that the charge that lies in shallow traps may be responsible for

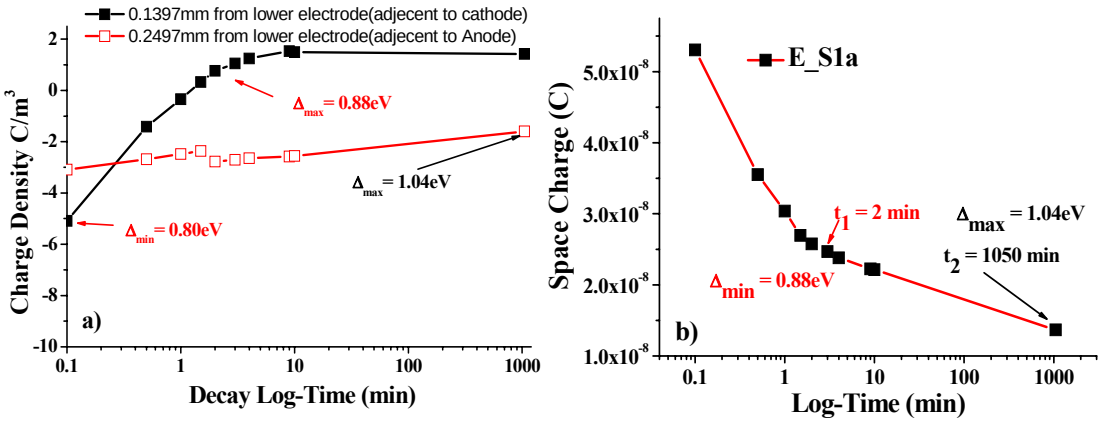

Figure 2.3.26: a) Charge density at 0.1397 and 0.2497mm adjacent to cathode and anode respectively, during accumulation and decay of E_S1a, b) Space charge decay of Figure 2.3.12b of E_S1a after 300min of poling, calculated using Equation (1).

the negative charge transit across the material. This characteristic may also be indicative of a situation where 2 hours of poling does not give enough time for the carriers in the traps to reach a thermal equilibrium. So instead of filling the traps at a given depth they only fill a fraction of them. Because of this the decay function is governed by the fraction in the traps at each depth. This behaves a bit like an exponential distribution of traps because more charge lies in the shallow traps than the deep traps which only a few carriers have time to reach. This could explain the kind of decay plot that is produced after 2 hours of poling whereas during 24 hours of poling the charges have time to come

near to thermal equilibrium in the traps and so fill them from bottom up as is assumed by Dissado et al (2006). The space charge behaviour of **E_S1a** is similar to the **SA** (Service Aged) material described in Figure 2.3.5 but there the negative charge transit is faster resulting in greater amounts of charge density adjacent to the anode.

Thermally stressed materials

As the decay of the thermally stressed material, **_TS1p**, was monitored for 220 minutes only, the maximum trap depth could not be calculated, see Figure 2.3.27a. However, an estimate of the minimum depth of trap that was occupied gives a value of **0.85eV** with a maximum depth greater than **1eV**. The maximum trap depth, Δ_{max}, estimated from Figure 2.3.27b is **>0.89eV** which is consistent with the estimated bounds of trap depths **≥1eV** for the other materials.

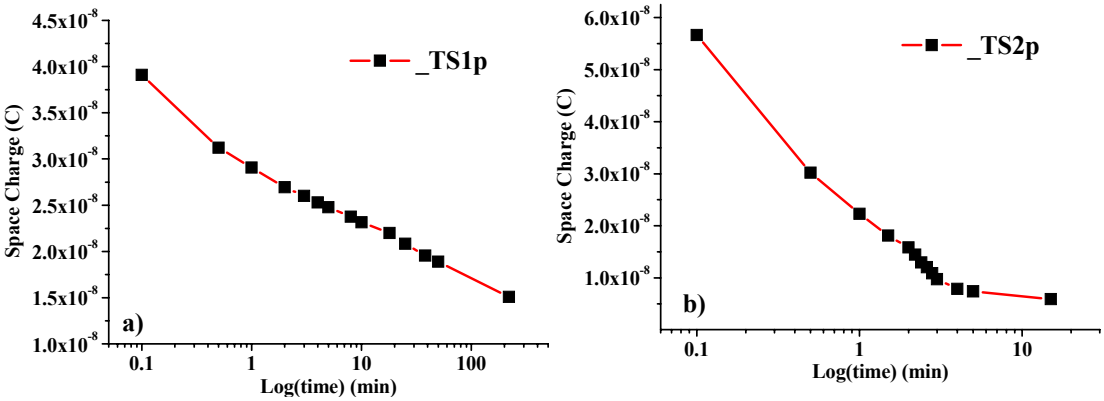

Figure 2.3.27: Space charge decay of Figure 2.3.14b after 120min of poling, calculated using Equation (1) a) of _TS1p and b) of _TS2p.

2.3.6 TSC measurements

The TSC measurements of the unstressed sample, **US_a**, were carried out at two different poling voltages, 4 and 6kV. At both voltages the pattern of the current measured is very similar with a current peak occurring at 110°C as is shown in Figure 2.3.28. The negative sharp spikes observed in Figure 2.3.28 especially under the 6kV poling may occur due to movement of charge within the material or charge escaping the material, or noise due to a high rate of data acquisition that is inadequately averaged.

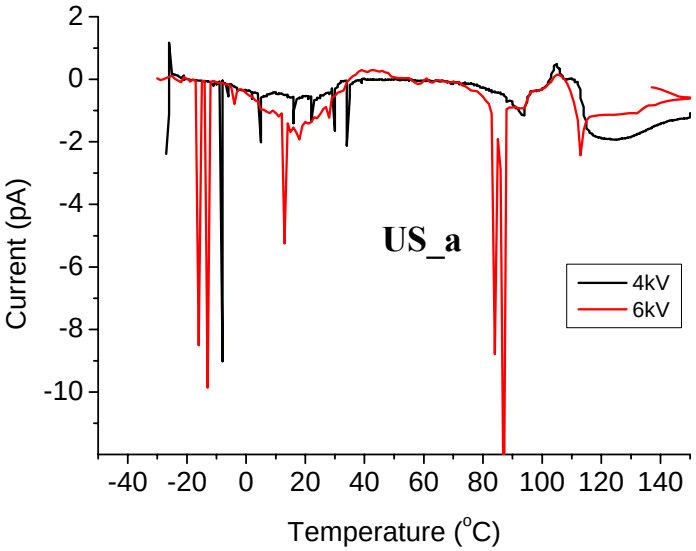

Figure 2.3.28: TSC measurement of the unstressed material, US_a at 4 and 6kV poling voltage.

The TSC currents were also measured at 4 and 6 kV for the thermally stressed sample, **_TS1a**. The current peaks for this material occurred around 120°C for both charging voltages as is shown in Figure 2.3.29. It should be noted that at the higher poling

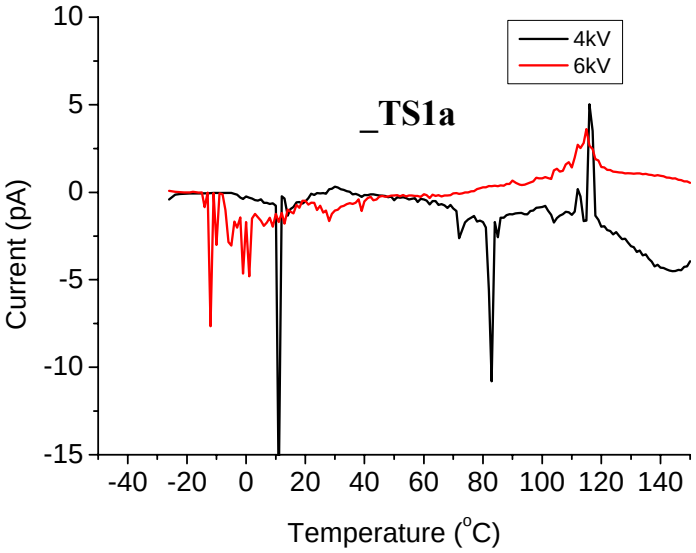

Figure 2.3.29: TSC measurement of thermally stressed material, _TS1a at 4 and 6kV poling voltage.

voltage the peak is wider and more uniform implying that more charge was injected during voltage application. The sharp negative spikes observed in the unstressed material, **US_a**, are also observed for the thermally stressed one. It was found out that these spikes were not present during when the experiment was repeated on the same specimen as is shown in Figure 2.3.30 where the data acquisition averaging was increased. It should also be noted that these measurements were conducted at a different

ramp rate, 4°C/min, rather at 2°C/min as the previous ones. The poling voltage is also lower (2kV) but the poling time has increased. Under these conditions high temperature peaks around 120°C are still observed with a similar magnitude as previously, Figure 2.3.28. However, a second narrow high temperature peak is observed at 90°C for the 30 minute poling and at 100°C for 60 minute poling. These sharp peaks around 100°C were attributed to the softening of XLPE in another study (Gubanski et al, 1992) and were present for all the compounds during that study. A low temperature peak is present around 23°C which is not very clear during the experiment reported in Figure 2.3.29. This peak also has a greater magnitude in the specimen that has the longest poling time.

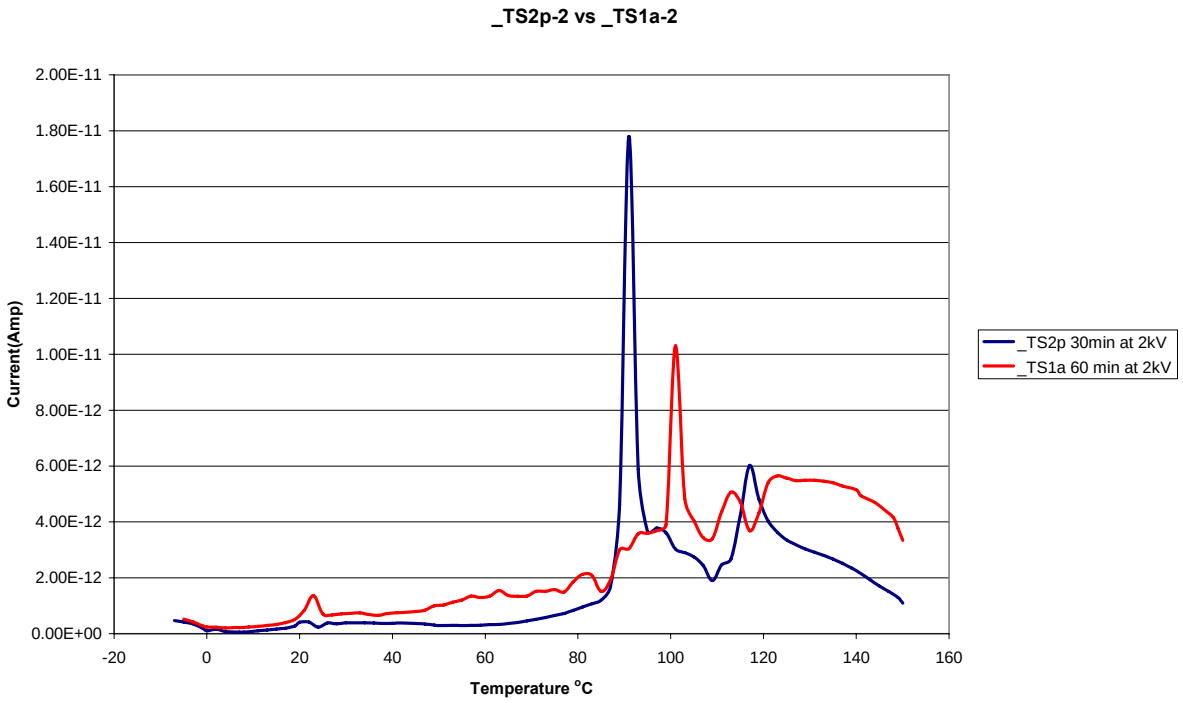

Figure 2.3.30: TSC measurements at 2kV for two thermally pre-stressed at 90°C materials for 5000 hours, _TS1a, and 10000 hours, _TS2p. These measurements were taken using the same specimen for a second repetition with a ramp rate of 4°C/min at two different poling times.

In the case of the electro-thermally stressed material, **_ETS1p**, during two replicate measurements (i.e. the TSC measurements are taking place for the first time) two current peaks were observed, one at a low temperature of 30°C and the other one around 110°C close to the peaks seen in the other two materials, see Figure 2.3.31. The high temperature peak is significantly greater in magnitude than the low temperature one. Thus, it could be assumed that most of the charge that was injected during the application of voltage got trapped into deeper trap regions as higher temperatures are

required to release it. A negative peak could also be observed just before the positive high temperature peak start to develop.

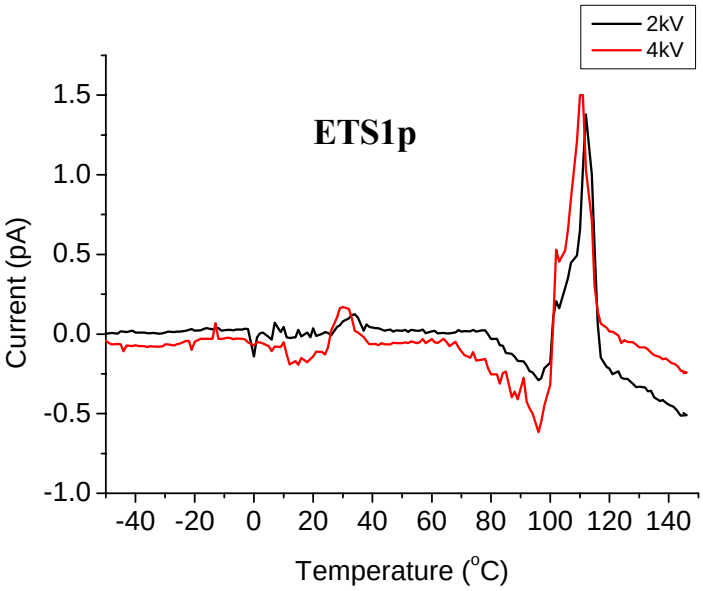

Figure 2.3.31: TSC measurement of the electro-thermally stressed material, ETS1pat 4 and 6kV poling voltage.

The behaviour of the electro-thermally stressed material was investigated further in order to gain more understanding on the origin of the low and high temperature peaks. Hence, a series of repeated experiments were conducted on the same specimens at the same poling temperature (90°C), voltage (2kV) and for the same poling time (30mins), see Figure 2.3.32.

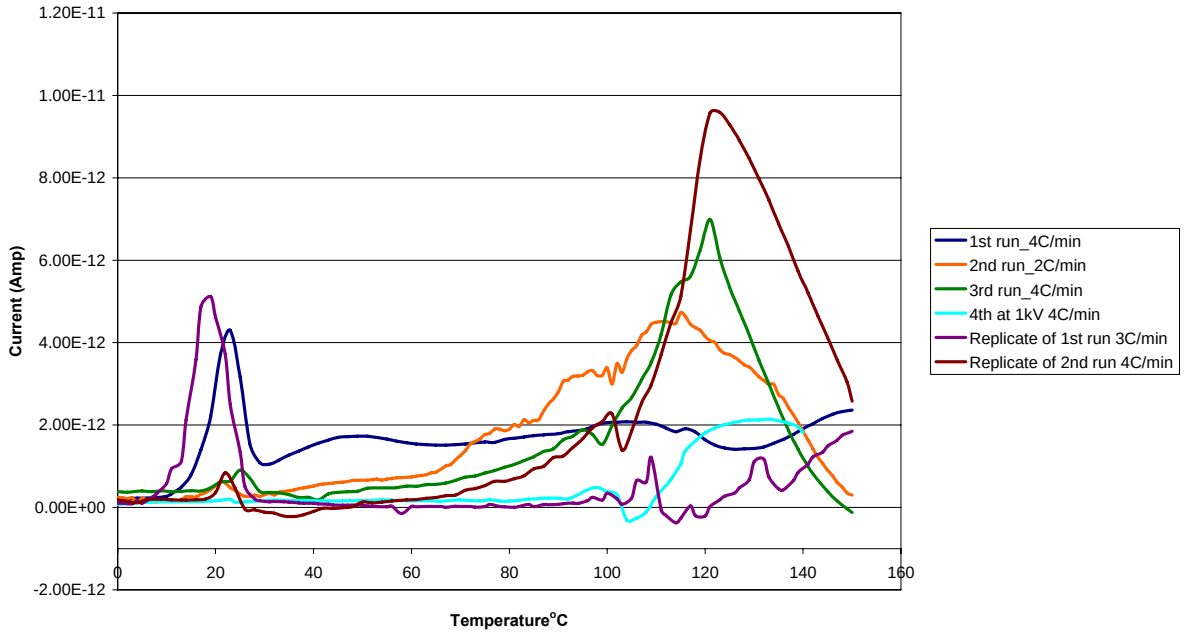

Figure 2.3.32: A series of repetition measurements on the electro-thermally pre-stressed material, ETS1p. The run and ramp rate are indicated in the legend. The poling temperature is 90°C and the applied voltage 2kV for 30 minutes otherwise specified in the legend.

Equations (4) and (5) are used to estimate the activation energies for the low and high temperature peaks and these are given in Table 2.3.1. The activation energies calculated (Table 2.3.1) show a great variation between different specimens and different repetitions on the same specimen. It also shows that Equation (5) gives a higher activation energies than Equation (4) especially for the narrow low temperature peak, as at the broad high temperature peaks there is a better agreement. According to the literature (Dissado & Fothergill, 1992, T. Mizutani et al, 1982 and Teyssedre et al, 2001) any activation energies above 1.5eV are not associated with de-trapping of either negative or positive charges. Activation energies of the order of 7eV and above are usually associated with ionization. Hence, unless ionization occurs during the TSC experiment, which is unlikely due to the low energy input to the system, any activation energies above 1.5eV should be ignored and accounted to the sensitivity of the TSC experiment and estimation approaches. In Table 2.3.1 only the average of the highlighted values was used to estimate the activation energies of the low and high temperature current peaks observed during the TSC measurements. It is found that the activation energy at the low temperature current peak corresponds at **0.871eV** and the high temperature one at **1.194eV**.

<table>
<tr><td rowspan="2">Experimental TSC run of ETS1p</td><td colspan="2">Low temperature peak activation energy (eV)</td><td colspan="2">High temperature peak activation energy (eV)</td></tr>
<tr><td>E_B (Eq. (4))</td><td>E_G (Eq. (5))</td><td>E_B (Eq. (4))</td><td>E_G (Eq. (5))</td></tr>
<tr><td>1st run (blue and purple coloured lines)</td><td>0.485</td><td>3.236</td><td>NA</td><td>NA</td></tr>
<tr><td>2nd run (orange and brown coloured lines)</td><td>5.13</td><td>5.587</td><td>1.267(average)</td><td>1.616</td></tr>
<tr><td>2nd and 3rd runs (orange and green coloured lines)</td><td>1.257</td><td>1.88
3.712</td><td>1.45</td><td>1.038
1.632</td></tr>
<tr><td rowspan="2">Average activation energies less than 1.5eV</td><td rowspan="2">0.871</td><td rowspan="2"></td><td>(1.35)</td><td>(1.038)</td></tr>
<tr><td colspan="2">1.194</td></tr>
</table>

Table 2.3.1: Activation energies calculated using Equations (4) and (5) for the low and high temperature peaks of the electro-thermally pre-stressed material, ETS1p, in Figure 2.3.32.

The service stress material, **SA**, behaved similarly to the electro-thermally stressed one with two current peaks being observed, one at a low temperature of 30°C and another one around 110°C as is shown in Figure 2.3.33. However, for the service stressed material the low temperature peak is greater in magnitude than the high temperature one.

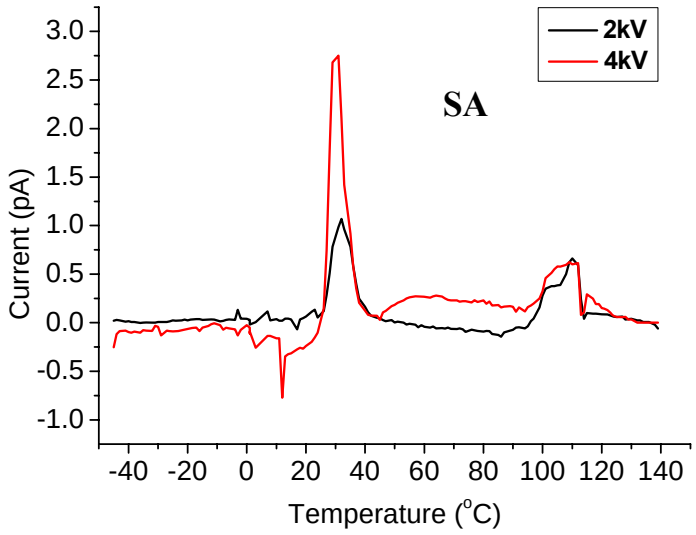

Figure 2.3.33: TSC measurement of the service aged material, SA at 2 and 4kV poling voltages.

2.3.7 Analysis of TSC measurements

Figure 2.3.34 shows the TSC measurements of samples with different electro-thermal histories under the same conditions as for the first run. All the samples have a high temperature peak occurring around 115 °C. The low temperature peak at 30 °C is only present for the electro-thermally (**ETS1p**) and service (**SA**) stressed materials. The current peak of the thermally (**_TS1a**) stressed material at the low temperature is also present at this poling field, but at a higher poling voltage appears to be of opposite polarity, see Figure 2.3.29. The trap depths at both low and high temperature peaks were very roughly estimated using the temperature ramp rate to estimate the time ($\mathbf{t_r}$) that the charges take to be released and assuming that the de-trapping of the charge is an activated process with the activation energy being the trap depth, **Δ**. It is also assumed that the traps are not distributed in energy. Setting $t_r \nu = \exp\left(\frac{\Delta}{kT}\right)$ as defined in Equation (3) a very rough estimation of the trap depth **Δ** could be made. Hence, the low temperature peak was found to correspond to a **Δ** of **0.92eV** and the high temperature peak to **Δ=1.18eV**. The low temperature trap depth is very close to the ones calculated in section 2.3.3b and 2.3.3c. These activation energies show a good agreement with the

ones estimated at different ramp rates using Equations (4) and (5) in Table 2.3.1 for the electro-thermally stressed material. These finding also agree with investigations of C. Lanca et al (2002a, 2002b and 2004) that were carried out in unstressed and electro-thermally stressed materials both in LDPE and XLPE (C. Lanca et al, 2007a). It should also be noted that in another study by S.M. Gubanski et al (1992) where different compounds of XLPE were studied under the TSC technique, it was found that the measurements are sensitive enough to differentiate the compounds according to their additives and cross-linking by-products which is also suggested by C. Lanca (2002a). Nevertheless, their studies were conducted at much lower poling fields than in this study. In this study the poling field are a lot higher, hence the space charge formation may superimpose and dominate over the other features of the materials.

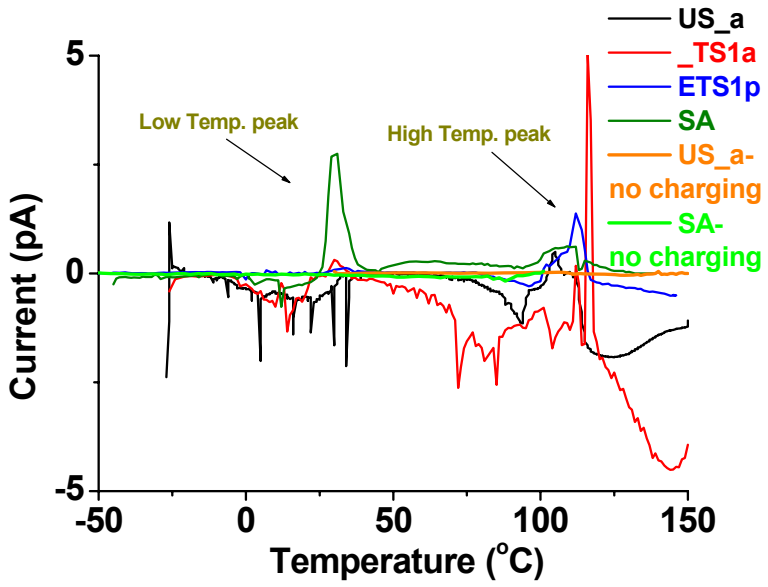

Figure 2.3.34: TSC comparison of materials with different electro-thermal stresses poled at 90°C for 15mins under 4kV. The TSC experiment was also conducted under no poling condition for the unstressed (US-a) and service stressed (SA) materials.

(a) Correlation of TSC peaks with PEA measurements

In order to understand the nature of the TSC peaks, PEA measurement were made at different points of the TSC experiment indicated by the arrows pointing upwards in Figure 2.3.35 for two runs on the **ETS1p** material. It was found out that during the 1st run both low and high temperature peaks occurred. After the charging dwell-time was completed the sample was cooled down to 10°C with liquid nitrogen and it was removed from the TSC apparatus to the PEA where the space charge stored could be measured. It was observed that during the poling of the material at 90°C positive charge was stored throughout the material with positive peaks formed adjacent to both

electrodes, Figure 2.3.35b. A similar space charge profile in XLPE during polarisation at 90°C was also observed by Y.L. Chong et al (2007), although at lower poling temperatures during the first hour of poling the space charge was dominated by negative carriers. Once the sample was installed back in the TSC apparatus, a current is found on ramping up the temperature giving a positive peak at 20°C. At 35°C the space charge retained is measured again under the PEA, where it is observed that a fraction of positive charge adjacent to the cathode has escaped which caused the formation of the low temperature peak. The decay of this positive charge occurred in 12 minutes which gives an estimation of the minimum and maximum trap depths of that positive fraction of the charge. Using Equation (3), this was found to lie between **0.85** and **0.95eV**. As the next PEA measurement was taken at the end of the TSC experiment, it is not clear if the formation of the higher temperature current peak is due to the de-trapping of space charge. However, the majority of space charge is still retained in the material after 35°C and resides in trap depths greater than **0.95eV**. The activation energies of the following current peaks were then estimated using Equation (5) as indicated in Figure 2.3.35a. By

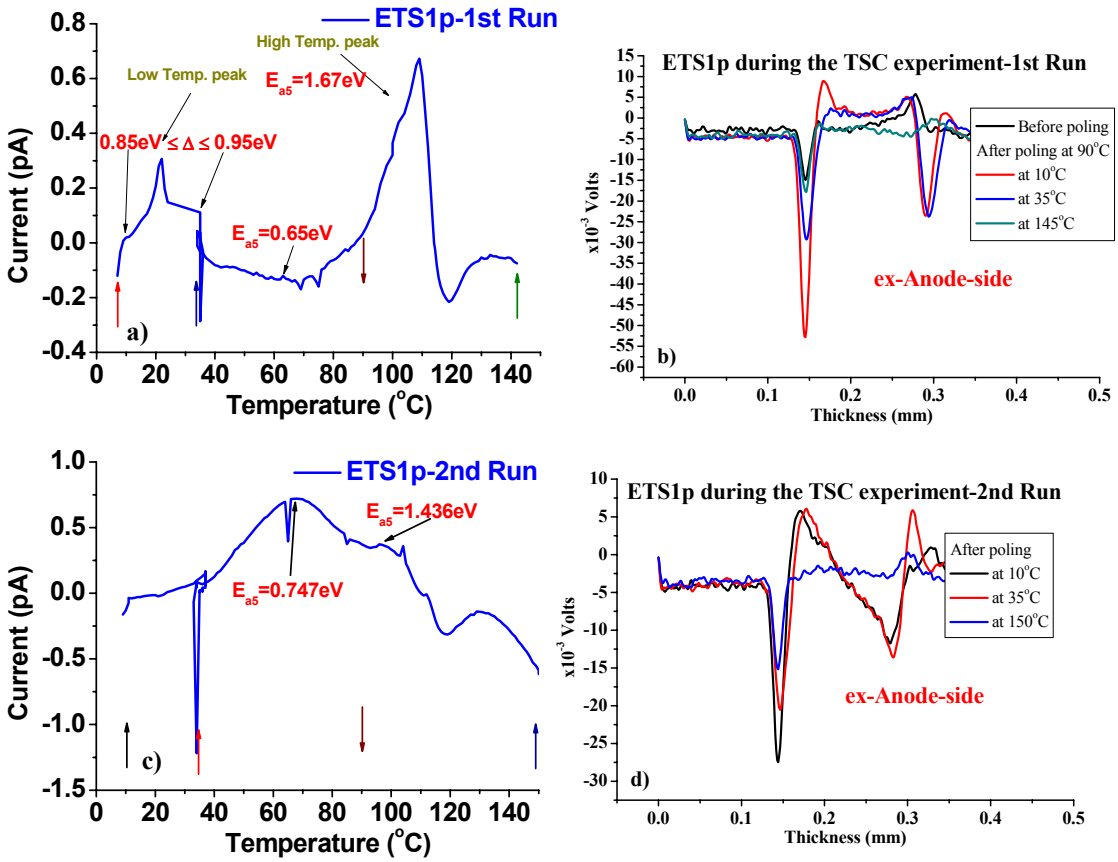

Figure 2.3.35: TSC measurement of ETS1p material a) 1st Run, c) 2nd Run with a ramp rate of 2°C/min, poled at 2kV for 30 minutes at 90°C (charging temperature is indicated with the arrow pointing downwards) and PEA measurements obtained by removing the sample at different temperatures indicated by the arrows pointing upwards for b) 1st Run and d) 2nd Run.

the end of the 1st run all the positive charge has escaped the material leaving a very small amount of negative charge adjacent to the anode which reduces the electrode charge induced by the HV pulse of the PEA system.

During the 2nd run totally different TSC and PEA measurements from the above are obtained, see Figure 2.3.35c and d, respectively. The space charge that is stored after polarisation is now negative at the anode and positive at the cathode. This type of space charge does not decrease between the 10 and 35°C interval, thus no current peak is observed around that temperature. A broad current peak begins to form just after that with its peak occurring at 67°C and an adjacent one at 97°C. The activation energies of these peaks were estimated using Equation (5) and are indicated in Figure 2.3.35c. Hence, the space charge profile of the material has changed, possibly because of the thermal stress experienced during the experiment. The elevated temperature may have caused the chemical composition and crystallinity of the XLPE material to change as high temperatures may cause further cross-linking or bond breakage (Dissado & Fothergill, 1992), and lamella thickening. It is also possible that concentration of chemical agents such as antioxidant and other material stabilizers have been altered leading to different space charge characteristics in both TSC and PEA techniques.

2.3.8 Discussion

The space charge profiles acquired via PEA for both conditioning types A and B hold the main features that characterise the materials. These are that the space charge in all materials is composed of carriers of the same polarity with similar distribution and that the magnitudes of the charge density are very similar if not the same. This picture of the space charge behaviour is also consistent with the data obtained during the ARTEMIS programme (Borealis, 2003) as well as by others studies in XLPE under similar conditions by Boudou et al (2004), G. Chen et al (2001, 2004), Y.L. Chong et al (2005, 2007), Mazzanti & Montanari (2003), Mazzanti et al (2003), Montanari (2000), Montanari et al (1999, 2001, 2003 and 2004). The main difference that is observed between the two thermal treatments is that in type A the space charge accumulation and decay occurs slower (Figure 2.3.2 - Figure 2.3.4) than in type B (Figure 2.3.7, Figure 2.3.10, Figure 2.3.11, Figure 2.3.14 and Figure 2.3.15). The PEA data for unstressed, **US_a**, and thermally stressed, **_TS1a**, samples are very similar with low negative charge densities and slow charge decays for the thermal conditioning A (and probably

peeling from cable manufacturer "a"). This indicates that mainly negative charge is injected in all materials regardless of the stressing that the materials experienced as a cable. There is evidence of positive charge injection in the thermally, **_TS1a** (Figure 2.3.3), and electro-thermally, **ETS1p** (Figure 2.3.4), stressed materials especially at high applied fields. Nevertheless, negative charge accumulation at the cathode characterises the space charge behaviour in most materials during 120 minutes of poling. However, for the serviced aged, **SA**, material negative charge that gets injected at the cathode transits rapidly to the region adjacent to the anode especially at high fields (Figure 2.3.5). A similar behaviour is also observed in the electrically stressed material, **E_S1a** (Figure 2.3.12) but the charge transit occurs at a much slower rate than in the **SA** one, suggesting that the density of shallow traps is greater in the **SA** material than the **E_S1a**. It was also found that if the unstressed material is poled long enough, in this case more than 226 minutes, negative charge can also migrate from the region adjacent to the cathode. Hence, during 120 minutes of poling the material may have not reached thermal equilibrium and trap sites are not filled from bottom energy states to the top. Therefore, the charges in this case are located in traps of all depths. Consequently the trap depth range in the unstressed material that was poled for 120 minutes is big (**0.90-1.05eV**) as found in the depolarization analysis. Table 2.3.2 shows the transit times of negative charge from the cathode to anode for materials under different pre-stressing conditions. It is clearly shown that for 120 minutes of poling the fastest transit occurs in the **SA** material and in the electrically stressed ones, **E_S1p** and **E_S1a**, considering a charge density of more than 2 C/m^3. The thermally stressed materials also show evidence of negative charge transport, see Figure 2.3.3 and Figure 2.3.13, by gradually spreading across the sample and eventually reaching the anode.

Under the depolarisation analysis of type A conditioning it was found out that the charge of the unstressed and thermally stressed materials resides in deep traps (**≥0.95eV**) (Tzimas et al, 2005), and these traps are not present in great density as it is shown in Table 2.3.2. This analysis is supported by the TSC data, which only shows evidence for the deeper traps related to the higher temperature peak. In the case of the electro-thermally aged samples (**ETS1p**), Figure 2.3.4 and Figure 2.3.10, the situation is different. They accumulate larger quantities of space charge, some of which seems to lie

Material Ref.	Poling time	Transit time of negative charge to Anode	Maximum Charge density after poling(C/m^3)	
			Adjacent to Cathode	Adjacent to Anode
US_a (A)	120min	NA	-5	1
_TS1a (A)	120min	600 sec	-3	-1
ETS1p (A)	120min	600 sec	-6	-1
SA (A)	120min	60 sec	5	-12
US_p (B)	120min	NA	-7	0
US_a (B)	26 hours	≥215 mins ≤21 hours	-4	-4
E_S1p (B)	120min	10 mins	-5	-2
E_S1a (B)	300min	10 mins	-6	-3
_TS1p (B)	90+120min	90+3mins	-3	-2
_TS2p (B)	120min	NA	-7.5	0
ETS2p (B)	120min	NA	-8	0

Table 2.3.2: Transit times of negative space charge to reach the anode electrode and its charge densities after poling. The letter in the brackets next to the material reference indicates the type of conditioning undertaken.

in a range of traps that are shallower than **~0.94eV** and hence can be released faster. This contention is supported by the TSC, Figure 2.3.36, which shows that a lower temperature current peak corresponding roughly to a de-trapping energy of around **0.92eV** exists in addition to the higher temperature peak present in all the samples. The larger proportion of charge in the TSC experiment lies in the deeper traps, Figure 2.3.34, and this would be consistent with the PEA experiment, which shows that only a small amount of charge decays in the first few minutes, Figure 2.3.36, i.e. almost all the charge here lies in the deepest trap range. For the SA sample this is not the case. The TSC indicates that a large proportion of charge lies in the shallower traps, and that this will decay in a few minutes at room temperature, Figure 2.3.36. This also fits with the PEA and TSC experimental analysis above. This is consistent with a picture in which the deep traps have been filled and the charge residing in shallower traps has been able to transit the sample and build up the negative hetero-charge observed (Delphino et al,

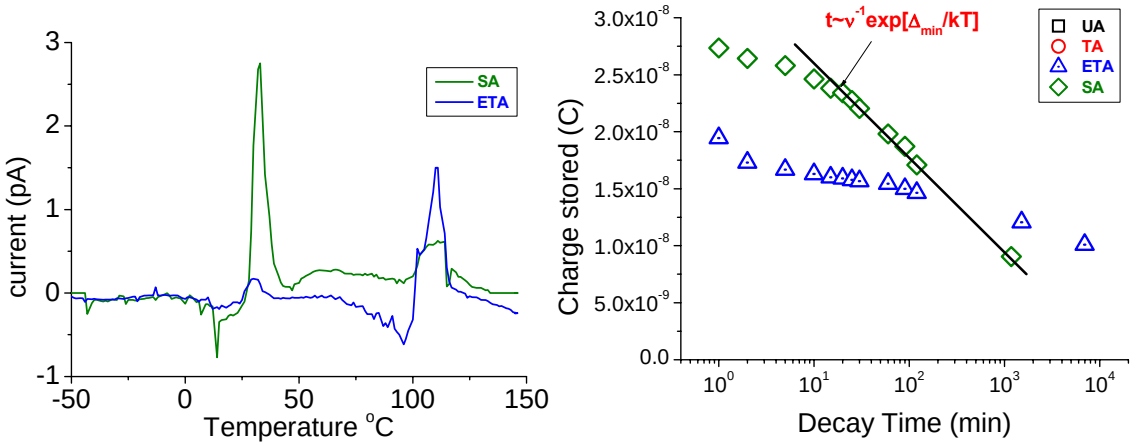

Figure 2.3.36: Correlation between a) TSC current peaks with b) space charge decay plots acquired with PEA.

2007). However the possibility of ionic dissociation leading to hetero-charge formation when the positive component is removed from the anode cannot be ruled out.

2.4 EFFECTS OF PRE-STRESSING HISTORY

- There is no evidence during 120 minutes of DC poling that thermal stressing over 5000h substantially modifies the space charge profile of the cable insulation.
- The electric stressing seems to introduce changes to the material by making easier the transit of negative charge from the cathode to the anode as was observed under dc poling for 120 and 300 minutes.
- The combination of an electric field and high temperature also introduces changes. These are:
    - Greater ability to accumulate net charge associated with a greater density of traps extending to shallower trap depths.
    - In the field aged cables the existence of shallow traps together with filled deep traps allow charge transit and the formation of heterocharge. The same effect is also observed in electrically stressed materials to a smaller extent.
- Negative charge accumulated adjacent to the cathode escapes faster on voltage removal than when it is trapped adjacent to the anode.

The low temperature peak observed in the TSC experiments occurs due to charge released adjacent to the cathode which reside in low energy trap states.

3 CHAPTER: ENDURANCE LIFE TEST OF ARTEMIS CABLE PEELINGS

3.1 INTRODUCTION

The tests described in this chapter are designed to determine whether or not the electro-thermal stressing that took place during the ARTEMIS programme had altered the inherent endurance capability of the XLPE insulation material under constant electro-thermal stress. This investigation is carried out by "a sudden death" test or endurance test which compares peelings (150μm thick) of cables that experienced different electro-thermal stresses with unstressed ones. All samples were conditioned before the test to remove any humidity and residual cross-linking by-products. A set of four samples was used for each material. The test was terminated once three out of four samples have failed leaving a sample near to failure for further investigation. In one case, the endurance life of the peelings is checked by the application of high a.c. field (rms70kV/mm) and high temperature (90^{o}C) in order to minimise the lifetime of the material. In a second case, of the field was kept at 70 kV/mm rms as in the former case but the temperature was reduced to 30^{o}C to investigate the effect the temperature has during the endurance test. Finally a lower electric field of 55kV/mm was applied at the higher temperature of 90^{o}C to check the endurance capability of the materials at a lower field. In all cases the influence of the pre-stressing of the material is considered to cause any possible change that was introduced to the material during electro-thermal stress as a cable.

Failure of solid insulation can be mostly described by extreme-value statistics, such as the Weibull and Gumbel distributions (Fothergill et al, 2003b) but historically, the lognormal function has also been used. The analysis of the endurance life time results was carried out by Weibull statistics because of the flexibility of the shape of the distribution function as is demonstrated in Figure 3.1.1. It is this flexibility that gives the Weibull distribution its wide applicability to electrical lifetimes (Dissado & Fothergill 1992, Dissado 2002a and Rowland et al 1986).

3.1.1 ARTEMIS programme contribution

The Artemis project demonstrated a very low rate of degradation of the cable materials in spite of the use of very high electric stress levels at elevated temperatures (Fothergill

et al 2003a). Nevertheless, it did provide a definite indication of the techniques that should be used to evaluate the state of the insulation, one of which is a check of its endurance capability as reported here.

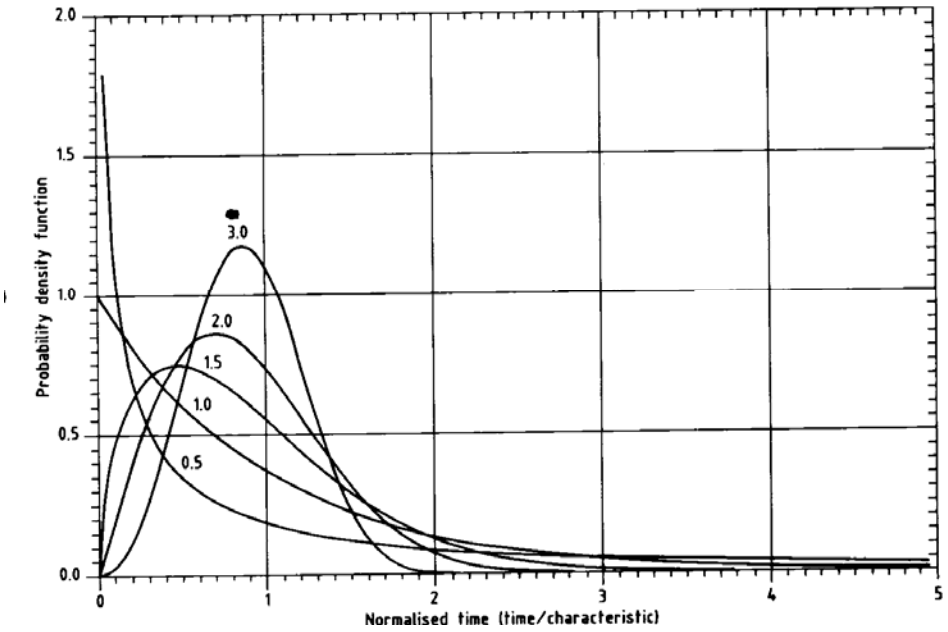

Figure 3.1.1: The probability density function of the Weibull distribution for the five cases of β= 0.5, 1.0, 1.5, 2.0 and 3.0. Taken from Dissado & Fothergill (1992).

The endurance life of peelings from unstressed cables was measured for electric fields varying from 30 to 80 kV/mm (rms) and two temperatures 293 (20°C) and 363°K (90°C) as part of the ARTEMIS programme (Borealis, 2003) and (Fothergill et al 2003a). The results shown in Figure 3.1.2 are typical of insulating materials and show

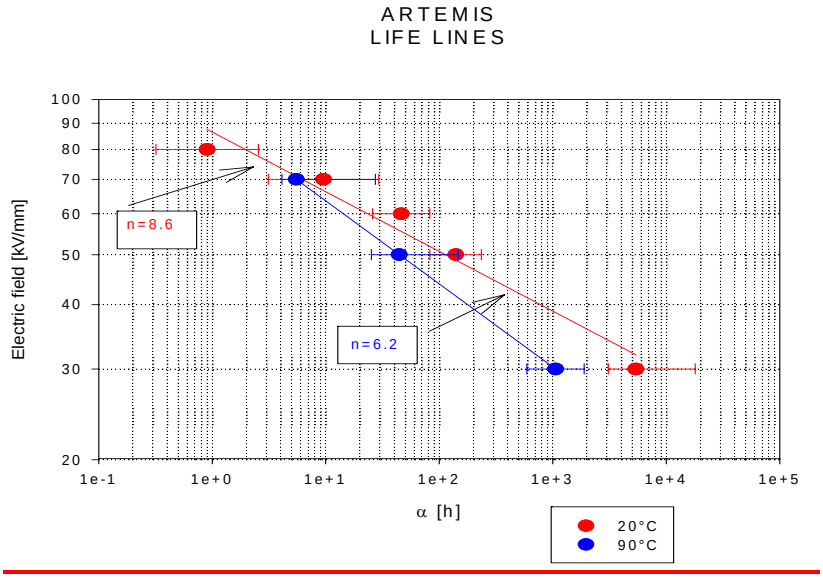

Figure 3.1.2: Endurance test on unstressed peelings from Artemis cables at 293 (20°C) and 363°K (90°C). Taken from Borealis (2003).

that the endurance capability of the material decreases as the field and temperature increases. This study is intended to check whether there is a decrease in the inherent endurance capability of the materials due to their different electro-thermal histories during the ARTEMIS programme.

3.2 THE WEIBULL DISTRIBUTION

The expression for the cumulative density function for the two-parameter Weibull distribution is:

$$F(t;\alpha,\beta) = 1 - \exp\left\{-\left(\frac{t}{\alpha}\right)^{\beta}\right\} \qquad \text{Equation (6)}$$

where:

t is the measured variable, usually time to break down or the breakdown voltage,

$F(t)$ is the probability of failure at a voltage or time less than or equal to t.

α is the scale parameter defining a characteristic value of the measured variable t and is positive, and

β is the shape parameter and is a positive number.

The probability of failure $F(t)$ is zero at $t=0$. The probability of failure rises continuously as t increases. As the time increases, the probability of failure approaches certainty, that is, $F(\infty)=1$.

The scale parameter α represents the time (or voltage) for which the failure probability is 0.632 (that is $1-1/e$ where e is the exponential constant). The units of α are the same as t, that is time to failure. The shape parameter β is a measure of the range of the failure times or voltages. The larger β is, the smaller is the range of breakdown voltages or times.

3.2.1 Weibull plots

In order to demonstrate that the Weibull distribution applies, Equation (1) is re-arranged so that the data should give a straight line, i.e.

$$\exp\left\{-\left(\frac{t}{a}\right)^{\beta}\right\} = 1 - F(t) \qquad \text{Equation (7)}$$

Therefore:

$$\left(\frac{t}{\alpha}\right)^{\beta} = -\ln\left[1 - F(t)\right] \qquad \text{Equation (8)}$$

and then:

$$\beta \log_{10}\left(\frac{t}{\alpha}\right) = \log_{10}\left(-\ln\left[1 - F(t)\right]\right) \qquad \text{Equation (9)}$$

So, $\log_{10}\left(-\ln\left[1 - F(t)\right]\right)$ is plotted on the y-axis and log(t) on the x-axis. The gradient gives β and the intercept on the y-axis gives $\log_{10}(\alpha)$.

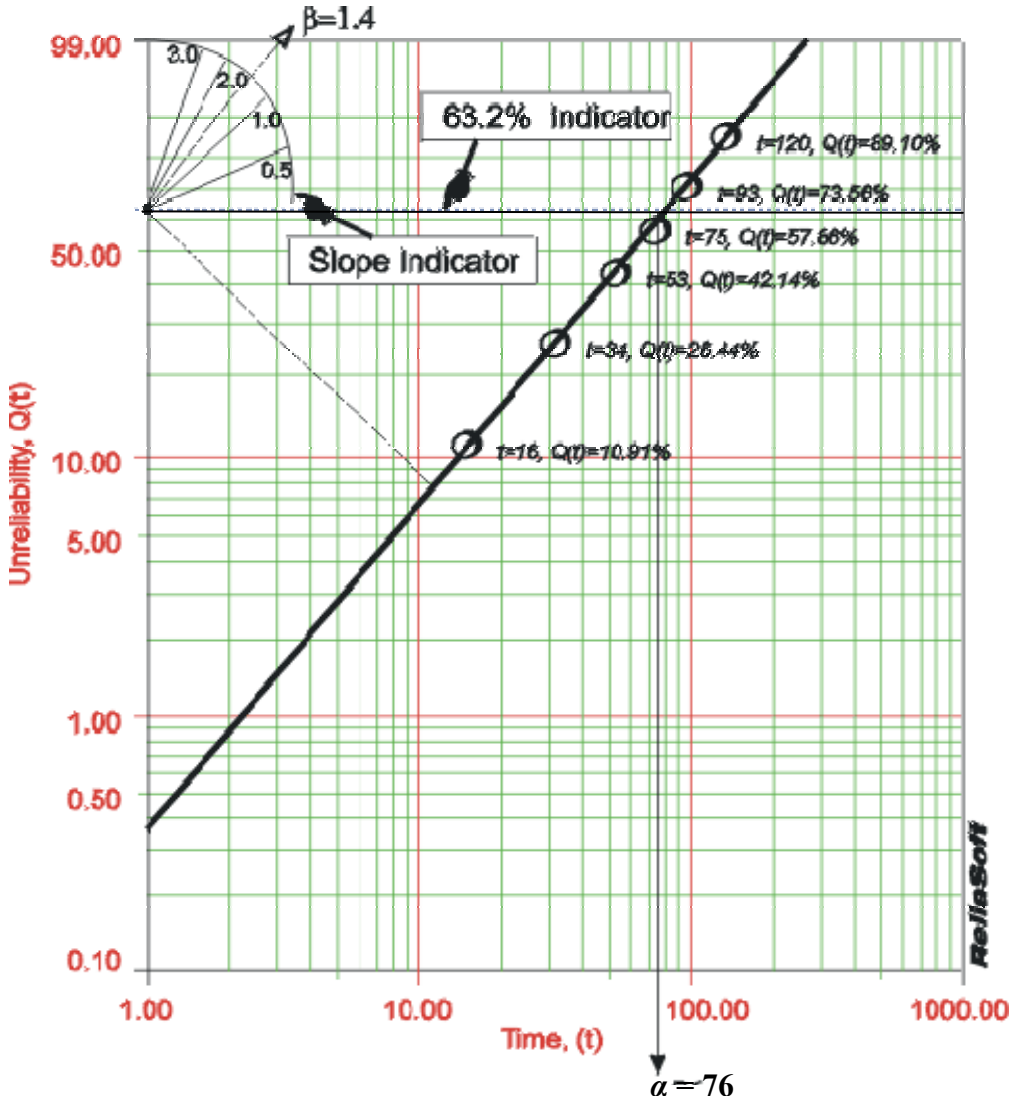

Figure 3.2.1: An example of a Weibull probability plot.

3.2.2 Estimation of plotting positions of the times to failure

According to IEEE P930 guide (Fothergill et al, 2003b) there are two types of data associated with solid insulation breakdown and each of them have to be treated differently for the estimations of the plotting positions. One type includes the data of an

experiment that is terminated once all the specimens are broken down and is usually referred as complete, or single censored if the experiment is terminated before all the specimens are broken down. The other type includes data from where the specimens can be withdrawn at any time or voltage and is referred as progressively censored. As the voltage is kept constant throughout the endurance test, the data that is being analysed in this chapter is characterised as single censored. This is the only method described here.

Before the Weibull plot probability paper is used, the appropriate failure probabilities need to be estimated. This is done by ranking the n times to failure from smallest to largest and assigning them a rank $i=1$ to $i=n$. Then a good, simple, approximation for the median probability of failure is found in (Fothergill et al, 2003b):

$$F(i,n) \approx \frac{i-0.44}{n+0.25} \times 100\% \qquad \text{Equation (10)}$$

Once the times to breakdown are known, they can be plotted against the median rank - probability to failure, to give the Weibull plot. Figure 3.2.1 shows an example of a set of data with six selected times to breakdown, where the plotting positions are indicated next to the times t_1, t_2, etc.

3.2.3 The shape of a Weibull probability Plot

The data plotted on Weibull probability paper can be used to check by eye the adequacy of the distribution. If the data does not produce a reasonably straight line on Weibull probability paper, it may not be represented statistically with the 2-parameter Weibull distribution function. Another way to check the adequacy is a computational method and is described in more detail in (Fothergill et al, 2003b).

3.2.4 Estimation of Weibull parameters

There are two ways to estimate the Weibull parameters, α and β, of the probability function. One way is to estimate them graphically using the Weibull probability paper and the other way is computationally. The graphical one is done by markers on the Weibull plot from which the value of α and β can be estimated as shown in Figure 3.2.1. The characteristic time to failure, α, is the projected point on the x-axis where the Weibull plot crosses the 63.2% of probability to failure. The shape parameter β

indicates the slope of the Weibull plot and can be graphically estimated using a Weibull paper as shown in Figure 3.2.1. If it is not possible to use this technique then an estimate for β may be found as follows. From the Weibull plot estimate the times corresponding to $F(t)$ = 10% and $F(t)$ = 90% denoted t_{10} and t_{90} respectively. An estimate for β is then given by:

$$\beta = \frac{1.340}{\log_{10}(t_{90}/t_{10})} \qquad \text{Equation (11)}$$

3.2.5 Estimation of Weibull percentiles

It is often useful to estimate the time, voltage or stress for which there is a given probability of failure p %; this is known as the p^{th} percentile. In constant stress life tests, these percentiles are sometimes referred to as "B lives". For example, the "B10 life" is the age at which 10% of the components will fail at a given voltage stress. The p^{th} percentile, t_p, may be estimated from:

$$t_p = \alpha\left[-\ln\left(1-\frac{p}{100}\right)\right]^{1/\beta} \qquad \text{Equation (12)}$$

where p is expressed as a percentage.

3.2.6 Estimation of 90% confidence limits for the Weibull function

If the same experiment involving the testing of many specimens is performed a number of times, the values of the parameter and percentile estimates, α, β and t_p from each experiment differ. This variation in estimates results from the statistical nature of insulation breakdown, see for example Dissado & Fothergill (1992). Therefore, any parameter estimate differs from the *true* parameter value that is obtained from an experiment involving an infinitely large number of specimens. Hence, it is common with each parameter estimate to give a *confidence interval* that encloses the true parameter value with high probability. In general, the more specimens tested, the narrower the confidence interval.

The method described in the IEEE statistical guide by Fothergill et al (2003b) provides a simplified procedure for estimating the bilateral 90 % confidence intervals, which exclude the highest 5 % and the lowest 5 % of the distribution, for sample sizes from *n=4* to *n=100* and is adopted in this chapter. The technique is applicable to complete

and singly-censored data; it is not applicable to progressively-censored data. The technique may be used with up to 50 % of the specimens being censored.

The following equations are used to obtain the bounds of the 90 % confidence intervals for the $p^{th.}$ Percentile Fothergill et al (2003b):

$$t_l(p) = \alpha \exp\{Z_l(p)/\beta\}$$
$$t_u(p) = \alpha \exp\{Z_u(p)/\beta\} \qquad \text{Equation (13)}$$

where $t_l(p)$ and $t_u(p)$ are the lower and upper bounds of the confidence interval for the $p^{th.}$ percentile.

Confidence interval tables have been calculated in Fothergill et al (2003b) and have been used in this study to estimate the 90% confidence limits according to the number of specimens used and failed/suspended for each test. In this study four specimens were used for each material (n=4) and the test was terminated once three of them failed (r=3). The values for the factors $Z_l(p)$ and $Z_u(p)$ were extracted from the confidence interval figures in Fothergill et al (2003b) for the percentiles p=0.1 %, 1.0 %, 5.0 %, 10 %, 30 %, and 95 % and the bounds of α (63.2%) are also included for n = 4 and r = 3 as presented in Table 3.2.1.

Percentile	**Values deducted from Fothergill et al (2003b) for n=4 and r=3**	
p	$Z_l(p)$	$Z_u(p)$
0.1 %	**-15.1**	**-2.3**
1 %	**-9.9**	**-1.1**
5 %	**-6.4**	**-0.65**
10 %	**-4.84**	**-0.415**
30 %	**-2.431**	**0.08**
63.21 % (α)	**-1.17**	**0.99**
95 %	**-0.55**	**2.98**

Table 3.2.1: Factors $Z_l(p)$ and $Z_u(p)$ extracted from Fothergill et al (2003b) in order to calculate the confidence limits for n=4 and r=3.

Such confidence limits enclose any particular percentile of the true population with 90 % probability. The greater the number of specimens tested, the closer the upper and lower curves. Confidence intervals can also be calculated for the shape parameter β, using the following equation:

$$\beta_l = W_l \beta$$
$$\beta_u = W_u \beta \qquad \text{Equation (14)}$$

where β_l and β_u are the lower and upper limits, respectively for the interval.

The factors W_l and W_u for $n = 4$ and $r = 3$ are obtained from Fothergill et al (2003b) and are *0.456* and *4.67* respectively.

3.3 EXPERIMENTAL PROCEDURE OF THE ENDURANCE TEST

The endurance tests were conducted at three different conditions **A**, **B** and **C** as is shown in Table 3.3.1. The endurance test under the condition **A** was carried out more than once; hence the subscripted number of **A** indicates the number of tests that were consequently conducted under these conditions. The alphabetical order of the endurance tests also corresponds to the order the tests were carried out. The first test, **A**, was carried out at an AC field of 70kV/mm (rms) and a temperature of 90^{o}C. The second test, **B**, was conducted at a field of 70kV/mm (rms) and a temperature of 30^{o}C and the third test was conducted at a field of 55kV/mm (rms) and a temperature of 90^{o}C. The materials that were used in each test are listed in Table 3.3.2 along with their stressing pre-histories as a cable during the ARTEMIS programme.

Endurance Test	Field E AC(kV/mm) $_{rms}$	Temperature (^{o}C)
$A_{1, 2, 3 \& 4}$	**70**	**90**
B	**70**	**30**
C	**55**	**90**

Table 3.3.1: Endurance test conditions.

3.3.1 Materials used

All the materials used for the Endurance tests are **peelings** of **XLPE** insulation with a **thickness of 150µm** but different stressing pre-histories as a cable, see Table 3.3.2. The insulation for the cables is manufactured by two different companies, which can be

distinguished by the small case letters, "p" and "a" under the reference name column in Table 3.3.2. It should be noted that the same batch of XLPE was supplied to the cable manufacturers. Hence the inherent differences of the insulation peelings, if any, come from the cable manufacturer's process and the electro-thermal stressing that they experienced as a cable.

No	Ref. name	REF. CODE	Endurance test	Pre-history of the material as a cable		
				E. stress AC (kV/mm)	Temp. (^{o}C)	Time (h)
1.	US_p	P11	A_2, B	-	20	-
2.	US_a	E22	A_2, C	-	20	-
3.	E_S1p	P20U6	A_2	19.5	20	5000
4.	E_S2p	PTHT 6/2 No11	A_4, B, C	19.5	20	7747
5.	E_S1a	ATHT 4/2 No3	A_4,	19.5	20	5581
6.	E_S2a	AVU6	A_2	12.5	20	5000
7.	_TS1p	PVT11	$A_{1,3}$	0	90	5000
8.	_TS2p	P90T3	A_3, B, C	0	90	10000
9.	ETS1p	P90TU11	A_1	19.5	90	5000
10.	ETS2p	PSM9	$A_{1,3}$,B, C	28	90	6000
11.	ETS2pm	PSM9	A_4	25	90	6000
12.	ETS3p	P90X2	A_2	28	90	3000
13.	ETS4p	PVTU6	A_1	12.5	90	5000
14.	SA	ABBV1	B, C	SERVICE	SERVICE	>18 YEARS

Table 3.3.2: Materials used for the endurance tests defined in Table 3.3.1 and their pre-history as a cable.

The aim of the endurance tests is to check whether the cable pre-history has had an identifiable effect upon the ability of the insulating material to withstand electrical and thermo-electrical stress. Four specimens were used per material to compare the statistical difference in the pre-history of each material. Once three specimens have failed the fourth specimen is suspended at the same time that the third one failed. The first test, $\mathbf{A_1}$, included materials from the same manufacturer that experienced very similar durations under stress, though not exactly identical. All of them experienced thermal stressing and four out of the five sets have also experienced different levels of

electrical stressing. This test aims to check whether the inherent endurance capability of the materials with a pre-history of different levels of electrical stress varies according to those levels with statistical significance. The second test under the same conditions, $\mathbf{A_2}$, included materials from both manufacturers with no stressing pre-history, **US_p** and **US_a,** and a couple of sample sets that experienced electrical stressing at two different levels, **E_S1p** and **E_S2a**. The aim of this test is to check whether there is any statistical difference between the unstressed materials and the electrically stressed ones and moreover between them and the thermally and electro-thermally stressed materials of the first test, $\mathbf{A_1}$. The following two tests at the same endurance test conditions, $\mathbf{A_3}$ and $\mathbf{A_4}$, are mainly aimed to replicate and verify the trends of the former tests.

The endurance test that was conducted under the conditions **B**, where the field was kept at 70kV/mm but a reduced temperature of 30^{o}C was used, consisted of materials that experienced stressing as a cable under different electro-thermal conditions, see Table 3.3.2. The aim of this test is to investigate the effect of temperature in the endurance test by comparison with the former test condition, **A**. Endurance test **B** compares an unstressed material, **US_p**, an electrically stressed one, **E_S2p**, a thermally stressed one, **_TS2p**, an electro-thermally stressed one, **ETS2p**, and a service stressed one, **SA**.

The materials that were used in the endurance test under condition **C**, lower field of 55kV/mm and high temperature of 90^{o}C, are the same materials that were used under condition **B** except that the **US_p** material was replaced with the **US_a** because of an insufficient length of tape. The aim of this test is to investigate the influence of a lower electrical field on the materials under a high temperature.

3.3.2 Conditioning of the tapes

The conditioning occurred at 50^{o}C at an ambient pressure for 48hours. The conditioning of the tapes was a feature of the ARTEMIS programme to remove volatile by-products and humidity as it has been shown to give reproducible results (Dissado et al, 2000 and Fothergill et al, 2003a).

3.3.3 Electrode design

Figure 3.3.1: HV electrodes set up to start an endurance test.

The HV electrode is a cylindrical brass shape with a radius of 2.5 cm, height of 3.0 cm and rounded edges to minimize corona discharges. The bottom electrode is an aluminium plate with a thickness of 5mm, where up to four HV electrodes can be placed. A good contact was ensured by placing a Perspex glass plate with thickness of 5mm above the brass electrodes and clamping the electrodes down like a sandwich, see Figure 3.3.1.

3.3.4 Sample handling

In the ARTEMIS programme, the same material supplier provided two cable manufactures with the same batch of XLPE resin in order to make EHV cables with insulation thickness of 14mm, as shown in Figure 3.3.2a. Once these cables were electro-thermally stressed, the insulation was peeled down to a thickness of 150μm with a specially designed cryotome. The peelings were rolled into tapes with a width of 8cm as is shown in Figure 3.3.2b and were distributed to the rest of the partners inside polyethylene-bags completely enclosed within aluminium bags, for them to investigate their properties with various techniques as mentioned in (Fothergill et al, 2003a). Once the tapes arrived at the University of Leicester, they were stored in a fridge at a temperature around 5^{o}C in order to prevent any further changes. The properties of the peelings were then investigated using samples taken from between the insulation

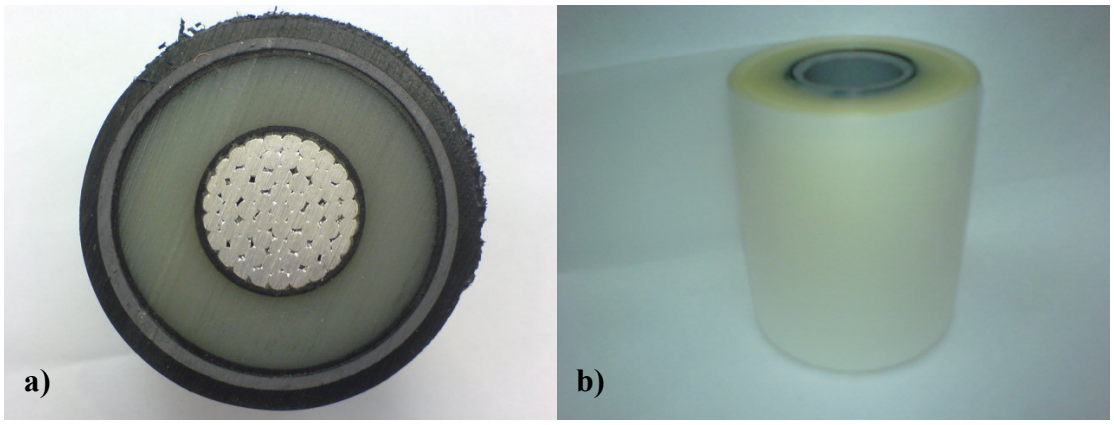

Figure 3.3.2: a) Section of the cable after any kind of stressing during ARTEMIS program and b) a tape roll after the insulation was peeled.

thickness of 2mm to 4mm (or as close as possible to those margins) from the inner semiconductive screen, once they were conditioned as described above.

After the conditioning process described in section 3.3.2 the samples used for the endurances tests **A**, **B** and **C** were placed between the electrodes and immersed in silicone oil as shown in Figure 3.3.1. The tray that is shown in Figure 3.3.1 could accommodate up to three different materials of four specimens each, which means up to twelve specimens. In order to avoid air bubbles being trapped between the specimen and the electrode interfaces the whole tray was placed under vacuum till no bubbles were observed and then was moved to the HV rig. The specimens were not removed from the HV rig till three out of four failures occurred for each material. Once they were removed they were characterised via space charge methods which are presented in chapter 4.

The time to breakdown was recorded by a high voltage circuit breaker with an accuracy of 1/100 of an hour. It should also be noted that once a specimen failed the power was cut off for all the specimens. Once the specimen was identified using a Mega-ohm meter, it was isolated from the high voltage rig, so that the power could be switched back on by carefully ramping the voltage up to the desired value. This means that the failed specimen remained in the tray shown in Figure 3.3.1 till three specimens of all the materials have failed, as removing would disturb the remaining on-going specimens.

3.4 RESULTS AND ANALYSIS

3.4.1 High electrical and thermal stress endurance test A

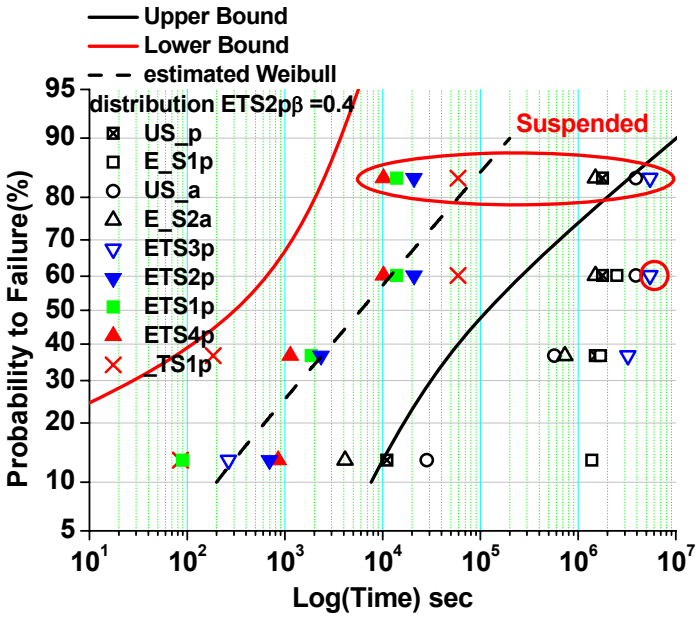

Figure 3.4.1: Weibull distribution for the times to failure from the peelings with different electro-thermal histories as a cable, including data that was obtained during endurance test A_1 & A_2.

The results of the endurance test, which was carried out at an electric field of 70kV/mm and a temperature of 90°C, (Tzimas et al, 2006), are shown in Figure 3.4.1. The estimated Weibull distribution for the samples with the most severe electro-thermal pre-history **ETS2p** is shown by the dashed line, together with its associated 90% confidence limits (continuous lines). The data of the **ETS2p** is represented in Figure 3.4.1 with the filled blue triangle symbol. In Figure 3.4.1, the coloured symbols represent the materials that have been stressed as a cable at 90°C and the black ones represent the materials that have been stressed at 20°C. It can be seen that all the coloured symbols lie within the 90% confidence limits of the most severely stressed material, except for **ETS3p**, for which only its first failure lies within the limits. All the black symbols, which represent materials that experienced no stress or just electrical stress as a cable, lay outside the 90% confidence limits, except the first failure of the electrically pre-stressed material, **E_S2a**. Thus, thermal stressing seems to be the dominating process causing a reduction in endurance life in the ARTEMIS programme. The electric field seems to have no significant effect. The data from the samples with 3000h of pre-history of electro-thermal stressing (**ETS3p**) indicates that this amount of time was insufficient to affect

the material. In general terms, the failures in Figure 3.4.1 can be separated into two groups with very similar statistical properties, one group with the coloured symbols and another group with the black ones.

After the results that are shown in Figure 3.4.1 were obtained from the endurance tests **A_1 & A_2**, another endurance test was conducted under the same conditions to check the validity of the separation into two groups. This endurance test (**A_3**) involved three materials and the Weibull plot of the times to failure is presented in Figure 3.4.2. The aim of this test was to check the statement that thermal stressing is the dominant component responsible for reducing the endurance capability of the material. Hence the materials that participated in this test were two with a thermal pre-history and one with electro-thermal pre-history. The thermally stressed material **_TS1p'** and the electro-

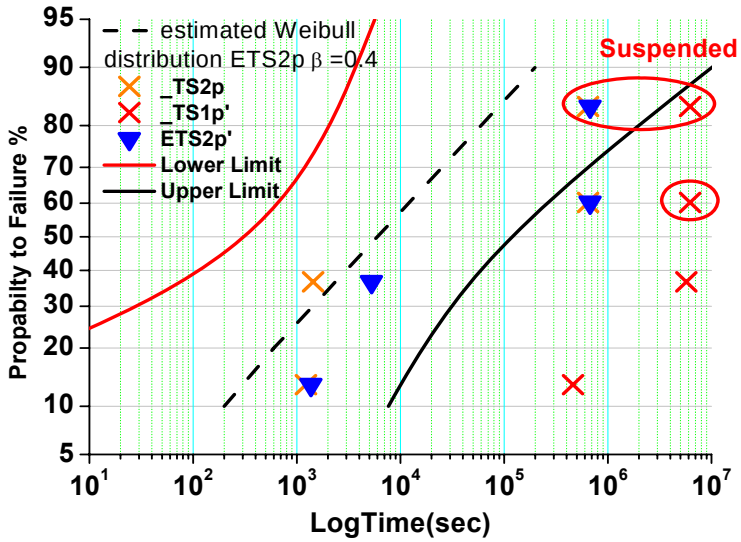

Figure 3.4.2: Weibull distribution for the times to failure from the peelings with different electro-thermal pre-histories as a cable, recorded during endurance test A_3 for three materials; two with thermal pre-histories, _TS2p and _TS1p', and one with an electro-thermal, ETS2p'. The 90% confidence limits are drawn according to the results recorded for ETS2p during the endurance test A_1 for comparison purposes.

thermally stressed one **ETS2p'** were also involved in the previous endurance test, hence the prime indication (') to denote them. The third material, **_TS2p**, was thermally stressed at 90°C for 10000h and was chosen to check how an extra 5000h of stressing affected the endurance capability of the material.

The result of this endurance test show that two out of three failures of the **_TS2p** and **ETS2p'** fall within the 90% confidence limits which were drawn for the results of

ETS2p. On the other hand, the two failures of the **_TS1p'** occurred outside the confidence limits in contrast to the previous endurance test $\mathbf{A_1}$. As the first two failures for the **_TS1p'** were already outside the confidence limits, it was not necessary to continue the endurance test $\mathbf{A_3}$. Hence, two out of four of the specimens of **_TSP1p'** were suspended as is shown in Figure 3.4.2.

The final endurance test $\mathbf{A_4}$ at high field and temperature involved three materials. Two of the materials had experienced only electrical stress as a cable at the same electrical field (**19kV/mm**) but different duration, **7747h** for **E_S2p** and **5581h** for **E_S1a**. The electro-thermally stressed material **ETS2p** was also used in this test, but with samples from a position further away from the inner semicon where the electric field is **25kV/mm** and it is named **ETS2pm**. The aim of this endurance test is to verify that electrical stress did not reduce the inherent endurance capability of the material. The reason for using the **ETS2pm** samples in this test is to check whether there is any difference in the endurance capability of the insulator at different radial distances from the inner semicon. The results of this test are presented in Figure 3.4.3.

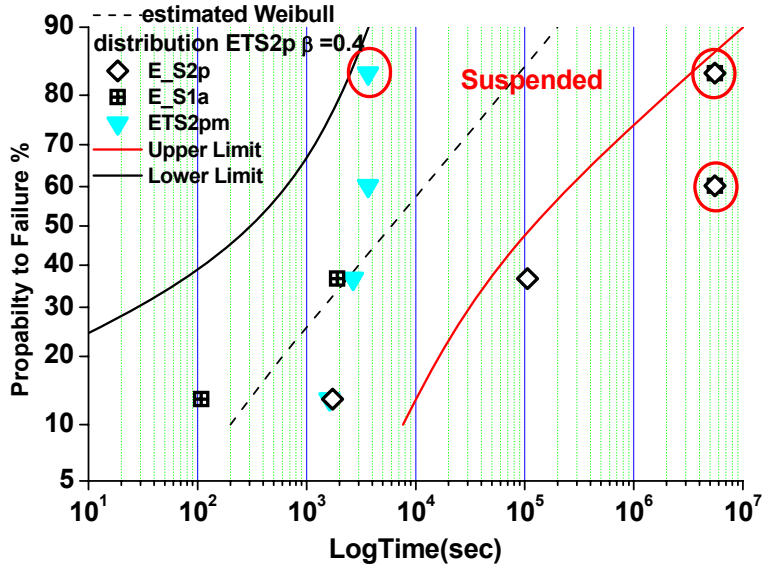

Figure 3.4.3: Weibull distribution for the times to failure from the peelings with different electro-thermal pre-histories as a cable, recorded during endurance test A_4 for three materials; two with electrical stress pre-histories, E_S2p and E_S1a, and one with an electro-thermal pre-history, ETS2pm. The 90% confidence limits are drawn according to the results recorded for ETS2p during the endurance test A_1 for comparison purposes.

According to Figure 3.4.3, three out of six failures of the electrically pre-stressed materials fall outside the 90% confidence limits of the **ETS2p** agreeing with the previous deductions (see Figure 3.4.1) that electrical stress on its own caused no significant reduction in the endurance life. The change of radial position of the insulation samples did not show any statistically significant difference for the electro-thermally pre-stressed material, **ETS2p**. The only difference that could be observed is an increase of the shape parameter **β** from 0.4 to 1.4 and consequently a decrease in the scale parameter α, as is shown in Table 3.5.1. In order to summarise the replicate results of the last two endurance tests, the data is plotted in the same Weibull plot as is shown in Figure 3.4.4. It can be deduced that nine out of the eighteen replicate failures fall in the same statistical group as those in Figure 3.4.1.

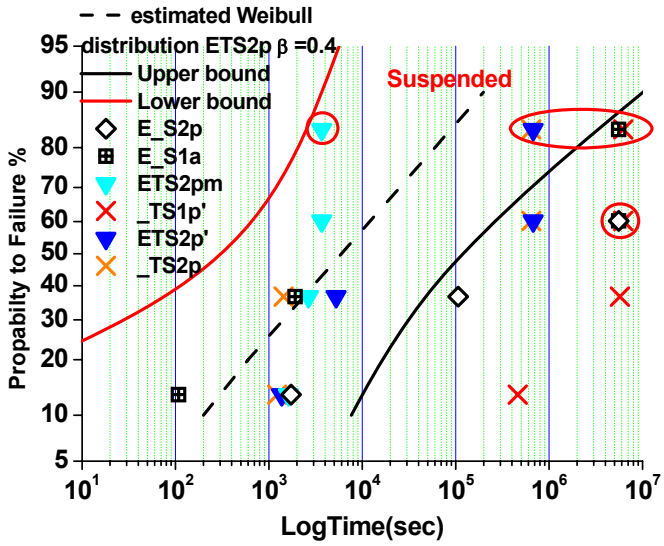

Figure 3.4.4: Data from Figure 3.4.2 and Figure 3.4.3 presented together.

The data points that are shown in Figure 3.4.4 have been obtained from peelings that experienced electrical, thermal and electro-thermal stress as a cable. Most of the failures of these peelings occurred within the 90% confidence limits that were estimated from the data for **ETS2p** shown in Figure 3.4.1, and involved materials that experienced both thermal and electrical stress as a cable. In contrast to the results in Figure 3.4.1 the material that experienced only a thermal stressing pre-history fell significantly beyond the 90% confidence limits at longer times. Furthermore, two out of the four failures of the materials that were just electrically pre-stressed, **E_S1a**, fall within the confidence limits whereas in Figure 3.4.1 almost all fall outside.

3.4.2 High electrical and low thermal stress endurance test B

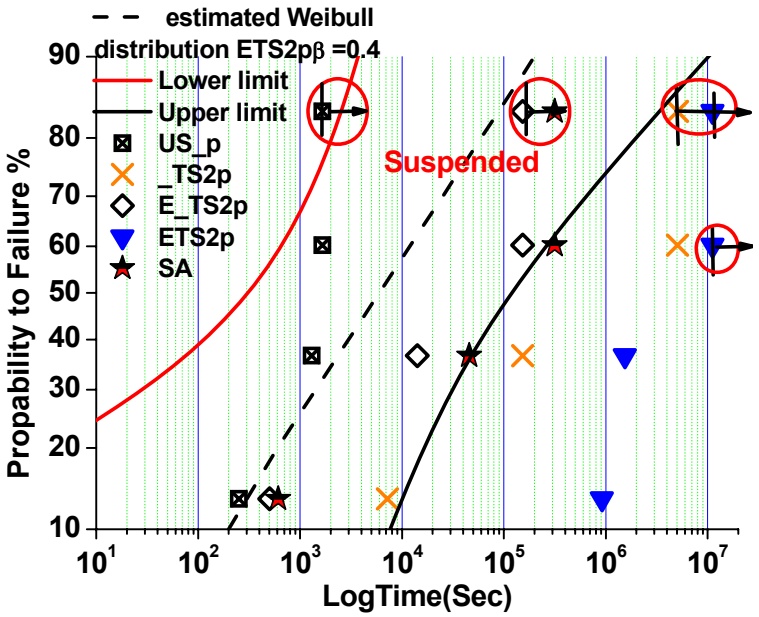

Figure 3.4.5: Weibull distribution of the failures that occurred during the endurance test B at 70kV/mm and 30°C for five materials with very different stressing histories as a cable; an unstressed US_a, an electrically stressed E_S2p, a thermally stressed _TS2p, an electro-thermally stressed ETS2p, and a service stressed SA. Again the 90% confidence limits of Figure 3.4.1 are used.

A further endurance test was conducted at the same electric field, 70kV/mm, but at a lower temperature of 30°C. The aim of this test was to determine the effect of the temperature on the endurance capability of the peelings. For this test, five materials with very different stressing pre-histories were used to check for reduction of the inherent endurance capability. Hence an unstressed, **US_p**, a thermally stressed **_TS2p**, at (**90°C** for **10000hours)**, an electrically stressed, **E_S2p**, (**19.5kV/mm** for **7747hours**), an electro-thermally stressed (**28kV/mm** and **90°C** for **6000hours**), and a service stressed, **SA**, (**18years**), material were put under the test.

Figure 3.4.5 shows the Weibull distribution on the failures that occurred during this test. If these materials would be ranked from this test, the unstressed material would be the worst, then the electrically stressed material would follow, after that the service stressed material, then the thermally stressed material and finally the electro-thermally stressed material. The ranking of these materials is shown more clearly in Figure 3.4.6b in the box and whisker format. However, it should be noted that the samples of the unstressed material were cut from a position of the peeling very near to the inner semiconductor of

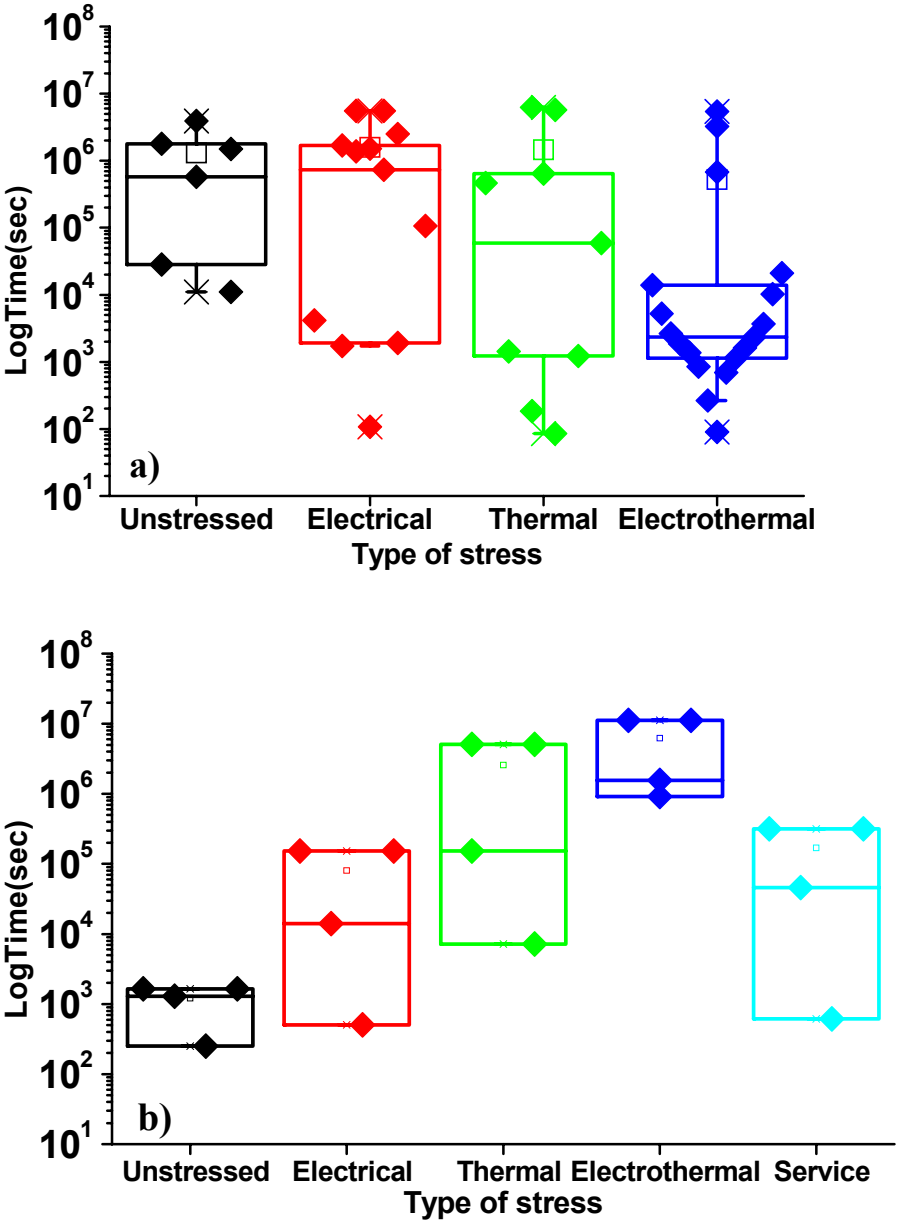

Figure 3.4.6: Box and whisker presentation of all the failures that occurred at 70kV/mm a) at 90°C and b) at 30°C of group of materials not necessary from the same cable but same type of stress as a cable. The box is determined by the 25th and 75th percentiles. The whiskers are determined by the 5th and 95th percentiles.

the cable. Hence, they may have been contaminated by semiconductor penetration into the material, which led them to fail before the other materials. The electro-thermally stressed material lasted the longest in the endurance test at 30°C in contrast with the previous endurance tests at 90°C where the electro-thermally stressed materials showed the most reduction in the inherent endurance capability as is shown in Figure 3.4.6a. From Figure 3.4.6a, it can be deduced that the unstressed and the electrically stressed

materials show the most endurance, with the thermally stressed materials following and the electro-thermal materials showing the least endurance.

3.4.3 Low electrical and high thermal stress endurance test C

This test uses a field of 55kV/mm and a temperature of 90°C, and involves materials with very different stressing pre-histories as a cable. The failures are presented in Figure 3.4.7. Six failures have occurred by 1.8×10^7s, but only five are presented in Figure 3.4.7. The first failure of the service aged material was eliminated because it occurred immediately after switching on the voltage. The only material that has not failed so far is the unstressed material. On the other hand two out of four specimens of the thermally stressed material, **_TS2p**, have failed. Thus so far the effect of the stressing pre-history of the materials upon the endurance life follows that found in endurance test **A** at high field and temperature, where the materials with thermal and electro-thermal stressing pre-history fail sooner than the others.

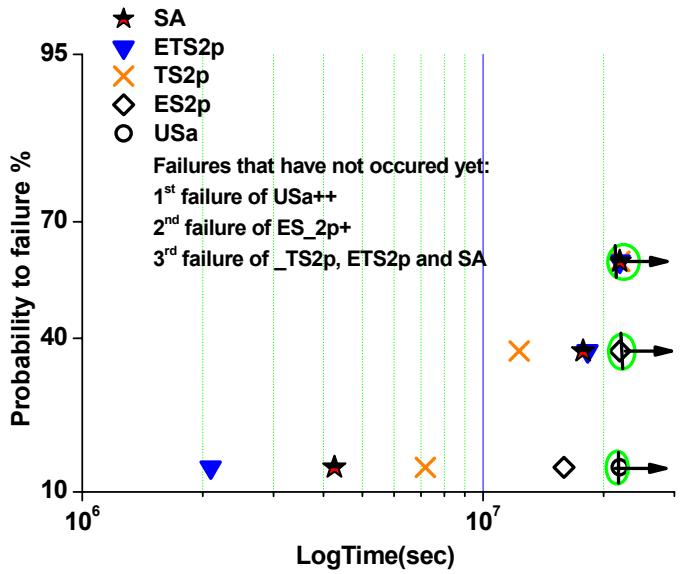

Figure 3.4.7: Weibull distribution for the times to failure, recorded during Endurance test C for five materials with very different stressing histories as a cable; an unstressed US_a, an electrically stressed E_S2p, a thermally stressed _TS2p, an electro-thermally stressed ETS2p and a service stressed SA.

3.5 DISCUSSION AND FURTHER ANALYSIS

The Weibull plots in the previous section exhibit contradictory behaviour for the endurance as can be seen by referring to Figure 3.4.6, where two sets of endurance data at the same field but for low and high temperatures are compared. The endurance data at the high temperature shows that the thermal and electro-thermal stressing experienced

by the material as a cable reduced its endurance capability. According to Figure 3.4.6a the endurance capability of the electrically pre-stressed materials has been reduced only at low percentiles such as the 25th while the other groups of materials show a reduction of the endurance capability at higher percentiles too in comparison with the unstressed material. The greatest reduction of endurance capability is observed for the electro-thermally pre-stressed materials. It should also be noted that the endurance test data **C** (obtained at 55kV/mm and 90^{o}C) agrees with the findings of the endurance test **A**. Mainly specimens with thermal and electro-thermal stressing histories have failed and only one with electrical stressing history. Specimens of the unstressed material did not fail. On the other hand the endurance test at low temperature gave the opposite result, i.e. the failures of the unstressed as well as the electrically pre-stressed material occurred before the failures of the thermally, electro-thermally and even service pre-stressed materials. Consequently a very obvious question arises as to why there is this contradiction in the endurance test results. First of all it should be noted that the unstressed specimens were cut from the part of the tape very near to the semicon, which may have been contaminated causing them to fail more quickly. However, all the other specimens were cut between 2-4mm from the inner semicon. So is there another feature/mechanism that dominates the failures at 30^{o}C but not at 90^{o}C?

In order to give an answer to this question we have to remind ourselves that Weibull statistics is an extreme value statistic and so failure is expected to occur at the weakest link of the system. Hence, any possible weakest links affecting this system need to be identified. Such weakest links may be due to local field enhancement by:

- Defects introduced during manufacturing, i.e. the extrusion process, such as voids due to the volatile by-products, see Figure 3.5.1a, and possibly like the ones in Figure 3.5.1b, which look like hollow tubes. The possibility that the electro-thermal stressing contributed to the creation of these defects cannot be ruled out either as their density increases in the materials that experienced electrical and electro-thermal stressing both as a cable and as a peeling, see Figure 3.5.3 to Figure 3.5.6;
- Defects that developed during the stressing of the material as cable and possibly increased during the endurance tests, perhaps like the ones in photographs taken of specimens that have been under the endurance test **A** and **B**, see Figure 3.5.1 to Figure 3.5.13;

- Defects at the interface of the specimens and the electrodes.

Due to the amorphous nature of polyethylene is very difficult to assign a particular type of defect to a specific origin such as manufacturing or degradation/ageing. However, the size and density of the tubular defects seem to increase in the regions of the specimen where the material has experienced electrical or electro-thermal stressing both as a cable and as a peeling. Moreover the density and size of the voids increases when the material undergoes electrical and electro-thermal stressing, see Figure 3.5.1, Figure 3.5.5, Figure 3.5.6b and Figure 3.5.13b. In the photographs that follow the red circles indicate tubular defects, the green arrows show the largest visible voids that were most probably introduced by the action of electro-thermal stressing during the endurance test. The orange circles indicate defects that may have occurred due to surface deterioration by partial discharges that lead to dendritic structures, see Figure 3.5.7, or a significant increase in the number of voids or tubular defects, see Figure 3.5.3b, Figure 3.5.6b and Figure 3.5.9a.

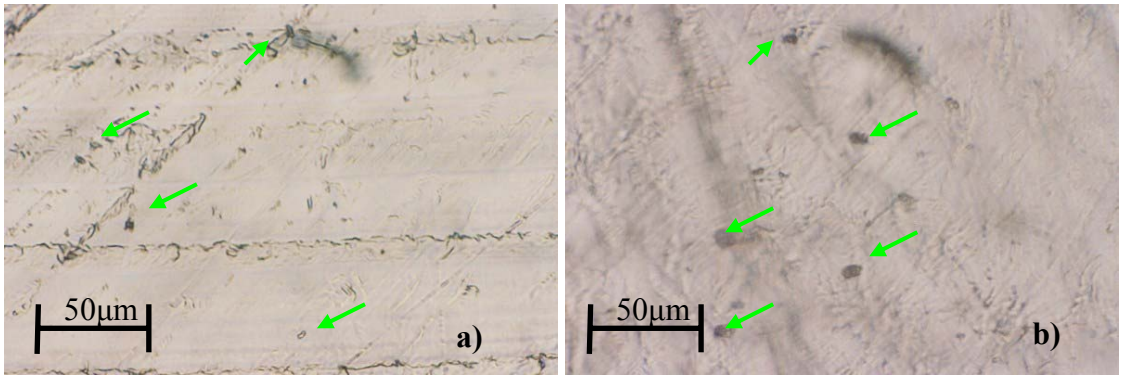

Figure 3.5.1: Photographs showing largest visible voids in XLPE peeling of unstressed material, US_p, taken by an optical microscope; a) outside and b) under the electrode area after the endurance test A. The area under the electrode of this sample has experienced electro-thermal stressing for 496 hours.

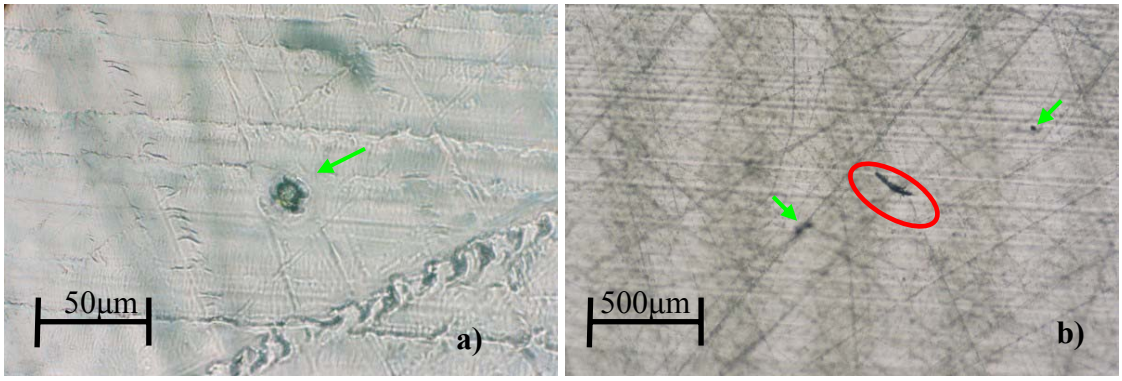

Figure 3.5.2: Photographs showing largest visible voids and defects in XLPE peeling of unstressed material, US_p, taken by an optical microscope after endurance test B; a) outside the electrode area and b) under the electrode area close to where the breakdown occurred. This specimen failed after 0.36 hours.

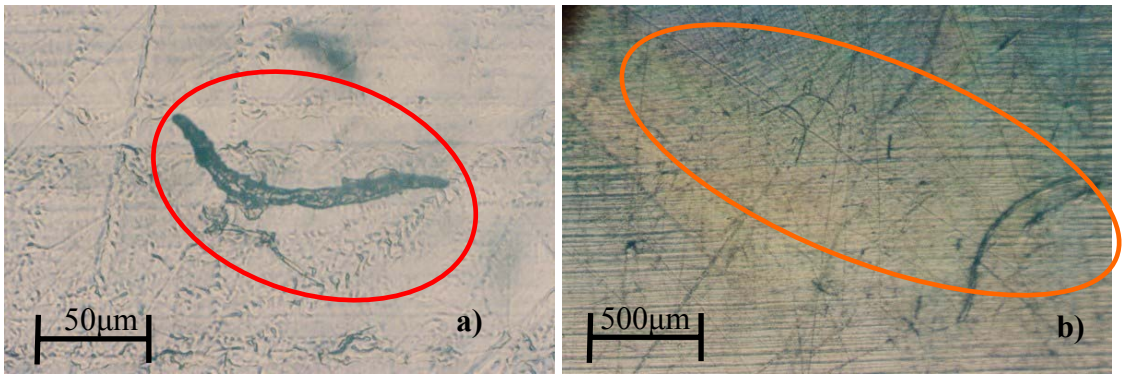

Figure 3.5.3: US_p endurance test A a) opposite edge of electrode experiencing the lower pressure b) edge of electrode experiencing the higher pressure.

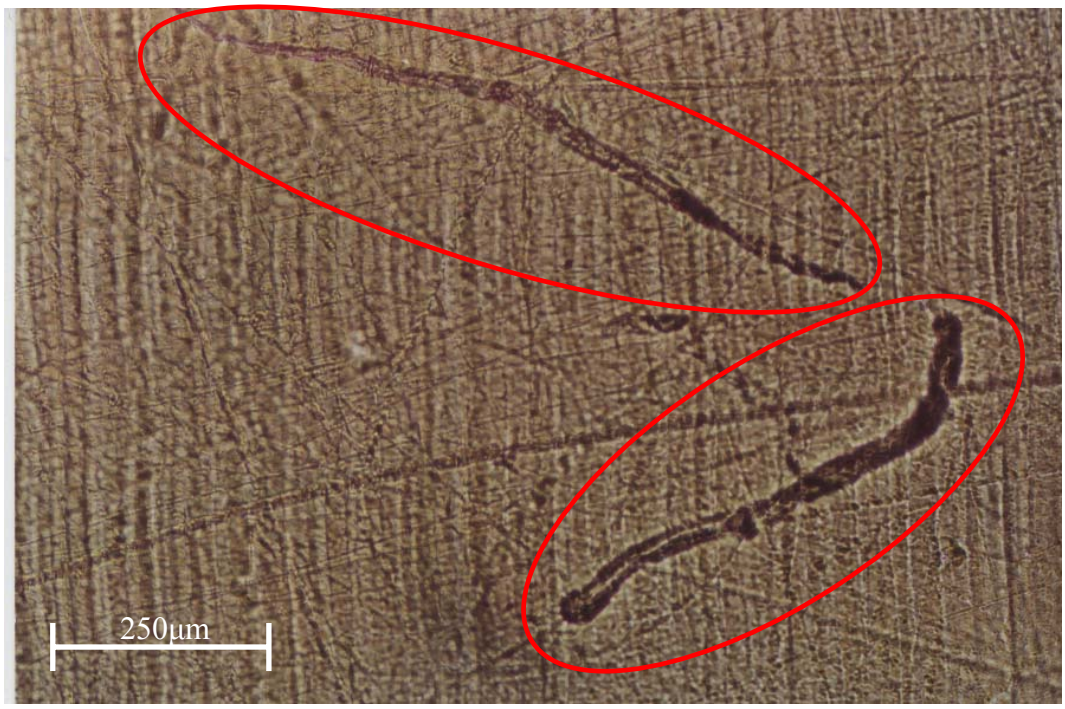

Figure 3.5.4: Photograph showing defects (in red circle) in XLPE peeling, E_S2p, taken by an optical microscope after the endurance test A for 1537 hours under the electrode area. The macroscopic scale of the defects suggests that they were introduced during manufacturing of the cables although the fact that electro-thermal stressing may have contributed to the creation of these defects can not be ruled out.

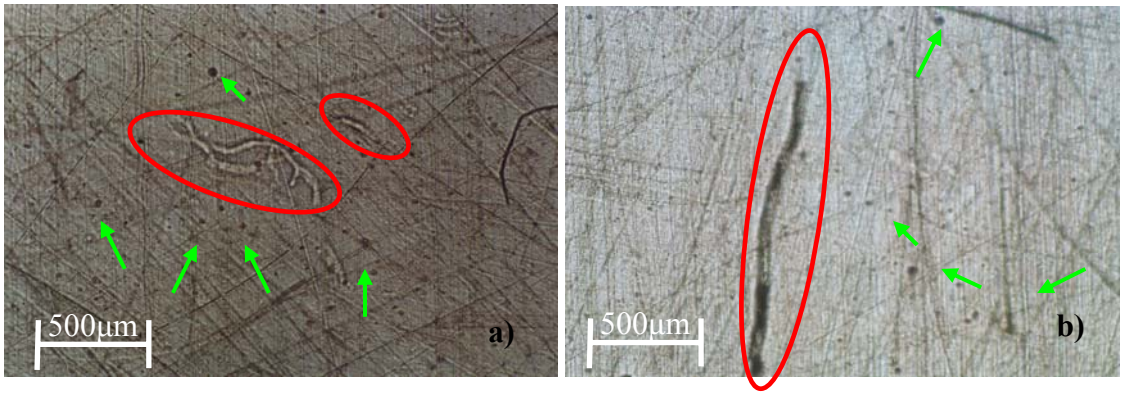

Figure 3.5.5: Photograph taken under the electrode area (near the edge) of E_S2p specimen that participated in the endurance test A for 1537 hours a), and b) under the electrode area near the

edge. The green arrows indicate the largest visible voids and the red circles tubular defects which were most probably introduced with the application of electro-thermal stress during the endurance test.

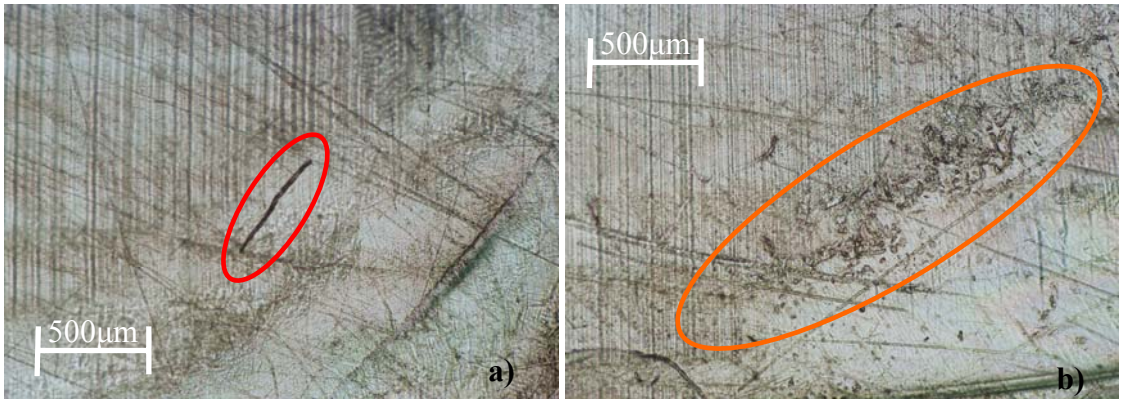

Figure 3.5.6: Photograph of a thermally pre-stressed peeling, _TS1p, near the edge of the electrode area, a) tubular defect, and b) significant increase in the density of voids and tubular defects after 1724 hour in endurance test A_3.

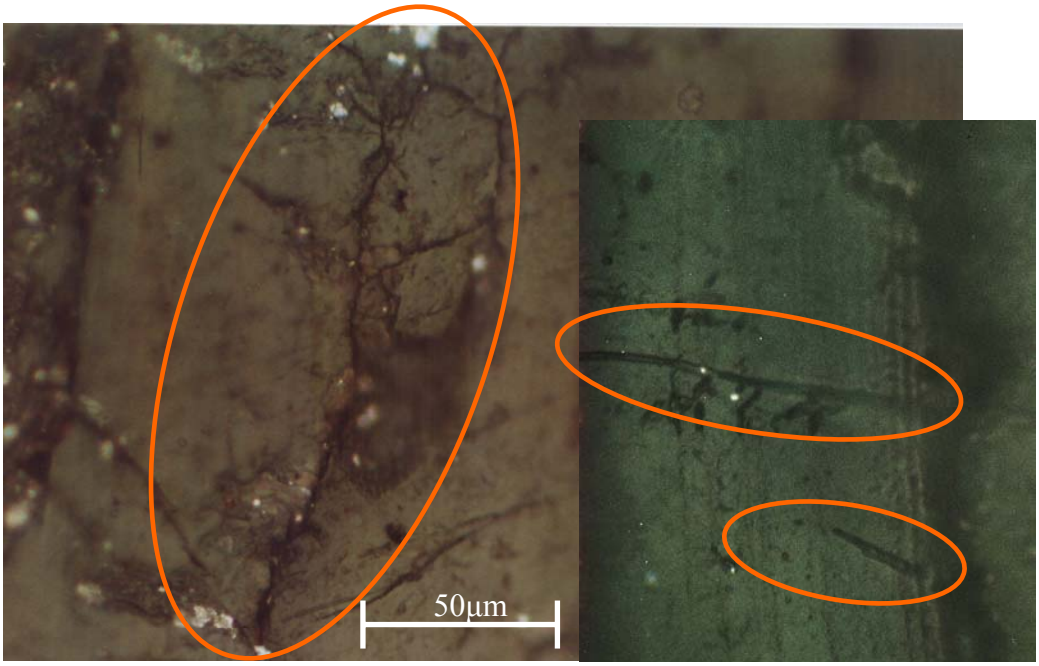

Figure 3.5.7: Dendrite-like deterioration of an E_S1p specimen that took place during 692hours of endurance test A near the edge of the electrode. This specimen showed a space charge double peak discussed further in chapter 4.

Figure 3.5.8: Magnification of a void under the electrode area of E_S2p specimen after the endurance test A for 1537 hour, with micro crack propagation whose long direction is indicated by the green arrow.

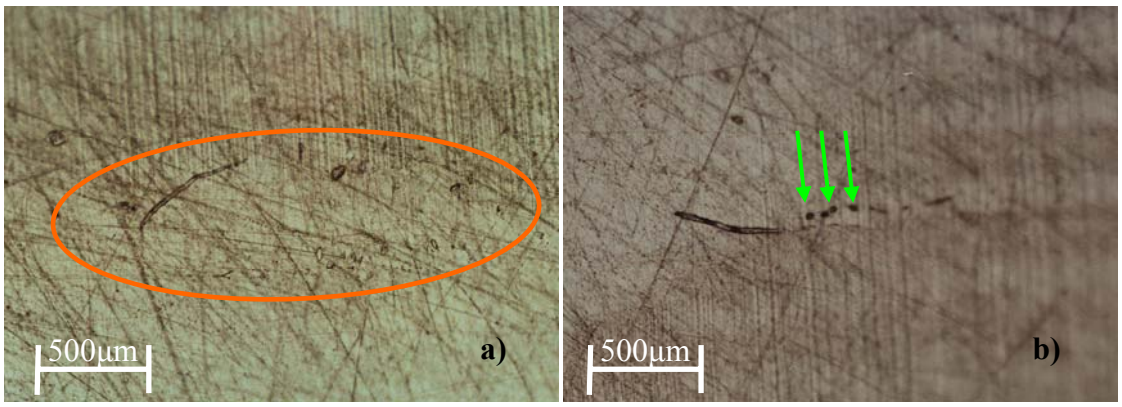

Figure 3.5.9: Void-clusters very close together from under the electrode area (near edge and breakdown) of ETS2p' that failed after 15 minutes of endurance test A.

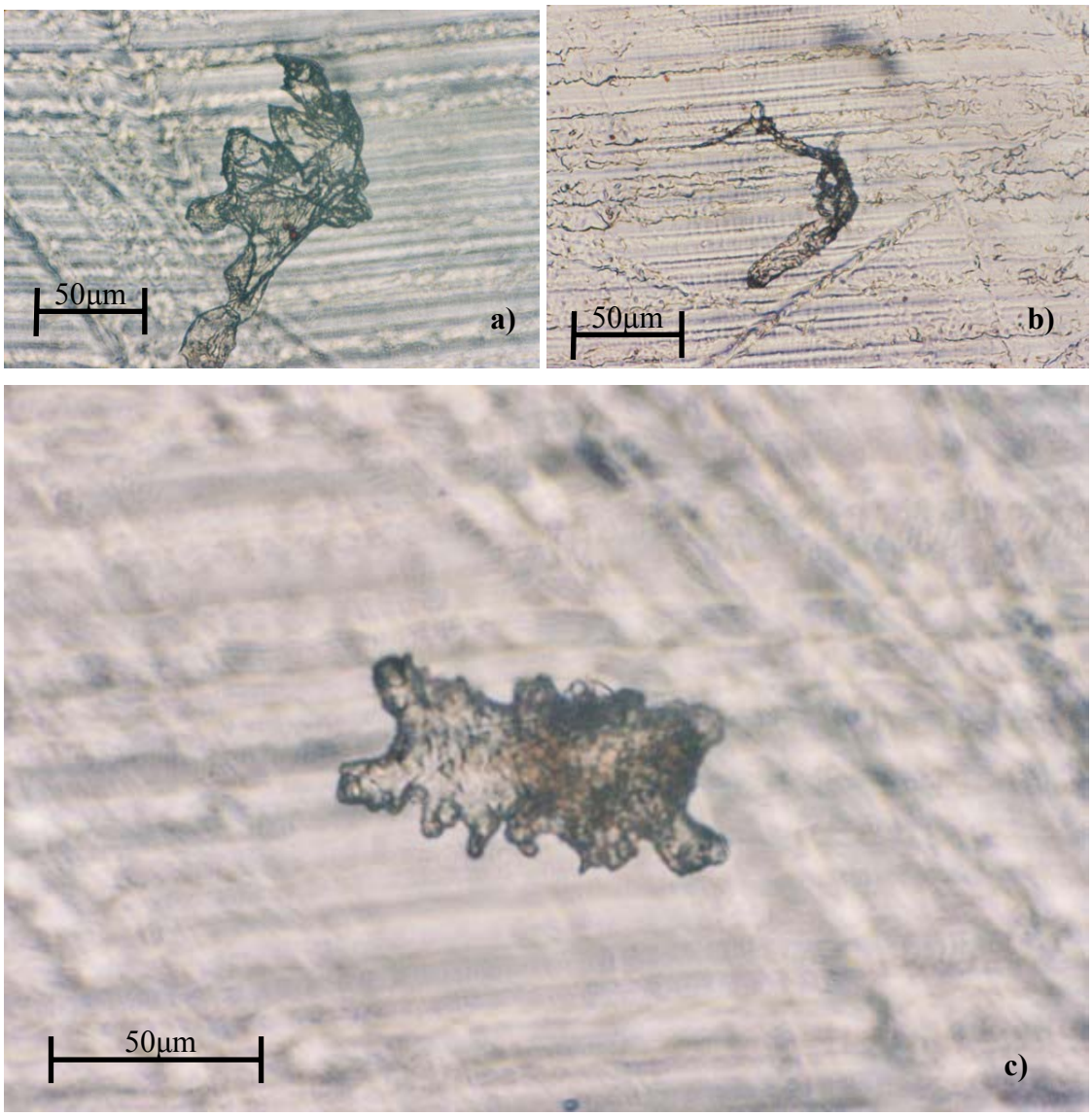

Figure 3.5.10: ETS2p after 3101endurance test A. a) under the electrode area, b) near the edge of the electrode area and, c) outside the electrode area.

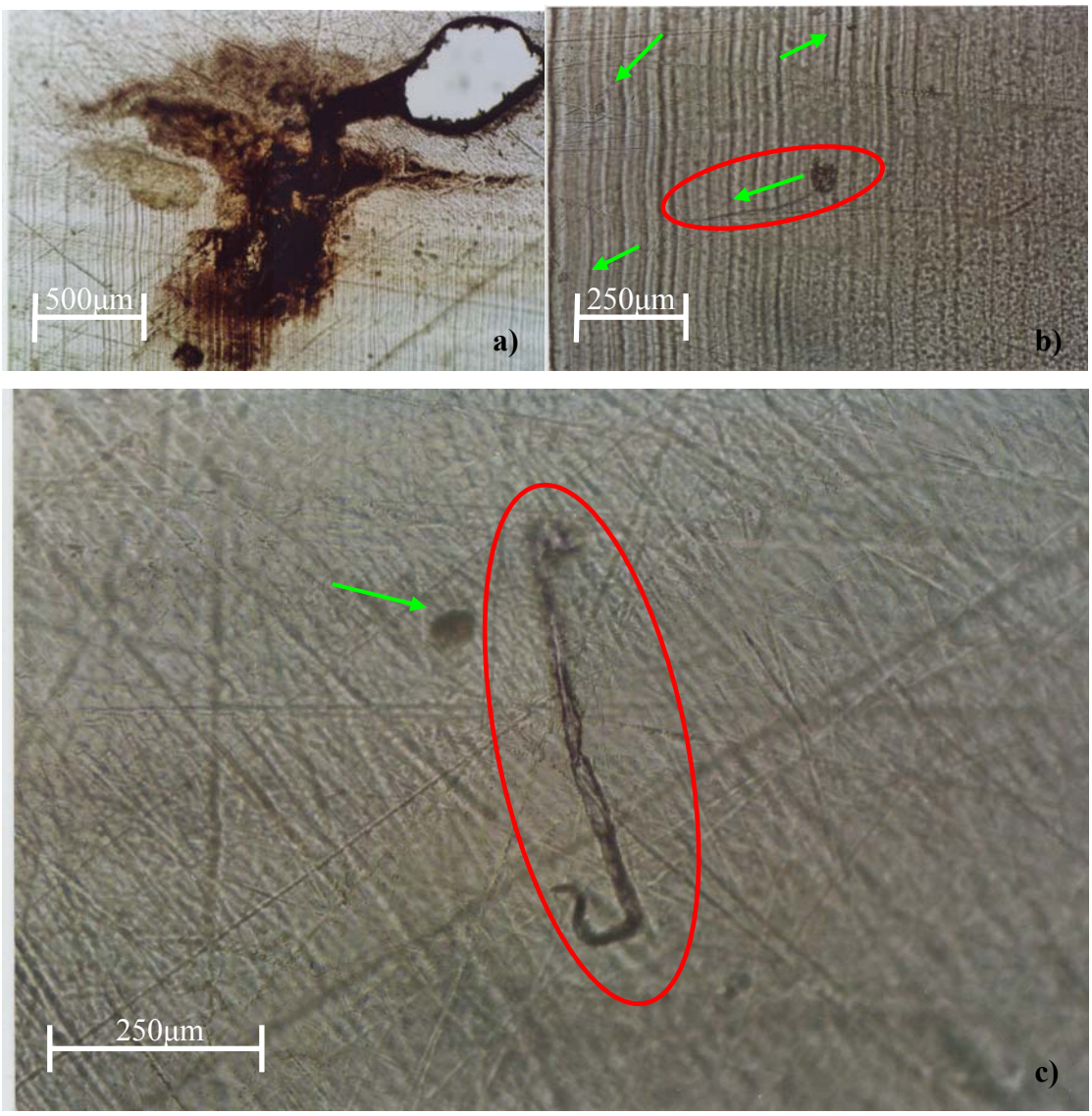

Figure 3.5.11: Photograph taken under the electrode area after the endurance test A of E_S1p, the specimen failed after 697 hours; a) Breakdown with a carbonised tail, b) Void-type defect in the red circle found under the centre of electrode area where the green arrow within indicates the direction of crack propagation-the rest of the green arrows show smaller void-type defects and c) Worm-type defect in red circle with a void indicated by the green arrow all of which lie next to the breakdown.

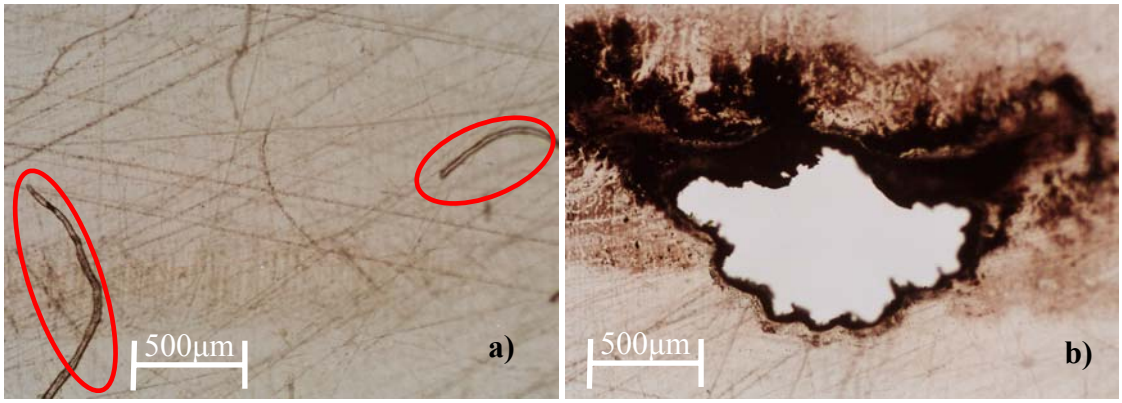

Figure 3.5.12: E_S1a specimen participating in the endurance test A that failed almost immediately after voltage ramp up a) tubular defects near the breakdown and b) breakdown shape that resulted in a carbonised tube.

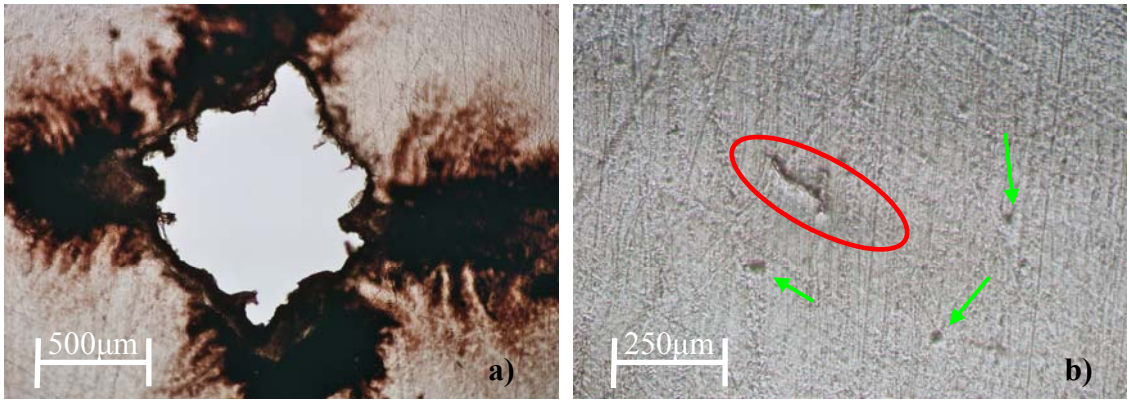

Figure 3.5.13: a) Breakdown possibly due to localised field enhancement of collapsing void clusters that occurred in the endurance test A of a E_S1a specimen after 30 minutes and b) voids and tubular defects not far from the breakdown region.

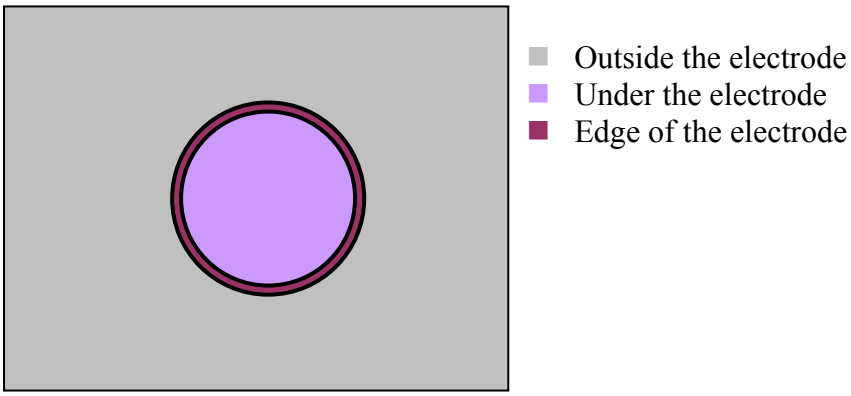

Figure 3.5.14: Schematic diagram of a typical sample and the areas that were observed via optical microscopy. The darkness of the colour filling an enclosed area indicates the relative concentration of defects (Dark =high concentration, Light =low concentration).

From the microscopic observations it was found that the number of voids was greatest under the electrode area and especially on the edge of the electrode where the mechanical force from the clamp could have been greater, see Figure 3.5.14. The visible voids under the electrode area of the unstressed material, **US_p**, also seem to be bigger in size in comparison with the ones observed outside that region which agrees with the idea that ageing causes void expansion.

The distribution and density of these defects, as is shown by Dissado (2002a) for tree lengths for instance, can be expected to determine the shape and scale parameters of the Weibull function for breakdown times as was demonstrated for water trees by Dissado (2002a) for example. As can be seen in Table 3.5.1 where all the shape parameters for the individual material are calculated with the method described in (Fothergill et al, 2003a), most of the values of β are around or below $\beta = 0.5$, although it should be noted

that the confidence limits on β are very wide so it is not certain that the true value of β is so low. This value of the shape parameter gives a Weibull distribution density function without a peak whose shape is shown in Figure 3.1.1, which means that the sample is more susceptible to failure at the beginning of its life. This form of statistic is known as "infant-mortality". As stated by Chan & Meeker (1999) the specimens with manufacturing defects will usually lead to an infant-mortality failure early in their lifetimes whereas the non-defective specimens will eventually fail from degradation/ageing of the matrix of the material. The observation of several relatively gross defects in the specimens under test and the infant mortality nature of the estimated Weibull exponent indicate that the failures in the endurance test may be defect-generated. In this study the materials used are from the same manufacturer in most cases and from the same material supplier. Hence, the differences in the endurance capability must be assumed to be due to defects that were introduced into the material during cable manufacture or during stressing as a cable.

Long tubular defects were found in samples of some of the electrically stressed samples (**E_S1p** and **E_S2p**) that survived for long times (~$5x10^6$sec) as is shown in Figure 3.5.4, Figure 3.5.5 and Figure 3.5.11. However, this type of defect has also been observed in the early failures of these materials very close to the breakdown region as is shown in Figure 3.5.13b and Figure 3.5.12a, where it can be suggested that the early failures of the materials occurred because of the existence of similar shaped defects. Microvoids were also found, sometimes in clusters, which it has been suggested are involved in ageing via coalescence by Dissado et al (2000) or the formation of percolation structures by Wu K. & Dissado (2004a). These appear to lead the electro-thermally pre-stressed, **ETS2p'**, material to fail early, see Figure 3.5.9. This finding suggests that the long tubular defects may have formed during the stressing of this material as a cable, possibly by coalescence of strings of small voids introduced during manufacture such as can be seen in Figure 3.5.9. On the other hand, Figure 3.5.10a and 3.5.10b show defects under the electrode area of a specimen from the same material, **ETS2p**, that lasted for 3101 hours under the endurance test **A** and are possibly a result of that test. Figure 3.5.10c shows a void type defect outside the electrode area that may have been introduced either during manufacture or cable stressing.

The difference in endurance capability of the peelings from cables with an electro-thermally and unstressed pre-history under the endurance test **A** conditions is shown in Figure 3.5.15. The data for each set in Figure 3.5.15 is a collation of data points from peelings that were not taken from the same cable/tape but had all experienced the same type of stress, in this case electro-thermal stress and zero stress. The suspended samples of each material set are censored. Both types of materials have very similar shape parameter values, denoted on the figure as "beta", but clearly very different characteristic values $\boldsymbol{\alpha}$, denoted on the figure as "eta". Consequently all materials can be compared together by plotting the 90% confidence limits of the parameter $\boldsymbol{\alpha}$, known as the characteristic life of the material, see Figure 3.5.16.

This plot implies that the electro-thermal stressing carried out during the Artemis programme did in fact alter the endurance capability of the materials with respect to the unstressed ones. The three electro-thermally pre-stressed samples in Figure 3.5.15 that fall closer to the unstressed ones at the higher percentiles might therefore be related to specimens where the electrode areas happened to surround less severe defects when they underwent their endurance test than occurred in the other cases.

On the left hand-side of the black vertical line in Figure 3.5.16 the characteristic values are for materials with either unstressed or solely electrical stress histories as a cable and have very similar characteristic values. Materials with thermal and electro-thermal histories are shown on the right hand side of the black line and can be seen to have characteristic values that generally are less than those to the left. There are two materials encircled in black whose characteristic values are similar to the unstressed ones, and are therefore exceptions to the general trend. There are also materials with narrow confidence limits, which show a consistency in the distribution of "weak links", i.e. defects. One of these has a short lifetime which suggests that it contains many severe defects of the same type, whereas the other is an exception to the general trend and hence has hardly any defects.

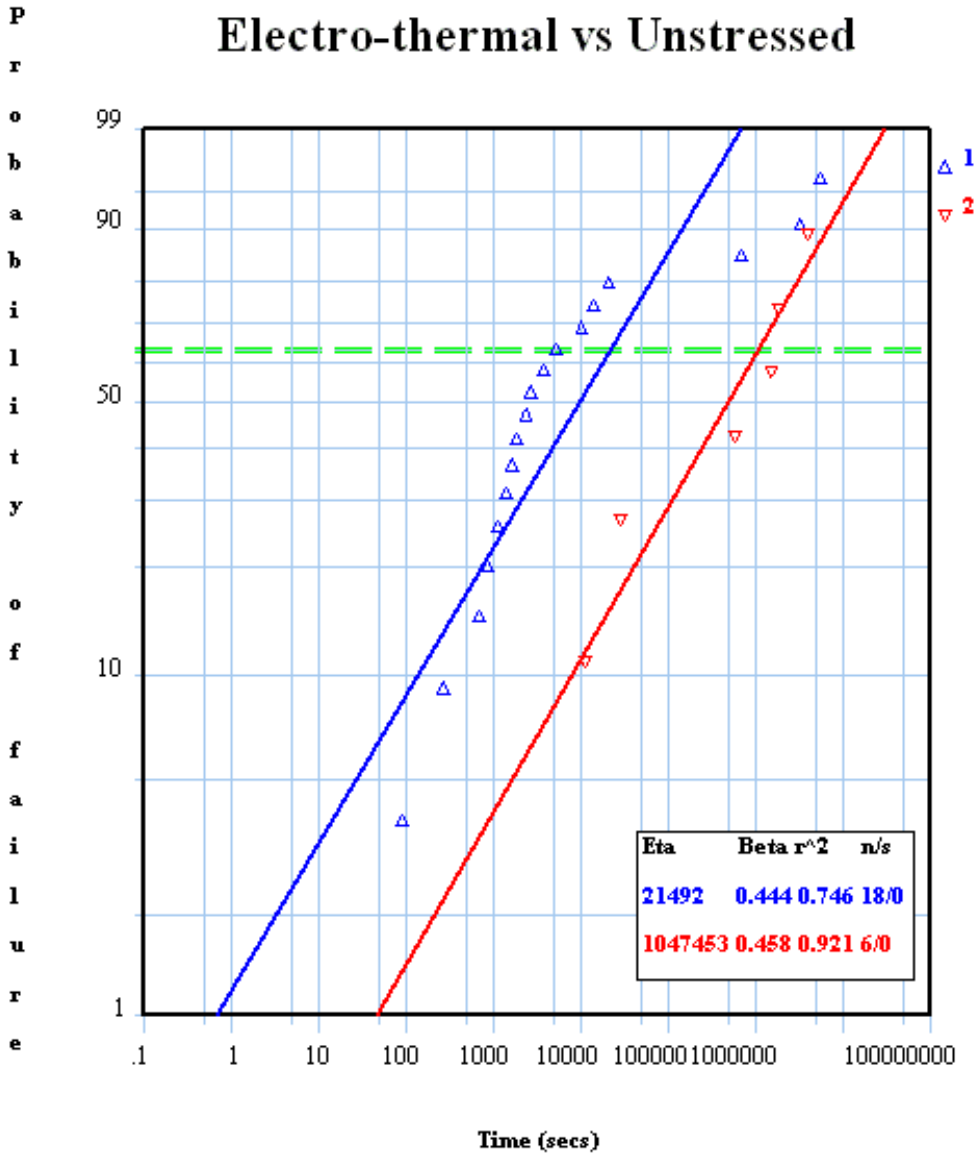

Figure 3.5.15: Comparison of the electro-thermally pre-stressed (in blue) and unstressed (in red) failures that occurred during endurance test A plotted by an evaluation software package, Relex Architect 2007.

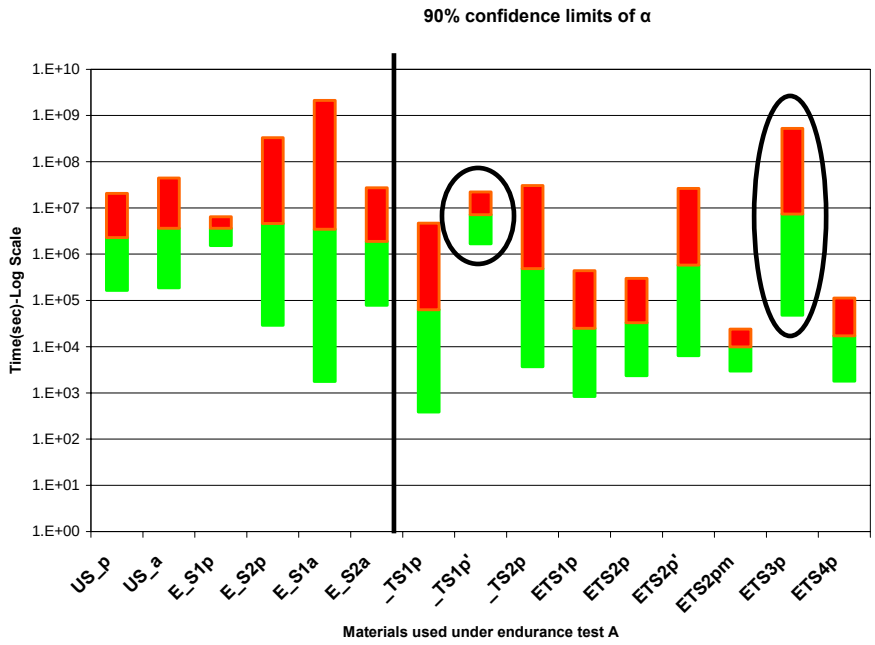

Figure 3.5.16: 90% confidence limits for the scale parameter *α*, commonly known as the characteristic value. The horizontal line is the estimated value of *α* and is the separation point between the green and the red boxes.

Rank according to Beta (β)	Ref. Name	Beta β	α alpha (seconds)
1.	E_S1p	3.650	2.112E+06
2.	ETS2pm	1.384212	6.911E+03
3.	_TS1p'	0.982943	5.519E+06
4.	ETS4p	0.544918	1.537E+04
5.	US_p	0.458	2.122E+06
6.	ETS2p	0.456	3.057E+04
7.	US_a	0.401	3.452E+06
8.	E_S2a	0.374	1.807E+06
9.	ETS1p	0.347	2.402E+04
10.	ETS2p'	0.260	5.767E+05
11.	_TS2p	0.240	4.839E+05
12.	ETS3p	0.232518	7.328E+06
13.	E_S2p	0.231	4.556E+06
14.	_TS1p	0.230	6.252E+04
15.	E_S1a	0.154	3.470E+06

Table 3.5.1: Ranking of the materials according to the shape parameter, β, of the Weibull distribution function.

The reduction in the endurance of the unstressed and electrically stressed specimens on going from a high temperature (T=90^{o}C) to a lower temperature (T=20^{o}C) at a field of E=70kV/mm, was unexpected. This feature does appear in the life expressions plotted in Figure 5.2.1, but corresponds to an unphysical extension of the theory to negative activation energies. In reality the failure time is likely to become essentially independent of temperature in this region of field, see Figure 5.2.1. The result obtained here may be caused by the presence of untypical samples containing defects in the limited region that is under the electrode.

3.6 CONCLUSIONS

The endurance test **A** at 70kV/mm and 90^{o}C suggests that:

- for the first 5000h of electrical and electro-thermal stressing only cables that experienced a thermal component (T = 90 °C) showed evidence of significant ageing as expressed through a reduction in endurance life at 70kV/mm and 90°C;
- for the same time of cable stressing there was no significant difference in endurance between samples from cables with different applied electrical fields, in the range from zero up to the maximum of 28kV/mm. This was found to be the case for both cables stressed at 90 °C and 20 °C.

The endurance test **C** at 55kV/mm and 90^{o}C agrees with the statements made from endurance test **A**.

The optical microscopy study shows that both voids and tubular type defects increase when the material is subjected to electrical and electro-thermal stress both as a cable and as a peeling.

4 CHAPTER: CHARACTERISATION OF THE ARTEMIS PEELINGS BEFORE AND AFTER THE ENDURANCE TEST

4.1 INTRODUCTION

The development of diagnostic tool that could assess the state of an insulator and predict its design life time for new HV cables and its remaining life time for the existing cables is essential. The investigation carried out in this chapter is designed to determine how the space charge behaviour evolves in XLPE peelings when they experience high electro-thermal stressing. It is believed that localized enhancement of the electric field can lead an insulation to failure. A measurable feature of the insulator that could cause electric field enhancement in a dielectric is the space charge built up. The space charge measurements provide us with information on the capability of the dielectric to accumulate charge that can be injected and transported. The polarity of the space charge that is injected and transported in the insulator can also be determined and consequently how the electric field is modified. The ability of the material to inject and transport space charge depends on the material properties such as morphology, crystallinity, free volume and chemical residues during polymerization (Dissado and Fothergill, 1992). Hence, ageing of the materials can be defined as a change of its properties with a reduction of its life as a consequence. As demonstrated in chapter 3 with the endurance tests at elevated temperatures and electric fields, electro-thermal pre-stressing of XLPE insulation as a cable resulted in reduction of the materials endurance life. An investigation is carried out in this chapter on how the space charge behaviour has been affected by the further electro-thermal stressing experienced by the peelings.

It has been demonstrated by Montanari (2000), G. Chen et al (2001, 2003 and 2004), Y.L. Chong et al (2004a, 2004b, 2005 and 2007), Abou-Daka et al (2004), Dissado (2006) and others (in “Space Charge in Solid Dielectrics” edited by Fothergill and Dissado, 1998) that space charge measurement is a sensitive technique to identify changes of the material properties, and that it could be used as an ageing marker by Fothergill et al (2003). It has been, though proved, very difficult to assign the changes that are being observed to a modification of the material property and thus to the life reduction of the materials, as observable changes may occur once the material life is very close to its end (Dissado, 2006). Hence, extensive studies have being carried out in

order to understand the space charge mechanism and use it as an ageing marker and develop life models that could predict the materials lifetime (Montanari 2000, Dissado et al 1997, 2001a and 2001b, Dissado 2002). The investigation that is carried out here aims to point out changes that occurred in the space charge behaviour before and after the endurances tests described in chapter 3 and explore the possibilities that could be used as an ageing marker.

4.2 PEA EXPERIMENTAL PROTOCOL AND SET UP

The experimental set up used in this section for the PEA measurement is exactly the same as the one described in chapter 2 and by Tzimas et al (2005). The space charge profiles presented in this section, in most cases, was obtained following the same protocol that is described in chapter 2. In some cases the charge in the material resided in very shallow trap depths and a great fraction of that charge escaped before measurement in transient volt-off (voltage off) conditions was made. Consequently space charge distributions were also derived by subtraction of the volt-on (voltage on) measurement at the zero time of stress (immediately once voltage is ramped up to the desire value) and the following volt-on measurements. Hereafter, these measurements are referred to in the text as "**volt-on**". On the other hand, the space charge accumulation measurements that are taken by transiently switching the voltage off and then back on are referred as "**volt-off**". The space charge measurements presented are volt-off measurements unless it is stated in the figure caption or text that they are volt-on. Nevertheless, all the space charge profile figures presented in this section regardless whether they are referring to accumulation or decay show the change in space charge density over time with the capacitive charge present on the electrodes during poling removed. The electrode that is the anode during dc poling is indicated on the figures. The decay of the space charge profile is measured immediately once the voltage is switched off and at subsequent times. Both the space charge accumulation and decay measurement times depend on how the charge changes with time. Hence, these times vary from sample to sample. The dc poling voltage was kept at 7.5kV during all the space charge measurements. As the thickness of the peelings is 150μm, this poling voltage produces an electric field of 50kV/mm.

4.3 CHANGES IN THE SPACE CHARGE BEHAVIOUR INTRODUCED BY THE ENDURANCE TEST

This section consists of changes in the space charge behaviour of the peelings before and after the electro-thermal stressing that they experienced under the three endurance test conditions described in chapter 3. Table 4.3.1 shows the endurance tests conditions and their durations. In the following subsection only the space charge profiles of the specimens that show a change in comparison with their profiles before the endurance tests are presented. Those specimens that are not included in the following subsections gave space charge profiles indistinguishable from the ones measured before the endurance test presented in chapter 2. Most of these were the specimens whose failures occurred early in the endurance test.

Endurance Test	E-Field AC (kV/mm) $_{rms}$	Temperature (^{o}C)	Test duration (hours)
A_1	**70**	**90**	**24**
A_2	**70**	**90**	**1507**
A_3	**70**	**90**	**1725**
A_4	**70**	**90**	**1537**
B	**70**	**30**	**3103**
C	**55**	**90**	**6088**

Table 4.3.1: Endurance tests conditions and durations.

The endurance tests **A** and **C** were carried out at high electric field and high temperature, see Table 4.3.1. The space charge profiles were measured both under the electrode area and outside it. The changes that were introduced by the influence of the electric field and the temperature component over the time until the specimen failed or was suspended were observed by measurements on the region under the electrode area. On the other hand, measurements made on the region outside the electrode area showed the changes that were introduced by the influence of the temperature component only. It should also be remembered that the failed specimens remained in the test rig until all the required specimens have failed. Consequently, the area under the electrode has undergone electro-thermal stressing until the failure occurred and just thermal stressing thereafter according to the conditions of the endurance test at the time. Measurements were made on the regions both inside the electrode area and outside so as to distinguish the effect of the electro-thermal stress from the purely thermal stress.

4.3.1 Space charge profiles before the endurance tests

Figure 4.3.1 recalls the behaviour of the space charge during accumulation of materials that experienced different electro-thermal stresses as a cable and were characterised in chapter 2. The main feature that characterises all the Artemis materials regardless of the pre-stressing condition is the negative and positive homocharge injection and

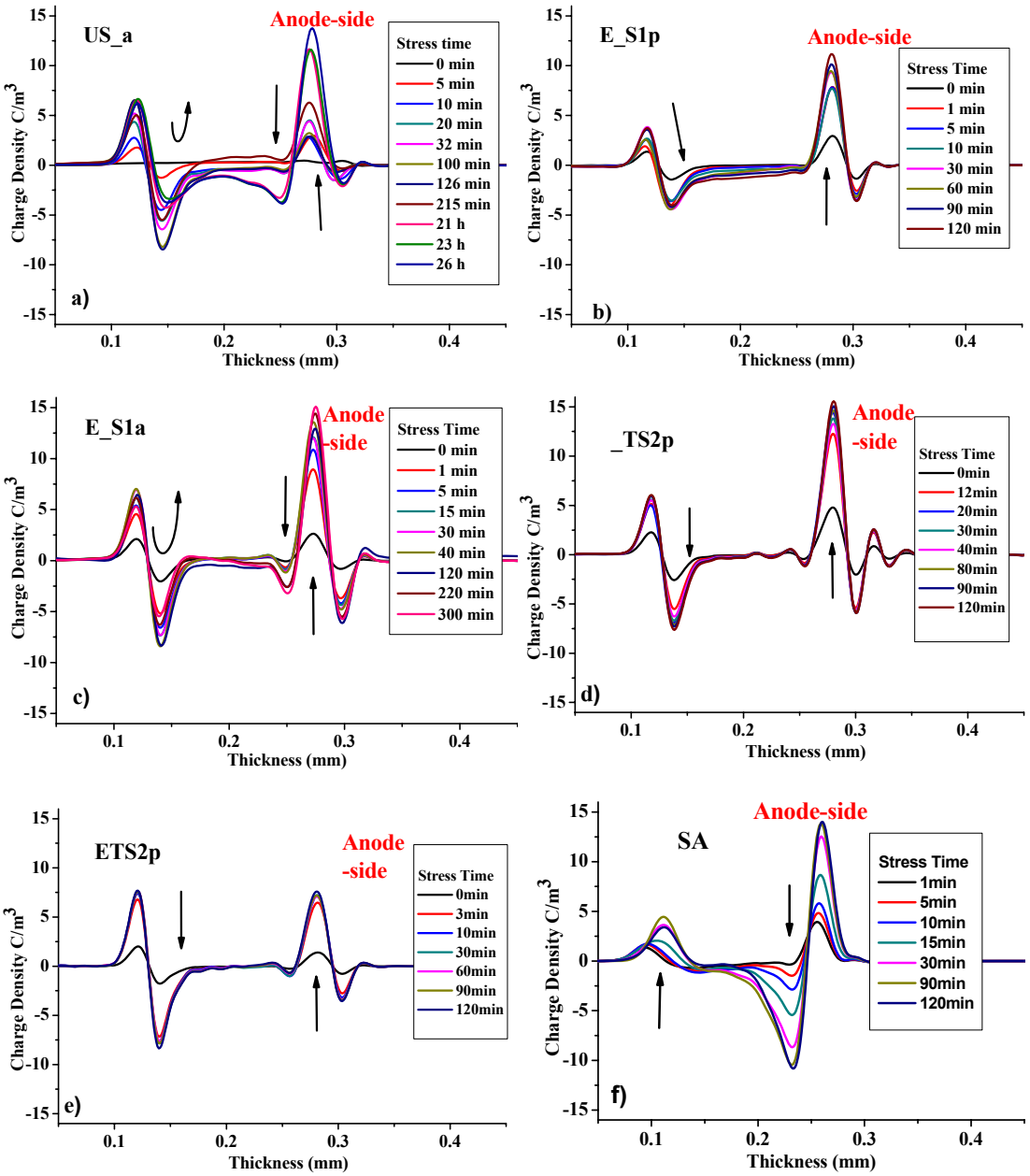

Figure 4.3.1: Space charge profiles obtained before the endurance tests during accumulation at 7.5kV for; a) an unstressed material, US_a, b) and c) two electrically stressed materials from different manufactures, E_S1p and E_S1a respectively, d) a thermally stressed material, _TS2p, e) an electro-thermally stressed material, ETS2p, and f) a serviced aged material, SA.

accumulation adjacent to the electrodes. Negative charge is also injected into the serviced aged material, **SA** Figure 4.3.1f, but in this case it transits rapidly to the anode

where it accumulates. It was also observed that negative charge transit to the anode occurs in the Artemis materials as is shown in Figure 4.3.1a, b and c for the unstressed and electrically stressed materials. In the Artemis peelings however, the transport occurs at a slower rate and involves smaller magnitudes than in the **SA** material.

4.3.2 Endurance test A (70kV/mm, 90°C)

As is reported in chapter 3 a wide range of peelings with different electro-thermal histories as a cable were used for this endurance test. The failures in this test range from within few minutes up to fifteen hundred hours. The space charge profile measurements of specimens that survived the endurance test for the longest times are mainly presented here as the material's properties are more likely to be altered. These are mainly specimens that experienced electrical stress or no stress at all as a cable.

(a) Unstressed peelings after the endurance test

The space charge profile from under the electrode area of the first failure of the unstressed material after the endurance test **A** does not change significantly during a dc poling duration of 120 minutes, and its consequent decay occurs quickly, see Figure 4.3.2. During the decay measurements it can be observed that some positive charge has built up in the bulk while the voltage was on but the overlay of negative charge did not make it possible to see it. Figure 4.3.3 shows the influence that 1083 hours of thermal stressing had on the space charge behaviour measured outside the electrode area of the specimen where the first failure occurred. Negative charge is injected from the cathode during accumulation of space charge, Figure 4.3.3a, and thermal stressing seems to have increased the magnitudes of the space charge density by about 50%. In both regions

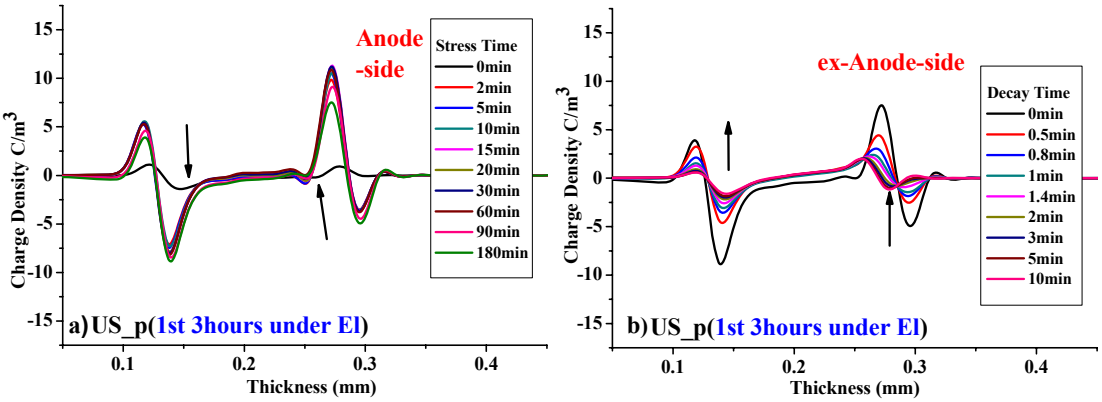

Figure 4.3.2: Space charge profile obtained under the electrode area after the endurance test A for the first failure of the unstressed material US_p; a) accumulation and b) decay. The parenthesis in this figure as well as in the following ones contains information on which failure of the sample set the figure refers to; the time to that failure and the location where the space charge profiles are being observed, i.e. under the electrode area (under El) or outside (out El).

most of the charge escapes the specimen within four minutes and the charge that is retained thereafter decays very slowly. For instance there is only a very small decrease of the negative and positive charge between the sixty fifth minute and two days of depolarization of the outer region. This observation suggests that the fraction of the charge that got retained after the fourth minute of decay resides in deep traps with depths estimated in chapter 2 to be ≥**1.05eV**.

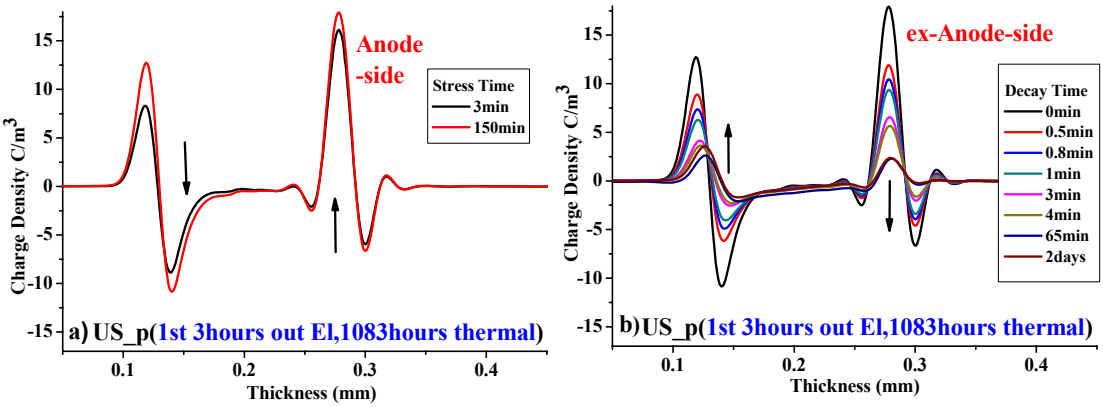

Figure 4.3.3: Space charge profile obtained outside the electrode area after the endurance test A for the first failure of the unstressed material US_p; a) accumulation and b) decay.

Measurements under the electrode area of the third failure of the unstressed material, **US_p** that occurred after 497 hours of electro-thermal stressing, Figure 4.3.4a, show that negative charge injection is observed throughout the 120 minutes of poling, which was not the case in the specimen where the first failure occurred, Figure 4.3.2a. In this case the injection rate of negative charge is probably higher than the positive one. The negative charge that has penetrated further into the bulk of the material, Figure 4.3.4b, decays very slowly in contrast with the negative charge adjacent to the electrodes which escapes/neutralises within the first two minutes. On the other hand when the same specimen is further poled for 135 minutes, Figure 4.3.4c, both negative and positive charge that is injected could be observed to penetrate further into the bulk from the cathode and anode respectively. In this case the decay occurs at a slower rate for both negative and positive charges as more that 30% of the charge is retained after the eighth minute while in the previous case 70% of the charge has escaped within the first minute of depolarization. Very similar space charge behaviour is also observed for the other unstressed material, **US_a**, thus its space charge profile is omitted.

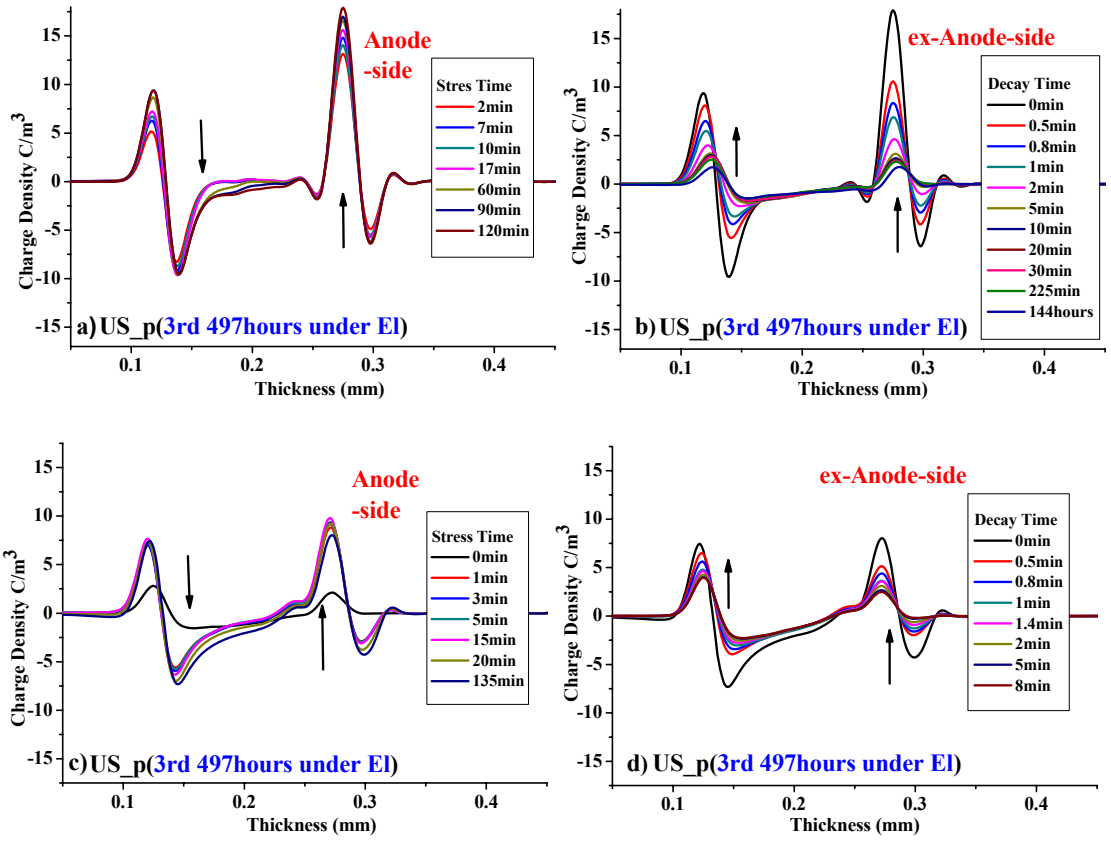

Figure 4.3.4: Space charge profile obtained under the electrode area after the endurance test A for the third failure of the unstressed material US_p; a) accumulation during 120 minutes, b) decay, c) consequent accumulation for further 135 minutes and d) decay.

(b) Electrically pre-stressed peelings after the endurance test

The electrically pre-stressed peeling showed good endurance ability under high electro-thermal stress, especially the **E_S2p** (19kV/mm for 7747 hours) and **E_S1a** (19kV/mm 5581 hours). The duration of the endurance test $\mathbf{A_4}$ was dependent on the time-to-failure of the third sample. The third failure for both the materials did not occur till 1537 hours, thus two specimens (noted by $\mathbf{ss_a}$ and $\mathbf{ss_b}$) of this test have been suspended. The space charge behaviour of these two materials is extensively analysed in this section in order to gain a better understanding of the changes that occurred in the space charge dynamics. First the behaviour of the **E_S2p** specimens is measured under the electrode area which had withstood electro-thermal stressing (70kV/mm, 90^{o}C) for 1537 hours. In some cases, the same specimen was poled again in order to observe its space charge behaviour over a longer period of time. It should be noted that the space charge profiles are presented in sequence with the first run of dc poling presented first and then next the second run.

Figure 4.3.5a shows the accumulation of the space charge in specimen **E_S2p** (ss_b) under the electrode area with the volt-on (subtracting the zero minute Volt-on measurement from the subsequent ones) method as the negative heterocharge that is building up at the anode could not be observed with the volt-off method. During 320 minutes of polarisation positive charge is injected from the anode into the bulk of the specimen forming a second positive peak while negative charge is building up at the anode and cathode. The negative heterocharge adjacent to the anode escapes/neutralises instantly once the voltage is switched off leaving positive charge, which within a couple of minutes decays forming negative charge. The negative charge adjacent to the cathode decays at a slower rate. The positive charge that penetrated further into the material seems to be less mobile as its decay occurs very slowly. The enhanced electric field produced by the positive and negative charge adjacent to the anode when the voltage is switched off encourages rapid positive charge injection and negative charge extraction. This could be the reason for the rapid changes of the charge adjacent to the anode.

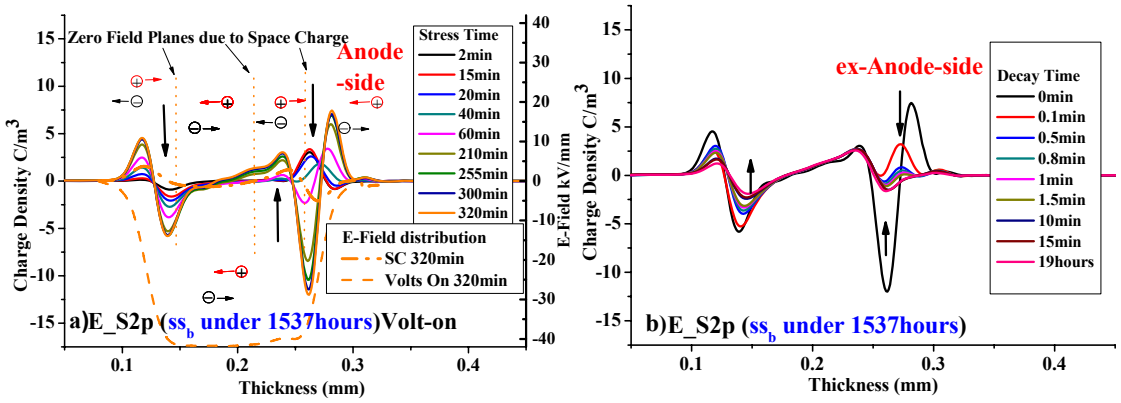

Figure 4.3.5: Space charge profile obtained under the electrode area after the endurance test A_4 for the suspended specimen of the electrically pre-stressed material E_S2p(ss_b); a) accumulation during 320 minutes "volt-on" measurements and the electric field distribution, b) decay.

Then the region outside the electrode area of the same specimen was poled for 200 minutes but this time the polarity was reversed, see Figure 4.3.6a. The aim of the polarity reversal is to check whether some features of the space charge behaviour are polarity dependent or dependent upon the side of the peeling. During these measurements positive charge is injected from the anode within the first minute and spreads across the sample forming positive heterocharge at the cathode. After about 10 minutes, negative heterocharge starts to form at the anode. It is probable that ionic dissociation from chemical reaction of the antioxidant and acetophenone (Sekii et al., 2001 & 2007) is involved in the heterocharge formation, though the possibility that

injected charges from the electrodes transit fast across the specimen and built up at the electrode interface due to a lower extraction rate cannot be ruled out (Delphino et al., 2007). However, this latter process is unlikely to be a major factor as once the voltage is switched off the charge density of the heterocharges continues to increase up to the fifteenth minute of depolarisation, as is shown in Figure 4.3.7. Even thereafter the decay process is very slow, possibly because ionic charges are difficult to extract/neutralise.

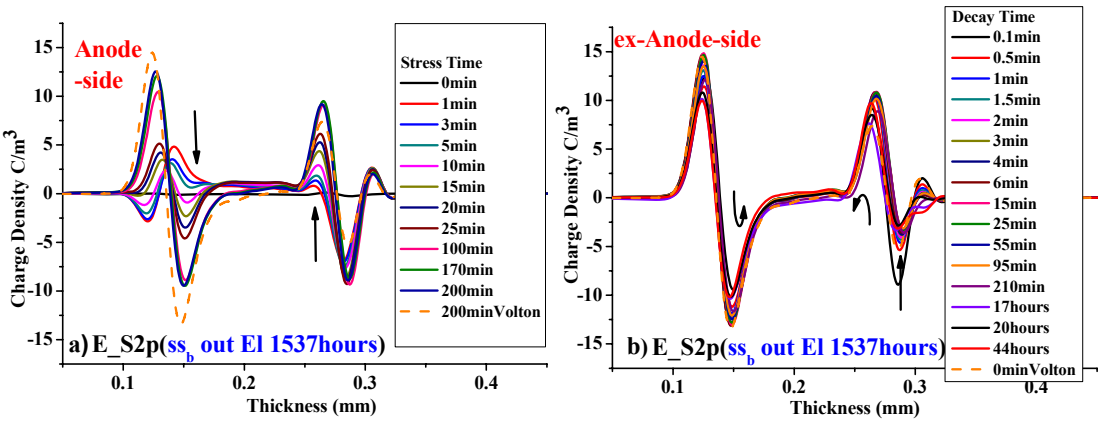

Figure 4.3.6: Space charge profile obtained outside the electrode area after the endurance test A_4 for the suspended specimen of the electrically pre-stressed material E_S2p(ss_b) with reversed polarity with respect to Figure 4.3.5; a) accumulation during 200 minutes "volt-off" measurements; the orange dashed line in this figure is taken with the volt-on method used hereafter in order to have an estimation of the charge lost between switching off the voltage and making the measurement, b) decay.

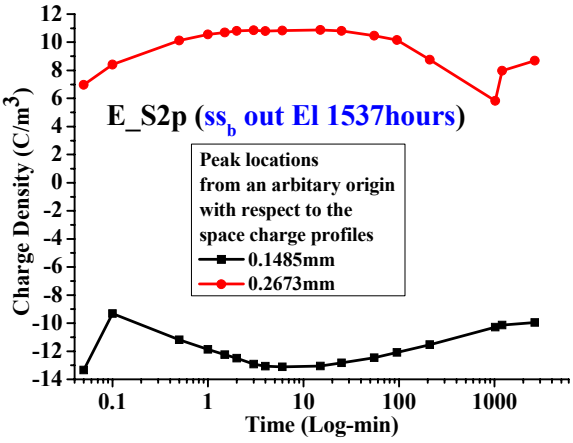

Figure 4.3.7: Change of the charge density of the charge peaks adjacent to the electrodes during the decay of Figure 4.3.6b.

The other suspended specimen **E_S2p** (ss_a) was poled for 230 minutes and the space charge distribution (Figure 4.3.8a) was found to be similar to that of the previous sample, Figure 4.3.5a. However, the negative charge magnitude adjacent to the anode can only be observed with the volt-on method during the 200th minute and is very small. In contrast to Figure 4.3.5b, the negative charge adjacent to the cathode escapes very

fast during depolarisation, Figure 4.3.8b, leaving behind positive charge. This most probably was accumulating during poling, but its observation was not possible then because the injection of the negative charge from the cathode cancelled out positive charge, giving a net negative charge region.

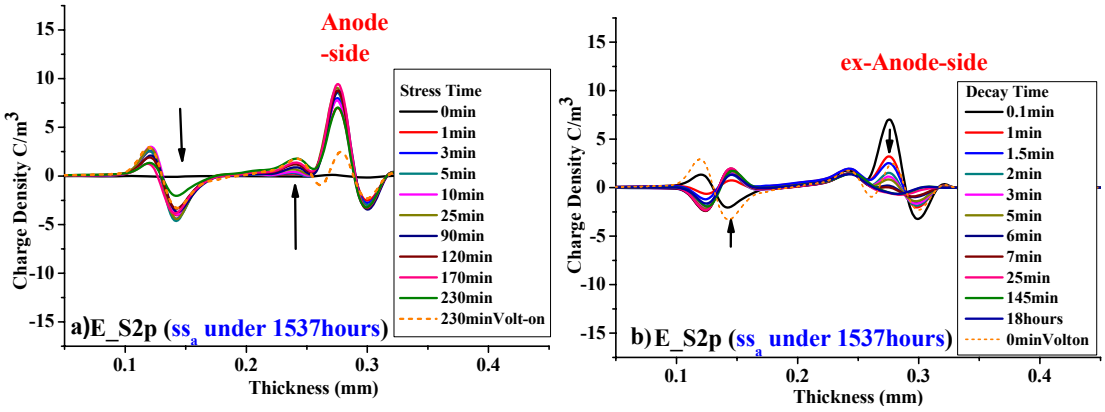

Figure 4.3.8: Space charge profile obtained under the electrode area after the endurance test A_4 for the suspended specimen of the electrically pre-stressed material E_S2p(ss_a); a) accumulation during 230 minutes "volt-off" measurements, b) decay.

When the polarity is reversed, Figure 4.3.9a, and the orientation of the sample remains the same, the space charge distribution has the same form as that in Figure 4.3.5a, but with reversed polarity. When the poling is continued for a further 360 minutes, Figure 4.3.9c, a double negative peak is formed at the cathode. As the charge increases in the second peak it reduces in the first peak, as can be seen from the red and green lines in Figure 4.3.10a.

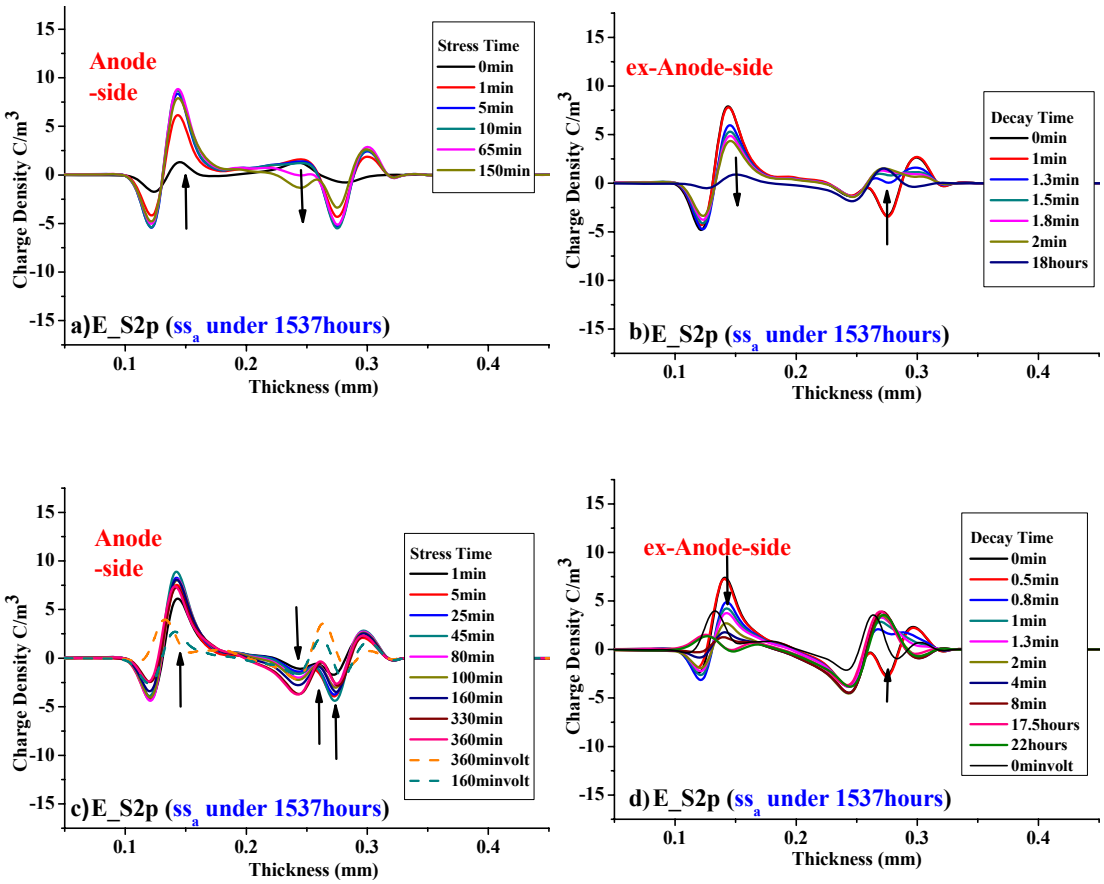

Figure 4.3.9: Space charge profile obtained under the electrode area after the endurance test A_4 for the suspended specimen of the electrically pre-stressed material E_S2p(ss_a) following on from Figure 4.3.8 by reversing the polarity; a) accumulation during 150 minutes "volt-off" measurements, b) its decay, c) further accumulation for 360 minutes and d) the subsequent decay.

These measurements show that the unusual double peak behaviour is associated with the top of the sample and not with the voltage polarity, and that it only appears in the region that experiences electrical stress and therefore cannot be related either to a thermal effect or to the voltage application of the PEA system. An estimation of the trap depths of the charge at the peaks can be obtained from Figure 4.3.10b using the method described in chapter 2. It was found that the negative charge that penetrated deepest into the material lies in a trap depth greater than **1.03eV** whereas that closer to the electrode decays faster and appeared to reside in shallower traps **≤0.85eV**.

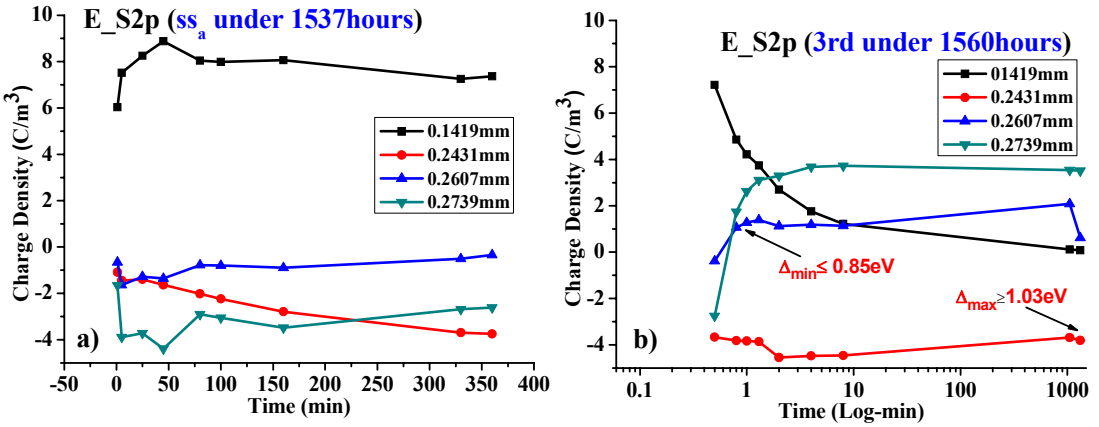

Figure 4.3.10: Change of the charge density at the charge peaks during a) the accumulation and b) the decay presented in Figure 4.3.9 c) and d) respectively.

In order to estimate the trap depths of the charge retained at the end of the depolarization experiments shown in Figure 4.3.6b and Figure 4.3.9d, the specimens were discharged using the Thermally Stimulated Current technique described in chapter 2. The results are given in Figure 4.3.11a. However, it should be noted that in this case it was not necessary to pole the specimen as is normally done in standard TSC measurements, as space charge was already retained in the specimens from the previous PEA experiment. It was found that a current peak occurred at a temperature of 80°C for both specimens corresponding to a detrapping activation energy of **0.95eV** using Equation (5) from chapter 2. The TSC profiles as well as the PEA ones shown in Figure 2.3.35c and Figure 2.3.35d in chapter 2 are very similar to these ones. Here, the current peak occurs at a higher temperature and its magnitude is greater as is the space charge observed by the PEA. Furthermore, the space charge density magnitudes retained after the PEA experiment are proportional to the peak current magnitudes observed in the TSC experiment. However, the total amount of space charge estimated from both techniques is not the same, as is shown in Table 4.3.2.

Specimen name and maximum magnitude of charge retained after PEA	Total amount of space charge (C)	
	PEA technique without the image charges	TSC technique
E_S2p(ss_a)-4C/m^3	1.3140×10^{-8}	9.4565×10^{-10}
E_S2p(ss_b)-10C/m^3	3.5360×10^{-8}	3.1981×10^{-9}

Table 4.3.2: Total amount of space charge retained after the PEA experiments presented in Figure 4.3.6b and Figure 4.3.9d estimated by both the last PEA decay measurement and the TSC data shown in Figure 4.3.11a.

The space charge estimated from the PEA is greater than the TSC one. Unless the area under the space charge profile after the de-convolution of the signal does not correspond

to the actual amount of the space charge stored in the material, the reduction of the space charge during the TSC experiment could be assigned either to an incomplete removal of the space charge, or to recombination of charge. This latter process gives currents in opposite direction to charge extraction and so results in a reduced net current or even opposite polarity (Tanaka Y. et al, 1998).

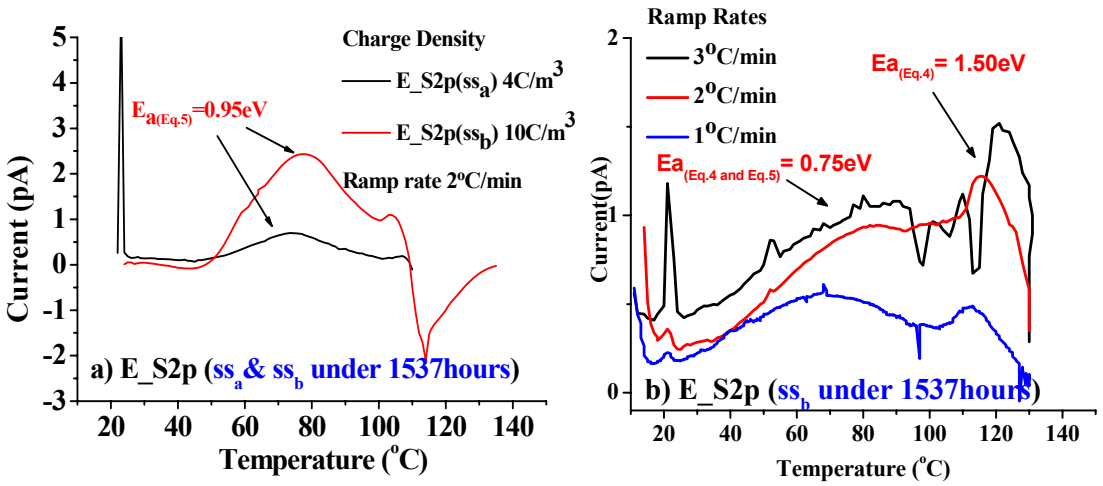

Figure 4.3.11: TSC measurements a) from the retained charge of Figure 4.3.6b and Figure 4.3.9d and b) at three different ramp rates in order to estimate the activation energies.

The de-trappping activation energy of the **E_S2p(ss$_b$)** specimen was further investigated by using the TSC technique with different ramp rates. The results are given in Figure 4.3.11b for the standard protocol described in chapter 2 and the following parameters; poling temperature 90°C and poling voltage 2kV for 60 minutes. The average activation energy using both Equations (4) and (5) was found to be **0.75eV** for the current peak occurring around **80°C** and **1.50eV** around **120°C** as shown on the figure. This estimation also agrees with the results presented in Figure 2.3.35c in chapter 2. It should also be noted that the sequence of the TSC experiments on the same specimen up to a temperature of 130°C did not significantly change the TSC and PEA profiles shown in and Figure 4.3.11 and Figure 4.3.12 in contrast to experiments presented in chapter 2 and shown in Figure 2.3.35.

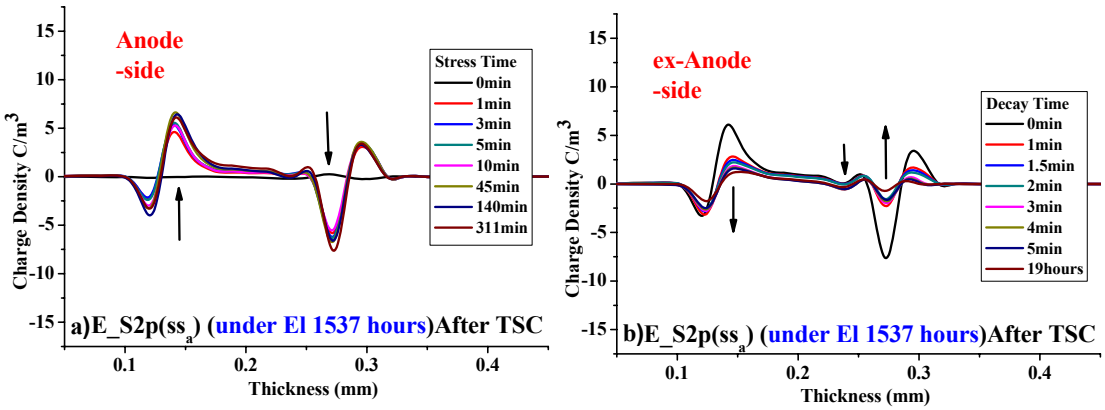

Figure 4.3.12: Space charge profile obtained under the electrode area after the TSC experiment for the suspended specimen of the electrically pre-stressed material E_S2p(ss$_a$) under reversed polarity; a) accumulation during 311 minutes "volt-off" measurements, b) its decay.

Figure 4.3.13 summarises the main features that electro-thermal endurance stressing (under the electrode area) and thermal (outside the electrode area) stressing introduced to all the electrically pre-stressed material experiencing the endurance test A. The space charge profiles show that extra electro-thermal stressing increased the charge injection at the interface between the specimen and the semicon electrode of the PEA system. This was the side of the sample next to the brass electrode during the ac endurance test. A second homocharge peak was formed further into the material. It is observed that there is a memory effect for these features. This is demonstrated in Figure 4.3.13f where the same specimen is re-poled following charge removal. Here the charge is injected almost directly into the second peak. In contrast charge is transferred from the peak nearest the electrode to the peak deeper in the peeling during the first poling experiment. Extra thermal stressing on the other hand increased the heterocharge concentrations at the electrode interfaces. This may be a result of the weakening molecular bonds of chemical impurities and additives, leading to dissociation into ions and their accumulation at the electrode interface.

(c) Thermally pre-stressed peelings after the endurance test

The thermally pre-stressed material failures generally occurred earlier than the electrically pre-stressed ones during the endurance test A conditions, and the space charge behaviour did not significantly change in comparison with that found before the endurance test. The main change is observed in the **_TS1p** shown in Figure 4.3.14b where negative space charge, which is injected from the cathode, is observed to

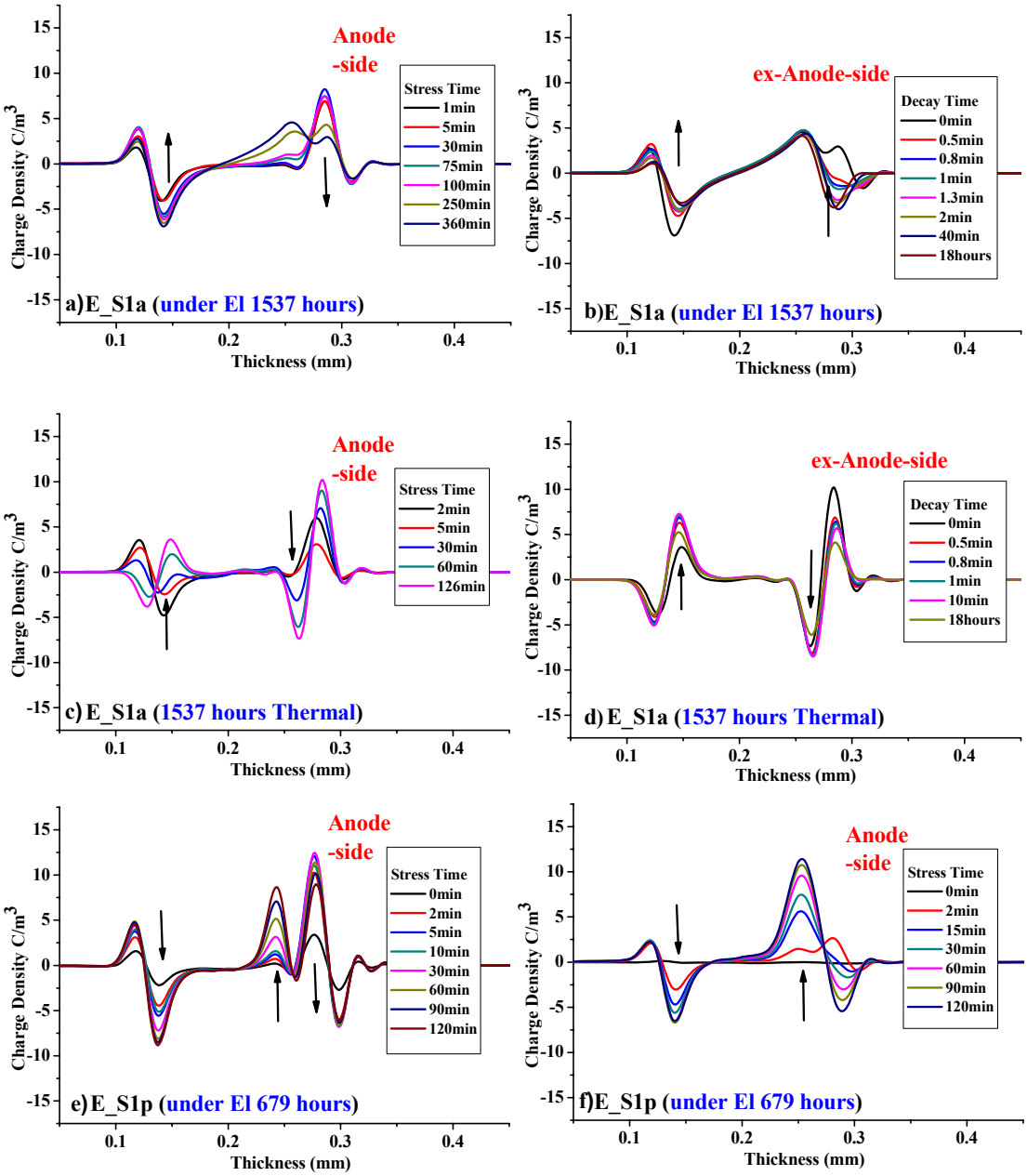

Figure 4.3.13: Space charge evolution obtained under the electrode area for electrically pre-stressed specimens with the volt-off method; a) E_S1a accumulation for 360 minutes, b) E_S1a the subsequent decay of a), e) E_S1p accumulation for 120 minutes and f) reapplication of voltage to e) for 120 minutes once the charge has decayed. c) and d) show the accumulation and decay of the E_S1a specimen outside the electrode area (Adapted from Tzimas et al, 2007).

penetrate further into the material. However, samples with more than 16.5 hours under the endurance test conditions show positive space charge forming adjacent to the anode that over time penetrates further into the bulk as shown in Figure 4.3.14a.

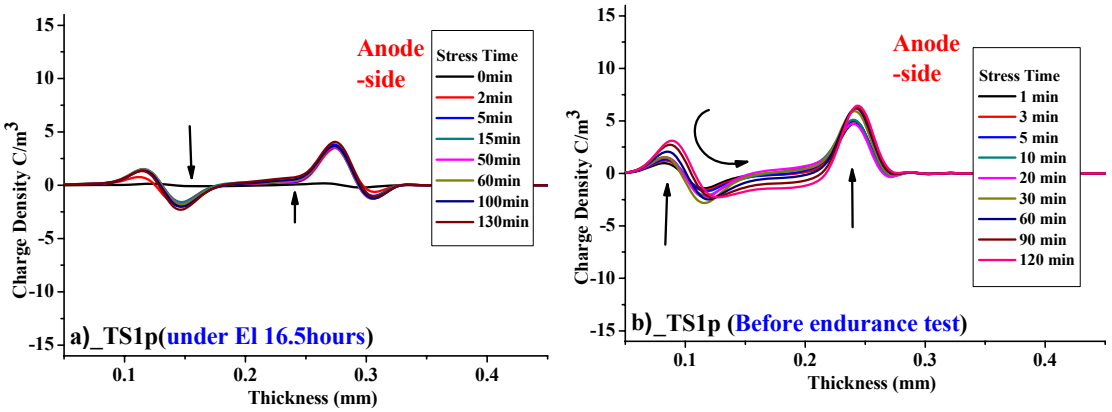

Figure 4.3.14: Space charge accumulation profile obtained under the electrode area a) after the endurance test A_4 for the suspended specimen of the thermally pre-stressed material _TS1p "volt-off" measurements, b) before.

(d) Electro-thermally pre-stressed peelings after the endurance test

The space charge profile of the electro-thermally pre-stressed specimens after the endurance test did not show a significant change in comparison to that found before the test as their failures occurred early in the test.

4.3.3 Endurance test B (70kV/mm, 30°C)

The specimens that participated in the endurance test B have experienced electrical stress of 70kV/mm under the electrode area till their failure occurred but only the thermal stress of 30°C outside the electrode area. The time to failure of the specimen whose space charge behaviour is investigated is presented in a parenthesis next to the material code. It should also be remembered that all the specimens remained in the test rig till the test was terminated. This endurance test was terminated after 3103 hours as indicated in Table 4.3.1.

(a) Unstressed peelings after the endurance test

The space charge profile under the electrode of the unstressed material after this endurance test, shown in Figure 4.3.15a, is very similar to the distribution before the test shown in Figure 2.3.7 in chapter 2 where positive charge injection and transit across the bulk could be observed. However here, the positive charge has the time to reach the cathode where it builds up. As is shown in Figure 4.3.15b this charge decays very slowly over a period of 90 hours, and is estimated to reside in traps with depths greater than **1.07eV**. It was only released under the TSC experiment where the activation energy was estimated to be **1.51eV** for the negative current peak occurring around 72°C, see Figure 4.3.17.

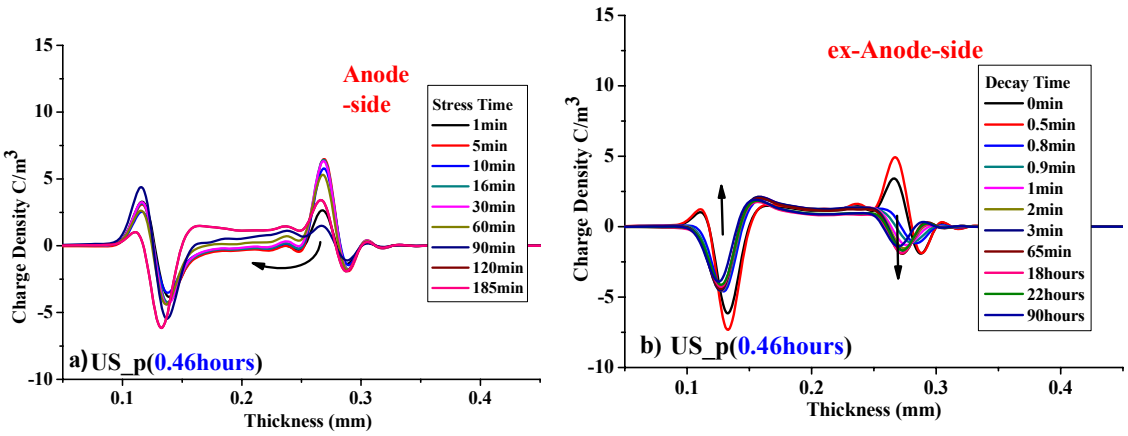

Figure 4.3.15: Space charge profile obtained under the electrode area for the unstressed specimen US_p with the volt-off method; a) accumulation for 185 minutes, b) the subsequent decay.

(b) Electrically pre-stressed peelings after the endurance test

The space charge profile under the electrode area of the electrically pre-stressed material after 60 hours of electrical endurance stressing, Figure 4.3.16a, behaves like the unstressed material, **US_a** before the endurance test as shown in Figure 4.3.1a. Here, the negative charge reaches the anode where it builds up a lot faster than in the **US_a** prior to endurance testing. As was also observed in the **US_a** Figure 2.3.8d the space charge retained after poling decays very slowly suggesting that it lies in very deep traps. The TSC experiment, whose data is given in Figure 4.3.17 showed a negative current peak occurring around 60°C with an estimated activation energy of **1.33eV**. A higher temperature current peak was also observed for both specimens (**US_p** and **E_S2p**) but the activation energies estimated using Equation (5) are too high to be physically possible and since the experiment was only conducted at a single temperature ramp rate, Equation (4) can not be used.

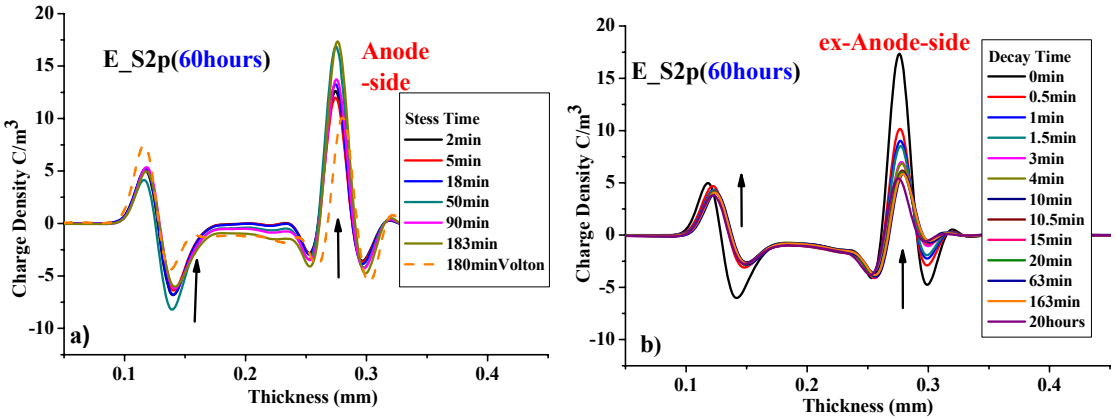

Figure 4.3.16: Space charge profile obtained under the electrode area for the electrically pre-stressed specimen E_S2p with the volt-off method; a) accumulation for 183 minutes, b) the subsequent decay.

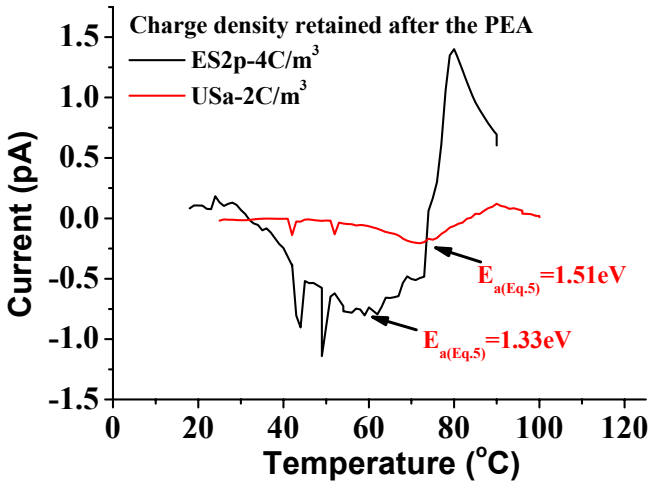

Figure 4.3.17: TSC measurements of the retained charge after the PEA experiment of the unstressed material US_p and electrically pre-stressed E_S2p whose space charge distributions are given in Figure 4.3.15b and Figure 4.3.16b respectively.

Specimen name and maximum magnitude of charge retained after PEA	Total amount of space charge (C)	
	PEA technique without the image charges	TSC technique
US_a 2C/m^3	1.8273x10^{-8}	7.3268x10^{-11}
E_S2p 4C/m^3	3.0752x10^{-8}	1.1485x10^{-9}

Table 4.3.3: Total amount of space charge retained after the PEA experiments presented in Figure 4.3.15b and Figure 4.3.16b estimated by both the last PEA decay measurement and the TSC data shown in Figure 4.3.17.

(c) Thermally pre-stressed peelings after the endurance test

Figure 4.3.18a shows the space charge profile under the electrode of the thermally pre-stressed material **_TS2p**. Here negative charge moves across the material to the anode where it accumulates whereas it stayed close to the cathode before the endurance test. In contrast with the electrically pre-stressed sample **E_S2p** a great fraction of the negative charge that has been accumulated both adjacent to the anode and cathode during poling escapes/neutralises within 30 seconds once the voltage is switched off. However the negative charge that is left after this time decays very slowly if it does so at all similar to **E_S2p**. The same specimen was further poled for two days, see Figure 4.3.19, and

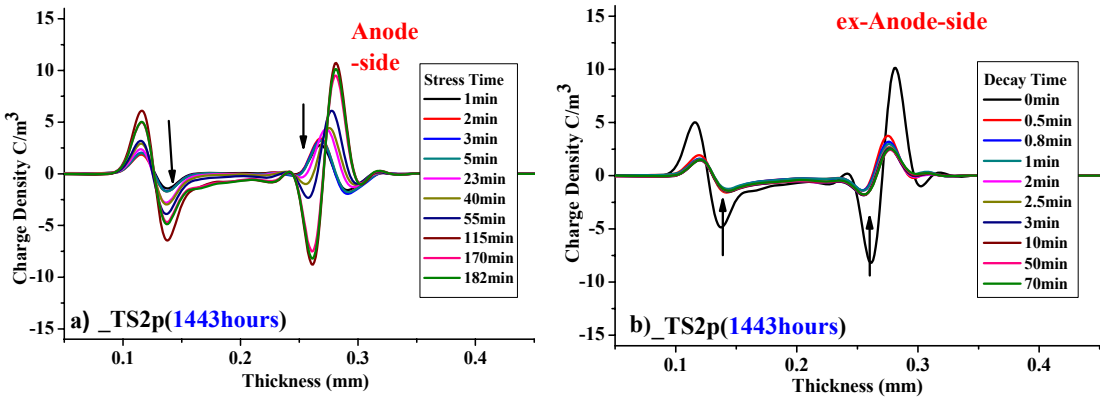

Figure 4.3.18: Space charge profile obtained under the electrode area for the thermally pre-stressed specimen _TS2p with the volt-on method; a) accumulation for 182 minutes, b) the subsequent decay.

during the volt-off accumulation measurements does not appear to change much. Nevertheless, with the volt-on method negative charge can again be observed to build-up rapidly at the anode. The volt-on method shows that positive charge accumulates at the cathode during poling. This can be seen clearer during the decay where negative charge escapes very fast leaving behind the positive charge that can be observed during poling with the volt-on method.

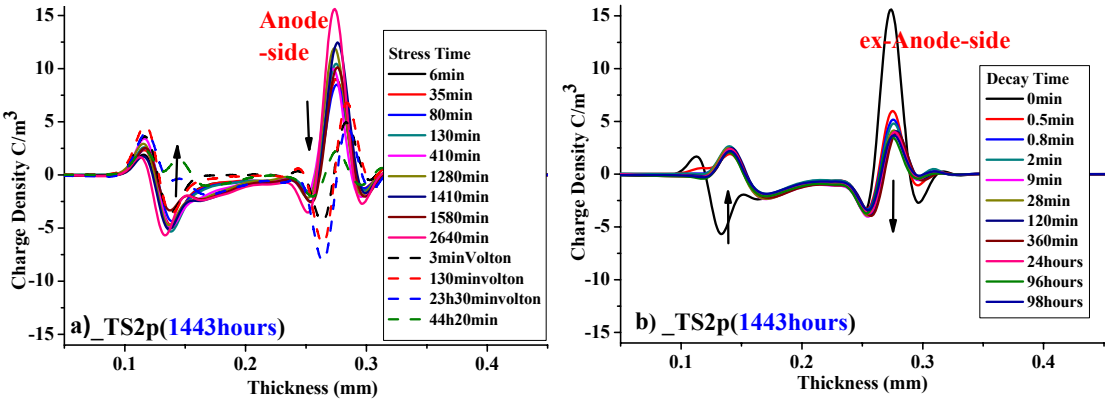

Figure 4.3.19: Space charge profile obtained for the thermally pre-stressed specimen _TS2p with the volt-off method under the electrode area; a) further accumulation for 2640 minutes after poling for 182 minutes, b) the subsequent decay.

(d) Electro-thermally stressed peelings after the endurance test

The space charge behaviour of the electro-thermally stressed material, see Figure 4.3.20, shows positive charge being injected from the anode and forming a second positive peak like the electrically pre-stressed materials in endurance test **A**. However the space charge density is small.

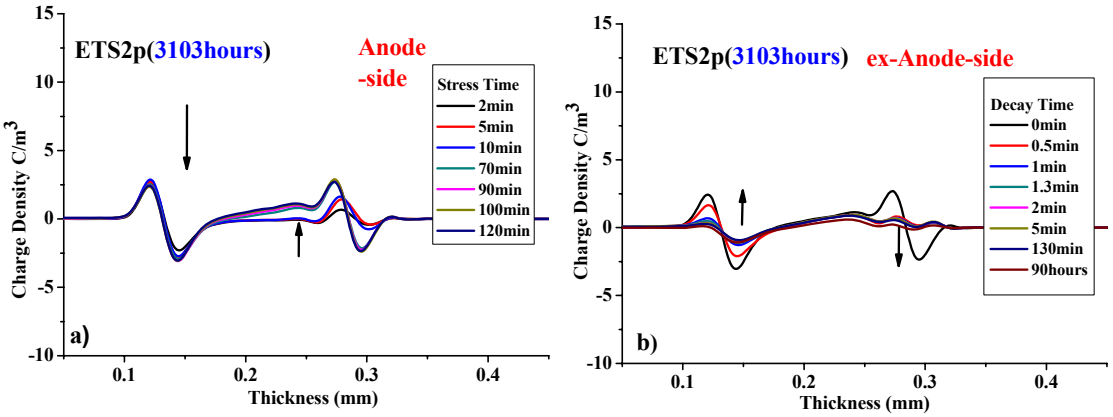

Figure 4.3.20: Space charge profile obtained under the electrode area for the electro-thermally pre-stressed specimen ETS2p with the volt-on method; a) accumulation for 120 minutes, b) the subsequent decay.

Figure 4.3.21 shows the space charge behaviour outside the electrode area of the **ETS2p** material after 3103 hours of just thermal stressing. The space charge profile is very similar to the ones of **E_S2p** and **_TS2p** but from under the electrode area. In these latter cases however, the hours for which they experienced electrical stressing are negligible in comparison with the 3103 hours of thermal stressing. Hence, we may only be observing the changes that were introduced solely by the thermal stressing in all these cases.

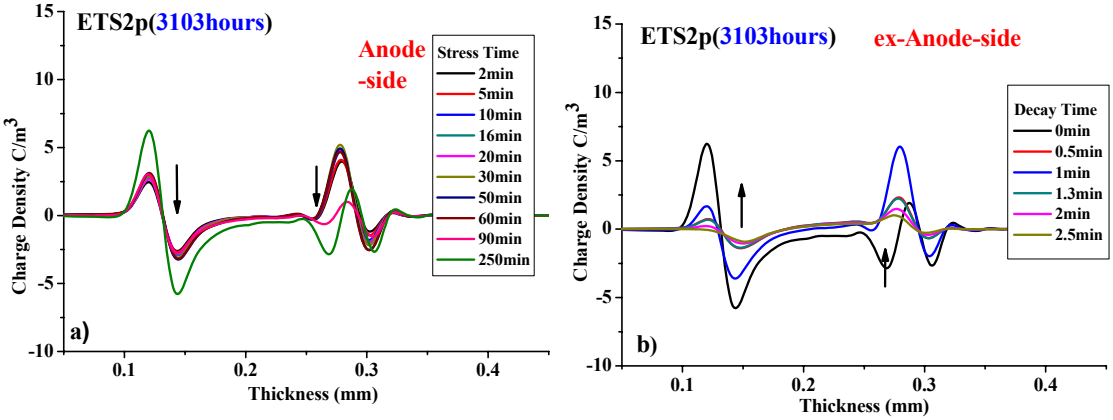

Figure 4.3.21: Space charge profile obtained outside the electrode area for the electro-thermally pre-stressed specimen ETS2p with the volt-on method; a) accumulation for 250 minutes, b) the subsequent decay.

(e) Service stressed peelings after the endurance test

The space charge behaviour of the service aged material, **SA**, has also changed. Measurements under the electrode area where the third failure occurred, Figure 4.3.22, show that instead of negative heterocharge accumulation at the anode, see Figure 4.3.1f, there is positive heterocharge at the cathode. Negative homocharge appears for the first 5 minutes next to the cathode and thereafter positive heterocharge accumulation

dominates. Positive homocharge accumulation is observed adjacent to the anode but this charge escapes/neutralises faster than that at the cathode, see Figure 4.3.22b. Similar space charge behaviour is observed outside the electrode area, see Figure 4.3.24. Hence, 87 hours of electrical stressing did not significantly influence the space charge behaviour compared to 3103 hours of thermal stressing.

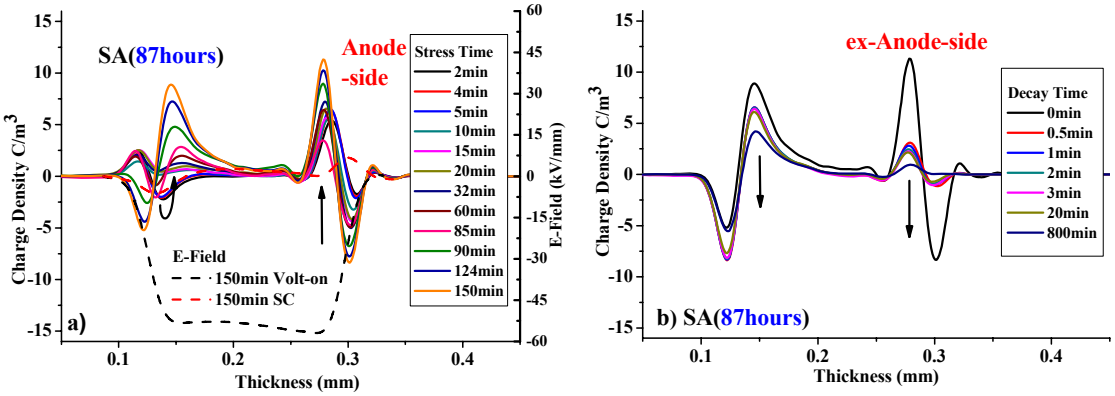

Figure 4.3.22: Space charge profile obtained under the electrode area of the 3rd failure for the Service stressed specimen SA with the volt-on method; a) accumulation for 150 minutes, b) the subsequent decay.

Measurements made under the electrode on the suspended sample of the **SA**, Figure 4.3.23, show positive charge injection and accumulation adjacent to the anode which within the twentieth minute of poling spreads across the bulk and reaches the cathode. Thereafter, it seems that the system arrived at an equilibrium as there is not a considerable change. Once the voltage is switched off the charge reduces at equal amounts across the sample as the electric field is balanced and charges of the same polarity have the same mobility.

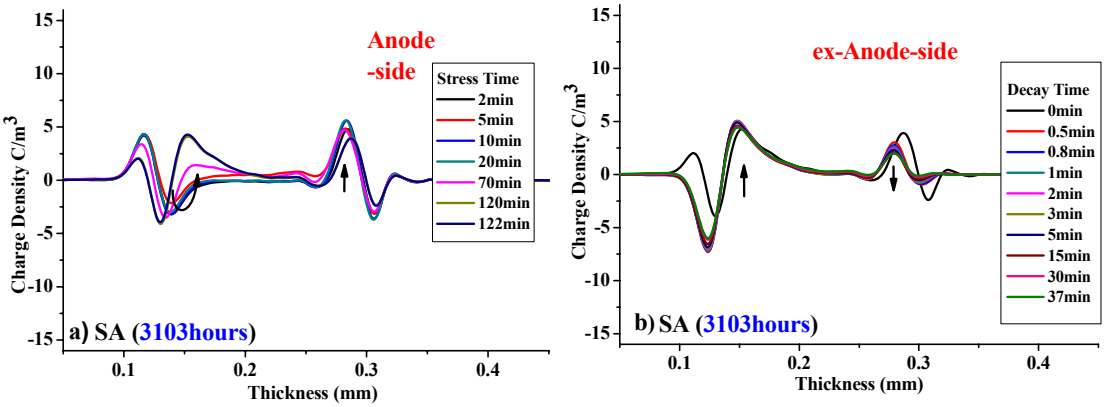

Figure 4.3.23: Space charge profile obtained outside the electrode area for the Service stressed specimen SA with the volt-on method; a) accumulation for 122 minutes, b) the subsequent decay.

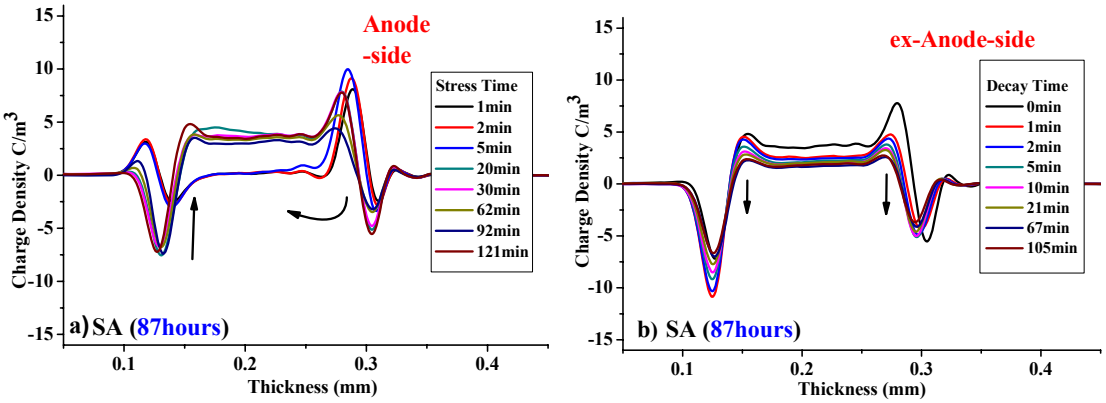

Figure 4.3.24: Space charge profile obtained under the electrode area for the Service stressed specimen SA with the volt-on method of the suspended sample; a) accumulation for 121 minutes, b) the subsequent decay.

4.3.4 Endurance test C (55kV/mm, 90°C)

The specimens that participated in the endurance test **C** as well as the endurance test **A** have experienced electro-thermal stress. In this case the electrical stress was 55kV/mm, 15kV/mm less than the former endurance test, but the thermal stress of 90°C is exactly the same. This endurance test was terminated after 6088 hours, as indicated in Table 4.3.1, before all the samples had failed as was described in chapter 3. Hence, all the space charge measurements presented here were conducted on suspended samples in order to investigate the maximum effect that the endurance test stressing may have had on the samples. The measurements under the electrode region are for samples that have undergone electro-thermal stressing for 6088 hours and the measurements outside the electrode for samples that just experienced thermal stressing for exactly the same duration. The changes that occurred in the space charge behaviour after this endurance test are consistent with the changes that were introduced by the endurance test **A** and **B**, and in some cases by the Artemis stressing. Hence, wherever this is the case, the similarities will be pointed out avoiding the detailed description which is done elsewhere.

(a) Unstressed peelings after the endurance test

Measurements under the electrode area of the unstressed material, **US_a**, Figure 4.3.25 show similar space charge behaviour to the electrically pre-stressed material (**E_S1a**, **E_S1p** and **E_S2p**, see Figure 4.3.13) after the endurance test **A** and the electro-thermally pre-stressed material (**ETS2p**, see Figure 4.3.20) after the endurance test **B**, where a second positive peak is formed.

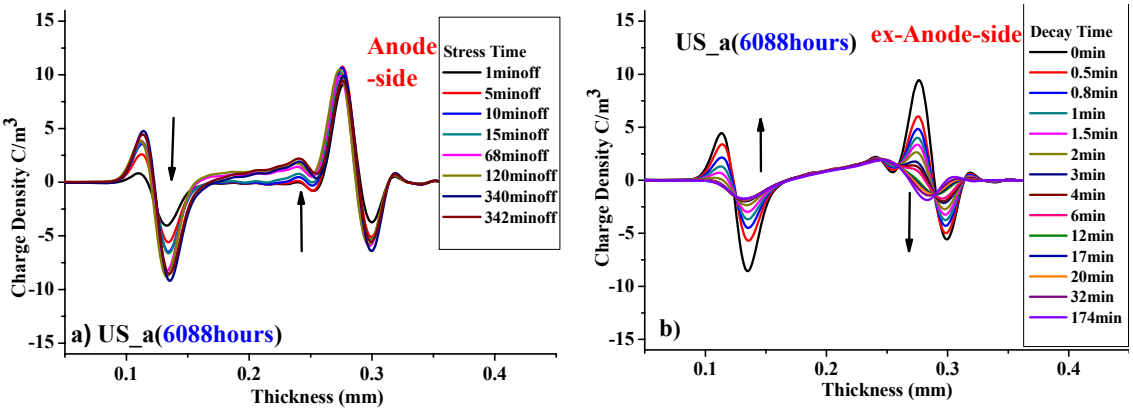

Figure 4.3.25: Space charge profile obtained under the electrode area for the unstressed specimen US_a with the volt-off method; a) accumulation for 342 minutes, b) the subsequent decay.

On the other hand, outside the electrode region of the same specimen, Figure 4.3.26, where just thermal stressing was applied, homocharge injection is observed at both

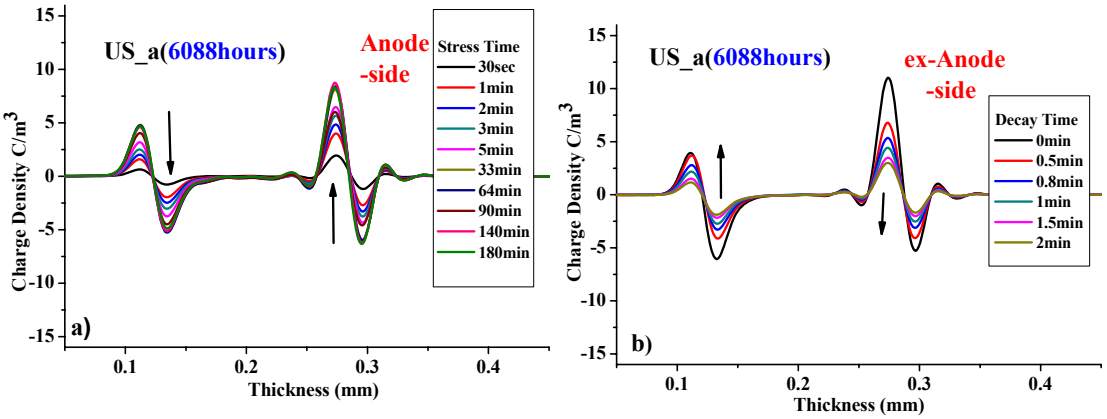

Figure 4.3.26: Space charge profile obtained outside the electrode area for the unstressed specimen US_a with the volt-on method; a) accumulation for 180 minutes, b) the subsequent decay.

electrodes. This space charge profile is consistent with the one obtained from the Artemis thermally stressed material, **_TS2p**, Figure 4.3.1d.

(b) Electrically pre-stressed peelings after the endurance test

Measurements under the electrode area of the electrically pre-stressed material, **E_S2p**, Figure 4.3.27 show positive charge injection and transit to the cathode within the thirty fifth minute without the formation of the second positive peak adjacent to the anode which was observed after the endurance test **A**. Hence, after this endurance test the penetration of the charge and its transport to the cathode became easier. The decay of this charge shown in Figure 4.3.27b occurs very slowly although the electric field produced by the charges encourages them to neutralise. These charges reside in energy states with trap depths greater than **1.04eV**.

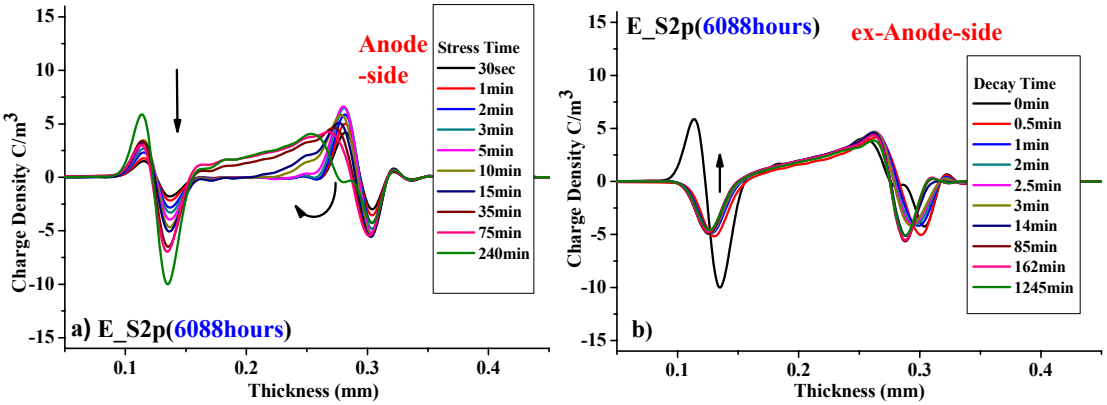

Figure 4.3.27: Space charge profile obtained under the electrode area for the electrically pre-stressed specimen E_S2p with the volt-on method; a) accumulation for 240 minutes, b) the subsequent decay.

Measurements outside the electrode area of the same sample, Figure 4.3.28, showed no observable change in the position of the charge during the 210 minutes of poling though the charge density of the injected charge increases. As is suggested in chapter 2 and by Dissado et al (2006) the system may not have reached thermal equilibrium by that time. As these charges only occupy very shallow energy states, their decay occurs very

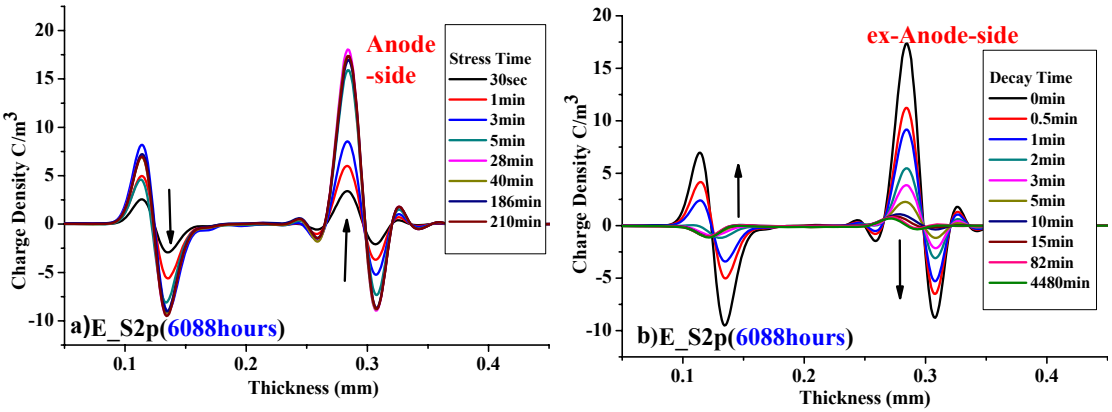

Figure 4.3.28: Space charge profile obtained outside the electrode area for the electrically pre-stressed specimen E_S2p with the volt-off method; a) accumulation for 210 minutes, b) the subsequent decay.

rapidly. This may indicate that the extra thermal stressing on the electrically pre-stressed material, **E_S2p**, gave rise to an increase in the shallow traps density.

(c) Thermally pre-stressed peelings after the endurance test

Measurements under the electrode area of the thermally pre-stressed material, **_TS2p**, Figure 4.3.29 show again positive charge injection spreading to the cathode as observed above in the **E_S2p**. Here, though the poling time was increased further to investigate any possible long time effects and it is observed that later on negative charge is injected into the material and penetrates into the bulk. As can be seen from the decay plot both

the negative and positive charges residing in the bulk have not decayed over a period of 6978 minutes. These charges have occupied energy states whose trap depths estimated to be greater than **1.08eV**. In contrast to the above measurements are the ones that were conducted outside the electrode area, Figure 4.3.30, show no significant change over the same period of poling. Here the injected homocharges at the anode and cathode have occupied very shallow energy states, thus their rapid decay.

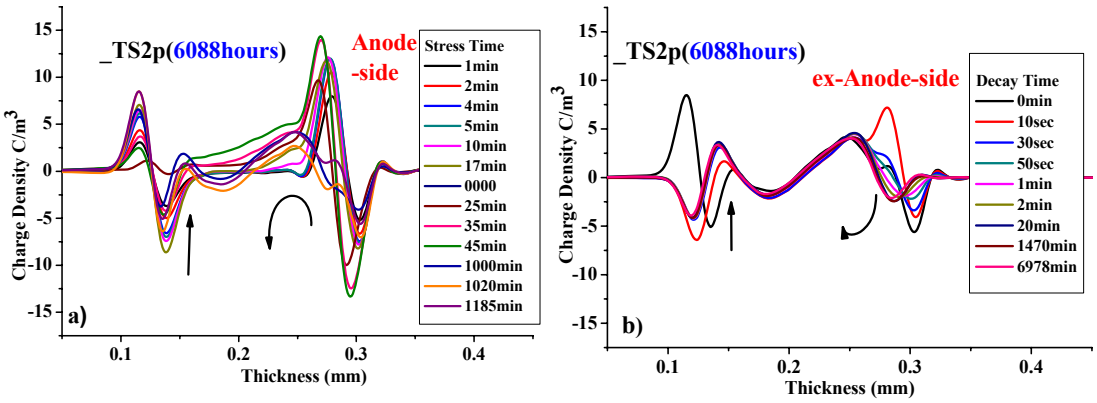

Figure 4.3.29: Space charge profile obtained under the electrode area for the thermally pre-stressed specimen _TS2p with the volt-on method; a) accumulation for 1185 minutes, b) the subsequent decay.

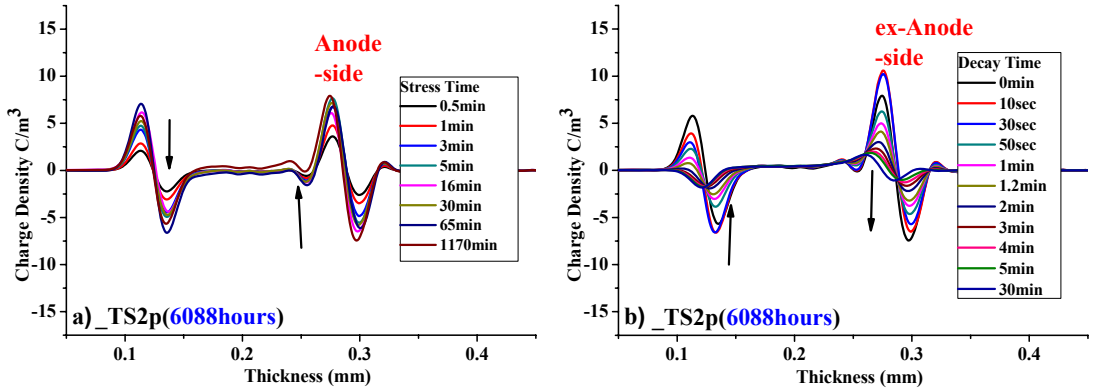

Figure 4.3.30: Space charge profile obtained outside the electrode area for the thermally pre-stressed specimen _TS2p with the volt-on method; a) accumulation for 1170 minutes, b) the subsequent decay.

(d) Electro-thermally pre-stressed peelings after the endurance test

Measurements made under the electrode area of the electro-thermally pre-stressed material, **ETS2p**, in Figure 4.3.31 show that positive and negative charge accumulation at the anode and cathode respectively has very similar charge densities after 1030 minutes of poling as was also observed for the electrically pre-stressed material after the endurance test **A**. These charges decay very slowly despite the fact that the electric field produced by them, encourages them to neutralise.

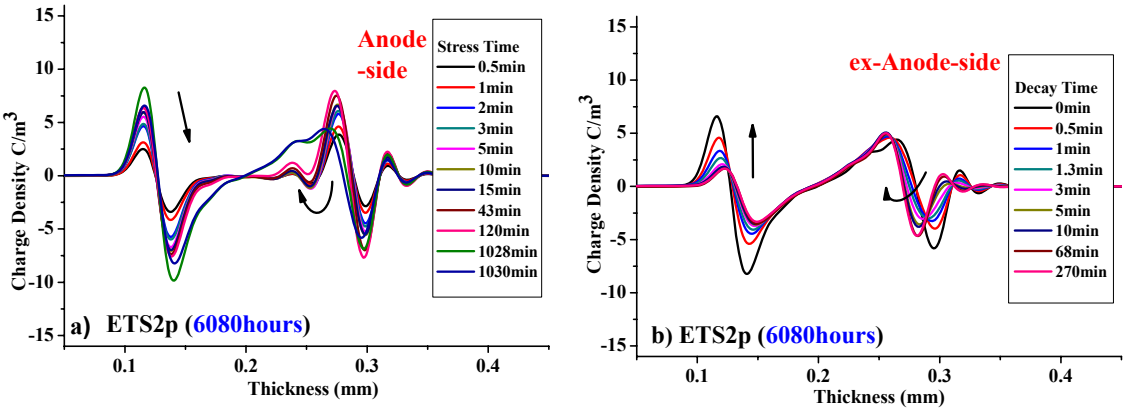

Figure 4.3.31: Space charge profile obtained under the electrode area for the electro-thermally pre-stressed specimen ETS2p with the volt-on method; a) accumulation for 1030 minutes, b) the subsequent decay.

Measurements outside the electrode area of the same sample, Figure 4.3.32, show totally different space charge behaviour to the one under the electrode but a very interesting one. During space charge accumulation over a period of time of 1140 minutes the only observable change is the reduction of the negative homocharge and the appearance of a small positive peak adjacent to the positive homocharge peak at the anode, see Figure 4.3.32a. However, during the decay of space charge, Figure 4.3.32b, the space charge change that was produced during accumulation can be observed more

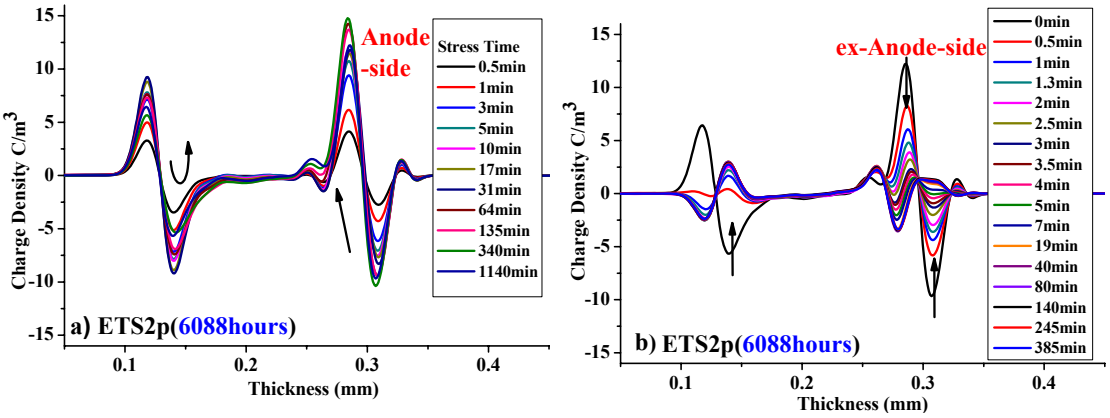

Figure 4.3.32: Space charge profile obtained outside the electrode area for the electro-thermally pre-stressed specimen ETS2p with the volt-on method; a) accumulation for 1140 minutes, b) the subsequent decay.

clearly. During poling we could only see the net charge changes that were occurring and these happen to be so well balanced that the net charge was almost unchanged. The decay plot though shows that during poling equal amounts of positive and negative charge transited to the cathode and anode respectively where they were masked by the injected charge. Once the injected homocharge adjacent to the electrodes decays, the charge that is left behind decreases very slowly possibly due to their mobility or nature.

Similar space charge behaviour was also observed under the electrode area of the electrically pre-stressed material **E_S2p** after the endurance test **A**.

(e) Service stressed peelings after the endurance test

Measurements of the service stressed material, **SA**, under the electrode area Figure 4.3.33, show positive charge injection and penetration to the cathode as was observed in most of the samples under the electrode area in this endurance test and endurance test **A**. However, the magnitude of the charge density is smaller in comparison to the other measurements presented in this section. It is similar though to the space charge profile obtained for the electro-thermally pre-stressed material, **ETS2p**, after the endurance test **B**, see Figure 4.3.20.

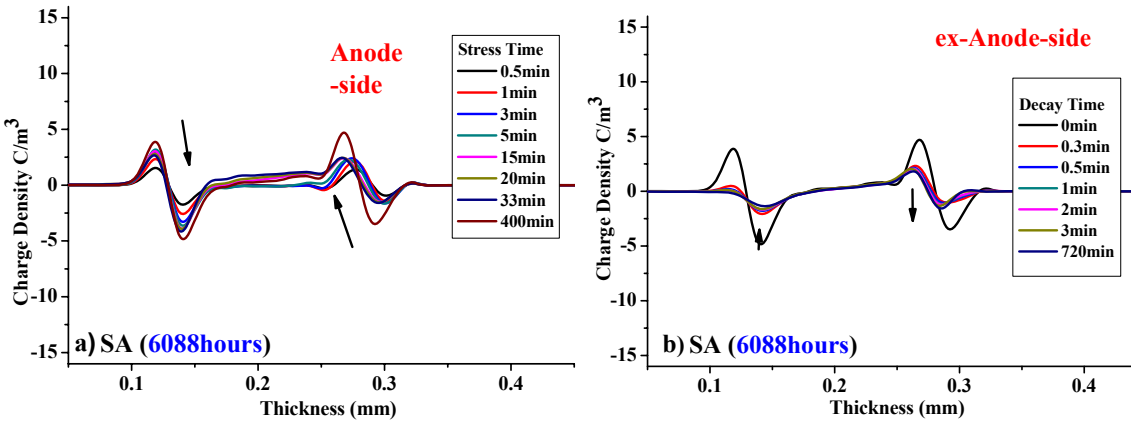

Figure 4.3.33: Space charge profile obtained under the electrode area for the Serviced stressed specimen SA specimen SA with the volt-on method; a) accumulation for 400 minutes, b) the subsequent decay.

On the other hand, measurements outside the electrode area of the same sample, Figure 4.3.34, show heterocharge accumulation of both positive and negative charges with the magnitude of the positive charge density dominating over the negative one. This finding is in contrast to the behaviour observed before the endurance test, see Figure 4.3.1f, where only negative heterocharge could be observed. During the decay the charge density of the positive charges continues to increase by a small fraction within the first minute similarly to the behaviour of electrically pre-stressed material, **E_S2p** see Figure 4.3.6b. Thereafter both polarity charges decay very slowly, indicating charge residing in energy states with deep trap depths.

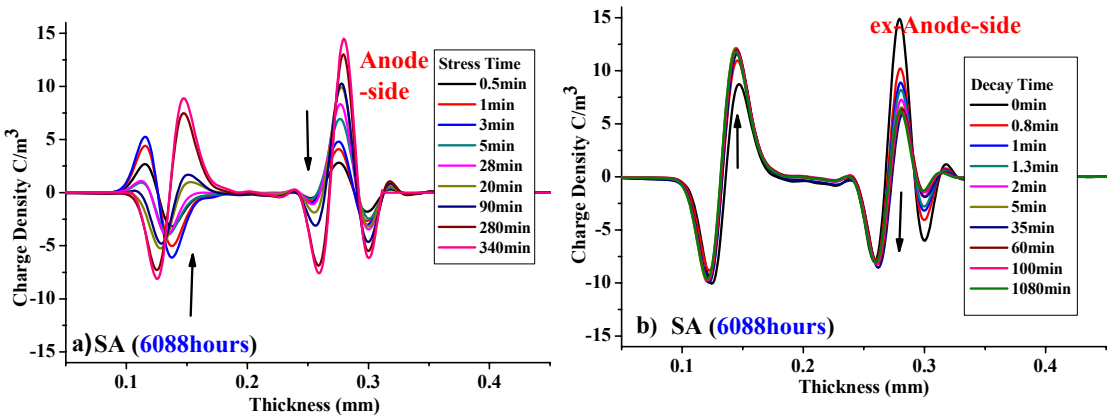

Figure 4.3.34: Space charge profile obtained outside the electrode area for the Serviced stressed specimen SA with the volt-off method; a) accumulation for 340 minutes, b) the subsequent decay.

4.3.5 Residual charge

Once the endurance tests were terminated and before any measurements were made on the specimens, the space charge retained after ac electro-thermal stressing was measured. These measurements were conducted without the application of any voltage. Only the voltage of the high voltage pulse was applied to the specimens. As this residual charge has a small charge density in some cases it was impossible for the system in use to de-convolute the signal. Wherever this was the case the residual charge is presented in mVolts rather than C/m^3. The residual charge measurements could provide us with information on the trap depths that the charge has reached during the ac stressing and on the type/polarity of the charge that is more likely to occupy these energy states.

(a) After the endurance test A

The charge retained after the endurance test A was very small as is shown in Figure 4.3.35. The largest amount of residual charge is seen in Figure 4.3.35g and h, and Figure 4.3.35j, of the thermally pre-stressed materials, **_TS1p** and **_TS2p**, and the electro-thermally pre-stressed one, **ETS2p** respectively. Hence, for these materials it seems that the charge had the time and the ability, due to the materials properties, to occupy deep energy states and be retained at 90^{o}C. However, this was not the case for the other materials although they showed good endurance capability. Hence, because space charge decays faster at higher temperatures leaving only small amounts of charge that are retained after this test, no real correlation can be made between the residual charge and the endurance life of the material.

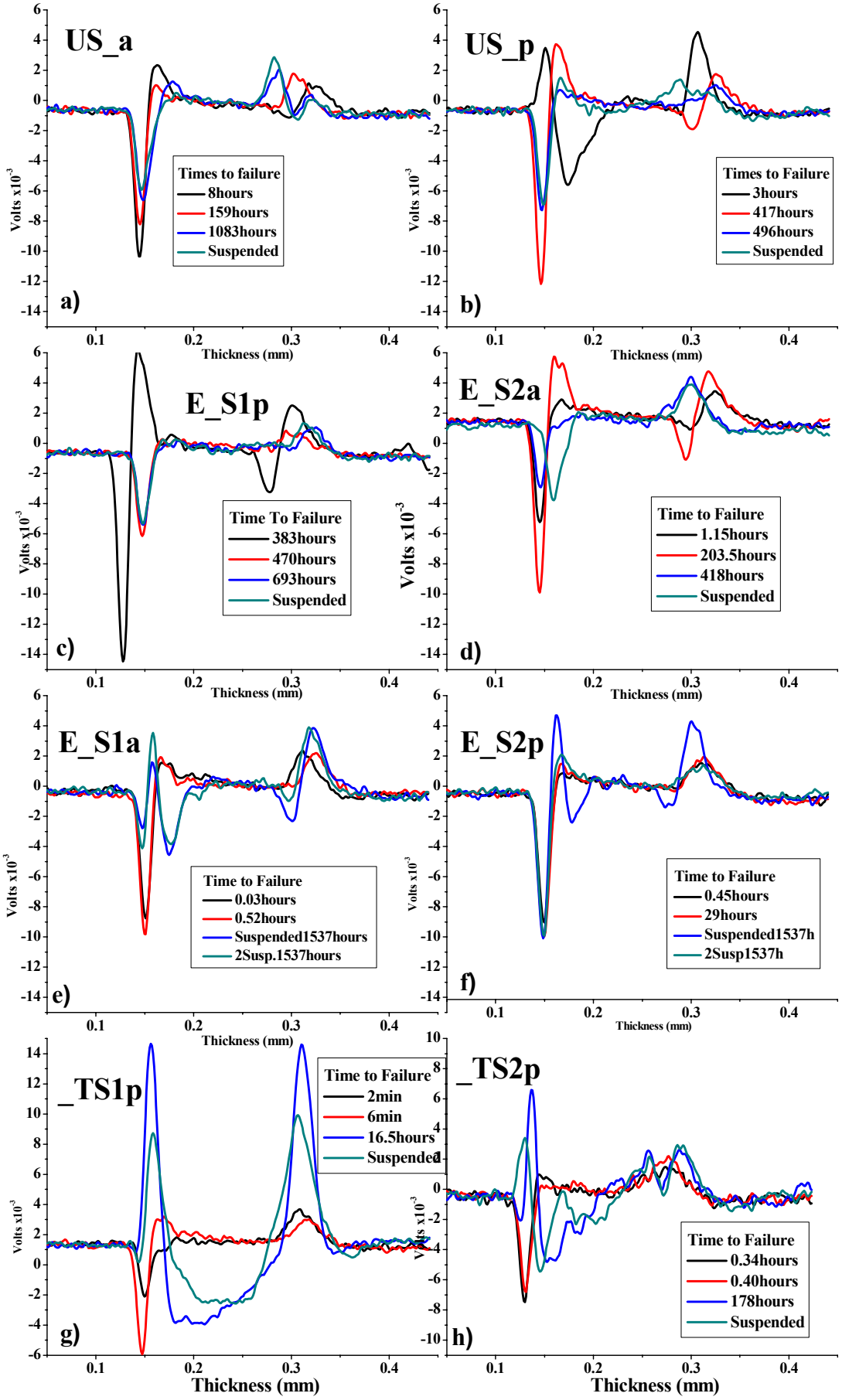
US_a
Times to failure
8hours
159hours
1083hours
Suspended
a)
US_p
Times to Failure
3hours
417hours
496hours
Suspended
b)
E_S1p
Time To Failure
383hours
470hours
693hours
Suspended
c)
E_S2a
Time to Failure
1.15hours
203.5hours
418hours
Suspended
d)
E_S1a
Time to Failure
0.03hours
0.52hours
Suspended1537hours
2Susp.1537hours
e)
E_S2p
Time to Failure
0.45hours
29hours
Suspended1537h
2Susp1537h
f)
_TS1p
Time to Failure
2min
6min
16.5hours
Suspended
g)
_TS2p
Time to Failure
0.34hours
0.40hours
178hours
Suspended
h)
Volts x10-3
Thickness (mm)

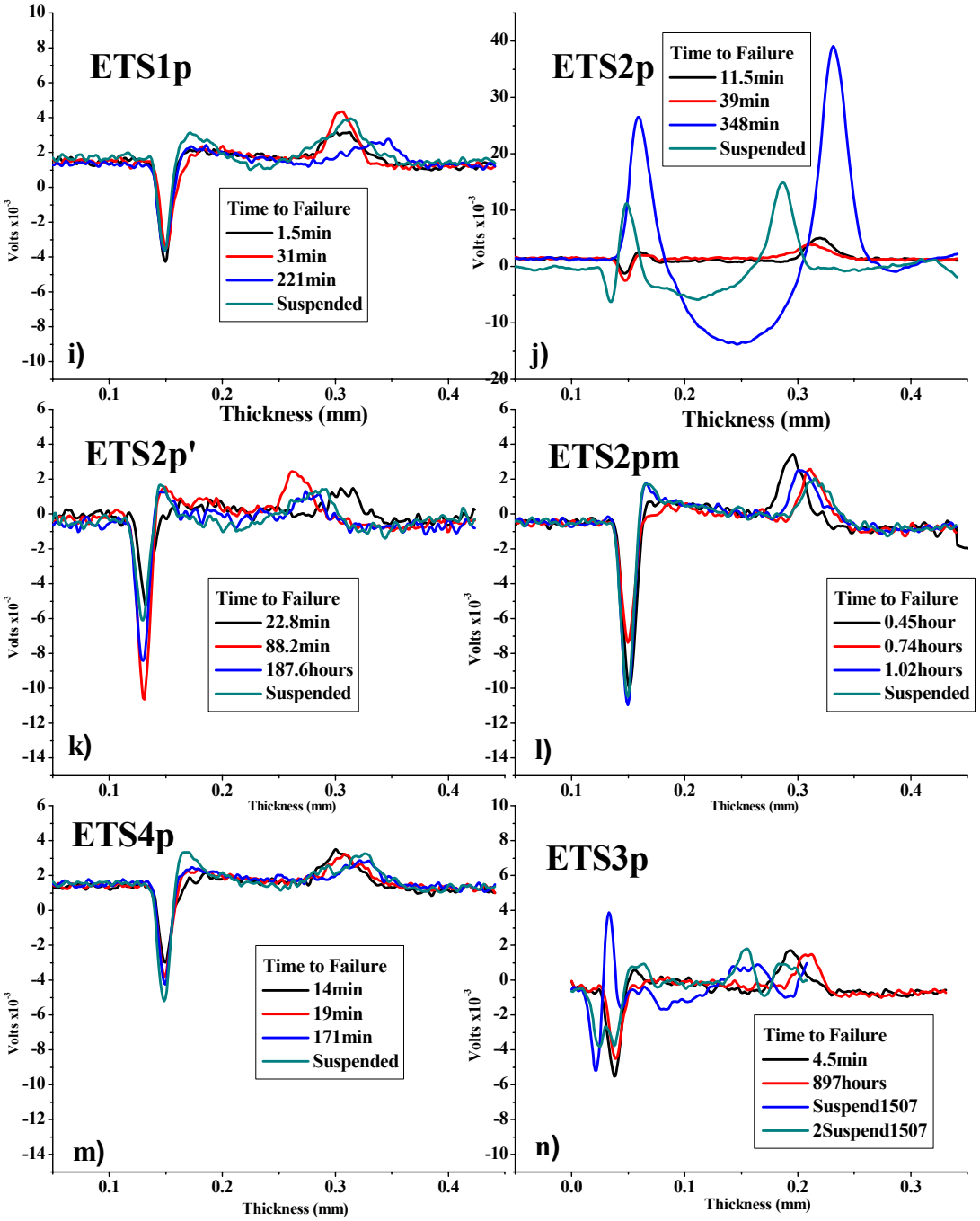

Figure 4.3.35: Retained charge after the endurance test A.

(b) After the endurance test B

The residual charge after the endurance test **B** is presented in Figure 4.3.36. Here the magnitude of the charge density is greater than in the previous test as this test temperature was 30^{o}C and once charge is trapped at this temperature it takes a longer time to escape than it would at a higher one (Dissado et al, 2006). It is observed that the residual charge profiles for most of the specimen (either failed or suspended) fit into a

single form. In this profile is that most of the specimens retain negative charge which is located adjacent to the electrodes, with an exception of the first failure of the **ETS2p** where it is retained in the bulk. The magnitude of the charge density of this negative charge for the suspended samples ranges between 1-2 C/m^3, see Figure 4.3.36f. The magnitudes in the other specimens vary according to the material and time to failure. The materials with the most retained charge are **E_S2p** and **ETS2p** with a charge density more than 2 C/m^3. The long times to failure of these specimens may also have something to do with the magnitude of the charge density.

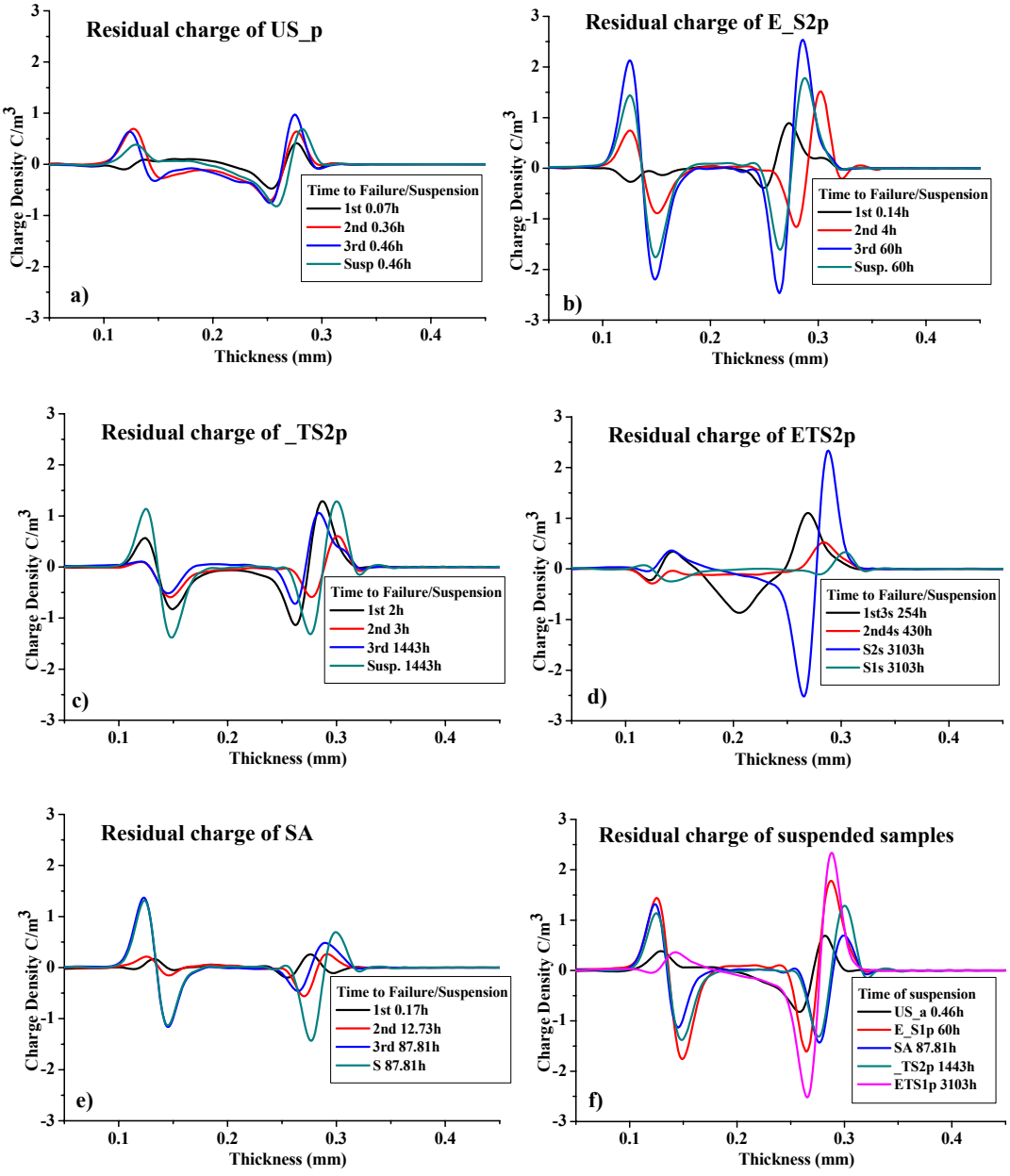

Figure 4.3.36: Retained charge after the endurance test B.

(c) After the endurance test C

The endurance test **C,** as well as **A,** was conducted at a high temperature of 90^{o}C. The charge escapes easily the material. Thus the residual charge profiles are similar to the ones from the endurance test **A** and are omitted from this section.

4.4 DISCUSSION

The space charge behaviour of Artemis peelings before and after endurance test conditions has been investigated in this chapter. The results show that the endurance stressing did alter the space charge behaviour of the materials both under and outside the electrode area, the latter being where only the temperature component was acting. It was found that the endurance stressing conditions of tests **A** and **C** where the temperature was kept at 90^{o}C, made the charge injection under dc poling easier on the side where the brass high voltage electrode was located. Both positive and negative charge can be injected into that side of the specimen dependent on the polarity of the field as can be seen from Figure 4.3.8 and Figure 4.3.9. This injected charge forms a second homocharge peak adjacent to the electrode that is found mainly in electrically pre-stressed specimens that had participated in the endurance test **A**, which showed good endurance capability. The magnitude and time of appearance of the second homocharge peak varies from sample to sample as indicated in Table 4.4.1. It appears the fastest in the electrically pre-stressed materials and decays very slowly in all cases although the electric field produced by these charges encourages them to neutralise suggesting that the charges forming it reside in deep traps. The retained charge after the PEA experiments only decays under the TSC experiment where the temperature is increased and thus the mobility of the charge increases, see Figure 4.3.11. The charge retained after the PEA experiment is more than the charge responsible for the current measured during the TSC experiment, as estimated in Table 4.3.2. This may happen because the trap hopping energy barrier is reduced and with the influence of the electric field these charges can recombine or neutralise easily creating currents in opposite polarity which results in a reduced net current (Tanaka Y. et al, 1998).

Ref name	Time to failure/ suspension (hours)	Time of first appearance ≤ (min)	Duration (min)		Magnitude of the second peak (C/m^3)	
			of dc poling	of recorded decay	at the end of dc poling	at the end of the decay
US_p	497	121	120+135	8	1.5	1.5
E_S2p(ss_b)	1537	40	320	1140	2.7	2.5
E_S2p(ss_a)	1537	10	230	1080	2.3	2.1
E_S1a	1537	30	360	1080	5	4.8

Table 4.4.1: Times and magnitudes of formation of the second peak after the endurance test A for the unstressed and electrically pre-stressed materials.

The charge injection for the specimens that participated in the endurance test **C**, appears to be easier than the ones in endurance test **A**. The charge that is injected penetrates the specimen a lot faster compared to test **A** samples, and it spreads across to the cathode within 68 minutes for the unstressed material, **US_a**, and within 35 minutes for **E_S2p**, **_TS2p** and **SA** materials, see Table 4.4.2. This charge decays very slowly although the electric field produced by the space charge encourages it to neutralise. However this field may not be big enough to overcome the trap hopping energy barrier that these charges occupy. For the **ETS2p** material, see Figure 4.3.31, the positive charge that is injected forms a small positive peak next to the anode for the first 120 minutes. Thereafter positive and negative charge is injected from the cathode and the anode respectively and penetrates the material. It seems that for this material the negative and positive charge injection occurs in equal amounts, thus the positive net charge does not extend to the cathode.

Ref name	Time to suspension (hours)	Penetration time of injected charge to cathode ≤ (min)	Duration (min)		Magnitude of the injected charge density(C/m^3)	
			of dc poling	of recorded decay	at the end of dc poling	at the end of the decay
US_a	6088	68	342	174	2.6	2.3
E_S2p	6088	35	240	1245	4	3
_TS2p	6088	35	1185	6978	3.5	3.1
ETS2p	6088	NA	1030	270	5	5
SA	6088	15	400	720	4.7	2.3

Table 4.4.2: Penetration times of injected charge to cathode and magnitudes after the endurance test C.

Positive charge injection and penetration to the cathode is also observed for the **US_p**, **ETS2p** and **SA** materials after the endurance test **B**, where the fastest charge penetration to the cathode occurs for the **SA** one, see Table 4.4.3. However for the **E_S2p** and **_TS2p** materials the space charge accumulated adjacent to the electrodes is negative and its magnitudes are indicated in Table 4.4.3. Positive charge appears in the **_TS2p** material adjacent to the cathode only when it is poled further, see Figure 4.3.19. This could mean that negative charge injection and transport dominates over the positive one and that ionic separation if it occurs is slow. It should also be noted that the space charge found in all the materials participated in this test is unipolar; positive for the **US_a** and **SA** materials, negative for the **E_S2p** and **_TS2p**. However in the **ETS2p** material the space charge formed is both positive and negative. The polarity of the retained charge after the endurance test **B** and the space charge accumulated during the subsequent dc poling is the same only for the **E_S2p** and **_TS2p** materials. This means that the positive charge injection and transport occurs easier in the other materials. The reason this happens needs to be investigated further.

Ref name	Time to failure/ suspension (hours)	Penetration time of injected charge to cathode ≤ (min)	Duration (min)		Magnitude of the injected charge density(C/m^3)	
			of dc poling	of recorded decay	at the end of dc poling	at the end of the decay
US_a	0.46	60	185	5400	1.8	2
E_S2p	60	NA	183	1200	-6.1**C**, -4**A**	-3**C**, -4**A**
_TS2p	1443	NA	182	70	-5**C**, -8**A**	-1.5**C**, -1.5**A**
ETS2p	3103	70	1030	270	5	5
SA(ss)	87	15	121	105	5	4.7

Table 4.4.3: Penetration times of injected charge to cathode and magnitudes after the endurance test B.

4.5 CONCLUSIONS

- There are two categories of charge, homocharge that is rapidly extracted and heterocharge that is only extracted very slowly.
- The endurance stressing has changed the space charge behaviour in the following ways:
    - Further thermal stressing decreased the time to hetero-charge accumulation.
    - Further electro-thermal stressing, on the other hand, resulted in a homo-charge double peak at the high-voltage electrode that was indicative of an irreversible change.
- Negative residual charge is retained after stressing at 30^{o}C and there is some indication that its magnitude is related to the length of time on stress and is a symptom of longevity not a cause. At higher temperatures the residual charge is rapidly extracted and cannot be measured easily.

5 CHAPTER: DISCUSSION

The previous three chapters reported experiments carried out on XLPE peelings that were cut from full size EHV cables with different electro-thermal stressing histories from the Artemis programme. The peelings were characterized mainly; via space charge measurements (Tzimas et al, 2005) reported in chapter 2; via endurance tests (Tzimas et al, 2006) reported in chapter 3 and via further space charge measurements after the endurance tests (Tzimas et al, 2007) reported in chapter 4. The purpose of these investigations was to identify possible "ageing markers" that can be extracted from space charge measurements. Space charge measurement has been chosen as a tool to identify possible "ageing markers" because after Artemis programme (Fothergill et al, 2003) it was suggested to be a sensitive technique to detect ageing of the material or rather changes in the material that were introduced from different conditions of electro-thermal stressing. The build up of space charge in polymeric insulation materials has been suggested to be the driving force behind the ageing mechanism in the model proposed by Dissado et al (1997). This model was shown to be the only model that fitted three sets of endurance test data at three different temperatures with the same set of parameters (Mazzanti et al, 2005). Hence, in this chapter the answers to the following questions in terms of quantities that can be extracted from space charge measurements will be the core of discussion:

1. *Did the stressing during the ARTEMIS programme change the material?*
2. *How did the electro-thermal prehistory of the XLPE peeling influence their endurance capability?*
3. *How do the field, temperature and stressing duration affect the material's space charge behaviour?*
4. *What properties of the material changed during the endurance tests?*
5. *What changes does the field introduce to the material at lower temperatures?*

The questions that arose from the data presented in the experimental chapters are also discussed. These are:

A. How long does it take for space charge changes to be observable?
B. When does ionic separation start to be observable and what conditions lead to its occurrence?
C. How does space charge evolve during different levels of electro-thermal stress?
D. Why do some samples fail earlier than the others?

E. Has the structural matrix of the material been degraded after ARTEMIS or the Endurance test? And if so, how and in which materials?
F. Do the specimens that last as long as the 3rd failure shows any evidence of degradation in the space charge measurements or other techniques?
G. Can we tell the difference between failures that occurred due to a defect or matrix degradation, i.e. bond scission etc?

5.1 SPACE CHARGE ORIGIN AND DISTRIBUTION

The types of charge that can be expected to form space charge in a dielectric can be electronic or ionic in nature as described in section 1.5.2. The wide range of possible origins for the space charge measured in insulating polymers make its interpretation very complex. For example, the space charge measured during accumulation could be formed by injection/extraction and/or by ionization of molecules or ions that might already exist in the material, with its spatial distribution being determined by transportation of charge to the opposing electrode, and recombination. Furthermore the space charge may decay by charge de-trapping and extraction at the injecting electrode, transit of the sample and extraction at the opposing electrode or neutralisation by injected charge of opposite polarity. However some general features can be derived from the space charge measurements during its accumulation and decay that could be used to characterize polymeric materials and evaluate their state. These are outlined below:

- Movement of injected charge boundary by:
  - Penetration of injected charge into the bulk of the material, where in some cases a second peak can be formed adjacent to the electrode or spread across the bulk to the opposing electrode;
  - Transit time of space charge boundary to the opposite electrode;
- Heterocharge formation, possibly due to ionic dissociation;
- Magnitude of the space charge density that is related to:
  - Density of shallow trap depths, i.e. density of charge that decays rapidly;
  - Density of deep traps, i.e. density of charge that decays slowly if it does at all for the given temperature.

5.2 EFFECT OF ARTEMIS STRESSING

The results reported in Chapter 2 show that the electro-thermal stressing that the XLPE experienced during the Artemis programme did introduce changes in the material.

These changes were observed mainly in quantities extracted from space charge measurements, such as the dc threshold, charge mobility and other, see section 2.1.3.

5.2.1 Space charge measurement findings

The space charge characterization that was carried out in this study showed that 5000h of thermal stressing did not substantially modify the space charge behaviour of the material although 10000h of thermal stressing may have increased the shallow trap density. On the other hand electrical stressing made it easier for the injected negative charge to transport, and to transit the sample and accumulate at the anode. The combination of electrical and thermal stressing increased the ability of the material to accumulate net charge associated with charge densities extending to shallower trap depths. This feature was even more enhanced in the serviced stressed material where negative heterocharge accumulated next to the anode possibly by fast negative charge injection and transit to the anode (Tzimas et al, 2005 and Delphino et al, 2007). The lower trap depths that were estimated for negative charge adjacent to the anode may also support this contention as it is shown in Table 5.2.1. However, the possibility that positive ionic charge may have accumulated adjacent to the anode reducing rapidly the net negative charge, cannot be ruled out. The trap depths estimated separately for the space charge regions adjacent to the anode and cathode show two kinds of behaviour in all materials. The negative charge adjacent to the cathode resides in traps with small trap depths whereas the negative charge adjacent to the anode resides in deeper traps.

The reason for this could lie with the injection and extraction properties of the electrode/insulation interfaces or could depend on the type of carriers that form the net charge peaks that are observed with the PEA technique. G. Chen et al (2001) investigated the injection properties of different electrode insulation interfaces in LDPE plaque samples where it was concluded that semicon electrodes inject more electrons and holes than the aluminium ones. When each electrode material is evaluated separately it was concluded that semicon electrodes inject more electrons than holes and aluminium ones more holes than electrons, (G. Chen et al, 2001). Hence, the injection rate of electrons and holes for the cathode electrode, which in this study is aluminium, is less than the one that can be expected for the anode which consists of semicon. Thus the rapid decay of the negative charge adjacent to the cathode could be assigned to positive charge injection on voltage removal that occurred while the electric field at the interface

is high enough. Furthermore, the maximum charge density that is recorded after poling at the cathode is greater than the one at the anode creating a higher interfacial electric field that could inject positive charge, see Table 5.2.1. The unstressed material, **US_a**, that was dc poled for 26 hours and was observed to have equal amounts of negative charge in peaks accumulated adjacent to the cathode and near to the anode after poling, see Table 5.2.1, even though the anode electrode, which consists of semicon, would inject holes at a higher rate than the aluminium cathode would inject electrons. However, it was estimated that the trap depth of the negative charge adjacent to the cathode is again less than the negative charge near the anode. A possible scenario is one in which injected electrons move quickly in shallow traps until they reaches the anode, where a delay in extraction allowed it time to be trapped in deeper states. Although the

Material Reference name	Poling time	Transit time of negative charge to Anode	Adjacent to Cathode		Adjacent to Anode	
			Maximum Charge density after poling(C/m^3)	**Trap Depth (eV)**	Maximum Charge density after poling(C/m^3)	**Trap Depth (eV)**
US_a (A)	120min	NA	-5	**0.95**	1	**1.10**
_TS1a (A)	120min	600 sec	-3	**0.95**	-1	**1.10**
ETS1p (A)	120min	600 sec	-6	**0.94**	-1	**1.10**
SA (A)	120min	60 sec	5	**0.93**	-12	**1.04**
US_a (B)	120min	NA	-7	**0.86-0.90**	0	**1.05**
US_a (B)	26 hours	≥215 mins ≤21 hours	-4	**0.86-0.98**	-4	**1.08**
E_S1p (B)	120min	10 mins	-5	**0.84-0.87**	-2	**1.05**
E_S1a (B)	300min	10 mins	-6	**0.88**	-3	**1.04**
_TS1p (B)	90+120min	90+3mins	-3	**0.85**	-2	**1.00**
_TS2p (B)	120min	NA	-7.5	**NA**	0	**NA**
ETS2p (B)	120min	NA	-8	**NA**	0	**NA**

Table 5.2.1: Adapted from Table 2.3.3 including the trap depths estimated in chapter 2 for charge adjacent to both cathode and anode.

small trap depth of the negative charge at the cathode indicates that its decay on voltage removal is mostly determined by de-trapping and extraction at the injecting electrode, it can also be speculated that a contribution may be made by some injected positive charge that has migrated from the anode to the cathode during dc poling. Such migration was not observable during accumulation because the injected negative charge density dominated over any positive charge contribution. This positive charge could be electronic, i.e. holes injected from the anode and transiting through the sample to the cathode where it accumulated possibly due to a low extraction rate. It could also be ionic, i.e. molecules that dissociate in the bulk into positive ions that migrate to the anode and negative ions that move towards the anode. In this case though, the negative charge that is accumulated at the anode could also be ionic, thus the transit time of negative charge to the anode indicated in Table 5.2.1, could also be the time that ionic separation begins to be observable by space charge measurements.

5.2.2 Endurance test findings

The endurance tests, **A** and **C**, at high electrical field (70 kV/mm and 55kV/mm) and high temperature (90^{o}C) showed that the pre-stressing history of the peelings as a cable did reduce the inherent endurance capability of the material especially when the pre-stressing was either just thermal or combined electrical and thermal (Tzimas et al, 2006). Peelings with only an electrical pre-history did not demonstrate a significant decrease in the inherent endurance capability under these endurance tests. On the other hand the endurance test **B** that was conducted at high electrical stress (70k/mm) and a lower temperature, 30^{o}C, contradicted the findings of the endurance tests at high electro-thermal stress, see Figure 3.4.6.

The reasons that lead a dielectric insulation to age and ultimately fail are multiple as Dissado and Fothergill demonstrated in (Dissado & Fothergill, 1992) and the theoretical models by Crine (2002 and 2005), Dissado (2002a), Dissado et al (1997 and 2001), Mazzanti el al (1999, 2001 and 2005), Paloniemi (1981), Wu K. & Dissado (2004), show that the attempt to describe it is very complex. These models approach a scientific explanation from different points of view; electrical, chemical, mechanical, electromechanical, etc, by the choice of the dominant mechanism that leads to failure, see chapter 1. Nonetheless they all present a good fit to experimental data (Crine, 2002 and 2005), (Mazzanti et al, 2005) and (Grifiths et al, 1998).

The reasons that lead to contradictory endurance test findings at two different temperatures are also multiple, for instance:

- different inherent features of the peeling due to the pre-stressing history as well as the radial position that the specimens were taken from;
- the limited number of specimens that participated in endurance test **B**;
- the effect of the high electric field of the endurance test at the two temperatures;
- the synergistic contribution of the above reasons all together.

Nevertheless, endurance test **B** did demonstrate that Artemis stressing had altered the endurance capability of the materials but in such away as to actually improve the endurance strength of the pre-stressed samples compared to the unstressed ones. This may be true at the conditions under which endurance test **B** was conducted, i.e. the low temperature. The reasons listed above will be discussed in the following sections in order to envisage the failure mechanisms that may have led to the contradictory findings of the endurance tests.

(a) The effect of Electric Field and Temperature in the Endurance Test

The endurance tests that were carried out on unstressed peelings at ac electric fields ranging from 30 to 80 kV/mm(rms) and two temperatures, 20 and 90^{o}C (see Figure 3.1.2), during the Artemis programme by Montanari and the group from Bologna (Borealis, 2003), showed that the influence of the endurance test temperature increases as the electric field decreases. At 70kV/mm the confidence limits of the failures of the unstressed peeling at both temperatures overlap giving lifetimes ranging between 3 and 30 hours with characteristic values of 9.5 and 5.5 hours at 20 and 90^{o}C respectively, suggesting temperature does not contribute significantly at high fields. Cooper (2004) calculated lifelines using equivalent parameters so as to illustrate the similarities and the differences between the DMM (Dissado, Montanari and Mazzanti, 1997) model and that of the Lewis et al (1996) for a wide range of electric fields at two temperatures, see for example Figure 5.2.1. Both models predict very similar lifetimes. In this case also the effect of temperature decreases as the electric field increases till it becomes insignificant.

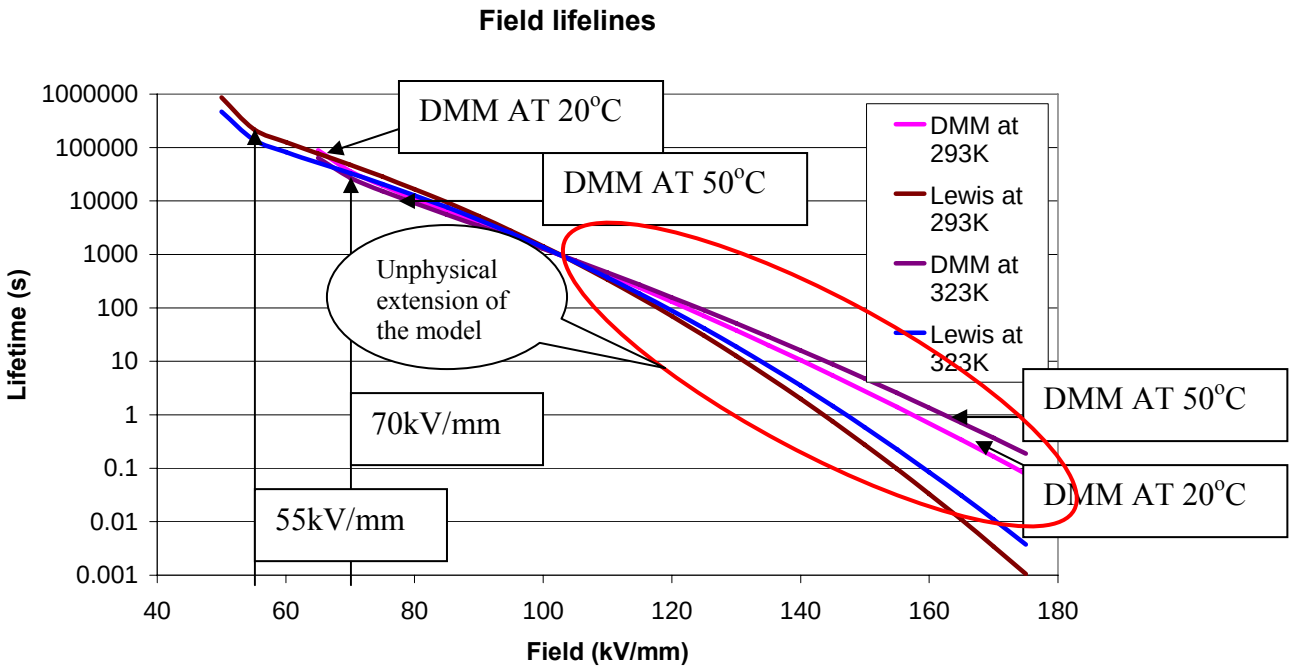

Figure 5.2.1: Comparison of the field life lines for the DMM and Lewis et al models at two different temperatures over a range of electric fields from 40-180kV/mm, taken from Cooper (2004).

In the current investigation the times to failure of the unstressed materials are *shorter* when the endurance test temperature is *lower* while the electrically and thermally pre-stressed materials do fall within the failure distribution range (see Figure 3.1.2). On the other hand the electro-thermally pre-stressed material showed a better endurance capability in the low temperature endurance test than in the high temperature test, as might be expected. Hence the greatest statistical difference occurs between the unstressed and the electro-thermally stressed materials.

This difference may lie in the effect that the temperature has on the space charge accumulation and transport at high electric fields and the inherent properties that may influence it (Herman et al, 2004). It was reported by Chong Y.L. et al (2007) that the charge injection threshold for dc poling decreases as the temperature increases for degassed XLPE plaques and that positive charge propagation increases as the temperature is increased. The space charge measurements reported in chapter 2 on the unstressed and electro-thermally stressed materials show that the former ones could accumulate less charge than the latter ones. Hence considering the temperature difference between endurance test **A** and endurance test **B**, positive charge could be injected and transported easier in the materials during endurance test **A** than **B**. Moreover if it is assumed that the ability of the materials to accumulated and transport

charge in ac field is similar to the one at dc fields then the electro-thermally stressed materials may have failed earlier in the endurance test **A** because of the large amounts of positive charge that were injected during each positive half cycle leading to high injection and extraction currents. It could have been easier for these positive charges to transport in the electro-thermally stressed material than the unstressed one, possibly because of shallow traps created during the stressing as a cable. The electro-thermally stressed material also behaved differently in endurance test **B**, but this time it exhibits a longer life than the unstressed material samples. The electro-thermally stressed samples also showed a different behaviour to all the other material samples in the measurements of the retained charge made after the endurance test. In all samples of the other materials negative charge accumulation adjacent to both electrodes was observed, even in the specimens of unstressed material that failed in less than an hour, see Figure 4.3.36. This means that this negative charge resides in deep traps and is not extracted during the positive half-cycle. Furthermore, its presence during the positive half-cycle increases the interfacial field at the electrode increasing the likelihood of specimen failure. Despite the longevity of all the specimens of the electro-thermally stressed material (that gave it a long time to accumulate charge) only one of the suspended specimen showed negative charge accumulation at one of the electrodes, suggesting that the interfacial field for these specimens were not as high as for the other materials. It is therefore possible that the contradictions in the endurance test results occurred because the injected charge had a different effect at the two temperatures, with the low temperature lifetimes governed by charge retention in deep traps increasing the interface field, and high temperature lifetimes governed by the injection/extraction currents favoured by charges in shallow traps. Other possible explanations for the contradictions are discussed in the following subsections.

It should also be pointed out that there is another question that arises from the residual charge measurements after the endurance test B and it lies in the origin of the retained charge. Negative charge during ac stressing was observed by Y.L. Chong et al (2006) via space charge measurements on XLPE plaques and it was found that it also accumulates adjacent to the electrodes. This charge could be ionic or electronic. If this charge is electronic then it could be injected during the negative half cycle at each electrode and possibly transported to the opposite one if it has a high mobility. The negative charge accumulation during ac stressing could also be attributed to the ability

of the material to trap negative charge. On the other hand, if this charge is ionic then it is suggested that negative ions are more mobile than the positive ones and manage to separate in the time interval of the positive half cycle. However if this is the case then positive charge should be observable in the bulk of the material. Unless the positive ions recombine with injected negative charge, the accumulated negative charge at the electrodes is electronic. The origin of ionic charge could also lie in the chemical composition of XLPE and the residual cross-linking by-products and chemical species that can be found in XLPE as is indicated in the next subsection, and possibly observed via space charge measurements on Artemis peelings by Thomas et al (2008).

(b) The effect of the inherent features of the peelings

The peelings were cut from 14mm thick cable insulation and the roll originally covered the full radial distance from inner to outer semicon. Different void sizes and number (Markey & Stevens, 1999 and 2003) were found at different radial locations from the semicon (see chapter 1). The electrical stress (Figure 5.2.2a) as well as thermal stress (Figure 5.2.2b) was also not exactly the same across the insulation width. The electric field at the 2-4mm region for the **ETS2p** material ranges from 28 to 24 kV/mm and the temperature from 88 to 86^{o}C.

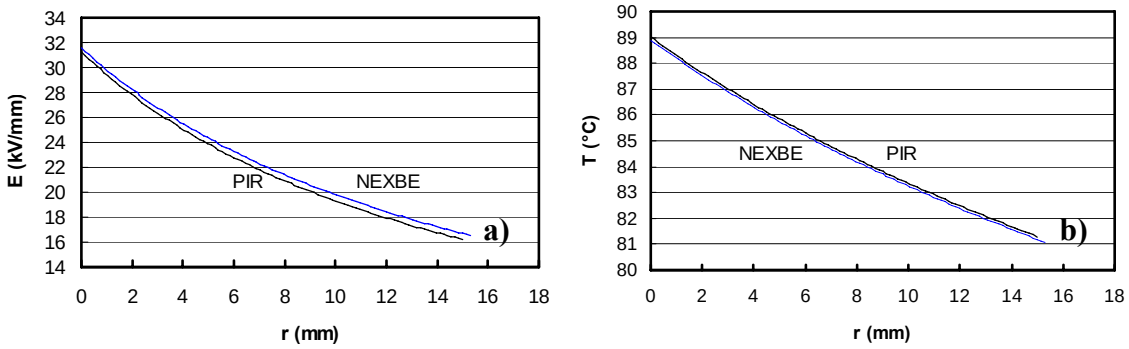

Figure 5.2.2: a) Electric field vs radial distance and b) Temperature vs radial distance from inner semicon of the two ARTEMIS cables. Taken from Borealis (2003).

As was pointed out in chapter 1 XLPE is far from a pure material, as it could contain chemical impurities, such as the DCP cross-linking by products, cumyl alcohol and acetophenone, and antioxidants as well as various kinds of stabilizers (Smedberg et al, 2004). During a spectroscopic analysis that was carried out during the Artemis programme it was found that the concentration and radial distribution of these chemical species depends on the type of stress that the peeling has experienced as a cable (Herman et al, 2005). Figure 5.2.3 shows the acetophenone concentrations as a function of the radial distance of the insulation for three peelings; an unstressed reference; an

electrically stressed and an electro-thermally stressed one. The acetophenone concentrations with respect to the reference material decrease at radial distances near to the inner semicon and increase near the outer semicon as the electrical and particularly thermal stress duration is increasing. It is true that the purpose of the thermal conditioning of the peelings was to remove as much as possible of the cross-linking by-products. However an examination that was carried out by Herman et al (2004) on the

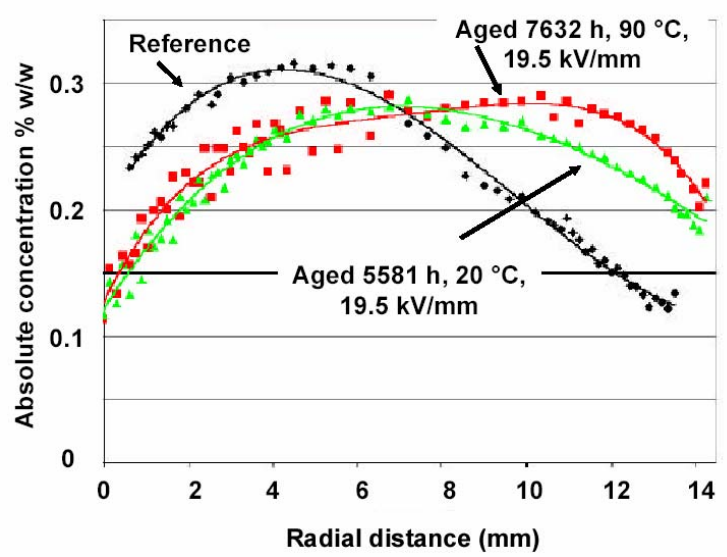

Figure 5.2.3: Acetophenone concentration for an unstressed material (probably US_a or US_p), (◆), electrically pre-stressed material E_S1a (5581 hours, 22°C, 225kV) (▲), and an electro-thermally stressed material, (7632 hours, 90°C, 225kV) similar conditions to ETS2p but at lower electric field stress (■). Taken from conference publications on Artemis peelings (Herman et al, 2004 and 2005).

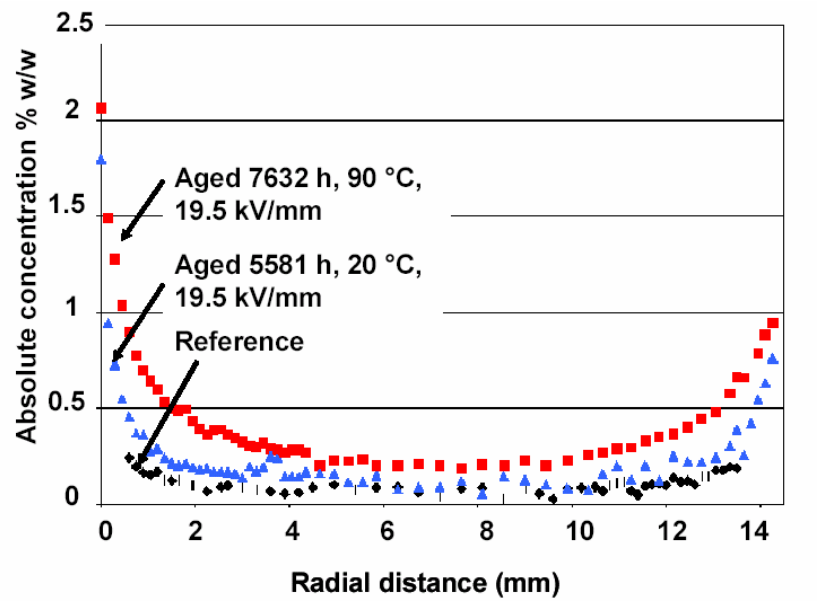

Figure 5.2.4 Acrylate concentration for an unstressed material (probably US_a or US_p), (◆), electrically pre-stressed material E_S1a (5581 hours, 22°C, 225kV) (▲), and an electro-thermally stressed material, (7632 hours, 90°C, 225kV) similar conditions to ETS2p but at lower electric field stress (■). Taken from conference publications on Artemis peelings (Herman et al, 2004 and 2005).

ETS2p material showed than up to 10% of both acetophenone and cumyl alcohol may remain in the polymer either attached onto the polymer chain or trapped within non-permeable voids, see Figure 5 of (Herman et al, 2004).

Not only the acetophenone concentration is altered by the stress type and duration but also the acrylate concentrations as is shown in Figure 5.2.4. Acrylate species migrate from both the inner and outer semiconductive screens into the insulation making its chemical composition even more complicated. It seems that thermal component of stress encourages the migration of acrylate species more than electrical stress alone. A multivariate statistical analysis (MVSA) that was carried out by Herman et al (2004) of the chemical species regressed against external properties of the peelings such as space charge measurements and electroluminescence led to a strong correlation providing a link between chemical information and the physical properties of the materials.

This correlation implies that space charge measurements are affected by the concentration of the above-mentioned chemical species as they could increase the chemical disorder of the polymer "matrix" and consequently increase the trap depths as well as the trap densities, and change its endurance life (Mazzanti et al, 2003a). Space charge measurements on the unstressed material, **US_p**, after the endurance test **B** showed positive charge accumulation across the bulk of the specimen and an increase in the trap density as well as the trap depth of the positive charge, see Figure 4.3.15. This positively trapped charge got released with the TSC technique and its activation energy was estimated to be **1.51eV**. As this specimen was cut very near to the inner semiconductive screen it is very likely that the acrylate concentration was high and has provided localised states for positive charge transport and accumulation that may have caused its rapid breakdown during endurance test **B**. On the other hand the space charge measurements of the electro-thermally pre-stressed material, ETS2p, showed charge densities of positive charge with smaller magnitudes in spite of the long period of time that it had to accumulate charge during the endurance test **B**. In contrast to the US_p material the positive charge does not distribute evenly across to the cathode, see Figure 4.3.20. This is indeed very peculiar as the stressing applied under the endurance test B for over 3000 hours would tend to increase more the trap depths and trap densities of the ETS2p material than would be the case over the period of less than an hour that the US_p material survived. Nevertheless, the contrary is observed, implying that these two

set of samples may be untypical. Their behaviour could be the consequence of very different concentrations of chemical species such as acetophenone and acrylates in combination with the antioxidant (Sekii, 2007) that is already present in the material.

(c) The limited number of specimens

The statistical difference of the failures with the endurance test **A** may also be attributed to the limited number of specimens that participated in the endurance test **B**, especially in the case of the unstressed material, **US_p**, whose limited length of tape forced the use of specimens near the inner semiconductive screen where the number of voids was found to increase and contamination of the semicon was very likely. As is shown above the inherent features of the material, either chemical or morphological, are dependent on the radial location that the specimens were taken from. Although the majority of the specimens that participated in the endurance tests were taken from a radial region between 2-4mm, a reasonable variation of inherent features can be observed between the 2mm and 4mm distance from the inner semicon. Hence this variation could be projected onto the endurance test results.

(d) The synergistic effect

It is more than likely that the synergistic contribution of all the above mentioned factors is responsible for the difference in behaviour observed in endurance test **A** and **B**. As was pointed out in the discussion section of chapter 3, at the high electric fields used in the endurance tests the early failures of the materials may well be occurring due to the presence of larger rather than smaller morphological defects. At such high field large morphological defects such as spheroidal or tubular voids observed in the peelings could develop partial discharges that will cause eventual breakdown. If non-permeable voids exist in the material and they contain aromatic chemical species such as acetophenone or cumyl alcohol partial discharging may be inhibited in electrical fields, however they could expand the void or even form cracks under thermal stressing if the material has lost its elasticity, probably like the ones shown in Figures 3.5.8 and 3.5.11 for example. Weibull distributions with a shape parameter $\beta=0.5$ that characterise the majority of the material failures (see Table 3.5.1) are termed in failure statistics “infant mortality” distributions (Chan & Meeker, 1999). This means that unless a failure occurs early in the material’s life time it has a great probability to exhibit longevity. Usually such early failures are regarded as due to the presence of defects, whose origin would lie in the manufacturing or stressing pre-history of the materials. The endurance lifetime

is associated with the severity of the defect. Specimens that withstand the endurance test beyond a certain period, i.e. later than the first failure of the group that this specimen belongs to, have a less severe defect, and so the longer the time on test the less severe the worst defect in the specimen and the longer the sample is likely to survive. However, this does not mean that morphological defects could not be created in this specimen during the stressing of the endurance test as was shown in chapter 3. Hence, the time to failure of the later rather than the earlier failures could depend more on the alteration of the inherent chemical properties of the peelings and the subsequent morphological ones, rather than on just morphological changes that possibly already exist in the specimens that fail quickly and cause their rapid breakdown. In other words, this means it is more likely that changes in the properties of the "matrix" of the polymer may be observed in specimens that fail later than in those that fail quickly. Thus, space charge measurements were carried out mostly on specimens that have lasted the longest under the endurance tests.

5.3 EFFECT OF ENDURANCE TESTS

Endurance testing did introduce changes of the space charge behaviour of the materials with respect to that found after Artemis stressing, but prior to the endurance test. Inherent features prior to the pre-stressing conditions are also reflected in the space charge behaviour after the endurance test stressing. In Table 5.3.1 the typical polarity of the charge that was accumulated after the three endurance tests is stated for the five pre-stressing conditions that the peelings experienced, both for under and outside the electrode area. Additionally, in Table 5.3.2 to Table 5.3.4, the main changes that were observed in endurance tests **A** to **C** are stated along with the trap depth estimations and are used in together with Table 5.2.1 in order to identify changes in the space charge behaviour of the materials.

Type of pre-Stressing \ Endurance test			Typical polarity of charge: A 70kV/mm,90°C	B 70kV/mm,30°C	C 55kV/mm,90°C
Unstressed	Under	A	Positive	Positive	Positive
		C	Negative	Negative (Bulk-slow positive)	Negative
	Outside	A	Positive	NA	Positive
		C	Negative	NA	Negative
Electrical	Under	A	Fast Negative (Bulk-slow positive peak)	Negative	Positive
		C	Negative-(E_S2p switches to Positive on voltage removal)	Negative	Negative
	Outside	A	Slow Negative	NA	Positive
		C	Slow Positive	NA	Negative
Thermal	Under	A	Positive	Fast Negative	Positive
		C	Negative	Negative (when further dc poled switches to Positive on voltage removal)	Positive
	Outside	A	NA	NA	Positive
		C	NA	NA	Negative
Electro-thermal	Under	A	Positive	Positive	Positive
		C	Negative	Negative	Negative
	Outside	A	NA	Fast Negative	Positive (switches to Negative on voltage removal)
		C	NA	Negative	Negative (switches to Positive on voltage removal)
Service	Under	A	NA	Positive	Positive
		C	NA	Positive	Negative
	Outside	A	NA	Positive	Negative
		C	NA	Positive	Positive

Table 5.3.1: Typical charge polarity in peelings with various pre-stressing conditions during accumulation both under and outside the electrode area adjacent to the anode and cathode.

5.3.1 Endurance test A

Table 5.3.1 shows that the polarity of the charge that is accumulated adjacent to the electrodes after the endurance tests remains the same in a lot of cases with what was observed before, i.e. positive and negative charge adjacent to the anode and cathode respectively. Despite this the space charge behaviour did change for all the materials after endurance testing as is shown in Table 5.3.2 to Table 5.3.4. For instance space charge measurements on the long lived specimens after endurance test **A** showed the formation of a double peak near the anode during accumulation. The time taken for this second peak to appear was different in the electrically and unstressed material, with it appearing faster in the former. The reason for this could be because the electrical pre-stressed material withstood the electro-thermal stressing of the endurance test **A** for a longer time. Hence the formation of the second peak could be an effect of the ac electro-thermal endurance stressing rather than a cause of material failure. It should also be noted that in all cases the charge that is trapped in the second peak decays very slowly if it does at all, see Table 5.3.2. This suggests that ac electro-thermal endurance stressing creates more deep traps (Mazzanti et al, 2003a, Wu K. & Dissado, 2005). Similar space charge features have also been observed in XLPE plaques by Abou-Dakka et al (2004) and Y.L. Chong et al (2006). Abou-Dakka et al (2004) observed a double peak during dc (50kV/mm) ageing for tree-retardant XLPE plaques where its magnitude also increased with ageing time and its first appearance occurred after 6000 hours. This observation may though be related to the effect of the tree-retardant additives rather than as a consequence of ageing. In normal type XLPE they observed opposite polarity peaks near the electrodes that moved closer together over time, which suggests that the space charge boundaries are extending with dc stressing. This agrees with the contention that ageing creates more traps and increases the trap density Wu K. & Dissado, 2005).

The origin of the double peak could either be physical or chemical and even in some case a combination of both. Physical in the way that it occurs in the tree-retardant XLPE plaques, where the intended action of tree-retardant additives is probably to become conducting in high fields and so reduce the enhancement of divergent stress points and hence inhibit the initiation of electrical trees. In the plaques such high field conductivity would move the injected charge further into the material until the field near the anode

reduced sufficiently for the additive to revert to low conductivity. A similar conductive path could have formed for the **E_S1p** material where surface deterioration observed, see Figure 3.5.7, and the second peak appeared the fastest, see Figure 5.3.1e.

On the other hand it could be chemical, in the way that it probably occurs in the **E_S2p** material, see Figure 4.3.5a, where fast negative charge accumulates adjacent to the anode increases the interfacial field and encourages further positive charge injection. Y.L. Chong et al (2006) observed similar space charge behaviour under dc poling after ac stressing XLPE plaques containing no antioxidant at ambient temperature. Hence, the occurrence of this double peak may be due to the consumption/oxidation of the antioxidant due to high temperature and the ac electrical stress as has also been suggested by Kon H. et al, (1996) for XLPE stressed under high fields. Antioxidant clusters are also known to lead to stress cracking and promote oxidation (B.S.Bernstein, 1984), so thermal and electrical stresses that produce such clusters will promote degradation. Overall it is probable that both chemical and physical routes will lead to local conducting patches penetrating into the polymer near the electrode, and hence to penetration of injected charge to the ends of the conducting region as is found in water trees (Y.Okhi, 2007). A similar result may occur for a discharging void next to the electrode, with the discharges creating a peak of charge with the same polarity as the electrode at the tip of the void, as well as the peak due to injected charge.

Sample Reference	Time to failure/ suspension (hours)	Double peak	**Trap depth (eV)**	Duration (min)		Magnitude of the second peak (C/m^3)	
		Time of 1st appearance ≤ (min)		of dc poling	of recorded decay	at the end of dc poling	at the end of the decay
US_p	497	121	**0.91**	120+135	8	1.5	1.5
E_S2p(ss_b)	1537	40	**1.035 (TSC 0.75-1.5)**	320	1140	2.7	2.5
E_S2p(ss_a)	1537	10	**1.033**	230	1080	2.3	2.1
E_S1a	1537	30	**1.03**	360	1080	5	4.8

Table 5.3.2: Estimated trap depths after Endurance Test A.

5.3.2 Endurance test B

If we assume that the positive charge injection and formation of the double peak is due to the consumption of the antioxidant then the space charge measurement after the endurance test **B** suggests that the antioxidant has not been consumed during the electrical or thermal stressing alone as both the electrically and thermally pre-stressed materials show no positive charge injection, see Table 5.3.3. This contention also agrees with the observations of Boudou et al (2004) in low-density polyethylene where the addition of antioxidant was shown to encourage negative charge injection and transport to the anode. The space charge behaviour of the electrically and thermally pre-stressed materials fits with that description. On the other hand the space charge behaviour of the electro-thermally, **EST2p**, and service, **SA**, pre-stressed materials do not fit into the same pattern as injection and transport of positive charge injection is observed, and this occurs the fastest in the **SA**, see Table 5.3.3. The positive charge accumulated in these materials decays very slowly indicating that it resides in deep traps. This observation also supports the contention that ageing creates deep traps.

Ref name	Time to failure/ suspension (hours)	Penetration time of injected charge to cathode ≤ (min)	**Trap depth (eV)**	Duration (min)		Magnitude of the injected charge density (C/m^3)	
				of dc poling	of recorded decay	at the end of dc poling	at the end of the decay
US_a	0.46	60	**1.074 (TSC-1.51)**	185	5400	1.8	2
E_S2p	60	NA	**1.038 (TSC-1.33)**	183	1200	-6.1C, -4A	-3C, -4A
_TS2p	1443	NA	**0.963**	182	70	-5C, -8A	-1.5C, -1.5A
ETS2p	3103	70	**0.998**	1030	270	5	5
SA(ss)	87	15	**0.974**	121	105	5	4.7

Table 5.3.3: Estimated trap depths after Endurance Test B. In the last two columns A stands for anode and C for cathode.

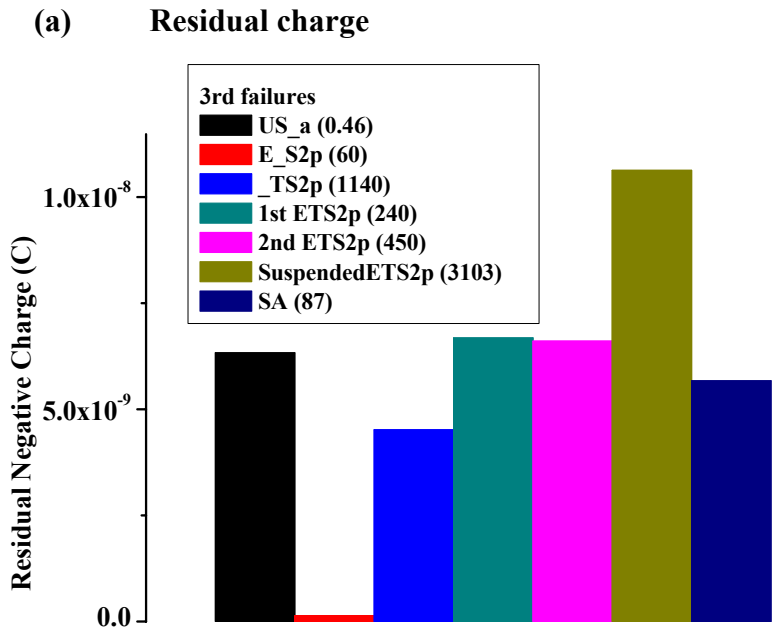

Figure 5.3.2: Residual negative charge after endurance test B for the 1st, 2nd failures and suspended specimens for ETS2p material and for the 3rd failures for all the other materials.

Figure 5.3.2 shows that a significant amount of charge is retained after endurance test **B** in a range of samples. There is some indication that the retained charge increases the longer the time to failure in the electro-thermally pre-stressed and service aged materials, but this correlation is not maintained when the other materials are taken into account. In particular the charge retained by the electrically pre-stressed material is very low but it should be remembered that the residual charge measurements were taken as

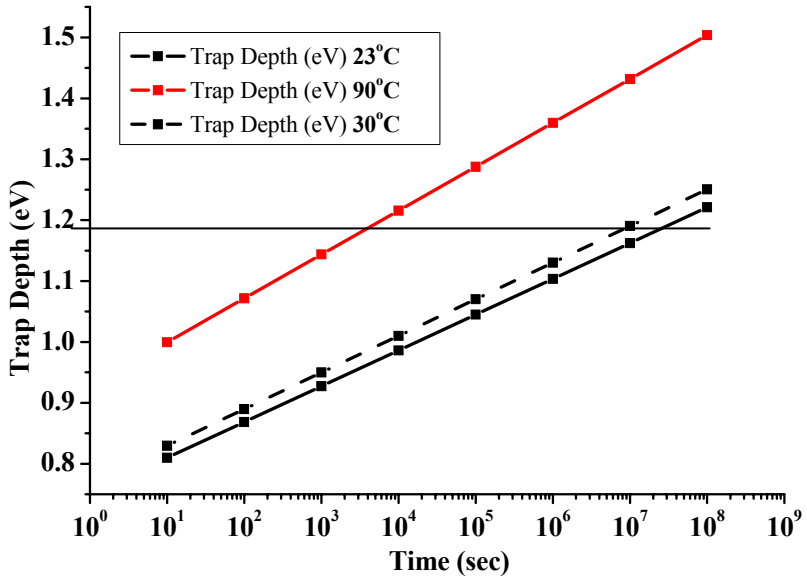

Figure 5.3.3: Space charge decay times and corresponding trap depths at three temperatures; 23; 90 and 30°C. Estimated using Equation (3) in chapter 2.

near as possible to the breakdown. Hence, depending on the location of the breakdown a greater portion of charge may be lost in some materials than in others. Further work is needed with more samples to clarify whether or not a correlation exists.

Figure 5.3.3 shows that the residual charge after endurance test **B** (at 30°C) could be residing in traps with depths greater than **1.2 eV,** and if we assume that any charge injected in tests A and C occupied similar trap depths it can be seen that it would decay within less than an hour. For this reason much smaller amounts of retained space charge would be expected after the endurance tests at 90^{o}C as was observed.

5.3.3 Endurance test C

The space charge behaviour of samples that underwent stressing for 6088 hours of endurance test **C** has also changed with respect to the behaviour measured before the test. In this case positive charge injection is observed after the endurance test **C** Once again regardless of the pre-stressing conditions of the materials positive charge injection and propagation is observed. This suggests, as argued previously, that the combination of ac electrical and thermal stressing has consumed the antioxidant in the materials. The fastest positive charge injection occurs in the thermally and electrically pre-stressed material see Table 5.3.4, whereas the greatest amount of net charge initially injected is found in the thermally pre-stressed sample, see Figure 5.3.4. However over time the total net charge is reduced in the thermally pre-stressed material probably because it is extracted at the cathode or neutralized by negative charge injection.

At the end of the dc poling though the space charge in this specimen increases rapidly, possibly because negative charge injection begins to dominate and propagate further into the bulk. This space charge behaviour is normally found in high dc fields where the heterocharge field produced by a negatively charged region that extends across the sample triggers the formation of positive charge packets that cross the sample to the cathode (See A. et al, 2001a, 2001b and 2001c, Hozumi N. et al, 1998, and Lanca et al, 2007a).

Heterocharge accumulation has been observed at the beginning of the measurements of space charge in the service stressed material before any endurance stressing. It was also observed in specimens that had experienced electrical or thermal stressing as a cable

and thermal or electrical stressing during the endurance tests. This may be due to the separation of ionic species, the relatively rapid transit of charge carriers to an electrode where extraction is slow, or the extension of a region of injected charge to the counter electrode as described above. Space charge measurements reported by Sekii et al (2007) suggest that hetero-charge formation in XLPE is caused by the separation of ionic species produced by chemical reaction between a sulfur type antioxidant and residues of ducumyl peroxide in the presence of acetophenone. As the XLPE material under study contains a sulphur type antioxidant as well as residues of cross-linking by products, it is very likely that the heterocharge formations observed are due to the separation of ions produced by these chemical species. Thomas et al (2008) observed regions of opposite polarity charges to exist in Artemis peelings prior to any poling, suggesting again ionic separation. Thus it is very likely that the combination of Artemis stressing and endurance test **C** stressing resulted in the generation of negative ions near the anode that encourage positive charge injection and its subsequent propagation to the cathode. Evidence of heterocharge accumulation at both electrodes is found in the service pre-stressed material, see Figure 4.3.34.

It is very difficult to distinguish whether heterocharge formation is due to the separation of ions or electronic charge injection as it is more than likely that both processes occur at the same time. The current conduction model of Heylen & Postoyalko (2008) based on the Schottky law managed to fit experimental conduction currents (Montanari, 2000) in XLPE film similar to that studied here by introducing a term accounting for ionic currents. Heylen & Postoyalko (2008) argued that above the threshold fields that were identified by Montanari (2000), where the conduction currents increase drastically and space charge accumulation occurs, the currents observed were due to a combination of ionic and electronic components. In contrast, numerical models based on the Schottky injection law with a part-blocking electrode can also generate heterocharge accumulation (Le Roy S. et al, 2007). The space charge profile outside the electrode of the **ETS2p** material after the endurance test **C**, see Figure 4.3.32 demonstrates that the injection of electronic charges at the electrodes and their transit to the opposite electrodes and/or ionic dissociation can occur simultaneously. There, no charge is observed until the voltage removal when opposite polarity charges to the electrode can be seen to have been accumulating. It is most likely that these charges are ions as it is easier for the electronic charge to be extracted or neutralised than ionic charge, though

these could be charges that are deep trapped. Regardless of the origin of the heterocharge its occurrence is a problem for the insulation system as it increases the interfacial field, which could reduce the insulation life.

Sample Reference	**Trap depth (eV)**	Penetration time of injected charge to cathode ≤ (min)	Duration (min)		Magnitude of the injected charge density(C/m^3)	
			of dc poling	of recorded decay	at the end of dc poling	at the end of the decay
US_a	**0.987**	68	342	174	2.6	2.3
E_S2p	**1.037**	35	240	1245	4	3
_TS2p	**1.08**	35	1185	6978	3.5	3.1
ETS2p	**0.998**	NA	1030	270	5	5
SA	**1.023**	15	400	720	4.7	2.3

Table 5.3.4: Estimated trap depths after 6088 hours in the Endurance Test C.

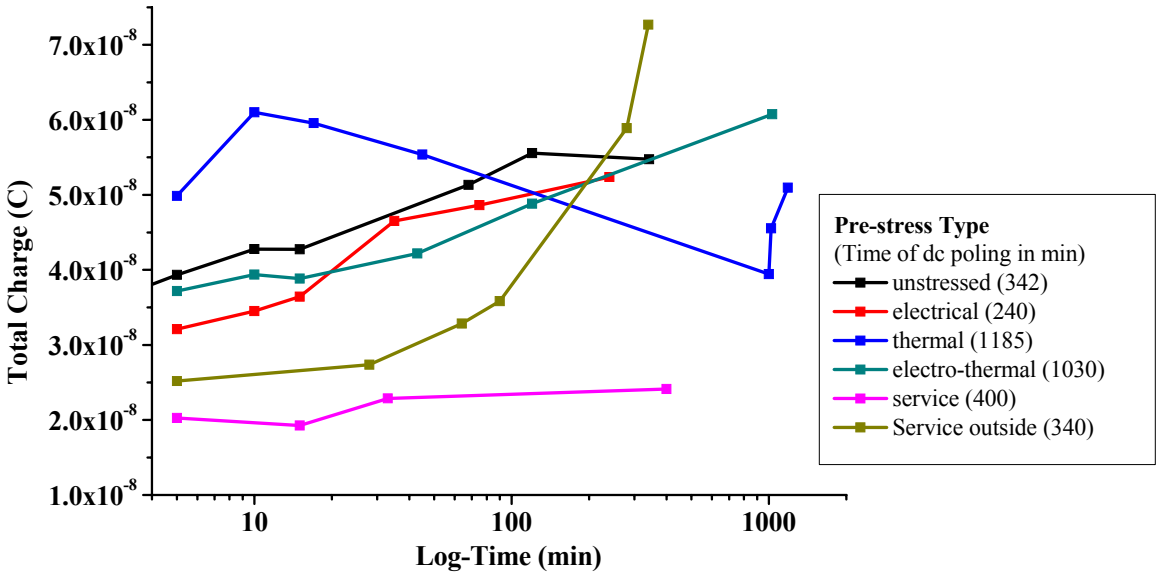

Figure 5.3.4: Total charge accumulation for the five types of materials that participated in endurance test C.

As is demonstrated by the charge still remaining in the material after ten minutes of decay following voltage removal, Figure 5.3.5, the total charge decay plot of the materials that participated in endurance test **C**, the deep trap density of the materials that underwent endurance test **C** has increased with respect to the ones reported in Table 5.2.1 and the charge of the unstressed material after 2 and 26 hours of dc poling before endurance stressing.

The greatest magnitude of total charge occurs in the service stressed material but outside the electrode area. On the other hand the least amount of total charge is observed for the serviced stressed material under the electrode area. This is very peculiar. This material as the space charge measurements outside the electrode area as well as the ones before any endurance stressing show, is the material in which the greatest accumulation of charge is also observed. The electro-thermally pre-stressed material exhibits similar space charge behaviour after 3108 hours under the endurance test **A** condition. One possible explanation would be that these materials have not reached a thermal equilibrium with the charge filling the traps from deep traps upwards (Dissado et al, 2006). This could mean that more time under dc poling is needed for charge to start filling the deep traps that were created during the endurance test. This contention is also supported by the space charge behaviour of the electro-thermally pre-stressed material after the endurance test **C** where its space charge distribution does not show any significant change over the first 120 minutes of poling, see Figure 4.3.31.

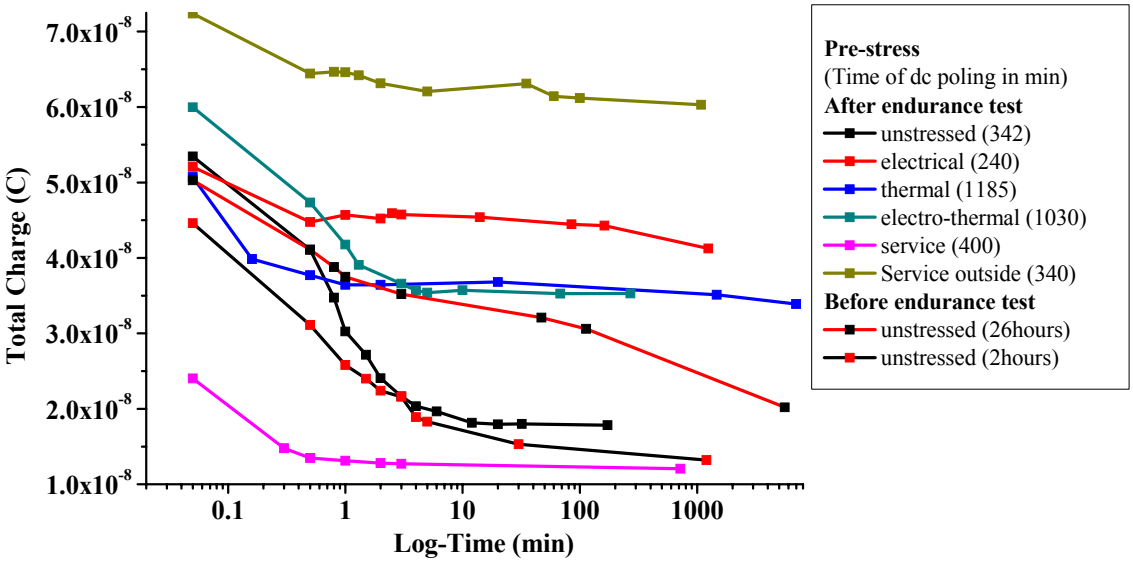

Figure 5.3.5: Total charge decay for the five types of materials that participated in endurance test C and the unstressed material before the endurance for comparison.

6 CHAPTER: CONCLUSIONS AND FURTHER WORK

Artemis stressing did change the inherent properties of the XLPE insulation peelings that were stressed under different electro-thermal conditions as cable. These changes were observed via space charge measurements and ac endurance tests at three different conditions. The space charge measurement before any further endurance stressing showed that:

- There is no evidence during 120 minutes of DC poling that thermal stressing over 5000h substantially modifies the space charge profile of the cable insulation.
- The electric stressing seems to introduce changes to the material by making easier the transit of negative charge from the cathode to the anode as was observed under dc poling for 120 and 300 minutes.
- The combination of an electric field and high temperature also introduces changes. These are:
    - Greater ability to accumulate net charge associated with a greater density of traps extending to shallower trap depths.
    - In the field aged cables heterocharge accumulation is observed which could be attributed to:
        - The existence of shallow traps together with filled deep traps allow charge transit and its formation at the electrodes, or
        - Ionic dissociation products of a chemical reaction between the antioxidant and ducumyl peroxide residues in the presence of acetophenone.
    - Heterocharge accumulation is also observed in electrically stressed materials, but to a smaller extent than in the field aged materials.
- Negative charge accumulated adjacent to the cathode escapes faster on voltage removal than when it is trapped adjacent to the anode. This could also be attributed to positive charge accumulation that is superimposed with negative charge injection, but further space charge measurements made simultaneously with the external current are required to verify this.
- The low temperature peak observed in the TSC experiments occurs due to charges released adjacent to the cathode which reside in low energy trap states.

The endurance test **A** at 70kV/mm and 90^{o}C suggests that:

- for the first 5000h of electrical and electro-thermal stressing only cables that experienced a thermal component (T = 90 °C) showed evidence of significant ageing as expressed through a reduction in endurance life at 70kV/mm and 90°C;
- for the same time of cable stressing there was no significant difference in endurance between samples from cables with different applied electrical fields, in the range from zero up to the maximum of 28kV/mm. This was found to be the case for both cables stressed at 90 °C and 20 °C.

The endurance test **C** at 55kV/mm and 90^{o}C agrees with the statements made from endurance test **A**.

- There are two categories of charge, homocharge that is rapidly extracted and heterocharge that is only extracted very slowly.
- The endurance stressing has changed the space charge behaviour in the following ways:
    - Further thermal stressing decreased the time to hetero-charge accumulation.
    - Further electro-thermal stressing, on the other hand, resulted in a homo-charge double peak at the high-voltage electrode that was indicative of an irreversible change.
- Negative residual charge is retained after stressing at 30^{o}C and there is some indication that its magnitude is related to the length of time on stress and is a symptom of longevity not a cause. At higher temperatures the residual charge is rapidly extracted and cannot be measured easily.

The optical microscopy study shows that both voids and tubular type defects increase when the material is subjected to electrical and electro-thermal stress both as a cable and as a peeling.

Chemical analysis by the FTIR technique in a correlated with a chemometric analysis could achieve concrete conclusions about the charge species and its relation to the chemical species that may pre-exist or may have generated during electro-thermal stressing.

REFERENCES:

ABOU-DAKKA, M., BULINSKI, A. & BAMJI, S. (2004) "Space charge development and breakdown in XLPE under DC field". *IEEE Transactions on Dielectrics and Electrical Insulation,*(ISBN: 1070-9878/1), Vol. 11, No. 1, pp. 41-49.

ALIJAGIC, J., MARSHUIS, P.H.F. & SMIT, J.J. (2004) "Possibilities for Using Space Charge Quantities as Aging Markers and as Tool for Material Ranking," *Proceedings of ICSD,* Toulouse, France, (ISBN.0-7803-8348-6), pp. 743-746.

ALISON, J. M. & HILL, R. M. (1994) "A model for bipolar charge transport, trapping and recombination in degassed crosslinked polyethylene", *Journal of Physics D: Applied Physics*, Vol. 27, pp. 1291-1299.

ANDREWS, T., HAMPTON, R. N., SMEDBERG, D. W., WASCHK, V. & WEISSENBERG, W. "The Role of Degassing in XLPE Power Cable Manufacture", *IEEE Electrical Insulation Magazine*, (DEIS) Vol. 22, No. 6, pp. 5-16.

ANTONIJEVIC, M. (2005) Chapter 3 of PhD Thesis, "The use of thermally stimulated currents spectroscopy in the physical characterisation of pharmaceutical systems". *Queens University Belfast*.

BAMBERY, K. R. & FLEMING, R. J. (1998) "Space Charge Accumulation in Two Power Cable Grades of XLPE". *IEEE Transactions on Dielectrics and Electrical Insulation,*(ISBN: 1070-9878/98), Vol. 5, No. 1, pp. 103-109.

BERNSTEIN, B.S. (1984) IEEE Int.Symp. Elec.Insul. (Montreal), pp11-21.

BLAISE, G. (2001) "Charge localization and transport in disordered dielectric materials". *Journal of Electrostatics,*(0304-3886/01), Vol. 50, pp. 69-89.

BOREALIS (2003) "Final Technical Report". *Borealis AB*, 11-11-2003.

BOUDOU, L. & GUASTAVINO, J. (2002) "Influence of temperature on low-density polyethylene films through conduction measurement". *Journal of Physics D: Applied Physics*, (0022-3727/02/131555) Vol. 35, pp. 1555-1561.

BOUDOU, L., GRISERI, V., GUASTAVINO, J. & DISSADO, L. A. (2004) "Effect of Temperature on Space Charge Formation in Low Density Polyethylene - Role of Antioxidant". *International Conference on Solid Dielectrics*, (0-7803-8348-6/04), pp. 252-255.

BOUFAYED, F., LE ROY, S., TEYSSEDRE, G., LAURENT, C., SEGUR, P., COOPER, E., DISSADO, L. A. & MONTANARI, G. C. (2004) "Numerical resolution of charge transport in cross-linked polyethylene by means of bipolar model with a distribution of traps.". *IEEE International Conference on Solid Dielectrics*, (ISBN:), 2, pp. 562-566.

BROWN, M. A., CHEN, G., DAVIES, A. E., DISSADO, L. A. & NORMAN, P. A. (2000) "Space charge characterization in aged LDPE amalgamated insulation regions from under water telecommunication systems" *IEEE Transactions on Dielectrics and Electrical Insulation*, Vol. 7, pp. 346-352.

CASTELLON, J. & MALRIEU, S. (2002) "Report on Artemis on-site cable measurements". *Advance Metrology for Electrical Engineering*, Artemis Project, 18/03/2002.

CHAN, V. & MEEKER, W. Q. (1999) "A Failure-Time Model for Infant-Mortality and Wearout Failure Modes". *IEEE Transactions on Reliability,*(ISBN: 0018-9529/99), Vol. 48, No. 4, pp. 377-387.

CHEN, G., TAY, T. Y. G., DAVIES., A. E., TANAKA, Y. & TAKADA, T. (2001) "Electrodes and Charge Injection in Low-density Polyethylene Using the Pulse

Electroacoustic Technique". *IEEE Transactions on Dielectrics and Electrical Insulation,*(ISBN: 1070-9878/1), Vol. 8, No. 6, pp. 867-873.

CHEN, G., FU, M. & LIU, X. Z. (2003) "Influence of ac ageing on space charge dynamics in LDPE". *13th International Symposium on High Voltage Engineering (ISH)*, (ISBN:), pp. 365-369.

CHEN, G., TANAKA, Y., TAKADA, T. & ZHONG, L. (2004) "Effect of Polyethylene Intereface on Space Charge Formation". *IEEE Transactions on Dielectrics and Electrical Insulation,*(ISBN: 1070-9878/1), Vol. 11, No. 1, pp. 113-121.

CHONG, Y. L., CHEN, G., MIYAKE, H., TANAKA, Y. & TAKADA, T. (2004a) "Effect of AC Ageing on Space Charge Evolution in XLPE". *Annual Report Conference on Electrical Insulation and Dielectric Phenomena*, (0-7803-8584-5), pp. 81-84.

CHONG, Y. L., MIYAKE, H., TANAKA, Y., TAKADA, T., NAKAMA, H. & CHEN, G. (2004b) "Space Charge in Polyethylene under AC Elctrical Stress using the Pulsed Electroacoustic Method". *Annual Report Conference on Electrical Insulation and Dielectric Phenomena*, (0-7803-8584-5), pp. 77-80.

CHONG, Y. L., CHEN, G., HOSIER, I. L., VAUGHAN, A. S. & HO, Y. F. F. (2005) "Heat Treatment of Cross-linked Polyethylene and its Effect on Morpholoy and Space Charge Evolution". *IEEE Transactions on Dielectrics and Electrical Insulation,*(1070-9878/05), Vol. 12, No. 6, pp. 1209-1221.

CHONG, Y. L., CHEN, G., MIYAKE, H., MATSUI, K., TANAKA, Y. & TAKADA, T. (2006) "Space Charge and Charge Trapping Characteristics of Cross-Linked-Polyethylene Subject to ac Electric stresses". *Journal of Physics D: Applied Physics,*(ISBN: 0022-3727/06/081658), Vol. 39, No., pp. 1658-1666.

CHONG, Y. L., CHEN, G. & HO, Y. F. F. (2007) "Temperature Effect on Space Charge Dynamics in XLPE Insulation". *IEEE Transactions on Dielectrics and Electrical Insulation,*(1070-9878/07), Vol. 14, No. 1, pp. 65-76.

COOPER, E. S. (2004), Chapter 2 of PhD Thesis, "Polymer Ageing Models", University of Leicester, 2004.

COOPER, E. S., DISSADO, L. A. & FOTHERGILL, J. C. (2005) "Application of Thermoelectric Aging Models to Polymeric Insulation in Cable Geometry". *IEEE Transactions on Dielectrics and Electrical Insulation,*(ISBN: 1070-9878/05), Vol. 12, No. 1, pp. 1-10.

CRINE, J.-P. (2002) "Aging and Polarization Phenomena in PE under High Electric Fields". *IEEE Transactions on Dielectrics and Electrical Insulation,*(ISBN: 1070-9878/2), Vol. 9, No. 5, pp. 697-703.

CRINE, J.-P. (2004) "On The Interpretation Of Some Electrical Aging Relaxation Phenomena In Solid Dielectrics". *Annual Report Conference on Electrical Insulation and Dielectric Phenomena*, (0-7803-8584-5), pp. 1-16.

CRINE, J.-P. (2005) "On The Interpretation of Some Electrical Aging and Relaxation Phenomena in Solid Dielectrics". *IEEE Transactions on Dielectrics and Electrical Insulation,*(ISBN: 1070-9878/05), Vol. 12, No. 6, pp. 1089-1107.

DELPHINO, S., FABIANI, D., MONTANARI, G. C., DISSADO, L. A., LAURENT, C. & TEYSSEDRE, G. (2007) "Fast charge packet dynamics in XLPE insulated cable models". *Annual Conference on Electrical Insulation Dielectric Phenomena*, (IEEE 07CH37929), pp. 421-424.

DISSADO, L. A. & FOTHERGILL, J. C. (1992) *"Electrical Degradation and Breakdown in Polymers"*, Peter Peregrinus Ltd on behalf of IEE.

DISSADO, L. A. & FOTHERGILL, J. C. (Eds) (1998) "Space Charge in Solid Dielectrics", *The Dielectrics Society,* (095335380X).

DISSADO, L. A., MAZZANTI, G. & MONTANARI, G. C. (1997) "The Role of Trapped Space Charges in the Electrical Aging of Insulating Materials". *IEEE Transactions on Dielectrics and Electrical Insulation,*(ISBN: 1070-9878/97), Vol. 4, No. 5, pp. 496-506.

DISSADO, L. A., PARIS, O., DITCHI, T., ALQUIE, C. & LEWINER, J. (1999) "Space Charge Injection and Extraction in High Divergent Fields". *IEEE International Conference on Electrical Insulation and Dielectric Phenomena*, (0-7803-5414-1/99), pp. 23-26.

DISSADO, L. A., FOTHERGILL, J. C., SEE, A., STEVENS, G. C., MARKEY, L., LAURENT, C., TEYSSEDRE, G., NILSSON, U. H., PLATBROOD., G. & MONTANARI, G. C. (2000) "Characterizing high-voltage XLPE cables through electrical, chemical, and micro-structural measurements performed on cable peelings: the effect of surface roughness, thermal treatment, and peeling location". *Annual Report Conference on Electrical Insulation and Dielectric Phenomena*), 1, pp. 136-140.

DISSADO, L. A., MAZZANTI, G. & MONTANARI, G. C. (2001) "Elemental strain and trapped trapped space charge in thermoelectrical aging of insulating materials Part 1: Elemental strain under thermo-electrical-mechanical stress". *IEEE Transactions on Dielectrics and Electrical Insulation,*(1070-9878/1), Vol. 8, No. 6, pp. 959-965.

DISSADO, L. A. (2002a) "Predicting electrical breakdown in polymeric insulators". *IEEE Transactions on Dielectrics and Electrical Insulation,*(1070-9878/2), Vol. 9, No. 5, pp. 860-875.

DISSADO, L. A. (2002b) "Understanding Electrical Trees in Solids: From Experiment to Theory", *IEEE Transactions on Dielectrics and Electrical Insulation*, (1070-9878/1), Vol. 9, No. 4, pp. 483-497.

DISSADO, L. A., GRISERI, V., PEASGOOD, W., COOPER, E. S., FUKUNAGA, K. & FOTHERGILL, J. C. (2006) "Decay of Space Charge in Glassy Epoxy Resin Following Voltage Removal". *IEEE Transactions on Dielectrics and Electrical Insulation,*(1070-9878/06), Vol. 13, No. 4, pp. 903-916.

DISSADO, L. A. (2007) "The Electrical Ageing of Polymeric Insulation", *Proc. Int.Conf. on Polymeric Materials in Power Engineering* (ICPMPE) Bangalore India, paper I-2 (10 pages).

FABIANI, D., MONTANARI, G. C., CAVALLINI, A. & MAZZANTI, G. (2004) "Relation between space charge accumulation and partial discharge activity in enameled wires under PWM-like waveforms". *IEEE Transactions on Dielectrics and Electrical Insulation,*(1070-9878/04), Vol. 11, No. 3, pp. 393-405.

FLEMING, R. J., HENRIKSEN, M. & HOLBOLL, J. T. (2000) "The Influence of Electrodes and Conditioning on Space Charge Accumulation in XLPE". *IEEE Transactions on Dielectrics and Electrical Insulation,*(1070-9878/0), Vol. 7, No. 4, pp. 561-571.

FLEMING, R. J. (2005) "Space Charge Profile Measurement Techniques: Recent advances and Future Directions". *IEEE Transactions on Dielectrics and Electrical Insulation,*(1070-9878/05), Vol. 12, No. 5, pp. 967-978.

FOTHERGILL, J. C., MONTANARI, G. C., STEVENS, G. C., LAURENT, C., TEYSSEDRE, G., DISSADO, L. A., NILSSON, U. H. & PLATBROOD., G. (2003a) "Electrical, Microstructural, Physical and Chemical Characterization of HV XLPE CAble Peelings for an Electrical Aging Diagnostic Data Base". *IEEE Transactions on Dielectrics and Electrical Insulation,*(1070-9878/03), Vol. 10, No. 3, pp. 514-527.

FOTHERGILL, J.C., HAMPTON, R.N. & MONTANARI, G.C. (2003b) “IEEE P930: the Statistical Analysis of Electrical Insulation Breakdown Data”, IEEE Standard.

FOTHERGILL, J. C. (2007) " Ageing, Space Charge and Nanodielectrics: Ten Things We Don’t Know About Dielectrics", *International Conference on Solid Dielectrics*, (1-4244-0750-8/07)pp. 1-10.

FU, M. & CHEN, G. (2003) "Space charge measurement in polymer insulated cables using flat ground electrode PEA system". *IEE Proc. – Sci. Meas. Technol.*), 150, pp. 89-96.

FU, M., CHEN, G. & LIU, X. (2004) "Space charge behaviour in LDPE after AC electracal ageing". *Proc. 8th International Conference on solid Dielectrics (ICSD2004)*, ((IEEE 04CH37539)), pp. 217-220.

GARROS, B. (1999) "Ageing and Reliability Testing and Monitoring of Power Cables: Diagnosis for Insulation Systems, The ARTEMIS Program". *IEEE Electrical Insulation Magazine,*(0883-7554/99), Vol. 15, No. 4.

GRANIER, O., TOUREILLE, A., SCHUE, F. & COLLET, A. (1999) "Manufacturing process effect on space charge evolution in high voltage XLPE cables: Correlation between thermal history and presence of space charge". *ARTEMIS Project*, (ISBN:), pp.

GRIFITHS, C. L., FREESTONE, J. & HAMPTON, R. N. (1998) "Thermoelectric Aging of Cable Grade XLPE". *IEEE ISEI*, (0-7803-4927-X/98), pp. 578-582.

GUBANSKI, S. M., NILSSON, U. & WANG, M. S. E. (1992) "Thermally Stimulated Depolarization Current Measurements of Different Polyolefin Compounds". *Nordic Insulation Symposium*, (1102-4925), pp. 8.5:1-10.

HAMPTON, R.N., HARTLEIN, R., ORTON, H. & RAMACHANDRAN, R. (2007) "Long-Life XLPE Insulated Power Cable", *Jicable*.

HEYLEN, A.E.D. & POSTOYALKO, V. (2008) "Classical Interpretation of Conduction Currents in Crosslinked Polyethylene (XLPE) and a Comparison with Ideal Polyethylene" *IEEE Transactions on Dielectrics and Electrical Insulation,*(1070-9878/07), Vol. 15, No. 2, pp. 342-349.

HERMAN, H., THOMAS, J. & STEVENS, G. (2004) "Spectroscopic and Chemometric Analysis of Cable Condition in the Artemis Program". *ICSD*, (0-7803-8348-6/04), pp. 623-627.

HIRAI, N., MINAMI, R., TANAKA, T., OHKI, Y., OKASHITA, M. & MAENO, T. (2003) "Chemical Group in Crosslinking Byproducts Responsible for Charge Trapping in Polyethylene". *IEEE Transactions on Dielectrics and Electrical Insulation,*(1070-9878/1), Vol. 10, No. 2, pp. 320-330.

HO, Y. F. F., CHEN, G., DAVIES, A. E., SWINGLER, S. G., SUTTON, S. J., HAMPTON, R. N. & HOBDELL, S. (2002) "Measurements of Space Charge in XLPE Insulation Under 50 Hz AC Electric Stresses Using the LIPP Method". *IEEE Transactions on Dielectrics and Electrical Insulation,*(1070-9878/1), Vol. 9, No. 3, pp. 362-370.

HO, Y. F. F., CHEN, G. & DAVIES., A. E. (2003) "Effect of Semiconducting Screen on the Space Charge Dynamic in XLPE and Polyolefin Insulation under dc and 50Hz ac Electric Stresses Conditions". *IEEE Transactions on Dielectrics and Electrical Insulation,*(1070-9878/1), Vol. 10, No. 3, pp. 393-403.

HOFFMANN, R., JANIAK, C. & KOLLMAR, C. (1991) "A Chemical Approach to the Orbitals of Organic Polymers". *Macromolecules,*(0024-9297/91/2224-3125), Vol. 24, No. 13, pp. 3725-3744.

HOZUMI, N., TAKEDA, T., SUZUKI, H. & OKAMOTO, T. (1998) "Space charge behaviour in XLPE cable insulation under 0.2-1.2 MV/cm dc fields". *IEEE Transactions on Dielectrics and Electrical Insulation,*(1070-9878/98), Vol. 5, No. 1, pp. 82-90.

JONES, J. P., LLEWELLYN, J. P. & LEWIS, T. J. (2005) "The Contribution of Field-Induced Morphological Change to the Electrical Aging and Breakdown of Polyethylene". *IEEE Transactions on Dielectrics and Electrical Insulation,*(1070-9878/05), Vol. 12, No. 5, pp. 951-966.

KON, H., SUZUOKI, Y. MIZUTANI, T., IEDA, M. & YOSHIFUJI, N. (1996) "Packet-like Space Charges and Conduction Current in Polyethylene Cable Insulation", *IEEE Transactions on Dielectrics and Electrical Insulation,*(1070-9878/96), Vol. 3, No. 3, pp. 380-385.

LANCA, M. C. (2002), PhD Thesis "Electrical ageing studies of polymeric insulation for power cables". University of Lisbon, Portugal.

LANCA, M. C., NEAGU, E. R. & MARAT-MENDES, J. N. (2002) "Combined isothermal and non-isothermal current measurements applied to space charge studies in low-density polyethylene". *Journal of Physics D: Applied Physics,*(0022-3727/02/080029+04), Vol. 35, No., pp. L29-L32.

LANCA, M. C., NEAGU, E. R., NEAGU, R. M. & MARAT-MENDES, J. N. (2004) "Space Charge Studies in LDPE Using Combined Isothermal and Non-isothermal Current Measurements". *IEEE Transactions on Dielectrics and Electrical Insulation,*(1070-9878/1), Vol. 11, No. 1, pp. 25-34.

LANCA, M. C., FU, M., NEAGU, E. R., DISSADO, L. A., MARAT-MENDES, J. N., TZIMAS, A. & ZADEH, S. (2005) "Comparative study of Space charge in the polymeric insulation of power cables using PEA, isothermal and non-isothermal discharge current measurements". *Proc. ISE12 - 12th Int. Symp. on Electrets*, (0-7803-9116-0), pp. 284-287.

LANCA, M. C., NEAGU, E. R., DISSADO, L. A. & MARAT-MENDES, J. N. (2006) "Space Charge Studies in XLPE from Power Cables using Combined Isothermal and Thermostimulated Current Measurements". *Material Science Forum, Trans Tech Publications,*(143.210.107.61-02/10/06), Vol. 514-516, No., pp. 935-939.

LANCA, M. C., NEAGU, E. R., DISSADO, L. A. MARAT-MENDES, J. N., TZIMAS, A. & ZADEH, S. (2007a) "Space charge analysis of electro-thermally aged XLPE cable insulation", accepted in *Space Journal of Non-Crystalline Solids*, February 2007.

LANCA, M. C., NEAGU, E. R., DISSADO, L. A., MARAT-MENDES, J. N., TZIMAS, A. & ZADEH, S. (2007b) "Space charge analysis of electro-thermally aged XLPE cable insulation", *4th Int. Conf. Int. Dielectric Soc. & 9th Int. Conf. on Dielectric and Related Phenomena,* 3-7 Sept., Poznan, Poland, Book of extended Abstracts, (ISSN 0458-1555), pp. 58-59.

LAURENT, C., TEYSSEDRE, G. & MONTANARI, G. C. (2004) "Time-resolved Space Charge and Electroluminescence Measurements in Polyethylene Under ac Stress". *IEEE Transactions on Dielectrics and Electrical Insulation,*(1070-9878/04), Vol. 11, No. 4, pp. 554-560.

LAVERGNE, C. & LACABANNE, C. (1993) "A review of Thermo-Stimulated Current". *IEE Electrical Insulation,*(0883-7554/93), Vol. 9, No. 2, pp. 5-11.

LE ROY, S., TEYSSEDRE, G., LAURENT, C., DISSADO, L. A. & MONTANARI, G. C. (2007) "Relative Importance of Trapping and Extraction in the Simulation of Space Charge Distribution in Polymeric Insulators under DC Potentials" *IEEE International Conference on Solid Dielectrics,*(1-4244-0750-8/07), pp. 494-497.

LE ROY, S., TEYSSEDRE, G. & LAURENT, C. (2006) “Numerical methods in the simulation of charge transport in solid dielectrics” *IEEE Transactions on Dielectrics and Electrical Insulation,* Vol. 13, No. 2, 239-246.

LEWINER, J., HOLE, S. & DITCHI, T. (2005) "Pressure Wave Propagation Methods: a Rich History and a Bright Future" *IEEE Transactions on Dielectrics and Electrical Insulation,*(1070-9878/05), Vol. 12, No. 1, pp. 114-126.

LEWIS, T. J., LLEWELLYN, J. P., SLUIJS, M. J. VAN DER, FREESTONE, J. & HAMPTON, R. N. (1996) “A new model for Electrical Ageing and Breakdown in Dielectrics” . IEEE DMMA, pp.220-224.

LIM, F. N., FLEMING, R. J. & NAYBOUR, R. D. (1999) "Space charge accumulation in Power Cable XLPE insulation". *IEEE Transactions on Dielectrics and Electrical Insulation,*(1070-9878/99), Vol. 6, No. 3, pp. 273-281.

MAENO, Y., HIRAI, N., OHKI, Y., TAKADA, T., OKASHITA, M. & MAENO, T. (2005) "Effects of Crosslinking Byproducts of Space Charge Formation in Crosslinked Polyethylene". *IEEE Transactions on Dielectrics and Electrical Insulation,*(1070-9878/05), Vol. 12, No. 1, pp. 90-97.

MARAT-MENDES, J. N., NEAGU, E. R. & NEAGU, R. M. (2004) "Electrical conduction and space charge trapping in highly insulating materials". *Journal of Physics D: Applied Physics,*(0022-3727/04/030343+05), Vol. 37, No., pp. 343-347.

MARKEY, L. & STEVENS, G. C. (1999) "Task 1 Interim Report: Microstructural and chemical characterisations of unaged cable samples". *University of Surrey*, 29/09/1999.

MARKEY, L., STEVENS, G. C., DISSADO, L. A. & MONTANARI, G. C. (2000) "Multi-stress electrical and thermal ageing of HV extruded polymeric cables: mechanisms and methods". *Eighth International Conference on Dielectric Materials, Measurements and Applications. (IEE Conf. Publ. No. 473)*, (0-85296-730-6), pp. 413-418.

MARKEY, L. & STEVENS, G. C. (2003) "Microstructural characterisation of high-voltage XLPE electrical insulation in power cables: Determination of void size distributions using TEM". *Journal of Physics D: Applied Physics,*(0022-3727/36/20/022), Vol. 36 No. 20, pp. 2569-2583.

MARY, D., LAURENT, C., TEYSSEDRE, G., BAMJI, S., BULINSKI, A., ABOU-DAKKA, M. & CISSE, L. (2004) "Threshold of Space Charge Injection and Electroluminescence in Polymeric Insulation". *Annual Report Conference on Electrical Insulation and Dielectric Phenomena*, (0-7803-8584-5), pp. 249-252.

MAZZANTI, G., MONTANARI, G. C. & DISSADO, L. A. (1999) "A space-charge life model for ac electrical aging of polymers". *IEEE Transactions on Dielectrics and Electrical Insulation,*(1070-9878/99), Vol. 6, No. 6, pp. 864 - 875.

MAZZANTI, G., MONTANARI, G. C. & DISSADO, L. A. (2001) "Elemental strain and trapped space charge in thermoelectrical aging of insulating materials: Life modeling". *IEEE Transactions on Dielectrics and Electrical Insulation,*(1070-9878/1), Vol. 8, No. 6, pp. 966-971.

MAZZANTI, G., MONTANARI, G. C. & ALISON, J. M. (2003a) "A Space-Charge Based Method for the Estimation of Apparent Mobility and Trap Depth as Markers for Insulation Degradation-Theoretical Basis and Experimental Validation". *IEEE Transactions on Dielectrics and Electrical Insulation,*(1070-9878/1), Vol. 10, No. 2, pp. 187-197.

MAZZANTI, G., MONTANARI, G. C. & PALMIERI, F. (2003b) "Quantities Extracted from Space-charge Measurements as Markers for Insulation Aging". *IEEE Transactions on Dielectrics and Electrical Insulation,*(1070-9878/1), Vol. 10, No. 2, pp. 198-203.

MAZZANTI, G., MONTANARI, G. C. & DISSADO, L. A. (2005) "Electrical Aging and Life Models: The Role of Space Charge". *IEEE Transactions on Dielectrics and Electrical Insulation,*(ISBN:), Vol. 12, No. 5, pp. 876-890.

MEUNIER, M., QUIRKE, N. & ASLANIDES, A. (2000) "Characterisation of charge carrier traps in polymeric insulators". *Annual Report Conference on Electrical Insulation and Dielectric Phenomena*, (0-7803-6413-9), 1, pp. 21-24.

MITSIMOTO, S., FU, M., DISSADO, L.A. & FOTHERGILL, J.C. (2006) "Short Time Decay of Space Charge in Epoxy Resin", Proceedings of ICPADM, Bali (06CH37773),pp 135-138.

MIZUTANI, T., SUZUOKI, Y. & IEDA, M. (1977) "Thermally stimulated currents in polyethylene and ethylene-vinyl-acetate copolymers". *Journal of Applied Physics,*(1977JAP....48.2408M), Vol. 48, No. 6, pp. 2408-2413.

MIZUTANI, T., TSUKAHARA, T. & MASAYUKI, I. (1980) "Thermally-Stimulated Currents in Oxidized Low-Density Polyethylene". *Japanese Journal of Applied Physics,*(00214922), Vol. 19, No. 11, pp. 2095-2098.

MIZUTANI, T., SUZUOKI, Y., MASAHIRO, H. & MASAYUKI, I. (1982) "Determination of Trapping Parameters from TSC in Polyethylene". *Japanese Journal of Applied Physics,*(19821120), Vol. 21, No. 11, pp. 1639-1641.

MONTANARI, G. C., MAZZANTI, G., FABIANI, D., ALBERTINI, M. & PEREGO, G. (1999) "Investigation of DC Threshold of Polyethylenes as a Tool for Insulation Characterization". *Annual Report Conference on Electrical Insulation and Dielectric Phenomena*, (0-7803-5414-1/99), pp. 559-563.

MONTANARI, G. C. (2000) "The electrical degradation threshold of polyethylene investigated by space charge and conduction current measurements". *IEEE Transactions on Dielectrics and Electrical Insulation,*(1070-9878/0), Vol. 7, No. 3, pp. 309-315.

MONTANARI, G. C. & DAS-GUPTA, D. K. (2000) "Polarization and Space Charge Behavior of Unaged and Electrically Aged Crosslinked Polyethylene". *IEEE Transactions on Dielectrics and Electrical Insulation,*(1070-9878/0), Vol. 7, No. 4, pp. 474-479.

MONTANARI, G. C., MAZZANTI, G., BONI, E. & ROBERTIS, G. D. (2000) "Investigating ac space charge accumulation in polymers by PEA measurements". *Annual Conference on Electrical Insulation and Dielectric Phenomena*, (0-7803-6413-9/00), pp. 113-116.

MONTANARI, G. C., RAFFAELLI, L., PALMIERI, F., MARTINOTTO, L. & SERRA, S. (2001) "Techniques for the estimation of ac space charge accumulation threshold for insulating materials". *Annual Report Conference on Electrical Insulation and Dielectric Phenomena*, (0-7803-7053-8/1), pp. 460-464.

MONTANARI, G. C. (2002) "Final Technical Report - Task 6: Ageing Diagnosis System". *University of Bologna*, ARTEMIS Project.

MONTANARI, G. C., PALMIERI, F., MAZZANTI, G. & TEYSSEDRE, G. (2003) "AC charge injection investigated by means of space charge measurement: threshold and frequency dependence". *Proceedings of the 7th International Conference on Properties and Applications of Dielectric Materials*, (0-7803-7725-7), pp. 895-899.

MONTANARI, G. C., TEYSSEDRE, G., LAURENT, C., CAMPUS, A., NILSSON, U. H. & SMEDBERG, A. (2004) "Charging of PE and XLPE specimens: effect of antioxidant and cross-linking on luminescence features, space charge and conduction current measurements". *Annual Report Conference on Electrical Insulation and Dielectric Phenomena*, (0-7803-8584-5/04), pp. 73-76.

MONTANARI, G. C., LAURENT, C., TEYSSEDRE, G., CAMPUS, A. & NILSSON, U. H. (2005) "From LDPE to XLPE: Investigating the Change of Electrical Properties. Part I: Space Charge, Conduction and Lifetime". *IEEE Transactions on Dielectrics and Electrical Insulation,*(1070-9878/05), Vol. 12, No. 3, pp. 438-446.

MONTANARI, G. C. & MORSHUIS, P. H. F. (2005) "Space Charge Phenomenology in Polymeric Insulating Materials". *IEEE Transactions on Dielectrics and Electrical Insulation,*(1070-9878/05), Vol. 12, No. 4, pp. 754-767.

MUROOKA, Y., TAKADA, T. & HIDAKA, K. (2001) "Nanosecond Surface Discharge and Charge Density Evaluation Part I: Review and Experiments". *IEEE Electrical Insulation Magazine,*(0883-7554), Vol. 17, No. 2, pp. 6-15.

NEXANS (2002) "Final Technical Report; Task 4: Determination of the cable insulation ageing.". *Nexans*, Artemis Project, October 2002.

NOTINGHER, P. & TOUREILLE, A. (2002) "42 months report from MONTPELLIER". *De Montpellier*, ARTEMIS Project, March 2002.

OKAMOTO, T., SUZUKI, H., UCHIDA, K., TAKADA, T., INAMI, M. & SHINAGAWA, J. (2000) "Interfacial diffusion method to improve the breakdown strength of XLPE power cable joints". *IEEE Power Engineering Society Winter Meeting*, (0-7803-5935-6/00), pp. 712-717.

OKHI, Y. (2007) "Aiming at a more rigorous understanding in electrical insulating materials research", *Annual Report Conference on Electrical Insulation and Dielectric Phenomena* (IEEE 07CH37929), pp.1-12,

PALONIEMI, P. & LINDSTROM, P. (1977) "Application of the equalized ageing process method on thermal endurance testing of polyhydantoin film". *IEEE Transactions on Electrical Insulation*, Vol. EI-12, No. 1, pp. 67-74.

PALONIEMI, P. (1981) "Theory of Equalization of Thermal Ageing Processes of Electrical Insulating Materials in Thermal Endurance Tests I: Review of Theoretical Basis of Test Methods and Chemical and Physical Aspects of Ageing". *IEEE Transactions on Electrical Insulation,*(0018-9367/81/0200-0001), Vol. EI-16, No. 1, pp. 1-6.

PAWLOWSKI, T., LANG, S. B. & FLEMING, R. J. (2004) "Space charge and polarization in crosslinked polyethylene". *Annual Report Conference on Electrical Insulation and Dielectric Phenomena*, (0-7803-8584-5), pp. 93-96.

PHILLIPS, P. J. (1983) "Polymer morphology and molecular structure", in Chapter 2, *Engineering dielectrics*, Vol. IIA, Eds, Bartnikas, R. & Eichhorn, ASTM, Philadelphia, USA.

ROWLAND, S.M., HILL, R.M. & DISSADO, L.A. (1986) "Censored Weibull statistics in the dielectric breakdown of thin oxide films". *Journal of Physics C: Solid State Physics.* (0022-3719/86/316263) Vol. 19, pp. 6263-6285.

SAFFEL, J. R., MATTHIESEN, A., MCINTYRE, R. & IBAR, J. P. (1991) "Comparing thermal stimulated currents (TSC) with other thermal analytical methods to characterize the amorphous phase of polymers". *Thermochimica Acta, Elsevier Science Publishers B.V.,*(0040-6031/91), Vol. 192, No., pp. 243-264.

SEE, A., DISSADO, L. A. & FOTHERGILL, J. C. (2001a) "Electric field criteria for charge packet formation and movement in XLPE". *IEEE Transactions on Dielectrics and Electrical Insulation,*(1070-9878/1), Vol. 8, No. 6, pp. 859-866.

SEE, A., DISSADO, L. A., FOTHERGILL, J. C., TEYSSEDRE, G., LAURENT, C., MONTANARI, G. C. & PALMIERI, F. (2001b) "The Relationship between Charge Distribution, Charge Packet Formation and Electroluminescence in XLPE under DC". *2001 IEEE 7th International Conference on Solid Dielectrics*, (IEEE Pub. 01CH3711), pp. 97-100.

SEE, A., DISSADO, L. A., FOTHERGILL, J. C., TEYSSEDRE, G., LAURENT, C., MONTANARI, G. C. & STEVENS, G. C. (2001c) "Evaluation of the onset of space charge and electroluminescence as a marker for cross-linked polyethylene ageing". *4th International Conference on Electric Charge in Solid Insulators (CSC4)*), pp. 185-188.

SEKII, Y., OHBAYASHI, T., UCHIMURA, T., HUKUYAMA, T. & MAENO, T. (2001) "A study of space charge formation in XLPE". *Annual Report Conference on Electrical Insulation and Dielectric Phenomena*, (0-7803-7053-8/1), pp. 469-472.

SEKII, Y. (2007) "Influence of antioxidants and cross-linking on the crystallinity of XLPE dielectrics", *Annual Report Conference on Electrical Insulation and Dielectric Phenomena,* (IEEE Pub. No. 07CH37929), pp. 719-722.

SEKII, Y., SUZUKI, H., NOGUCHI, K. & MAENO, T. (2007) "The Negative Heterocharge Generation Mechanism in Polymeric Dielectrics", *Annual Report Conference on Electrical Insulation and Dielectric Phenomena,* (IEEE Pub. No. 07CH37929), pp. 404-408.

SMEDBERG, A., GUSTAFSSON, B. & HJERTBERG, T. (2004) "What is Crosslinked Polyethylene?". *Annual Report Conference on Electrical Insulation and Dielectric Phenomena*, (0-7803-8348-6/04), 1, pp. 415-418.

STEVENS, G. C. & BAIRD, P. J. (2005) "Nano- and Meso-measurements Metods in the Study of Dielectrics". *IEEE Transactions on Dielectrics and Electrical Insulation,*(1070-9878/05), Vol. 12, No. 5, pp. 979-992.

SUH, K.-S., TANAKA, J. & DAMON, D. (1992) "What is TSC?". *IEE Electrical Insulation,*(0883-7554/92), Vol. 8, No. 6, pp. 13-20.

SUZUOKI, Y., YASUDA, K., MIZUTANI, T. & IEDA, M. (1977) "The influence of oxidation on thermally stimulated currents from trapped carriers in high density polyethylene". *Journal of Physics D: Applied Physics,*(0022-3727/10/14/015), Vol. 10, No. 14, pp. 1985-1990.

TAKADA, T., TANAKA, Y., ADACHI, N. & XIAOKUI, Q. (1998) "Comparison Between the PEA Method and the PWP Method for Space Charge Measurement in Solid Dielectrics". *IEEE Transactions on Dielectrics and Electrical Insulation*, Vol. 5, No. 6, pp. 944-951.

TAKEDA, T., HOZUMI, N., SUZUKI, H., HARA, M., MURATA, Y., FUJII, K., TERASHIMA, K., WATENABE, K. & YOSHIDA, M. (1998) "Space charge behavior in full-size 250 kV DC XLPE cables". *IEEE Transactions on Power Delivery,*(0885-8977/98), Vol. 13, No. 1, pp. 28-39.

TAMAYO, I., BELANA, J., DIEGO, J. A., CANADAS, J. C., MUDARRA, M. & SELLARES, J. (2004) "Space Charge Studies of Crosslinked Polyethylene Midvoltage Cable Insulation by Thermally Stimulated Depolarization Current, Infrared/Fourier Transform Infrared, and Scanning Electron Microscopy". *Journal of Polymer Science: Part B: Polymer Physics,*(10.1002/polb.20268), Vol. 42, No., pp. 4164-4174.

TANAKA, Y., KITAJIMA, H., KODAKA, M. & TAKADA, T. (1998) "Analysis and Discussion on Conduction Current Based on Simultaneous Measurement of TSC and Space Charge Distribution". *IEEE Transactions on Dielectrics and Electrical Insulation,*(1070-9878/98), Vol. 5, No. 6, pp. 952-956.

TANAKA, Y., CHEN, G., ZHAO, Y., DAVIES., A. E., VAUGHAN, A. S. & TAKADA, T. (2003) "Effects Additives on Morphology and Space Charge Accumulation in Low Density Polyethylene". *IEEE Transactions on Dielectrics and Electrical Insulation,*(1070-9878/1), Vol. 10, No. 1, pp. 148-154.

TEMMEN, K. (2000) "Evaluation of surface changes in flat cavities due to ageing by means of phase-angle resolved partial discharge measurement", J. Phys. D. Appl. Phys., Vol. 33, pp. 603 - 608.

TEYSSEDRE, G., LAURENT, C., ASLANIDES, A., QUIRKE, N., DISSADO, L. A., MONTANARI, G. C., CAMPUS, A. & MARTINOTTI, L. (2001) "Deep trapping centres in crosslinked polyethylene investigated by molecular modeling and luminescence techniques". *IEEE Transactions on Dielectrics and Electrical Insulation,*(1070-9878/1), Vol. 8, No. 5, pp. 744-752.

TEYSSEDRE, G., LAURENT, C., MONTANARI, G. C., CAMPUS, A. & NILSSON, U. H. (2005) "From LDPE to XLPE: Investigating the Change of Electrical Properties. Part II: Luminescence". *IEEE Transactions on Dielectrics and Electrical Insulation,*(1070-9878/05), Vol. 12, No. 3, pp. 447-454.

TEYSSEDRE, G. & LAURENT, C. (2005) "Charge Transport Modeling in Insulating Polymers: From Molecular to Macroscopic Scale". *IEEE Transactions on Dielectrics and Electrical Insulation,*(1070-9878/05), Vol. 12, No. 5, pp. 857-875.

THOMAS, C., TEYSSEDRE, G. & LAURENT, C. (2008) "A New Method for Space Charge Measurements Under Periodic Stress of Arbitrary Waveform by the Pulsed Electro-Acoustic Method" *IEEE Transactions on Dielectrics and Electrical Insulation,* Vol. 15, No. 2, 554-559.

TOUREILLE, A. & GRANIER, O. (2000a) "Report on ARTEMIS Cable Pieces". *De Montpellier*, 7/08/2000.

TOUREILLE, A. & GRANIER, O. (2000b) "Report on Artemis Cable Pieces". *LABORATOIRE D'ELECTROTECHNIQUE*, 6/09/2000.

TZIMAS, A., FU, M. & DISSADO, L.A. (2005) "Characterization of electro-thermally aged XLPE cable peelings through space charge measurements", *Annual Report Conference on Electrical Insulation and Dielectric Phenomena.* (IEEE Pub. 05CH37702), pp. 30-33.

TZIMAS, A., FU, M., DISSADO, L.A. & HAMPTON, R.N. (2006) "Comparison of XLPE peelings with different electro-thermal histories using endurance test and residual charge methods", *Proc. ICPADM* (IEEE Pub. 06CH37773), Bali 26-30th June, pp. 293-296.

TZIMAS, A., FU, M., DISSADO, L.A., NILSSON, U.H. & CAMPUS, A. (2007) "Space Charge Characterization of XLPE peelings with a Cable prehistory: Before and After AC Endurance Tests", *Proc. ICSD07 – 9th Int. Conf. on Solid Dielectrics*, 8th -13th July, Winchester, U.K.(IEEE Pub. No. 07CH37848C), pp. 474- 477.

VARLOW, B. R. (1984) "Thermally Stimulated Current and Morphology in Low Density Polyethylene". *IEE Conference Publication*, (ISBN:), pp. 64-67.

WANG, X., LEWIN, P. L., DAVIES., A. E. & SUTTON, S. J. (2000) "Method to determine the trapping level of a polymeric material from thermally stimulated

discharge current measurements". *Proc.-Sci. Meas. Technol.*, (20000075), 147, pp.

WU, K. & DISSADO, L. A. (2004a) "Percolation Model for Electrical Breakdown in Insulating Polymers". *Annual Report Conference on Electrical Insulation and Dielectric Phenomena*, pp. 514-518.

WU, K. & DISSADO, L. A. (2004b) "Model for Electroluminescence in Polymers during the Early Stage of Electrical Tree Initiation". *IEEE International Conference on Solid Dielectrics*, Vol. 2, pp. 505-508.

WU, X., CHEN, G., DAVIES, A. E., HAMPTON, R. N., SUTTON, S. J. & SWINGLER, S. G. (2001) "Space Charge Measurements in Polymeric HV Insulation Materials". *IEEE Transactions on Dielectrics and Electrical Insulation,*(1070-9878/1), Vol. 8, No. 4, pp. 725-730.

aa)

ZANINELLI, D. & BALLOCCHI, G. (2000) "Fault analysis on AC/HV cable transmission lines". *IEEE Transactions on Power Delivery,*(0885-8977/00), Vol. 15, No. 2, pp. 616-622.

ZOU, C. (2007), PhD Thesis "The effect of humidity and surface functionalisation on the dielectric properties of nanocomposites", University of Leicester.

PUBLICATIONS:

1. M.C. Lança, M.Fu, E. Neagu, L.A.Dissado, J. Marat-Mendes, A.Tzimas and S. Zadeh, "*Space charge analysis of electrothermally aged XLPE cable insulation*", Journal of Non-Crystalline Solids, vol. 353, issue 47-51, pp. 4462-4466.
2. A.Tzimas, M.Fu, L.A.Dissado, U.H. Nilsson and A. Campus, "*Space Charge Characterization of XLPE peelings with a Cable prehistory: Before and After AC Endurance Tests*", Proc. ICSD 2007 – 9th Int. Conf. on Solid Dielectrics (8th -13th July, Winchester, U.K.).
3. M. Carmo Lança, M. Fu, E. Neagu, L. A. Dissado, J. Marat-Mendes, A.Tzimas and S. Zadeh, "*Space charge analysis of electro-thermally aged XLPE cable insulation*", 4th Int. Conf. Int. Dielectric Soc. & 9th Int. Conf. on Dielectric and Related Phenomena, 3-7 Sept., Poznan, Poland, Book of extended Abstracts, (ISSN 0458-1555), pp58-59, 2007.
4. A.Tzimas, M.Fu, L.A.Dissado, and R.N.Hampton, "*Comparison of XLPE peelings with different electro-thermal histories using endurance test and residual charge methods*", Proc. ICPADM (IEEE Pub. 06CH37773, ISBN 1-4244-0190-9), Bali 26-30th June, pp293-296, 2006.
5. A.Tzimas, M.Fu, L.A.Dissado, "*Characterization of electro-thermally aged XLPE cable peelings through space charge measurements*", Ann.Rep.CEIDP (IEEE Pub. 05CH37702), pp30-33, 2005.
6. M.C. Lança, M. Fu, E. Neagu, L.A. Dissado, J. Marat-Mendes, A. Tzimas and S. Zadeh," *Comparative study of SC in the polymeric insulation of power cables using PEA, isothermal and non-isothermal discharge current measurements*", Proc. ISE12 - 12th Int. Symp. on Electrets (11-14 Sept 2005, Salvador, Bahia, Brazil), eds. J.A. Giacometti, O.N. Oliveira Jr., R.M. Faria, (ISBN: 0-7803-9116-0), pp 284-287, 2005.

SPACE CHARGE ANALYSIS OF ELECTROTHERMALLY AGED XLPE CABLE INSULATION

M.C. Lança[1,*], M. Fu[2], E. Neagu[3], L. A. Dissado[2], J. Marat-Mendes[1], A.Tzimas[2] and S. Zadeh[4]

[1] *Departamento de Ciência dos Materiais, Secção de Materiais Electroactivos (CENIMAT), Faculdade de Ciências e Tecnologia, Universidade Nova de Lisboa, 2829-516, Caparica, Portugal*
[2]*Department of Engineering, University of Leicester, LE1 7RH Leicester, UK*
[3]*Department of Physics, Technical University of Iasi, B-dul D. Mangeron 67, Iasi 6600, Romania*
[4]*19 Gatwick Road London, SW18 5UF, U.K.*

Abstract:

Cross linked polyethylene (XLPE) is today widely used as an insulating material for power cables due to its good physical properties, however when in use it undergoes an electrical ageing process. Its ability to trap electric charge can give rise to space charge accumulation in the bulk of the polymer and produce localised electric stresses that can lead to cable failure, since the electric field will be increased above the design stress in some regions favouring the initiation of degradation there. In this work the PEA (pulsed electro-acoustic) method was used to compare the charge dynamics in three samples (XLPE cable peelings) aged in different ways (electro-thermally in the laboratory, field aged in service and thermally aged in the laboratory), and in particular the influence of the space charge trapping and de-trapping in the ageing phenomena. The results seem to support the idea that the electrical ageing creates charge traps whose characteristics are very much dependent on the ageing conditions, while samples that have been thermally aged show less ability to trap space charge.

PACS codes: 77.22.Jp; 77.20.Jv; 77.65.Dq

Keywords: electrical ageing; power cables; space charge, pulsed electroacoustic method (PEA); crosslinked polyethylene (XLPE)

1. Introduction

The polymeric insulation of power cables undergoes electrical ageing. Different types of ageing phenomena can appear, such as, water and electrical treeing that will not cause an immediate failure of the insulation, but in the long run contribute to dielectric breakdown and consequent cable failure [1]. Space charge accumulation plays a very important role in all the electrical ageing

* Tel:. +351 21 294 8565, fax: +351 21 294 8571
E-mail address: carmo@dcm.fct.unl.pt

phenomena, because it may raise the electric field locally and hence initiate a degradation mechanism, [2].

The most common insulating polymer used in medium and high voltage power cables is cross-linked polyethylene (XLPE) It is, therefore, important to understand how electrical ageing occurs in this polymer. On the other hand it is also well known that space charge accumulation leading to the formation of new traps by electro-oxidation and/or chain scission) plays a major role in the electrical ageing process [2]. Therefore the influence of space charge trapping and de-trapping characteristics needs to be studied, so as to gain a better understanding of the ageing phenomena and to be able to predict the lifetime of power cables

The space charge profile of XLPE peelings from power cables was studied using the PEA (pulsed electro-acoustic) method. This technique has been used extensively to obtain the space charge profile in polymers including polyethylene (both low density and cross-linked) [3-5].

2. Experiment

2.1 Sample ageing

In this work peelings from aged XLPE cables were used to measure the space charge profile. The peelings of XLPE received from the manufacturers were from cables aged as follows:

Type A – electro-thermally aged in the laboratory (25 MV/m at 90°C for 5000h);

Type B – field aged for 18 years in service and

Type C – thermally aged in the laboratory (90°C for 5000h).

(*A* and *C* were made from the same batch of XLPE).

2.2 PEA measurements

Prior to the space charge measurement the samples were pre-conditioned for 48h in vacuum at 50°C in order to remove volatiles and possible residual charge introduced during ageing process. The PEA measurements were performed at 30°C with a DC field applied of 120 MV/m. The results reported here were obtained with the electric field applied.

3. Results and discussion

3.1 Type A – XLPE cable electro-thermally aged in the laboratory

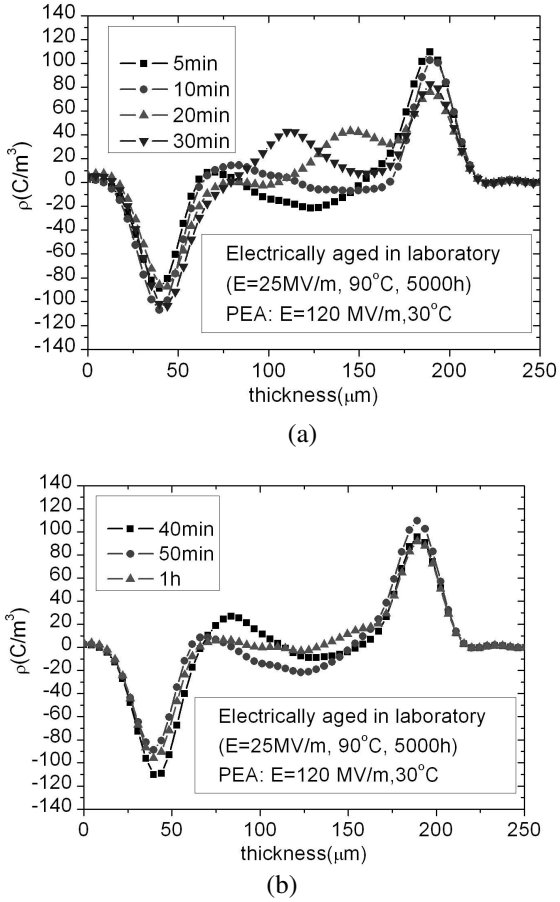

Fig. 1 – Space charge profile for XLPE cable peelings electro-thermally aged in the laboratory (type *A*) obtained by PEA measurements.

Fig. 1 shows the space charge profiles obtained during 1h of measurement with the DC field applied. In the space charge profile at 5 min (Fig.

1-(a)) a small and broad negative charge peak is observed in the bulk. By the end of 20 min a positive charge packet can be clearly seen near to the anode that begins to travels through the sample to the cathode. At 50 min (Fig. 1-(b)) the charge profile is similar to the one observed at 5 min: the positive charge packet has travelled across the insulation and has disappeared at the cathode so it possible to observe again the negative peak in the bulk, which has remained relatively unchanged. At 1h a new positive charge packet is distinguished near the anode. The amplitude of this second positive charge packet is smaller than the first one, and it is difficult to see its progress towards the cathode because it is partly masked by the negative peak in the bulk. However it is possible to determine that the transit time is similar to that found for the first packet.

The electric field profile is plotted in Fig. 2. The highest local field is observed for the charge packet front and its maximum value is around 160 MV/m at ≈30 min.

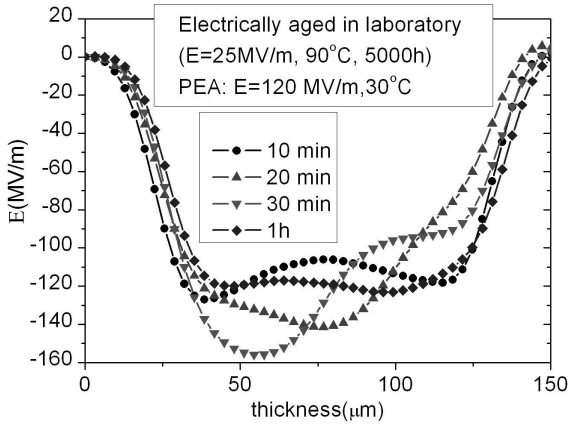

Fig. 2 – Electric field profile for XLPE cable peelings of a field aged cable (type *A*) obtained by PEA measurements†.

A rough estimation gives an average propagation speed of $v \approx 5\times10^{-8}$ ms^{-1} for the positive charge packets (calculation made based on the first packet transit time). Assuming that the positive carriers have a constant mobility and that the electric field average value (E) for the packet is 145 MV/m, an estimation of the charge mobility (μ) gives:

$$\mu = \frac{v}{E} = 3.4\times10^{-16}\ \mathrm{m^2\,V^{-1}\,s^{-1}} \qquad (1)$$

Peelings from unaged cables made with the same batch of XLPE have previously been analysed by PEA at the same DC field (120MV/m) but at 20°C [6]. The results also showed positive charge packets travelling from anode to cathode (with inception time of ~3.5h and transit time of 2.5 h for the first packet). The results presented here are similar with positive charge packets having similar amplitudes but faster inception and transit times (which may be the result of the higher temperature, 30°C, and not of the ageing process). Alison [5] has also observed positive and negative charge packet formation in unaged LDPE at 40°C and a higher electric field (≈130 MV/m), resulting in shorter inception and transit times than the ones observed in this work. The mobility estimated in [5] is one order of magnitude higher than the one obtained here. However, as stated above, it is difficult to compare because the measurement conditions are not the same.

3.2 Type B – XLPE cable field aged for 18 years in service

The most complex space charge profile is found for this type of sample, see Fig.4. At first, the formation of large heterocharge peaks is observed (t = 15 min), with a maximum attained at the anode of nearly –130 Cm^{-3} at t = ~18 min. This value of space charge is much higher than the ones seen for samples *A* and *B* and partially conceals the other features of the space charge profile. The positive heterocharge peak near the cathode does not change much with time, while the larger negative heterocharge peak near the cathode decreases appreciably during the first hour of the measurement.

A detailed observation of the space charge profile evolution during the first 15 minutes reveals that there is also negative charge present in the bulk. Moreover heterocharge build up is caused by

† The scale of the *xx* axis in the plots of the electric field corresponds to the thickness of the sample, while in the graphs of space charge profile is related to the PEA system sample holder, which includes the electrodes.

charge separation near the middle of the sample but closer to the anode. The positive charge moves faster and the heterocharge peak at the cathode quickly reaches its maximum. The negative charge takes longer to travel to near to the anode (the maximum is reached at about 18 min). Within the first 5 min a small positive charge peak is observed forming at the anode and moving towards the cathode. This is very difficult to observe because at the same time negative charge is drifting to the anode and masking this positive peak.

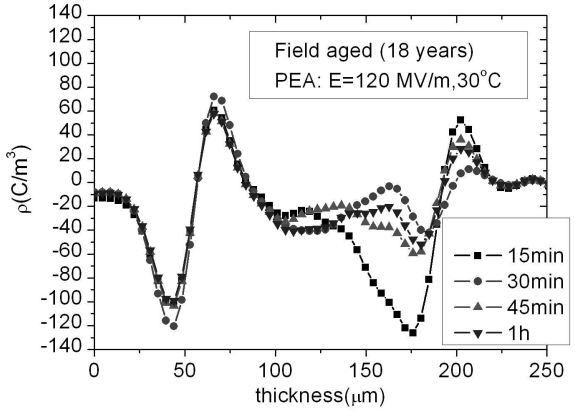

Fig.3 - Space charge profile for XLPE cable peelings of a field aged cable (type *B*) obtained by PEA measurements.

To have a better understanding of the space charge motion it was necessary to subtract the charge of the heterocharge peaks from the total charge. This was done by choosing as the baseline the profile at t = 18 min when the negative peak near the anode reached its maximum value. The results of this calculation are plotted in Fig.4 at every 5 min in the first 40 min of the measurement. As can be seen in Fig.4-(a) a small positive charge appears to be travelling from anode to cathode at the same time that negative charge is moving in the opposite direction. At t = 18 min, when the maximum is achieved at the negative peak near the anode, the electric field there is high enough to cause positive charge injection from the anode (Fig.4-(b)) that builds up and then drifts to the cathode. Simultaneously negative charge is moving from cathode to anode masking the positive charge. The injected positive charge leads to a permanent decrease in the negative heterocharge peak at the anode and only a small fraction of injected positive charge travels to the cathode.

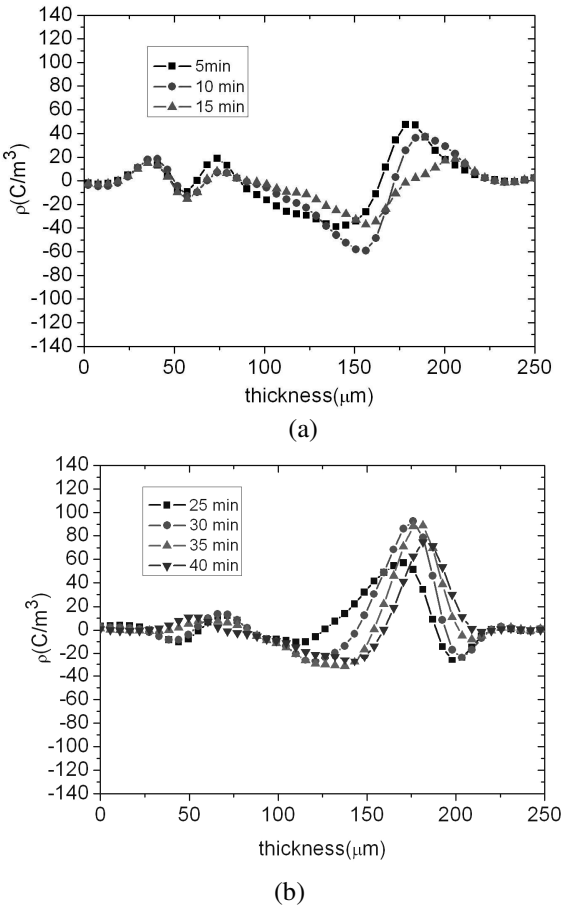

Fig.4 – Space charge profile with subtraction of heterocharge peaks at 20 min for XLPE cable peelings field aged obtained by PEA.

These results are very different from the other two types of samples. Even though positive charge forming packets at the anode is observed as in type *A* XLPE, there is a very high heterocharge build up that originates positive charge injection and smaller packets travelling to the anode against a background of negative charge injection and penetration.

After 40 min (Fig.3) is possible to see positive charge leaving the anode again, but this time the amplitude is smaller. At the end of 50 min the charge profile is no longer changing much with the

presence of the positive heterocharge peak near the cathode (which remained relatively unchanged after building up), a broad negative peak that can be observed in the bulk between the cathode heterocharge and the anode, and a negative heterocharge peak at the anode. The amplitude of this negative heterocharge peak near the anode is about -50 Cm^{-3} while the positive one is +60 Cm^{-3}, so the sample may be close to a net neutrality.

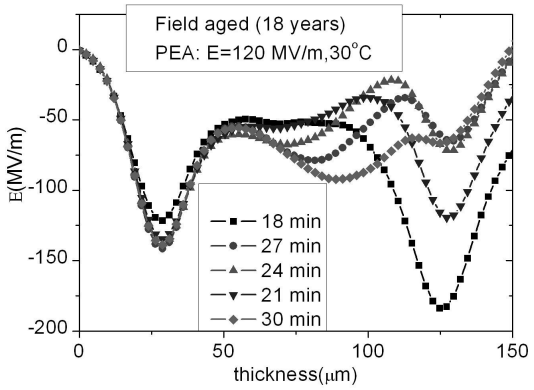

Fig. 5 – Electric field profile for XLPE cable peelings field aged obtained by PEA.

The electric field profile from 18 to 30 min plotted in Fig. 5 shows both the effect of positive charge injection from the anode and that of the negative charge in the bulk moving towards the anode.

3.3 Type C – XLPE cable thermally aged in the laboratory

The space charge profiles of type *C* samples (Fig. 6) show that almost no space charge is accumulated during the measurement time in contrast to what is found for type *A* and *B* samples (Fig. 1 and 2). Also no charge packets are formed. There is a relatively small heterocharge build up (less than –15 Cm^{-3} near the anode and less than +11 near the cathode Cm^{-3}). In thermal ageing of polyolefins it is well known that oxidation occurs via chain scission by attack of oxidized species at temperatures between 50 and 100°C [7]. However it seems that if such phenomenon occurs here it reduces the amount of space charge, probably due to a reduction in the rate of trapping and/or increase of charge transport perhaps via many shallower traps.

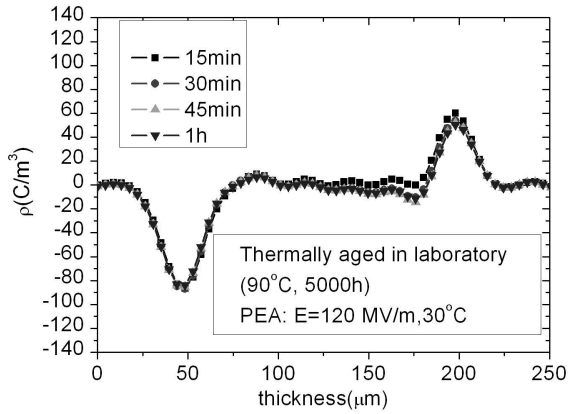

Fig. 6 – Space charge profile for XLPE cable peelings thermally aged in the laboratory (type *C*) obtained by PEA measurements.

A comparison of the data from electro-thermally aged and thermally aged samples suggest that electrical ageing creates charge traps that allows for an increased space charge accumulation. However the electro-thermally aged samples showed little difference from unaged samples, perhaps only insofar as the repetition of charge packets was reduced. Thermal ageing resulted in very little charge accumulation, possibly because oxidation has produced an increased number of shallow traps thereby allowing an increased transport rate.

4. Discussion and Conclusions

The characteristics of the traps are very dependent on ageing conditions as can be seen by comparing the space charge profiles obtained for samples that are field aged with those that are electro-thermally aged in the laboratory. The most complex profile arises from the field aged samples where no control of the ageing conditions was possible. The field-aged sample is the only one showing significant heterocharge from pre-existing charge separation. It is known that field aged and laboratory aged specimens show different ageing features [1]. In field ageing the electrochemical mechanisms seem

to dominate while in laboratory accelerated aged specimens the dominant phenomena appear to be electromechanical (higher stresses and temperature are often used). It is therefore possible that the heterocharge originates with ionic charge produced by a chemical process during service, although the mobility of the ions of different polarity must be different, perhaps the positive ion is reasonably mobile while the negative ion is effectively attached to the chains. In addition these samples exhibit charge injection during the stressing period, though the near balance of positive and negative charges at the end indicate that most of the stable charge originates with ion separation.

It is clear that electrical ageing is a complex process involving different mechanism (mechanical, chemical, etc.) enhanced by the presence of an electrical field. The measurements here show that space charge may play a dual role in both enhancing effects such as additional charge injection, and as an indicator of changes brought about in other ways.

5. References

[1] Dissado L.A., Fothergill J.C.: *Electrical Degradation and Breakdown in Polymers*, IEE, Peter Peregrinus, London, 1992

[2] Mazzanti C., Montanari G.C., Dissado L.A.: *IEEE Trans. Diel. and Elect. Ins.*, **12(5)**, 2005, 876-890

[3] Maeno T., Futami T., Kushibe H., Takada T. and Cooke C.M.: *IEEE Trans. Elect. Ins.*, **23(3)**, 1988, 433-439

[4] Li Y., Yasuda M. and Takada T.: *IEEE Trans. Diel. and Elect. Ins.*, **1(2)**, 1994, 188-195

[5] Alison J.M.: *Meas. Sci. Technol.*, **9**, 1998, 1737-1750

[6] See A., Dissado L.A., Fothergill J.C.: *IEEE Trans. Diel. and Elect. Ins.*, **8(6)**, 2003, 859-866

[7] Xu J.J. and Boggs S.A.: *IEEE Elect. Ins. Mag.*, **10(5)**, 1994, 29-37

Space Charge Characterization of XLPE peelings with a Cable prehistory: Before and After AC Endurance Tests

A. Tzimas[1]*, M. Fu[1], L.A. Dissado[1], U.H. Nilsson[2], A. Campus[2]
[1] Department of Engineering, University of Leicester,
Leicester, LE1 7RH, United Kingdom
[2] Borealis AB Sweden
* E-mail : at50@le.ac.uk

Abstract: In the E.U. research programme ARTEMIS 90 kV cables insulated using the same batch of XLPE were stressed under different electro-thermal conditions for various durations. Thin peelings of the insulation of the cable sections stressed in this way are compared with peelings taken from an unstressed cable section, through their ac electro-thermal endurance measured under the same test conditions, to see whether or not the cable stressing had altered the inherent endurance capability of the insulation material i.e. aged it, and to identify markers for the dominating process/es that degraded the materials. Their space charge behaviour was also measured by the Pulse-Electro-Acoustic (PEA) technique before and after the endurance test, in order to characterise the material from the stressed cables and to identify changes brought about during the endurance test. The measurements focussed on the accumulation of space charge under a standard measuring condition of 50kV/mm at room temperature, and its subsequent decay. The results show that the ARTEMIS stressing as well as the endurance test introduced changes to the space charge behaviour.

THE ARTEMIS PROJECT

Polymeric cables have now been in service for several decades that is why it is important to be able to ascertain their current state. There is therefore a need to understand the degradation processes involved, and identify diagnostic factors. Much work has already been carried out in this respect [1], but more is needed, hence the EU-sponsored ARTEMIS programme [2] was set up. Cross- linked- polyethylene (XLPE) from a single supplier was used by two different companies to manufacture 90kV cables to the same MV-design. Sections from the cable were placed under electrical, thermal, and electro-thermal stress for varying lengths of time (up to about two years), after which their insulation was peeled and the peeling subjected to a number of diagnostic measurements designed to characterise the state of the insulating material in comparison to its state in an unstressed (i.e. unaged) cable. The peelings have a thickness of 150μm. An analysis of the results did not show significant differences in the properties that were examined. The Artemis project demonstrated a very low rate of degradation of the cable materials in spite of the use of very high electric stress levels at elevated temperatures. Nevertheless, it did provide a definite indication of the techniques that should be used to evaluate the state of the insulation. Two of which are a check of its endurance capability and its space charge behaviour, both of which have now been used to further characterise the ARTEMIS peelings. This paper is focused on the space charge behaviour before and after the endurance test rather on the endurance test lifetimes, which were presented in [3]. We have excluded defects and screening layers from the peelings considered.

ENDURANCE TEST

Our 'sudden death' tests, i.e. endurance test, are intended to determine whether or not the stressing pre-history has had an effect on the electrical endurance of the material, i.e. whether or not the material has been irreversibly 'aged'. They were carried out at an ac electric field of 70kV/mm (rms) and a temperature of 363°K (90°C) to ensure failures within a reasonably short time. Four specimens were taken from as near as possible the same positions in the peeled roll to ensure that they experienced identical ageing conditions during the Artemis programme, and conditioned in a vacuum oven at 50 °C for 48 hours. The **H**igh-**V**oltage (**HV**) electrode is brass with a cylindrical shape of a diameter of 25mm, height 30mm, and rounded edges to avoid corona discharges. The bottom electrode is an aluminium plate with a thickness of 5mm allowing for up to four **HV** electrodes to be set in place. Good contact is ensured by placing a Perspex glass plate with a thickness of 5mm and clamping it down on the electrodes. Immersing the electrodes in silicon oil and degassing them in vacuum minimized the possibility of air accumulation between the interfaces and hence the occurrence of a breakdown due to partial discharges. The test is terminated when three of the specimens fail from each peeling leaving one specimen that can be taken to be just reaching the point of failure, which is available for further investigation e.g. space charge characterisation techniques as used in [4].

SPACE-CHARGE CHARACTERISATION

This section reports the effect that high ac electric field and temperature application has on the insulation through PEA measurements [5] under high dc electric field stressing. DC stressing was used to identify any changes that occurred in the XLPE peelings after electro-thermal stressing, as measurements using ac-stressing are very difficult.

1-4244-0750-8/07/$20.00 ©2007 IEEE.

Measurements of the space charge profile were taken for all the samples that were tested for their inherent endurance capability, before, and after the endurance test at 90°C and reported in [3]. Here the focus is on the space charge profile of XLPE as a 150μm peeling from a cable, following the sequence: 1) before experiencing any stressing, 2) after experiencing electrical stressing as cable, 3) after experiencing electro-thermal and thermal stressing under the endurance test. In the space charge profiles presented the anode is on the right-hand-side and the arrows indicate the change in space charge density.

Pulse-Electro-Acoustic technique (PEA) protocol

The HV electrode is semicon material and the ground electrode aluminium. A drop of silicon oil was placed between the electrodes and the sample to ensure good acoustic propagation. A DC poling field of 50kV/mm was applied at ambient temperature for up to 24 hours, during which a series of measurements were made with the voltage removed for the time of the measurement. The results, shown in the figures, therefore yields the space charge and corresponding image charges on the electrodes without the overlay of the capacitive charge on the electrodes.

Space charge in unaged peelings

A reference space charge profile for the material was first obtained using a peeling that was taken from a cable that did not experience either electrical or thermal stressing during the ARTEMIS programme. This peeling was kept sealed and refridgerated until needed. Its space charge behaviour was monitored for 26 hours of dc stressing at the same electric field. It can be seen from Figure 1 that during the first 270min negative charge accumulates adjacent to the cathode just as in all the ARTEMIS peelings [4]. Over 21hours of stressing the negative charge adjacent to the cathode reduces and an increasing negative heterocharge peak is formed at the anode while the net charge stays constant. This implies that some of the negative charge has migrated from the cathode to the anode.

Space charge profile after the ARTEMIS stressing

The effect of the ARTEMIS stressing pre-history has been evaluated by measuring the space charge profile over 300mins of a peeling from a cable that had experienced an electrical stress of 19kV/mm at 20°C for5500hours. During the space charge accumulation negative charge carriers transit from the cathode to the

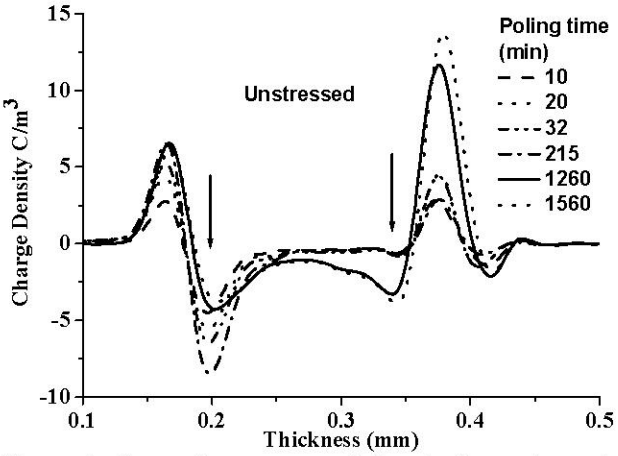

Figure 1: Space charge accumulation in the unstressed material during 26hours of dc stressing at 50kV/mm.

anode where they start to accumulate, as is shown is Figure 2a. A comparison with the profiles of the unstressed material shows that for the ARTEMIS stressed material the transit of negative charge to the anode is noticeable after 30min whereas previously it required about 215 minutes. Furthermore, during the space charge decay which is shown in Figure 2b the negative charge which accumulated near the anode decays very slowly in contrast to the negative charge adjacent to the cathode which escapes very fast leaving behind positive charge.

Space charge after electro-thermal stressing

Samples taken from the same peeling whose post-ARTEMIS space charge is shown in Figure 2 were further stressed in an ac electric field of 70kV/mm and at a temperature of 90°C. The space charge profile of a specimen that withstood further electro-thermal endurance stressing for 1537 hours was measured and is shown in Figure 3. There seem to be no significant changes in the first 40 minutes. However, after forty min. positive charge which is accumulated adjacent to the anode begins to move to a place further into the specimen where it forms an additional positive peak.

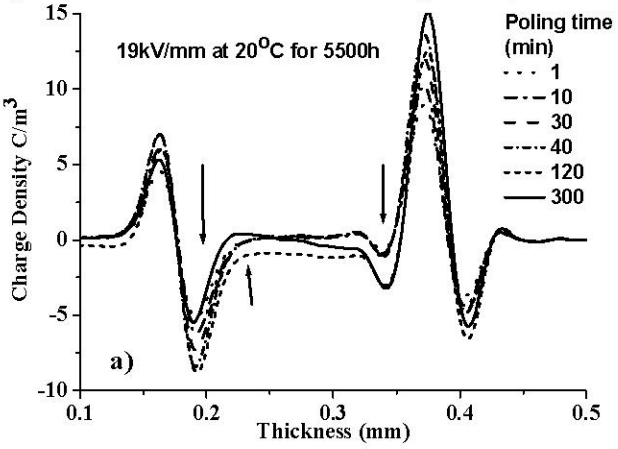

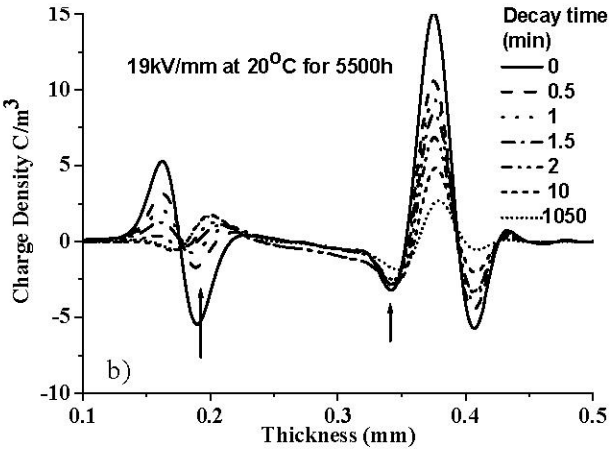

Figure 2: Space charge of an electrically stressed sample before the endurance test, a) accumulation and b) decay.

Eventually the positive charge is equally distributed between the two peaks. Over the same period of time negative charge accumulated adjacent to the cathode extends into the bulk of the material without forming a second peak, see Figure 3a.

The decay of the space charge profile over 18 hours is shown in Figure 3b, where two types of decay processes can be seen. In the first phase of decay some positive and negative charge adjacent to the anode and cathode respectively escape within the first two minutes. In the second phase both the negative and positive charges that are left in the bulk of the material decay very slowly. The field distribution corresponding to the space charge has two zero-field planes, which means that the charges in the bulk between the planes will have to transit the sample for neutralization, which will be a slow process.

Space charge profile after thermal stressing

Space charge measurements were also carried out on the parts of the peeling that lay outside of the electrode region during the endurance test, and hence did not experience any electrical stress. These measurements allowed us to distinguish the effect of the thermal component of the endurance testing from the electro-thermal effect. The space charge profiles observed during accumulation and decay are shown in Figure 4. Figure 4a shows the accumulation over a period of 120mins, and it can be seen that negative charge starts to accumulate adjacent to the anode after the fifth minute. Eventually the charge density reaches a magnitude of -7.3 C/m^3. Negative charge with a charge density of -4.8 C/m^3 is present at the second minute of poling, in the region adjacent to the cathode. Thereafter the charge density starts to decrease and eventually becomes positive reaching a value of 3.6 C/m^3. Thus, the ***change*** of charge density at the cathode is 8.4 C/m^3 and at the anode is 7.3 C/m^3, which makes them very similar. This observation suggests that the charge that is

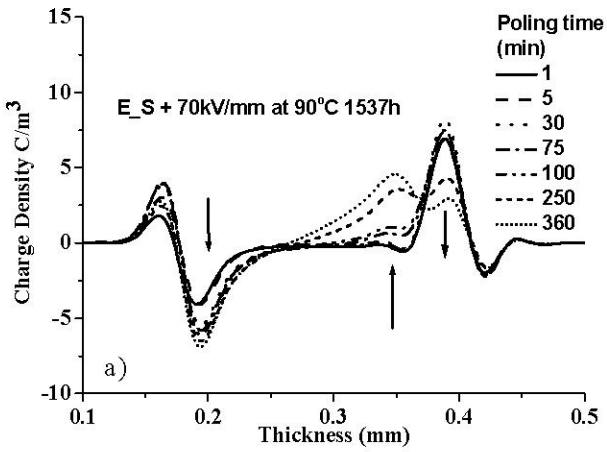

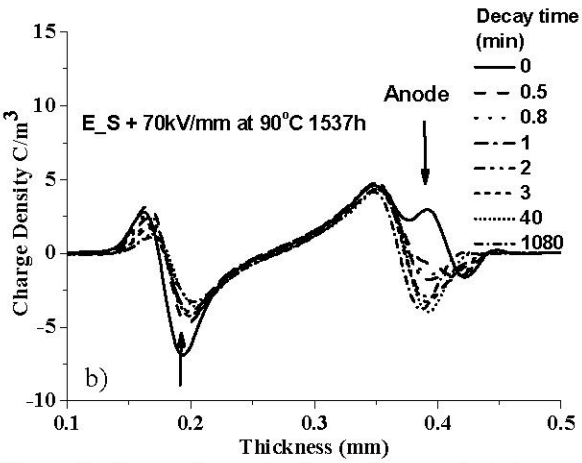

Figure 3: Space charge in the endurance tested sample that survived electro-thermal stressing for 1537h, a) accumulation and b) decay.

accumulating at the anode has migrated from the cathode. Surprisingly once the voltage is removed by short-circuiting the sample, the charge peaks near to the electrodes continue to increase, see Figure 4b. During the first minute the positive charge density doubles its magnitude from 3.6 to 7.1C/m^3, while at the same time the negative charge density only increases its magnitude from 7.3 to 8.4 C/m^3. Now the residual charge densities are equal to the same extent as found for the change in density during poling. This implies that injected negative charge has been removed leaving behind separated charge peaks corresponding to species dissociated in the bulk.

Double peak as ageing marker

In order to verify that the double positive peak adjacent to the anode after the endurance test, see Figure 3, was not a feature of the specific peeling investigated, a peeling from an electro-thermally stressed cable made by the other ARTEMIS manufacturer was also investigated. This material had experienced an identical electrical stress as a cable and as a peeling under the endurance test. Figure 5a shows that a double positive

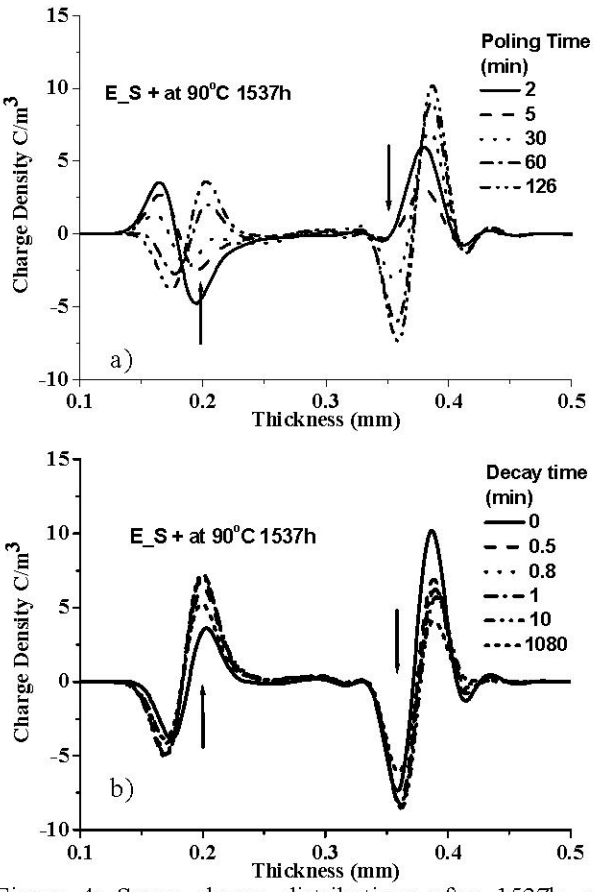

Figure 4: Space charge distributions after 1537h of thermal stressing in the endurance test, a) accumulation and b) decay.

peak was formed near the anode in this material also. The same sample was used for a repeat experiment after the original charge had been removed. As can be seen in Figure 5b the positive charge moves directly to the inner peak within the first two minutes, leaving very little charge in the outer peak. There is therefore a memory of the second peak's existence, i.e. the sample has been irreversibly aged. A repeat with reversed field showed that the second peak could also hold negative charge, and thus the charge accumulated in this peak is injected from the high voltage electrode.

CONCLUSIONS

- The time required for injected negative charge to cross the samples of insulation peeled from XLPE cables subjected to an ac field of 19.5kV/mm and 20°C has been substantially reduced, compared to that in unaged peelings.
- Additional thermal stressing of the peelings from aged cables resulted in a very rapid heterocharge separation that was retained for some time after short-circuiting.
- Further electro-thermal stressing, on the other hand, resulted in a homo-charge double peak at the high-voltage electrode that was indicative of an irreversible change.

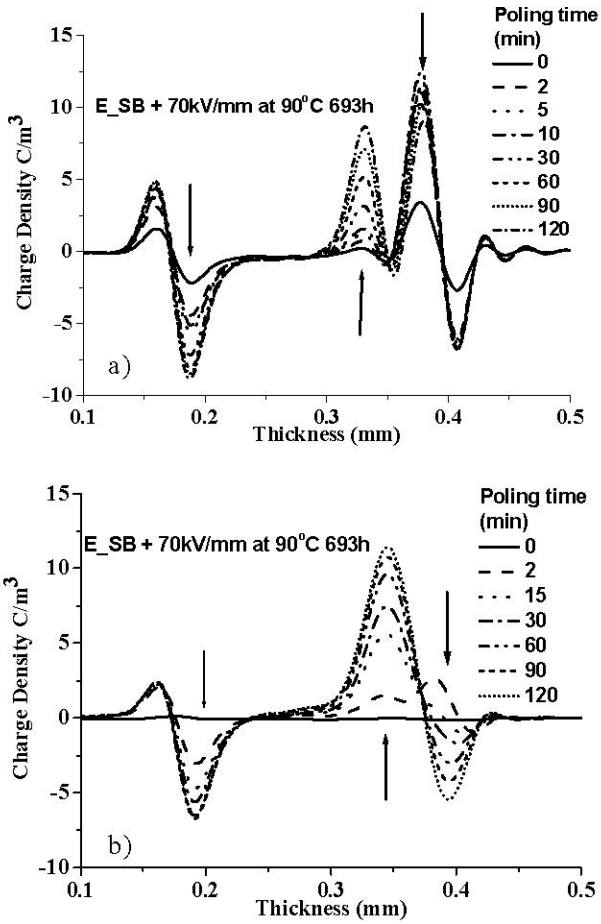

Figure 5: Space charge profile accumulation for electrically stressed ARTEMIS sample followed by endurance testing of 693h, a) first 120min of stressing b) a repeated 120min of stressing.

Acknowledgements

The authors would like to thank ARTEMIS for access to the samples and for permission to publish. A. Tzimas also thanks Borealis for financial support.

REFERENCES

[1] L.A. Dissado and J.C. Fothergill, *Electrical Degradation and Breakdown in Polymers*, P. Peregrinus Press, London, U.K., 1992.

[2] Fothergill, J.C., Montanari, G. C., Stevens, G. C., Laurent, C., Teyssedre, G., Dissado, L. A., Nilsson, U. H., Platbrood., G., "Electrical, Microstructural, Physical and Chemical Characterization of HV XLPE Cable Peelings for an Electrical Aging Diagnostic Data Base". *IEEE Trans. on Diel. and El. Ins.*, 2003. **10**(3): p. 514-527.

[3] A. Tzimas, M. Fu, L.A. Dissado, R.N. Hampton. "Comparison of XLPE Cable Peelings with Different Electro-Thermal Histories using Endurance Test and Residual Charge Methods", *International Conference on Properties and Applications of Dielectric Materials* (**ICPADM**), July 2006, Bali, Vol. 1, pp 293-296.

[4] A. Tzimas, M. Fu, L.A. Dissado. "Characterization of Electro-Thermally aged XLPE Cable Peelings through Space Charge measurements", *Conference on Electrical Insulation and Dielectric Phenomena* (CEIDP), October 2005, Nashville, pp 30-33.

[5] Takada, T., Tanaka, Y., Adachi, N., Xiaokui, Qin, "Comparison Between the PEA Method and the PWP Method for Space Charge Measurement in Solid Dielectrics". IEEE Trans. on Diel. and El. Ins., 1998. 5(6): p. 944-951.

Comparison of XLPE Cable Peelings with Different Electro-Thermal Histories using Endurance Test and Residual Charge Methods

A. Tzimas[1*], M. Fu[1], L.A. Dissado[1], R.N. Hampton[2]
[1]Department of Engineering, University of Leicester U.K.,
[2] Borealis AB Sweden
* E-mail: at50@le.ac.uk

Abstract: In a previous programme sections of the same XLPE-insulated ac-cables were stressed under different electro-thermal conditions and for various durations. Here, thin peelings from the cable insulation have their electrical endurance compared with peelings taken from an unstressed cable section, under the same test conditions. The aim is to verify whether or not the cable stressing had altered the **inherent** endurance capability of the insulation material i.e. aged it, and to identify markers for the dominating process/es that degraded the materials. The contributions from defects and screening layers have been excluded from this study. The endurance test was set at very high ac field and high temperature to maximise the stress and minimise the life of the material. All samples were conditioned before the test to remove any humidity and residual cross-linking by-products. A set of four samples was used for each material and the breakdown times were analysed by Weibull statistics. The results clearly show that only sample sets from cables that included a thermal stressing component display a reduction in the inherent lifetime, compared to the unstressed reference. The residual charge after the endurance test was measured by the Pulse-Electro-Acoustic (PEA) technique for all the failed samples as well as the suspended ones. Two types of behaviour were observed but it was found that the amount of retained charge was not related to the endurance life of the material.

THE ARTEMIS PROJECT

The advent of polymer cable insulation has led to a large amount of research into the way in which such materials lose their insulating qualities during service leading to eventual failure [1]. Now that such insulating materials have been in service for several decades it is particularly important to be able to ascertain their current state so that decisions can be taken regarding a costly replacement. There is therefore a need for an understanding of the degradation process and an identification of diagnostic factors. The EU-sponsored ARTEMIS programme [2] was an attempt to resolve these problems. In this programme, Cross- Linked-Polyethylene (**XLPE**) from a single supplier was used by two different companies to manufacture cable to the same MV-design. Sections from the cable were placed under electrical, thermal, and electro-thermal stress for varying lengths of time (up to about two years), after which their insulation was peeled and the peeling subjected to a number of diagnostic measurements designed to characterise the state of the insulating material in comparison to its state in an unstressed (i.e. unaged) cable. An analysis of the results did not show significant differences in the properties that were examined. The Artemis project demonstrated a very low rate of degradation of the cable materials in spite of the use of very high electric stress levels at elevated temperatures. Nevertheless, it did provide a definite indication of the techniques that should be used to evaluate the state of the insulation, one of which is a check of its endurance capability reported here.

Electrical and Thermal Stressing Employed in Artemis

The endurance capability of sets of four samples of insulation peelings from six cable sections with different stressing history is investigated, see Fig.1. All samples were cut from cable peelings whose thickness was 150μm and were conditioned for 48 hours at 323°K (50°C). The conditioning was a feature of the Artemis programme shown to remove volatiles and demonstrated to give reproducible results.

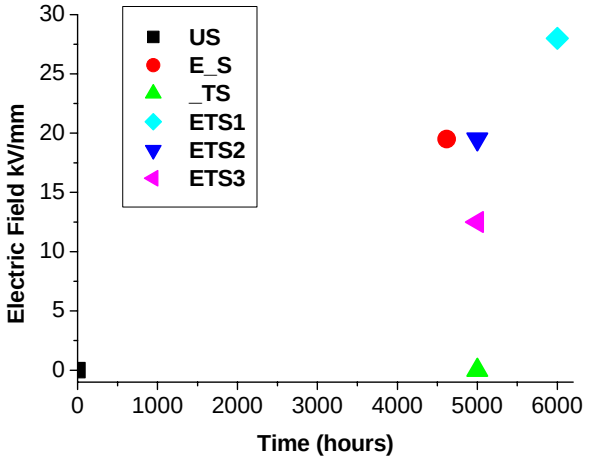

Figure 1: Electrical and thermal stress of the insulation as a cable.

Fig.1 shows the duration of the electro-thermal stress that the insulation material experienced as a cable. The acronyms used in Fig.1 for each different peeling stand for; **US**- **U**n**S**tressed, i.e. reference material, **E_S**-**E**lectrically **S**tressed only, **TS**-**T**hermally **S**tressed only, **ETS1** - **H**igh **E**lectro- **T**hermal **S**tress, **ETS2** -

Electro-**T**hermal **S**tress and **ETS3** - **L**ow **E**lectro-**T**hermal **S**tress. The temperature used to thermally stress the cables was 363°K (90°C). We chose peelings from cables that had experienced stress for approximately the same duration, so that the outcome of different electro-thermal conditions could be studied.

The endurance life of peelings from unstressed cables were measured for electric fields varying from 30 to 80 kV/mm (rms) and two temperatures 293 (20°C) and 363°K (90°C) as part of the ARTEMIS programme [3]. The results, Fig. 2., are typical of insulating materials and show that the endurance capability of the material decreases as the field and temperature increases.

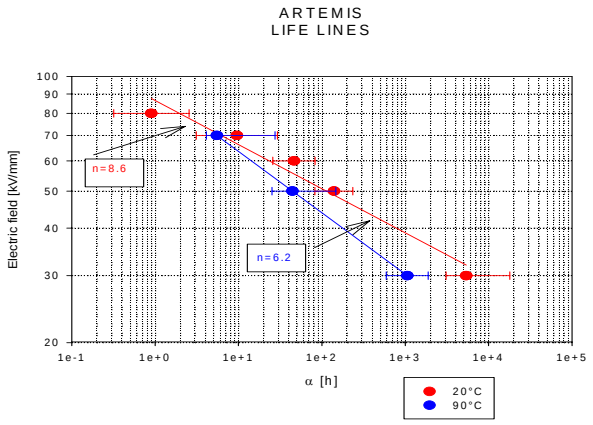

Figure 2: Endurance test on unstressed peelings from Artemis cables at 293 (20°C) and 363°K (90°C) [3].

ENDURANCE TEST

Our 'sudden death' tests, i.e. endurance test, are intended to determine whether or not the stressing pre-history has had an effect on the electrical endurance of the material, i.e. whether or not the material has been irreversibly 'aged'. They were carried out at an electric field of 70kV/mm (rms) and a temperature of 363°K (90°C) to ensure failures within a reasonably short time. Four specimens were taken from as near as possible the same positions in the peeled roll to ensure that they experienced identical ageing conditions during the Artemis programme. The High-**V**oltage electrode is brass with a cylindrical shape of a diameter of 25mm, height 30mm, and rounded edges to avoid corona discharges. The bottom electrode is an aluminium plate with a thickness of 5mm allowing for up to four **HV** electrodes to be set in place. Good contact is ensured by placing a Perspex glass plate with a thickness of 5mm and clamping it down on the electrodes. Immersing the electrodes in silicon oil and degassing them in vacuum minimized the possibility of air accumulation between the interfaces and hence the occurrence of a breakdown due to partial discharges. The test is terminated when three of the specimens fail from each peeling leaving one specimen that can be taken to be just reaching the point of failure, which is available for further investigation e.g. space charge characterisation techniques as used in [4].. Statistical analysis of the time to breakdown is carried out using Weibull statistics as is shown in Fig.3**.** The time up to the third failure is compared to that of the **US** material. The 90% confidence limits were calculated using the estimated shape parameter β = 0.4 for the **ETS1** material, given in Fig.3 as the dashed line. The value of β is less than unity and implies a large range of breakdown times. All the material that during the Artemis programme experienced electro-thermal or thermal stressing, alone i.e. **ETS1**, **ETS2**, **ETS3** and **TS**, lie within the confidence limits of **ETS1**, the material that experienced the most severe stressing as a cable, as is shown in Fig.3. However, the materials that did not experience any stressing at all or just experienced electrical stressing, i.e. **US** and **E_S**, lie outside the confidence limits of **ETS1**.

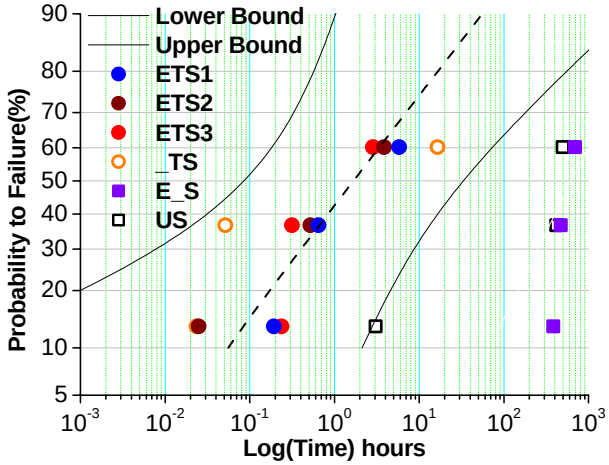

Figure 3: Weibull endurance plot of Artemis cable peelings at different electro-thermal conditions.

The E_S samples have a Weibull exponent β > 1, which indicates a narrow range of failure times than the other sets possibly because there have been no defects introduced into the sample by ageing.

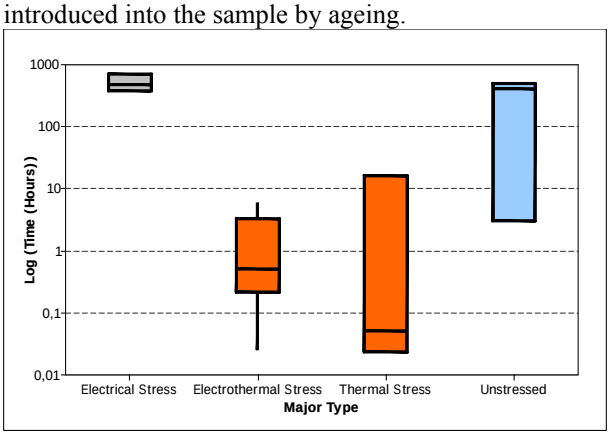

Figure 4: Comparison of different Artemis treatments in a Box and Whisker format (Box encloses 50% of the data, the bar within the box shows the median)

The difference of the time to breakdown statistics of the electro-thermally stressed materials and the non-thermally stressed ones is significant as is clear

from Fig.4. This figure shows that the failures of the materials that include a thermal component all occur within 15 hours while the ones that do not extend up to 722 hours. The former material failures occur within the time bars at 70kV/mm shown in Fig 2., whereas the latter do not. We were concerned about improvement in our test method so replicate tests have been made that verify this trend.

RESIDUAL CHARGE

Pulse-Electro-Acoustic technique (PEA)

The HV electrode side consists of semicon material whereas the ground electrode is aluminium. A drop of silicon oil was placed between the interface of the electrodes and the sample to ensure good acoustic propagation. A DC poling field of 40kV/mm was applied to the **TS** sample for $7.2x10^3$seconds. During this period the voltage was removed for a short time to enable a measurement to be made, and then the voltage was re-applied. The result, shown in Fig. 5, therefore yields the space charge and corresponding image charges on the electrodes without an overlay of capacitive charge on the electrodes.

Space charge profile before endurance test

Fig 5. shows the space charge accumulation profile of the **TS** material before the endurance test. There is a continuous accumulation of negative space charge, but during the first 3000 seconds it is located near the cathode, and after that it starts to extend into the bulk of the sample and eventually reaches the anode.

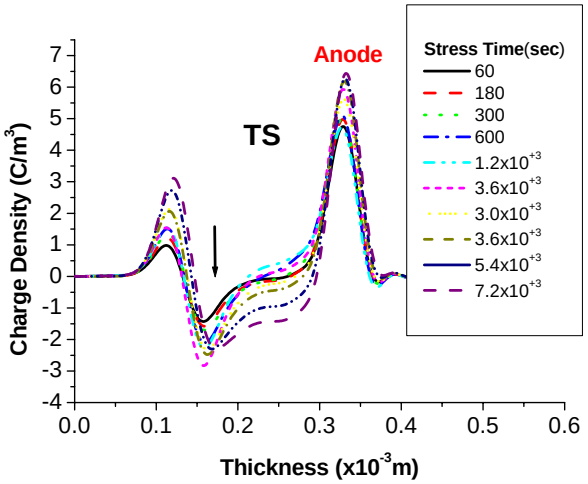

Figure 5: Accumulation of space charge within Artemis peelings-voltage on measurements.

Residual charge measurement after endurance test

The residual charge of the samples that experienced the endurance test was measured approximately a month after the end of the test; the exact time varies according to the failure times. The PEA measurements [5] were done by just applying the pulse voltage with amplitude of 600V and recording the raw signal acquired from the oscilloscope. Thus, the y-axis of the following figures, Fig.6 and Fig.7, is in volts and not in C/m^3. The electrode of the PEA apparatus (diameter of 1cm) was placed as near as possible to the breakdown site within the boundaries of the ac HV electrode (diameter of 2.5cm) used in the endurance test.

Two types of charge profile can be distinguished in the residual charge of the **TS** material samples as shown in Fig.6. In one of them a very small amount of charge is retained. This is found in the first and second failures, which occur within 360 seconds from voltage application. The second type is observed in the third failure and the suspended sample where a significantly greater amount of charge is retained in the bulk of the sample. The distribution of the charge is similar to that observed in Fig.5 with negative space charge penetrating into the bulk of the material. It should be noted that the greatest amount of space charge is observed in the 3rd failure and is mostly nearer to the cathode in contrast to the suspended sample where it is nearer to the anode.

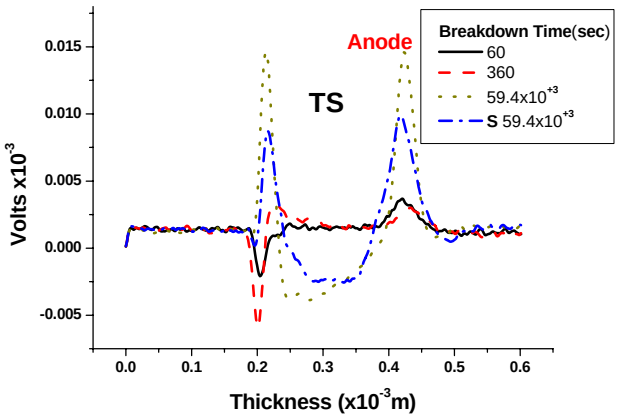

Figure 6: Residual charge remaining in endurance test samples of TS peelings.

Fig.7 shows the residual charge measured in the first failures of eight different endurance experiments where the first failures occur at various times. The results could be separated into two groups, which are indicated by the dashed and solid lines. The group represented by dashed lines consist of the failures that occurred within 840 seconds and retain the least amount of charge. These are all the materials that experienced electro-thermal stressing as a cable. The other group represented by the solid lines, consists of the failures that occurred after $4.14x10^3$ seconds and retain more charge than the dashed line group. These are the materials that did not experience any thermal stressing as a cable and lie outside the confidence limits of the Weibull plot in Fig.3.

The residual charge data shows that although under AC conditions the injection and extraction of charge is very fast, it may be trapped at deep trap regions where escape can be very difficult. In consequence charge may be retained in the sample from cycle to cycle.

There have been speculations that the quantity of retained charge may be indicative of the progress to failure, but the results for a given sample set, Fig.6 does not substantiate this. In many cases the samples that fail earliest are the ones with the least retained charge, i.e. the longer the sample survives the ac endurance test the more charge is likely to be retained.

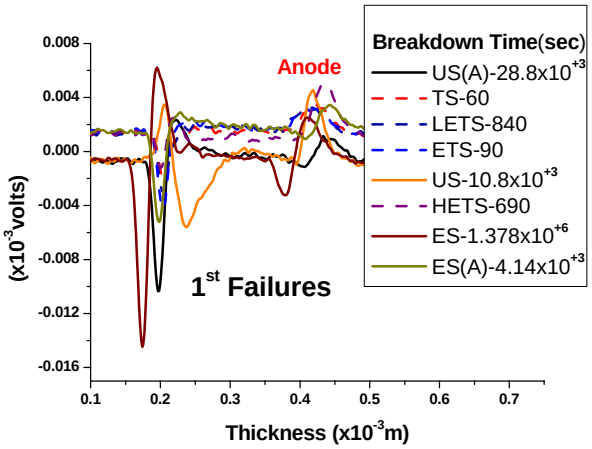

Figure 7: Residual charge measurements for the first failure in 8 separate endurance experiments (cable peelings with different electro-thermal stressing) zero voltage measurements.

DISCUSSION

Endurance

These tests have looked at the ageing of the insulation only within the very controlled electro-thermal stressing employed in the Artemis programme, i.e. no electrical surges, temperature gradients or fluctuations were allowed. With this proviso the measurements show that thermal stressing has a greater influence on reducing the subsequent peeling endurance than an electrical stress. These findings raise a number of issues for the future:

- Is there a threshold electrical stress for ageing? – the endurance tests conducted at a single electrical stress of 70kV/mm (rms) caused failure, but the pre-stressing showed no discernible evidence for the effect of electrical fields up to 28kV/mm (rms).
- Is there a threshold thermal stress for ageing? – the pre-stressing at 90°C caused a reduction in endurance (at 90°C and 70kV/mm) but pre-stressing at 20 °C and 19.5kV/mm showed no evidence for such a reduction.

Residual Charge

The pre-endurance accumulation of space charge in the Artemis peelings follows the expected behaviour – space charge develops throughout the sample with time, with dynamics that are different at the two electrodes. There are some rather small differences observed for the samples with different pre-stresses. There is a residual charge retained in all samples after they have been subjected to a subsequent electro-thermal endurance test.

All peelings within a series (Fig.6) show residual charge – even those which have experienced electrical failure. This feature is common to all test series e.g. all the first failures, Fig.7.

We conclude that the de-trapping of any accumulated charge as a result of the electrical failure is incomplete in ac-fields. We feel that an evaluation of the relative strengths of injected/extracted charge and retained charge in ac-fields may be a useful study to attempt to gain a better understanding of the sequence of the peeling failures.

CONCLUSIONS

The endurance test at 70kV/mm suggests that:

- for the first 5000h of electrical and electro-thermal stressing only cables that experienced a thermal component (T = 90 °C) showed evidence of significant ageing as expressed through a reduction in endurance life at 70kV/mm and 90 °C
- for the same time of cable stressing there was no significant difference in endurance between samples from cables with different applied electrical fields, in the range from zero up to the maximum of 28kV/mm. This was found to be the case for both cables stressed at 90 °C and 20 °C.
- The residual charge measurements under the conditions reported here do not follow a pattern that could be used to evaluate progressive degradation of the material.

Acknowledgements

The authors would like to thank Prof. Gian Carlo Montanari from the University of Bologna for providing the electrical endurance data shown in Fig.2. The authors would also like to thank the members of the ARTEMIS consortium for access to the samples from this project. A. Tzimas also thanks Borealis AB for financial support.

REFERENCES

[1] L.A. Dissado and J.C. Fothergill, "Electrical Degradation and Breakdown in Polymers", P. Peregrinus Press, London, U.K., 1992.

[2] Fothergill, J.C., Montanari, G. C., Stevens, G. C., Laurent, C., Teyssedre, G., Dissado, L. A., Nilsson, U. H., Platbrood., G., "Electrical, Microstructural, Physical and Chemical Characterization of HV XLPE Cable Peelings for an Electrical Aging Diagnostic Data Base". IEEE Trans. on Diel. and El. Ins., 2003. **10**(3): p. 514-527.

[3] G.C. Montanari, private communication.

[4] A. Tzimas, M. Fu, L.A. Dissado. "Characterization of Electro-Thermally aged XLPE Cable Peelings through Space Charge measurements", Conference on Electrical Insulation and Dielectric Phenomena (CEIDP), October 2005, Nashville, (ISBN 0-7803-9257-4), pp 30-33.

[5] Takada, T., Tanaka, Y., Adachi, N., Xiaokui, Qin, "Comparison Between the PEA Method and the PWP Method for Space Charge Measurement in Solid Dielectrics". IEEE Trans. on Diel. and El. Ins., 1998. 5(6): p. 944-951.

Characterization of Electro-Thermally aged XLPE Cable Peelings through Space Charge Measurements

A. Tzimas, M. Fu, L.A. Dissado
Department of Engineering
University of Leicester
LE1 7RH
UK

Abstract: Space charge results under dc-voltages have been used to compare samples taken from peelings of cables ac-aged under different specified thermal and electrical conditions with unaged and service-aged specimens. The aim is to identify quantities that have been altered during ageing. All samples were thermally treated to remove volatiles before measurement and ensure reproducible measurements appropriate to just the state of the polymer. Both the **P**ulsed-**E**lectro-**A**coustic (PEA) and **T**hermal-**S**timulated-**C**urrent (TSC) techniques were used. This allowed us to obtain information both on the ability of the polymer to transport and accumulate charge, and the trap depth distribution and relaxation barriers in the various XLPE samples. The combination of both techniques gives a more detailed picture of the state of the XLPE specimens than each technique on its own. PEA measurements show that materials that have undergone electro-thermal ageing accumulated the most charge, and that the charge resides in both deep and shallower traps. Differences between the field aged material and the electro-thermally aged 'laboratory' sample are identified in both the PEA and TSC measurements, and are taken to indicate that a larger fraction of charge lies in the less shallow traps in the service-aged material.

Introduction

The advent of polymer cable insulation has led to a large amount of research into the way in which such materials lose their insulating qualities during service leading to eventual failure [1]. Now that such insulating materials have been in service for several decades it is particularly important to be able to ascertain their current state so that decisions can be taken regarding a costly replacement. There is therefore a need for an understanding of the degradation process and an identification of diagnostic factors. The EU-sponsored ARTEMIS programme [2] was an attempt to resolve these problems. In this programme, Cross-Linked-Polyethylene (**XLPE**) from a single supplier was used by two different companies to manufacture cable to the same design. Sections from the cable were placed under electrical, thermal, and electro-thermal stress for varying lengths of time (up to about two years), after which their insulation was peeled and the peeling subjected to a number of diagnostic measurements designed to characterize the state of the insulating material in comparison to its state in an unstressed (i.e. unaged) cable. Insulating material from a service-aged cable of similar design with a similar but not identical XLPE was used to provide a comparison between the 'laboratory aged' cable sections and a cable that had been under service conditions.

Here we focus on a comparison between peelings from cables that had been Electro-Thermally-Aged (**ETA**) and Thermally-Aged (**TA**) for the same time, with Serviced-Aged (**SA**) samples originally intended as test bed for diagnostic factors. Peelings from UnAged (**UA**) samples are used as a control. The experiments reported relate to the trapping and release of space charge under a specified protocol, with measurements being made via the PEA [3] and TSC [4] techniques. These two techniques are carried out at different DC voltage field levels, and are used in a complementary way, with PEA measurements used to characterize the accumulated space charge distribution and its manner of decay upon removal of the voltage, and the TSC measurements being used to gain a clearer idea as to the energy distribution of the trapped charge.

Materials and experimental techniques

The samples used in this paper are all cut from peelings taken from XLPE-insulated cables with different ageing histories. The first material, **UA**, is unaged and is used as a reference. The second material, **TA**, was thermally-aged for 5000 hours at 90°C. The third material, **ETA**, was electro-thermally-aged at 19kV/mm and 90°C for 5000 hours. The last sample, **SA**, was taken from a cable, which was in service for 18 years. All the peelings had a thickness of 150μm and were conditioned in vacuum at 80°C for 48 hours. The conditioning was a feature of the ARTEMIS programme shown to remove volatiles and demonstrated to give reproducible results [2]. One sample, taken from the same radial position, was used from each peeling.

0-7803-9257-4/05/$20.00 ©2005 IEEE

Space charge measurement

The HV electrode side consists of semicon material whereas the ground electrode is aluminium. A drop of silicon oil at the electrode/samples interfaces ensured good acoustic propagation. Three DC poling fields, 33, 40 and 47 kV/mm were applied to all samples for 120 min. During this period the voltage was removed for a short time to enable a measurement to be made, and then the voltage was re-applied. The results therefore yield the space charge and corresponding image charges on the electrodes without an overlay of capacitive charge on the electrodes. The space charge decay was also measured at appropriate time intervals during 120 minutes or more of depolarization following removal of the applied voltage. As the space charge profile was similar at all fields, with only a small increase in the magnitude of the space charge density as the field increases, we will just present the poling field data acquired at 40kV/mm in this paper, see Fig.1 to Fig. 4. The space charge at time t (either during voltage application or during subsequent depolarization) is estimated via the absolute charge stored, Q(t), in the sample calculated with equation (1).

$$Q(t) = A\int_{x_1}^{x_0} |\rho(x,t)|dx \qquad (1)$$

Here A is the surface area of the HV electrode and ρ(x,t) is the space charge density and t is the time at which the measurement is carried out. The integral is taken between positions x_0 and x_1 and includes the image charges on the electrodes as it is difficult to estimate exactly where the electrode charge ends and the space charge begins. The actual space charge is taken to be half the amount deduced from equation (1). The space charge decay behaviour, after voltage removal, is characterized by a plot of Q(t) vs log (t) (t = decay time), see Fig.5. As long as the space charge profile retains its shape during the decay, which is essentially the case here, the decay of the absolute charge Q(t) can be related to the charge de-trapping [5-7]. It was shown in [6] that if it can be assumed that the charges are trapped in states whose density has a top-hat energy distribution, the decay follows the form

$$Q(t) \approx eNkT(C-\ln(t)) \qquad (2)$$

over the decay time range, t, defined by equation (3).

$$\exp\left(\frac{\Delta_{min}}{kT}\right) < \nu t < \exp\left(\frac{\Delta_{max}}{kT}\right) \qquad (3)$$

Here N is the density of states per unit energy interval. Δ_{min} and Δ_{max} are the depths of the minimum and filled trap depths respectively, which can be obtained from the times at which the plot deviates from a straight line, as long as, ν, the de-trapping attempt frequency can be estimated. We have taken ν = kT/h for our estimation as this frequency relates to incoherent thermal vibrations of the trap site.

TSC measurement

For the TSC measurements the sample was placed between two brass electrodes and was charged for 15 mins at 90°C for two different fields 27 and 40 kV/mm. The sample is then cooled down to -50°C, where the voltage is switched off, and the thermally stimulated currents are measured as the temperature is gradually increased up to 150°C. The temperature ramp-up rate is 1.7°C/min. Plots of the temperature-dependent discharge currents are given in Fig.6. Peaks in these currents can be associated with the release of dipoles or charges from their electric field imposed orientations.

Results

Space charge accumulation and decay

Figures 1 to 4 show the space charge accumulation, at 40kV/mm during 120mins of polarization, for all four samples. In the unaged sample, UA, Fig.1, a small density of negative space charge is seen to predominate, although there is some slight evidence for positive charge near the anode. Over time the negative space charge region penetrates deeper into the insulation.

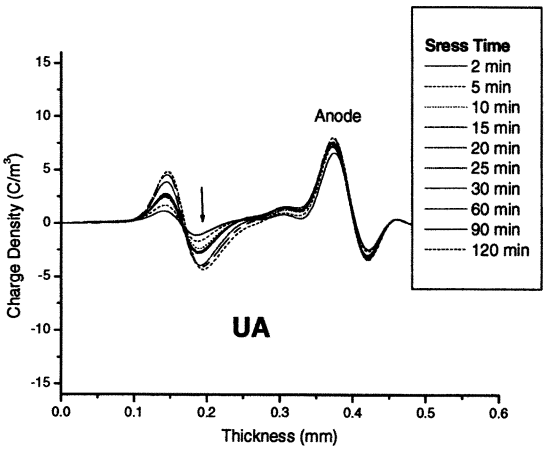

Figure 1: Space charge in the unaged sample during voltage stress.

The space charge behavior of the thermally aged sample, TA, is almost identical to that of the unaged sample. Here the transport of the negative carriers across the sample is even slower.

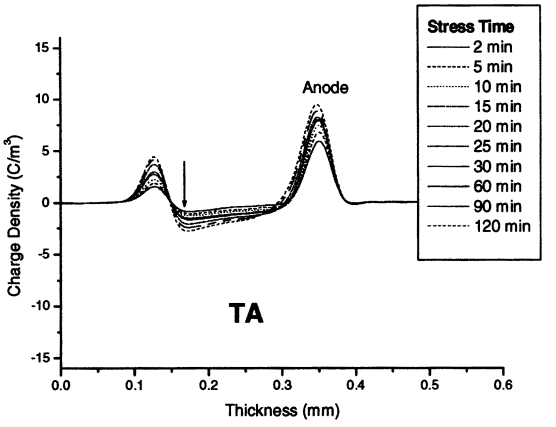

Figure 2: Space charge in the TA-sample during voltage stress.

Negative space charge again dominates in the electro-thermally aged sample, ETA, but here the charge density reaches significantly higher values (6 Cm^{-3}) than in the UA (4 Cm^{-3}) and TA (3 Cm^{-3}) samples.

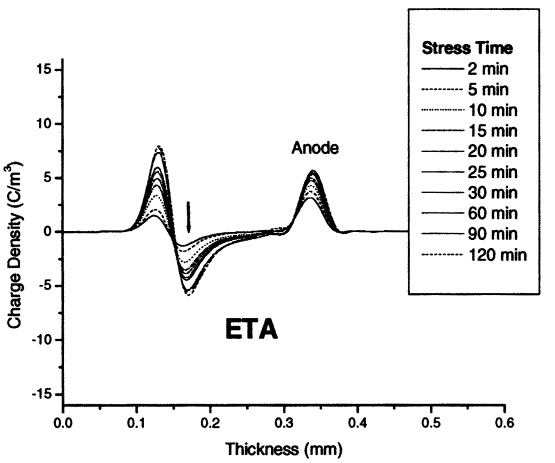

Figure 3: Space charge in the ETA sample during voltage stress.

In the service-aged sample, SA, the space charge behavior has significant differences to those of the other samples. Although negative space charge is still dominant, it has now accumulated next to the anode with a large density (15 Cm^{-3}).

Figure 5 shows the decay of Q(t) with time once the voltage has been removed after 120 minutes of stressing.. It is clear that the SA sample has the most space charge initially and that it decays fastest. For both the UA and TA samples the charge decay is very slow. In all cases the space charge decay obeys equation (2) over a range of times. Using equation (3), estimates of the minimum depth of filled trap can be made. These lie in around 0.93eV for SA and 0.94 to 0.95eV for the other samples. However it is noticeable that the two electro-thermally aged samples contain some charge that is removed quicker and hence that can be assumed to lie in shallower traps.

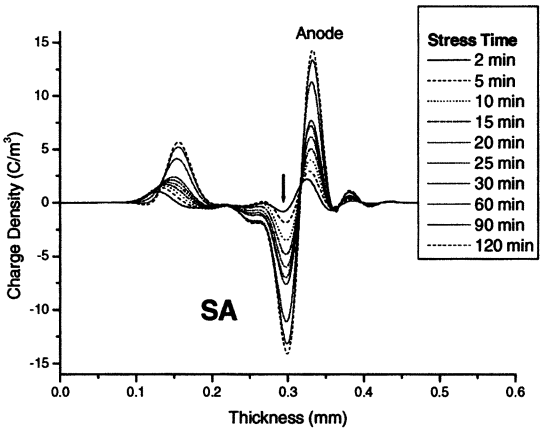

Figure 4: Space charge in the SA sample during voltage stress.

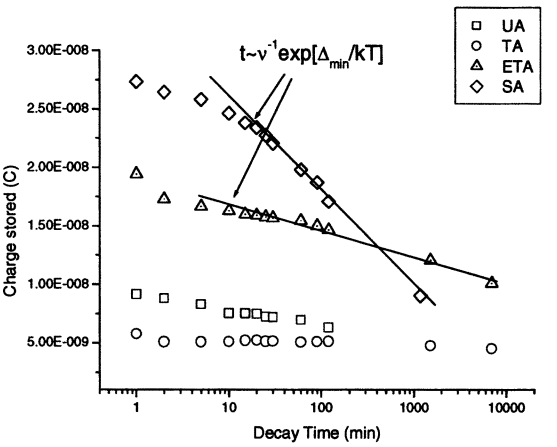

Figure 5: Decay of the stored space charge after voltage removal. The lines show the region of fit to equation (2) for SA and ETA.

No evidence for a cessation of the de-trapping process can be found and hence only a bound can be obtained for the deepest occupied traps using the longest time of the experiment (~ 7000 minutes). This gives,

$$\Delta_{max} \geq 1.10\text{eV} \qquad (4)$$

TSC current peaks

The TSC current (following poling at 27kV/mm) shows peaks for all four samples. The current peak for the UA sample is very weak and occurs around 115°C. For the TA sample, there are two sharp current peaks next to each other with the greatest in magnitude occurring at 120°C. Both the ETA and SA samples have two current peaks at 30 and 110°C with the high temperature peak being more intense than the low temperature one in the

ETA sample and the opposite being the case for the SA sample. Estimates for the de-trapping energy made from the position of the peak give 0.92eV for the peak at T≈303 K and 1.18eV for the peak at T≈383K. A similar result has been obtained by Mizutani et al [4] for LDPE.

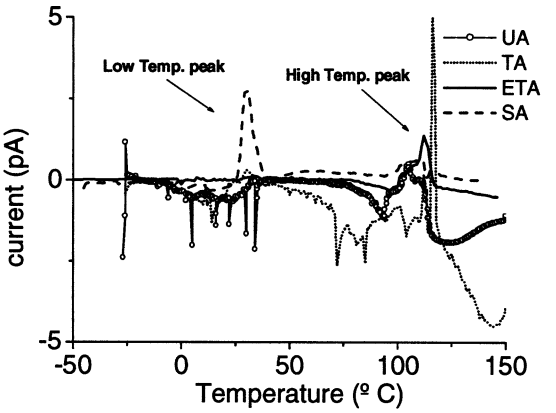

Figure 6: Current peaks of all four samples after 15mins of poling at 27kV/mm.

Discussion

The PEA data for UA and TA samples are very similar with low negative charge densities and slow charge decay. This indicates that mainly negative charge is injected, that it lies in deep traps (≥0.95eV), and these traps are not present in great density. This analysis is supported by the TSC data, which only shows evidence for the deeper traps related to the higher temperature peak. In the case of the electro-thermally aged samples the situation is different. They accumulate larger quantities of space charge, some of which seems to lie in a range of traps that are shallower than ~0.94eV and is hence faster to release. This contention is supported by the TSC that shows a lower temperature current peak corresponding roughly to a de-trapping energy of around 0.92eV exists in addition to the higher temperature peak present in all the samples. In the case of the ETA sample the larger proportion of charge in the TSC experiment lies in the deeper traps and this would be consistent with small amount of charge that can be seen to decay in the first few minutes of the PEA experiment, i.e. almost all the charge here lies in the deepest trap range. For the SA sample this is not the case. The TSC indicates that a large proportion of charge lies in the shallower traps, and that this will decay in a few minutes as seen in the PEA data. This is consistent with a picture in which the deep traps have been filled and the charge residing in shallower traps has been able to transit the sample and build up the negative hetero-charge observed. However the possibility of ionic dissociation leading to hetero-charge formation when the positive component is removed at the anode cannot be ruled out.

Conclusions

Thermal ageing over 5000h does not substantially modify the cable insulation. However, the combination of an electric field and high temperature does introduce changes. These are:

Greater ability to accumulate net charge associated with a greater density of traps extending to shallower trap depths.

In field aged cables the existence of shallower traps together with filled deep traps allows for charge transit and the formation of heterocharge.

Acknowledgements

The authors would like to thank ARTEMIS for access to the samples and for permission to publish. A. Tzimas also thanks Borealis for financial support.

References

[1] L.A. Dissado and J.C. Fothergill, *Electrical Degradation and Breakdown in Polymers*, P. Peregrinus Press, London, U.K., 1992.

[2] Fothergill, J.C., Montanari, G. C., Stevens, G. C., Laurent, C., Teyssedre, G., Dissado, L. A., Nilsson, U. H., Platbrood., G., *Electrical, Microstructural, Physical and Chemical Characterization of HV XLPE Cable Peelings for an Electrical Aging Diagnostic Data Base*. IEEE Trans. on Diel. and El. Ins., 2003. **10**(3): p. 514-527.

[3] Takada, T., Tanaka, Y., Adachi, N., Xiaokui, Qin, *Comparison Between the PEA Method and the PWP Method for Space Charge Measurement in Solid Dielectrics*. IEEE Trans. on Diel. and El. Ins., 1998. 5(6): p. 944-951.

[4] Mizutani, T., Suzuoki, Y., Masahiro, H., Masayuki, I., *Determination of Trapping Parameters from TSC in Polyethylene*. Japanese Journal of Applied Physics, 1982. **21**(11): p. 1639-1641.

[5] G.Mazzanti, G.C.Monatanri, J.M.Alison, *A space-charge based method for the estimation of apparent mobility and trap depth as markers for insulation degradation. Theoretical basis and experimental validation*, IEEE TDEI, vol 10, pp187-197, 2003

[6] L.A. Dissado, O. Paris, T. Ditchi, C. Alquie and J. Lewiner, *Space charge injection and extraction in high divergent fields*, Ann. Rep. CEIDP (IEEE Pub. No. 99CH36319), 1999, pp.23-26

[7] Dissado, L.A., G. Mazzanti, and G.C. Montanari, *The Role of Trapped Space Charges in the Electrical Aging of Insulating Materials*. IEEE Trans. on Diel. and El. Ins., 1999. 4(DEI): p. 496-506.

Comparative study of space charge in the polymeric insulation of power cables using PEA, isothermal and non-isothermal currents measurements

M. Carmo Lança[1], M. Fu[2], E. Neagu[1,3], L.A. Dissado[2], J. Marat-Mendes[1], A. Tzimas[2], S. Zadeh[4]

[1] Departamento de Ciência dos Materiais, Secção de Materiais Electroactivos (CENIMAT), Faculdade de Ciências e Tecnologia, Universidade Nova de Lisboa,2829-516, Caparica, Portugal
[2]Department of Engineering, University of Leicester, LE1 7RH Leicester, UK
[3]Department of Physics, Technical University of Iasi, B-dul D. Mangeron 67, Iasi 6600, Romania
[4]19 Gatwick Road London, SW18 5UF, U.K (work carried out at The University of Leicester).

***Abstract*-An understanding of space charge build-up in the polymeric insulation of power cables is important in determining how aging occurs and progresses and, also in predicting cable lifetime. In this investigation electric-field induced space charge in peelings from XLPE (cross-linked polyethylene) cables was measured using two different methods: the pulsed electro-acoustic technique (PEA) and the combined procedure of isothermal and non-isothermal charging/discharging currents (FTSDC). These two methods allow the study of space charge in highly insulating materials. Also, since electric fields of different orders of magnitude are applied to the sample in the two methods, it is possible to analyze different characteristics of the space charge traps. Prior to the measurements the samples were subjected to conditioning to remove volatiles. Cable peelings from various brands aged under different conditions (including field aged and thermally aged samples) were studied as received from the manufacturers. Some of the samples have undergone further ageing in AC electric field (50Hz) for 1000h to see the influence of further ageing on space charge build-up. The results for the different types of samples are compared in an attempt to correlate different ageing parameters.**

I. INTRODUCTION

Polyethylene (PE), mainly in its cross-linked form, has been used for many years as the polymeric insulation of medium and high-voltage power cables (both AC and DC). It is well known that the polymer suffers electrical ageing that limits the useful lifetime of the cables [1]. Dielectric breakdown is the ultimate consequence of electrical ageing but before, at earlier stages of ageing, new traps are formed and space charge accumulates. Since PE is a highly insulating material it is difficult to study the characteristics of space charge accumulation and the trap parameters (such as, relaxation times and activation energies).

In this work two different procedures to investigate space charge are used and the results compared.

FTSDC (final thermally stimulated currents): This procedure combines isothermal and thermo-stimulated measurements of current during charging and discharging. It is composed of four steps [2]:

1) ICC (isothermal charging current): the sample is isothermally (temperature - T_i) DC charged (applied electric field - E) for a given time, t_c;
2) IDC (isothermal discharging current): the sample is isothermally (T_i) discharged for a given time, t_d;
3) FTSDC (final thermo-stimulated discharging current): the sample is discharged and heated (from (T_i to T_f) at a constant heating rate (β);
4) FIDC (final isothermal discharging current): the sample is discharged for a given time, t_{fd};

The final step (FIDC) allows the almost complete discharge of the sample. Since the charges are in traps with long relaxation times, if the discharge is not carried out for long enough time before the next run, it is not possible to control the remnant charge and results are not reproducible [2]. For a more detailed overview of the procedure, mainly its application to the study of aged PE, see [3-6].

PEA (pulsed electro-acoustical technique): This technique gives the space charge profile of the samples along the axis perpendicular to the electrodes. An electrical pulse (with width in the order of nanoseconds) applied to the sample (with or without a continuous voltage), disturbs its electro-mechanical equilibrium generating propagating pressure waves at the locations of space charge. These are measured at a piezo-electric detector, where the amplitude gives the space charge magnitude and the delay gives its location. For details of the technique see [7].

The two techniques allow space charge characteristics to be studied at different electric field ranges (high electric field for PEA and medium electric field for FTSDC). In this work three different cable peelings from different sources and aged under different conditions are investigated using the two techniques described above.

II. EXPERIMENTAL

The three different cables peelings analyzed were received from the sources aged as following: Type A – electrically aged in the laboratory at high temperature (25 MV/m at 90°C for

5000h), Type B – service aged for 18 years and Type C – thermally aged at high temperature (90°C for 5000h). Cables A and C were made from the same batch of XLPE, but manufactured by different companies. Prior to measurement the samples were pre-conditioned in vacuum (48h at 50°C).

Some type A samples were further aged in a 1M solution of NaCl at 50°C for 1000 h with an applied 50 Hz -AC electric field of 7 MV/m. These type A samples are denoted by (a) and those investigated as received by (b).

The measurement procedure for FTSDC has been described in [5]. Here we present just the two first runs performed on each type of sample. The charging conditions were: DC electric field E = 2 MV/m, temperature during ICC+IDC T_i = 30°C with charge/discharge time ratio t_c/t_d = 1h/2h. For the FTSDC step the heating rate β = 1°C/min and the final temperature T_f = 100°C (corresponding also to the temperature of FIDC step). PEA was performed at temperatures between 20 and 40°C, with applied DC field varying from 20 to 120 MV/m.

III. RESULTS AND DISCUSSION

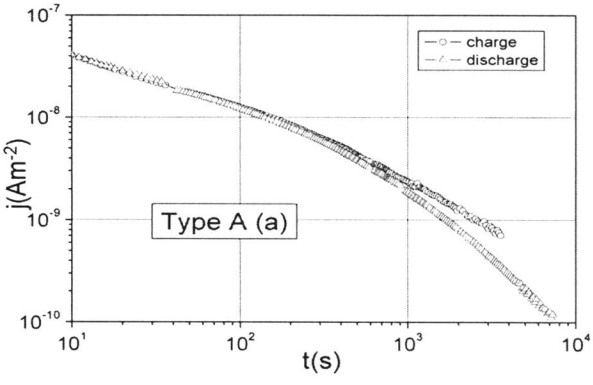

Fig. 1. ICC+IDC plot for Type A sample further AC aged (a). First run performed on the sample (E = 2 MV/m, T = 30°C, t_c/t_d = 1h/2h).

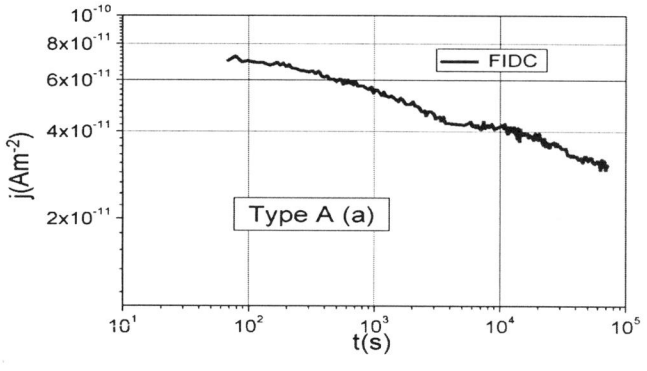

Fig. 2. FIDC plot for Type A sample further AC aged (a). First run performed on the sample (E =2 MV/m, T = 30°C, t_c/t_d = 1h/2h). Same sample as in Fig. 1.

A. FTSDC measurements

Figs. 1 and 2 show the results for the isothermal steps of the measurement ICC, IDC (Fig. 1) and FIDC (Fig. 2) of the first run performed on a type A-(a) sample. Usually the charging and discharging current results can be fitted by an exponential decay function with three or four different relaxation times. For example, the ICC in Fig. 1 was fitted with 3 relaxation times (τ_1 = 15s, τ_2 = 180s and τ_3 = 2100 s). These are typical values for PE where the longest relaxation time does not usually exceed 1h [5]. It is known that the observed current is due to trapping/de-trapping of space charge [3-6].

In Fig. 3 the second runs performed on type A-(a) and (b) samples are compared for ICC and IDC. Taking into account that the charging conditions are exactly the same it is clear that in the sample further aged (a) there is a greater amount of space charge. The second run was selected because type A-(a) samples were not conditioned prior to FTSDC measurements.

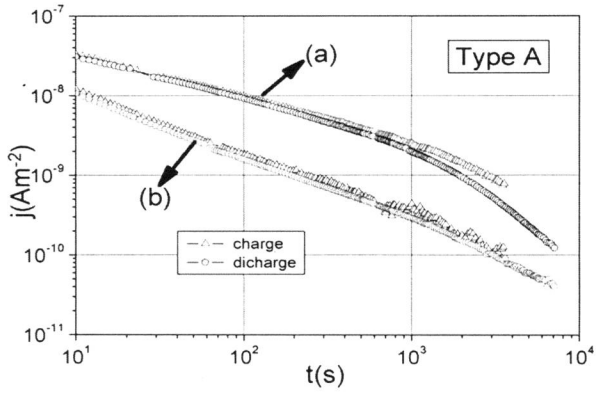

Fig. 3. ICC+IDC plot for Type A sample: (a) further AC aged and (b) no further ageing. Second run performed on the samples (E = 2 MV/m, T = 30°C, t_c/t_d = 1h/2h).

The FTSDC thermograms also can give very important information about different samples types: Figs. 4 and 5 compare samples of type A further AC aged (a), with no AC ageing (b). Figs. 6 to 8 compare runs 1 and 2 for samples of type A, B and C with no further ageing, respectively.

Type A: In Figs. 4 and 5 the effect of AC ageing is observed. The type A-(b) samples show a very broad peak which indicates the presence of a great amount of charge previously injected and retained in the sample. The calculation of the total charge in the charging process (Q_c = Q_{ICC}) and of the total charge released during the total discharge processes (Q_d = Q_{IDC} + Q_{FTSDC} + Q_{FIDC}) confirm this: Q_c < Q_d, especially for run 1. The calculated values of the total charge (Q_c and Q_d) are of the order of 10^{-9} C, similar to those reported in [4, 5]. The result also applies to type A-(a) even if further AC ageing has resulted in a much narrower and higher peak. It seems that this type of ageing creates new traps from which the excess amount of SC is de-trapped during the non-isothermal step. In this case it was possible to calculate activation energies (E_a) by the initial rise method [8]. The values are indicated in the plots for run 1 (E_a = 0.36 eV) and run 2 (E_a = 0.48 eV). This range of values is in good agreement with the ones found in the literature [9] for peaks in this temperature range (T_m = 50-60 °C).

The two first runs performed on a type A-(b) sample are plotted in Fig. 6. As can be seen the current density is lower for run 2 than for run 1. Also the peak is broader and flatter in run 2 indicating that the more carriers are trapped at a wider

range of trap depths than in run 1 and, also that some of the charge is trapped during the previous ageing. If the comparison is made between ICC and IDC, it is seen that the initial currents (until ≈1000s) are smaller for run 2 than for run 1 (both ICC and IDC), while for t_c and t_d > 1000s they are similar for both runs (results not presented here). These differences are much smaller than the ones seen in Fig. 3. If charging/discharging steps are analyzed it is possible to conclude that: (1) the charges trapped in deeper traps (with longer relaxation times) still remain in the sample after the first run and (2) the traps with shorter relaxation times are released during run 1 and not replaced by the DC charging of run 2, consequently these charges are deposited during the AC ageing.

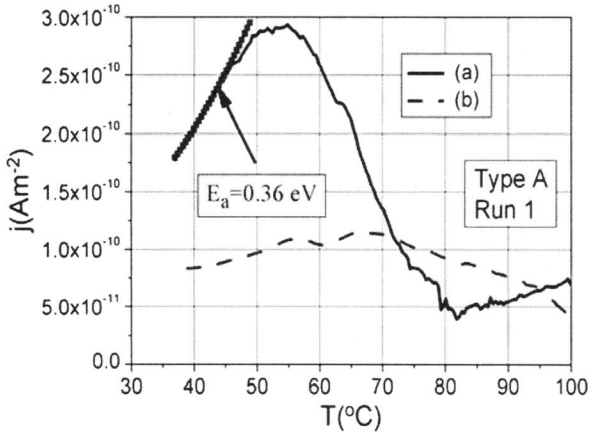

Fig. 4. FTSDC plot for Type A sample: (a) further AC aged and (b) no further ageing. First run performed on the samples (E = 2 MV/m, T = 30°C, t_c/t_d = 1h/2h).

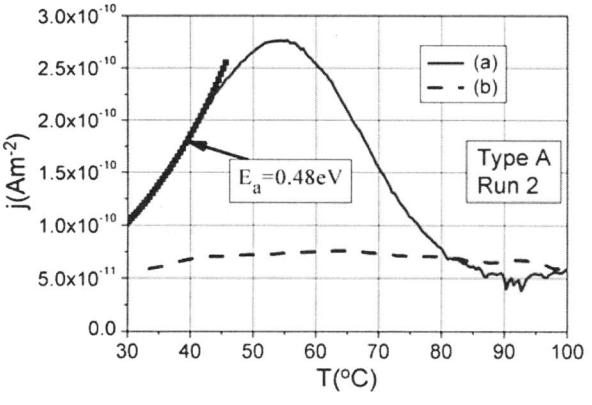

Fig. 5. FTSDC plot for Type A sample: (a) further AC aged and (b) no further ageing. Second run performed on the samples (E = 2 MV/m, T = 30°C, t_c/t_d = 1h/2h).

Type B: Runs 1 and 2 are plotted in Fig. 7 for a XLPE peeling from a service-aged cable. For run 1 the spectra is very different from the one seen in Fig. 6 for a type A sample (electrically aged in the laboratory). Two peaks can be distinguished, one broad with no clear maximum (below 80°C) and probably composed of different individual peaks (at least two shoulders are observed). The second peak at higher temperature (maximum around 90°C) is much sharper and narrower. For run 2 a peak similar to the ones seen for Type A (Fig. 6) is observed. It seems that during the first run (including FIDC step) SC that was trapped during ageing was released. The peak appearing at higher temperature indicates the presence of deeper traps in the service-aged samples.

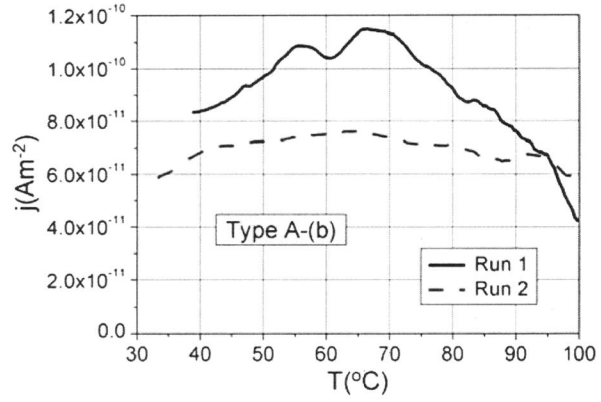

Fig. 6. FTSDC plot for Type A sample: (b). First and second run performed on the sample (E = 2 MV/m, T = 30°C, t_c/t_d = 1h/2h).

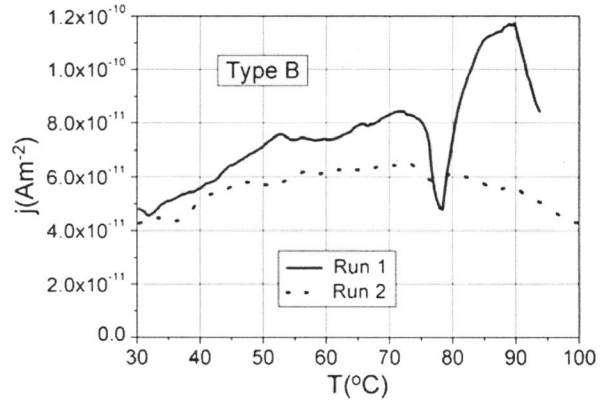

Fig. 7. FTSDC plot for Type B. First and second run performed on the sample (E = 2 MV/m, T = 30°C, t_c/t_d = 1h/2h).

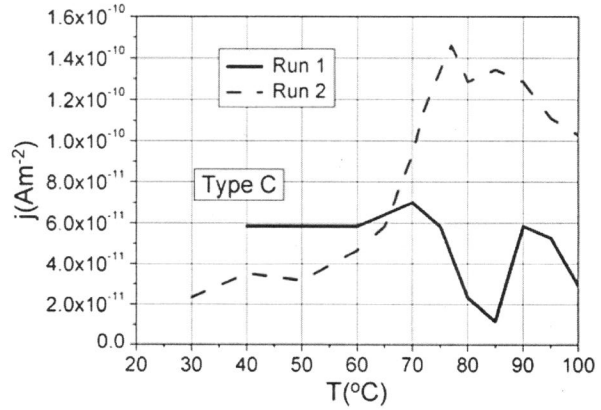

Fig. 8. FTSDC plot for Type C. First and second run performed on the sample (E = 2 MV/m, T = 30°C, t_c/t_d = 1h/2h).

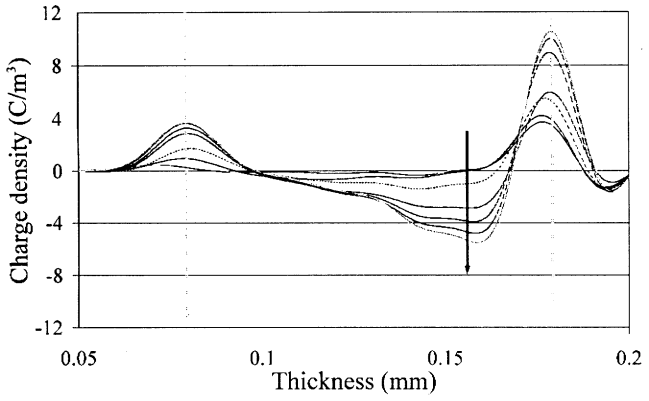

Fig. 9. PEA results for a type B sample with no further ageing (applied field 50 MV/m at 20°C). Measurements made by transiently removing the applied voltage. Stressing times from 1min to 120 min (as indicated by the arrow).

Type C: This sample did not undergo electrical ageing, only thermal ageing. In this case both runs 1 and 2 are different from the ones observed in either two types of samples as is shown in Fig. 8. The magnitude of the current is lower for this third type of ageing. The main difference is that the broad peak, related to SC traps, is no longer visible and sharper peaks appear. This could be due to SC charge trapped near the dipoles formed by thermal-oxidation.

B. PEA measurements

The PEA measurements were performed by applied DC fields one to two orders of magnitude higher then the ones used in FSDC. As an example, Fig. 9 shows the SC profile obtained for a type B-(b) sample with a DC field of ≈50 MV/m at 20°C for times from 1min to 120 min. Negative heterocharge build-up at the anode is observed. For an applied field of 120 MV/m it was possible to see charge packet formation in the type A samples even if the total amount of charge is not high. For experiments performed at 50 MV/m and near room temperature for the three types of samples the main characteristics were (with no AC ageing):

Type A: Negative charge was observed in the bulk with build up at the cathode and a maximum charge density of 6 C/m^3.

Type B: Negative heterocharge with a maximum density of 10 C/m^3.

Type C: Negative charge was measured in the bulk with a maximum density of 2 C/m^3.

Similar results were obtained for 60 MV/m for type A and C samples. For a lower field (20 MV/m) homocharge was observed with maximum density less than 2 C/m^3. The service-aged sample has a larger maximum charge density and differed from the others in exhibiting a negative heterocharge. This reveals the presence of more SC in deeper traps. The service aged XLPE peeling therefore shows the highest SC magnitudes with lower values for the electro-thermally aged and thermally aged laboratory samples, in order.

C. Comparing FTSDC to PEA measurements

If the total charge is considered in PEA measurements it is clear that the service aged sample shows higher values, while for the results presented here for FTSDC (runs 1 and 2) the higher charge values are found in the electrically aged samples in the laboratory. However if further runs are analyzed [10] the sample revealing the greater amount of charge is again the one aged in service. In both methods the sample aged only thermally is the one with the least SC. Therefore electrically aged samples have more space charge, but the long time ageing occurring during service places the charges in deeper traps necessitating larger field values, longer times and higher temperatures for their release. Thus higher fields (PEA) or longer times (FTSDC successive runs or very long FIDC) are needed to release the charge in the service-aged sample.

IV. CONCLUSIONS

PEA and FTSDC measurements can be used as complementary methods since different electric field levels are applied. Service aged samples are the ones with more SC present and with deeper traps. Thermo-electrically laboratory-aged samples also retain SC, but thermal ageing on its own results in less charge being retained as is visible in the thermograms. The service-aged samples show more and deeper traps with more SC present. The formation of SC deep traps therefore requires electrical stress, and it is probably also enhanced by the temperature.

ACKNOWLEDGMENT

The British Council Treaty of Windsor award LIS/992/2 is thanks for facilitating exchange visits between the two institutions.

REFERENCES

[1] L.A. Dissado, J.C. Fothergill: *Electrical Degradation and Breakdown in Polymers* (IEE P. Peregrinus, London 1992).

[2] E.R. Neagu, , R.M. Neagu, "Analysis of Charging and Discharging Currents in PET at Elevated Temperatures" Phys. Status Solidi A, Vol. 144, pp. 429-438, 1994.

[3] E.R. Neagu, J.N. Marat-Mendes, "Combined Isothermal and Non-isothermal Techniques to Analyze Charge Trapping and Satbility in Insulating Materials", Jpn. J. Appl. Phys., Vol. 40, pp. L1160-L1162, 2001.

[4] M.C. Lança, E.R. Neagu, J.N. Marat-Mendes: "Combined Isothermal and Non-isothermal Current Measurements Applied to Space Charge Studies in LDPE", J. Phys. D: Appl. Phys., Vol. 35, pp. L29-L32, 2002.

[5] M.C. Lança, E.R. Neagu, J.N. Marat-Mendes, "Space Charge Studies in LDPE using Combined Isothermal and Non-isothermal Current Measurements", IEEE Trans. On Diel. Elect. Ins., Vol. 11, pp.25-33, 2004.

[6] M. Carmo Lança, E.R. Neagu, J.N. Marat-Mendes, "Space Charge Studies of Aged XLPE Using Combined Isothermal and Thermostimulated Current Measurements", Mat. Sci. Forum., Vol. 480-481, pp.501-504, 2004.

[7] J.M. Alison, "A high-field pulsed electro-acoustic apparatus for space charge and external circuit current measurement within solid insulators", Meas. Sci. Technol., vol.9, pp. 1737-1750, 1998.

[8] J. Vanderschueren, J. Gasiot, "Field-induced thermally stimulated currents", in *Thermally Stimulated Relaxation in Solids*, edt. P. Bräunlich, Springer-Verlag, Berlin, 1979

[9] H. von Seggern, "Detection of Surface and Bulk Traps", J. Appl. Phys., vol. 52(6), pp. 4084-4089, 1981.

[10] M. Carmo Lança, E.R. Neagu, L. Dissado, J.N. Marat-Mendes, "Space charge studies in XLPE from power cables using combined isothermal and thermostimulated current measurements", Materiais 2005 – III Int. Materials Symp, pp. 222, 20-23 Mar. 2005, Aveiro, Portugal.